Ribosomal proteins in zebrafish haematopoiesis and human disease

Payne, Elspeth

Ribosomal Proteins in Zebrafish Haematopoiesis and Human Disease

Elspeth Payne MB ChB, BSc, MRCP, FRCPath

A Thesis Submitted to the University of London

DOCTOR OF PHILOSOPHY in the Faculty of Medicine

January 2011

Queen Mary University of London, Barts and The London Medical School, Charterhouse Square, London

DEDICATION

For Jeff and Romy

ABSTRACT

Several congenital disorders of human haematopoiesis including Diamond-Blackfan anaemia result from heterozygous loss of genes involved in ribosome biogenesis. Further, hemizygosity for ribosomal protein gene *RPS14* has been implicated in the pathogenesis of myelodysplastic syndrome with loss of 5q, suggesting that genes involved in ribosome biogenesis may act as both haploinsufficient tumour suppressors and regulators of normal haematopoiesis.

Ribosome biogenesis is highly conserved through evolution and readily studied in simple organisms such as yeasts. However the zebrafish provides a well-established genetic model system which is ideally suited to rapid assessment of vertebrate haematopoiesis. I have therefore used the zebrafish to study genes involved in ribosome biogenesis and their effects on developmental haematopoiesis relevant to human disease.

Presented in this work is investigation of the effect of disruption of 4 genes known to be involved in ribosome biogenesis on zebrafish haematopoiesis. Firstly, I describe a gene, Dead-box 18 (*ddx18*), identified in a forward genetic screen, whose disruption results in defective haematopoiesis and embryonic lethality. Secondly, I have studied the effects of loss of zebrafish orthologues of the human nucleophosmin gene (*NPM1*), the most frequently mutated gene in human acute myeloid leukaemia. Loss of Npm1 resulted in aberrant numbers of myeloid cells. Heterologous overexpression of mutated NPM1(NPMc+) resulted in increased production of haematopoietic stem cells suggesting a role for NPMc+ in pathogenesis of AML. Finally, I have shown that loss of Rps14 and Rps19 result in anaemia in developing zebrafish and have investigated p53-independent mechanisms for this effect.

The findings described herein demonstrate that disruption of normal ribosome biogenesis frequently results in abnormal developmental haematopoiesis. Further genetic assessment of these tissue-specific pathways deregulated by loss of normal ribosome function may represent an important common mechanism underlying the pathogenesis of congenital and acquired disorders of haematopoiesis, and may provide novel pathways for therapeutic targeting.

CONTENTS

LIST OF TABLES

LIST OF FIGURES

ABBREVIATIONS

ADA ……………………………………………………………….adensine deaminase

AGM…………………………………………….……………..aorta-gonad-mesonephros

ALK…………………………………………………......anaplastic lymphoma kinase

ALPM………………………………………………………….anterior lateral plate mesoderm

AO……………………………………………………………………….acridine orange

APML…………………………………………………….acute promyelocytic leukaemia

BCIP……………….………… (5-bromo-4-chloro-3-indolyl-phosphate) 4-toluidine salt

bp………………………………………………………………………….base pair

BRDU…………………………………………………………...bromo-deoxyuridine

BSA………………………………………………………….....bovine serum albumin

CAB………………………………………………………......caspase antibody block

CDR……………………………………………………….…critically deleted region

CHH………………………………………………………….….cartilage hair hypoplasia

CHOP………………………………………….……….C/EBP homologous protein 10

CHT………………………………………………….………..caudal haematopoietic tissue

DBA…………………………………………………….……Diamond-Blackfan anaemia

ddH$_2$O……………………………………………………….……double distilled water

DEPC…………………………………………………….…..diethylpyrocarbonate

DIG………………………………………………………………………digoxigenin

DKC…………………………………………………….…...dyskeratosis congenita

dNTPs……………………………………...deoxynucleotides (ATP, CTP, GTP, and TTP)

dpf…………………………………………………………...days post fertilisation

dsRNA…………………………………………………………....double stranded RNA

EIF2alpha…………………………..……eukaryotic initiation factor subunit 2 alpha

ELB……………………….…………………………………embryo lysis buffer

EMP……………………………………….………………erythro-myeloid progenitor

ENU……………………………………………………………… ethyl nitrosourea

ER………………………………………..…………………endoplasmic reticulum

EST………………………………………..……………expressed sequence tags

FBS…………………………………….....…fetal bovine serum (heat inactivated)

FeLV-C………………………………………… feline leukaemia virus subgroup C

FITC………………………………………….………….. fluorescein isothiocyanate

FLVCR1………………………….…… feline leukaemia virus subgroup C receptor 1

GCN2…………………………...…………… general control non-derepressible 2

GFP……………………………………..….………………green fluorescent protein

HbF……………………………………………………….….…haemoglobin F

Hpf………………………………………………….…… hours post fertilisation

HRI …………………………………………….……haem regulated inhibitory kinase

HRP………………………………………….………….. horse radish peroxidase

HSC……………………………………………………….haematopoietic stem cells

Hyb(-) ………………………….…..50% formamide; 5x SSC buffer; 0.1% tween 20

Hyb(+)………… Hyb(-)+ 5mg/ml torula (yeast) RNA Type IV and 50ug/ml heparin

ICM……………………………..………………………. intermediate cell mass

IP……………………………………………………………....immunoprecipitation

IPTG…………………………………………..isopropyl β-D-1-thiogalactopyranoside

ISR……………………………………………………… integrated stress response

Kb……………………………………………………………………….……kilobases

LDS…………………………………………………….…..lithium dodecyl sulfate

lmo2……………………………………………………….……… lim domain only 2

LPM……………………………………………….………lateral plate mesoderm

MABT………………………………………..... maleic acid buffer with 0.1% tween 20

MDS……………………………………….…………...myelodysplastic syndrome

MDS5q………………………………….…………………..MDS with loss of 5q

MGG…………………………………………….…....May-Grunwald-Giemsa

mg………………………………………..….……….….………………milligrams

MgCl$_2$……………………………………………………….….. magnesium chloride

ml……………………………………………………,…………………...millilitres

MLF1………………………………………………,… myeloid leukaemia factor 1

mM…………………………………………………….……………. millimolar

MO……………………………………………………………morpholino

mpx………………………………………………………….myeloid peroxidase

mpx+…………………………………………………….………mpx-expressing

MrDB………………………………………………..... Myc-related DEAD-box 18

mRNA………………………………………………….……………. messenger RNA

NBT…………………………………………...……….4-nitro blue tetrazolium chloride

NCBI……………………………...…. National center for biotechnology information

NEB…………………………………………….……….……… New England Biolabs

nsSNSV………………… non-synonymous single nucleotide sequence variants

p53e7/e7 or p53m/m………………………………………………………..zebrafish
line with a mutation within the DNA binding domain of the p53 gene in exon 7

PBI……………………………………………………….. posterior blood island

PBS……………………………………….…… .phosphate buffered saline

PBST………………………………………….…….. PBS + 0.1% tween 20

PCR………………………………………….........polymerase chain reaction

PDT…………………………………………..PBST, 1%DMSO, 0.3% Triton-X

PERK……………………………………... pancreatic endoplasmic reticulum kinase

PFA……………………………………………………….. paraformaldehyde

PI…………………………………………………….……propidium iodide

PKR………………………………………………… …protein kinase regulated by RNA

PolRI …………………………………………….……………..RNA polymerase I

PolRIII………………………………………………………... RNA polymerase III

ProK…………………………………………………...…………… proteinase K

PTU…………………………………………………………………… phenylthiourea

rag2……………………………………………… …recombinase activating gene 2

RNA……………………………………………………….……….ribonucleic acid

RP…………………………………………………………………...ribosomal protein

RPS19…………………………………………………...ribosomal protein S19

rRNA……………………………………………………………….. ribosomal RNA

RT……………………………………………………..………….. .room temperature

RT-PCR………………....... PCR following reverse transcription of RNA into cDNA

S……………………………………………………………………. sedimentation rate

SBDS……………………….…………..……Shwachman-Bodian-Diamond syndrome

SFII……………………………………..…………………………………..superfamily II

snoRNAs…………………………………………………………… small nucleolar RNAs

19

snoRNPs…………………………………..… small nucleolar ribonuclear proteins

SOCS……………………………………....….. super optimal broth with catabolite

SSCT…………………………………….…………………………..saline-sodium
citrate buffer (sodium chloride 150mM; trisodium citrate 15mM) + 0.1% tween20

TA……………………………………….……………………….. transactivating

tal1(or scl)…………………………………T cell acute lymphoblastic leukaemia gene

T-ALL……………………………….......…..……………..T lymphoblastic leukaemia

TBST…………………………………….……Tris buffered saline with tween (0.1%)

TERC……………………………….………………telomerase RNA component

TERT………………………………………………..telomerase reverse transcriptase

TILLING…………………………..……. targeting induced local lesions in genomes

Tg…………………………...……………..transgenic(promoter:expession construct)

tRNA……………………………………………………………. transfer RNA

TSG……………………………………………………..….tumor suppressor gene

UBF1………………………………………………….. upstream binding factor 1

VHL……………………………………………….……...….. Von Hippel Lindau

WISH or ISH…………………………….....…………whole mount in situ hybridisation

WT……………………………………………………………………….wild-type

X-gal …………………………………………5-bromo-4-chloro-3-indolyl-D-galactoside

ACKNOWLEDGEMENTS

My thanks go to Tom Look without whom I would never have had this remarkable experience. I shall take with me his immortal words of scientific wisdom "stay away from the dog poop".

To Finbarr Cotter for his support from afar.

To the myeloid team – thanks to Jen Sbrogna for her friendship and commitment to teaching a novice, to Clemens Grabher for guidance and to Niccolo Bolli for making sure that I finished things.

To other members of the Look lab especially Ujwal Pyati, Sam Sidi and Alex Kentis thanks for helping me to think like a "real" scientist.

I am indebted to Hong Sun and Maria Virgilio for their commitment and help in the final months.

To Shizhen Zhu for keeping me sane and always making me realise I could do more.

To Ellen Church – one of the most remarkable people I know for her friendship and time.

Finally and most importantly to my family; to my wonderful husband Jeff for putting up with me and being an excellent editor, and to my beautiful little American girl Romy.

"Perhaps I am doomed to retrace my steps under the illusion that I am exploring, doomed to try and learn what I should simply recognize, learning a mere fraction of what I have forgotten."

Andre Breton 1928

1. Introduction

1.1 Haematopoiesis in zebrafish

The first descriptions of haematopoiesis in teleost fish were annotated in 1872 by Joseph Oellacher (Detrich et al, 1995). A century later the first zebrafish blood mutant was described (Stainier et al, 1995). The appeal of the zebrafish as an organism in which to study developmental haematopoiesis arises from the fact that this small vertebrate produces eggs fertilised outside the mother (up to 200 eggs per pair per week) and is totally transparent during early development. Thus embryonic blood development can readily be studied in vivo with little or no manipulation of the embryo. In the past decade the development of transgenic animals expressing fluorescent proteins under blood-specific promoters have allowed direct visualisation of specific blood lineages (Hall et al, 2007; Hsu et al, 2004; Lin et al, 2005; Mathias et al, 2006; North et al, 2007; Renshaw et al, 2006; Traver et al, 2003). Such transgenic lines have facilitated fate-mapping studies that allow tracking of cell fate from haematopoietic stem cells (HSC) to mature cells (Bertrand et al, 2008; Bertrand et al, 2007; Kissa et al, 2008; Murayama et al, 2006). Fate mapping studies have also been carried out by injecting individual cells of the developing blastocyst between 1000 and 4000 cells with tractable rhodamine dye. This has allowed mapping of the origin of mono- and multi-potent blood cells to a specific location in the early embryo, as well as identifying at what time point such cells are committed to becoming a blood cell versus other mesodermal cell fate (Warga et al, 2009a). These studies suggest that with the exception of macrophages, all blood lineages seen in the embryo at 26 hours post fertilisation (hpf) are derived from a common progenitor located in the ventral blastocyst at 3 hpf (Warga et al, 2009a).

Legend Figure 1-1: Cartoon depicting the timeline of embryonic haematopoietic development in the zebrafish. Primitive haematopoiesis occurs in 2 phases, erythroid and myeloid. Definitive haematopoiesis begins at around 24 hpf and also occurs in 2 phases, transient erythro-myeloid progenitors followed by formation of definitive HSC in the aorta.
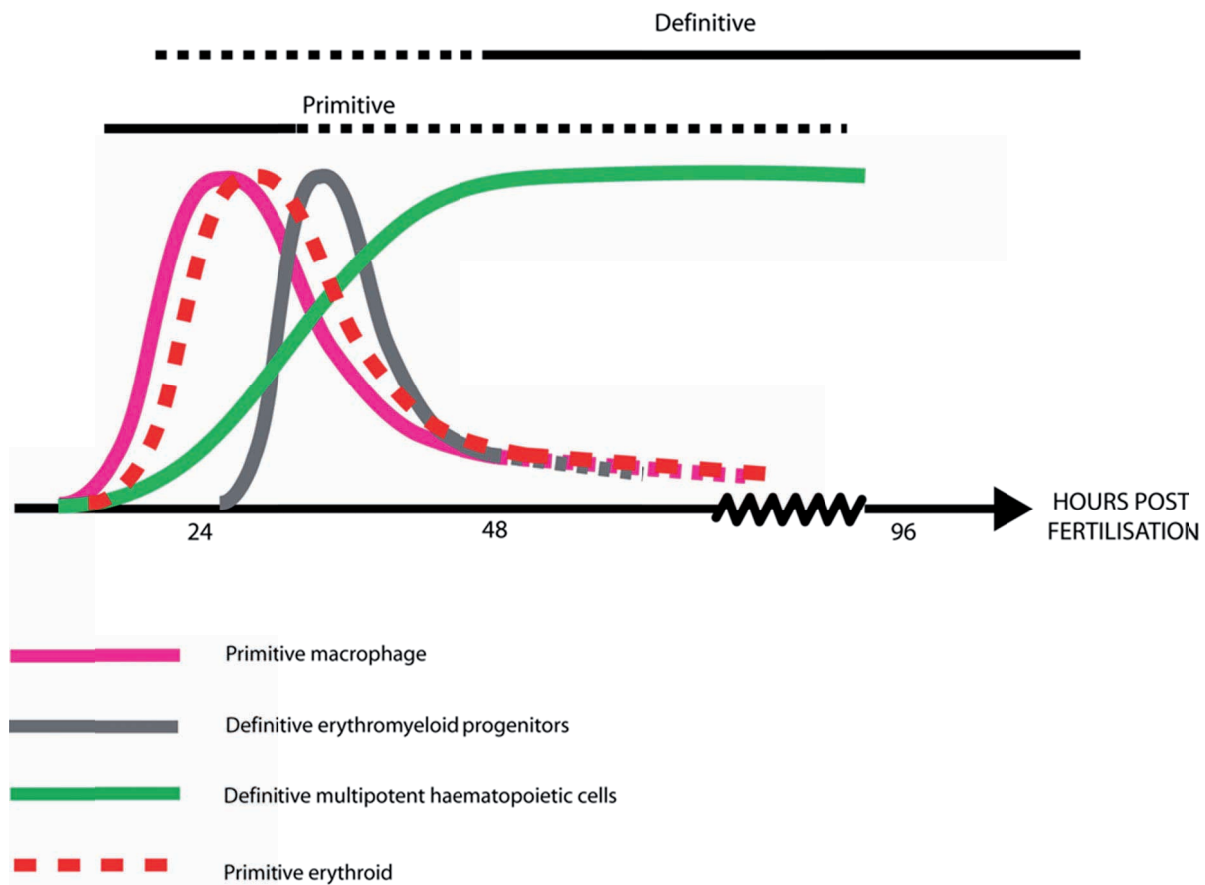
Figure 1-1 : Cartoon of timeline of zebrafish blood development

Zebrafish haematopoiesis occurs in 2 distinct waves, primitive (monopotent) and definitive (multipotent). Each wave comprises 2 phases; in primitive haematopoiesis erythroid and myeloid cells arise separately as two mono-potent populations, while definitive haematopoiesis occurs initially by production of transient bi-potent erythro-myeloid progenitors (EMPs) followed by the production of pluripotent HSCs. A cartoon showing the timeline of primitive and definitive blood development is shown in Figure 1-1.

Primitive haematopoiesis in zebrafish initiates from mesodermal precursor cells in the ventral and lateral marginal zone of the gastrula that can give rise to endothelium, blood, and cardiac tissue (Gering et al, 1998; Gering et al, 2003; Lee et al, 1994; Stainier et al, 1993; Traver et al, 2003). The mesodermal tissue that gives rise to blood cells is the lateral plate mesoderm (LPM), which comprises cells that express genes indicative of primitive blood cells or haemangioblasts, such as the T cell acute lymphoblastic leukaemia gene, *tal1* (or *scl*) and lim domain only 2 transcription factor gene, *lmo2.* respectively. The anatomical location of these early blood progenitors is different in teleost fish compared to their mammalian counterparts. In mammals, primitive haematopoiesis begins in the blood islands of the yolk sac as predominantly erythroid cells. In zebrafish before the onset of circulation primitive haematopoiesis occurs in three regions in the embryo: the anterior lateral plate mesoderm (ALPM) under the head, the intermediate cell mass (ICM) in the trunk and the posterior blood island (PBI) in the tail (Burns et al, 2002; Detrich et al, 1995; Herbomel et al, 1999; Lieschke et al, 2002). Red blood cells, which can be identified by brightfield microscopy develop in the posterior ICM and PBI, are marked by the expression of erythroid genes such as *gata1*, *globins* and *band3* (Brownlie et al, 2003; Detrich et al, 1995; Paw et al, 2003). At the ALPM, amoeboid cells with multi-lobed, eccentric nuclei begin to emerge from under the head, exhibiting the behaviours of functional leukocytes (Herbomel et al, 1999). At around 24 hpf definitive haematopoiesis commences with the emergence of bi-potent EMPs in the PBI. This is followed by budding of multipotent HSCs from endothelial cells in the ventral wall of the dorsal aorta, the aorta-gonad-mesonephros (AGM) equivalent in zebrafish (Bertrand et al, 2010; Boisset et al, 2010; Kissa & Herbomel, 2010). HSCs then migrate to the tail of the fish in the region of the PBI, which now, during definitive haematopoiesis, is referred to as the caudal haematopoietic tissue (CHT). This is thought to represent the fetal

liver equivalent in zebrafish. Cells in the CHT begin to differentiate into definitive myeloid, erythroid and thrombocyte (platelet) lineages, and subsequently enter the circulation. Some HSCs also enter the circulation or migrate up the pronephric ducts to seed the pronephros and the thymus, the adult haematopoietic organs in zebrafish (Bennett et al, 2001; Burns et al, 2002; Stachura et al, 2009; Thompson et al, 1998; Willett et al, 1999).

Mammalian studies indicate that following the establishment of self-renewing HSCs, a progressively more committed hierarchy of haematopoietic cells is formed. Zebrafish orthologues have been found for most of the genes expressed in mammalian blood cell types, including haemangioblasts (*scl*, *runx1*, *lmo2*, and *gata-2*), myeloid/erythroid and lymphoid progenitor cells (*pu.1*, *c/ebpalpha*, and *gata-1*), HSC *(runx1*, *cmyb*, *cd41*)*, T and B lymphocytes (*ikaros*, *rag1*, and *lck*), erythroid cells (*globin* genes and *band3*) and mature myeloid cells including granulocytes (*mpx*) and monocyte/macrophages (*c-fms*, *l-plastin*) (Bennett et al, 2001; Brownlie et al, 2003; Burns et al, 2002; Detrich et al, 1995; Gering et al, 1998; Herbomel et al, 1999; Kalev-Zylinska et al, 2002; Lieschke et al, 2002; Lyons et al, 2001; Thompson et al, 1998). The conservation of genes between mammals and zebrafish argues strongly that the regulatory mechanisms directing lineage specification are likewise conserved in these species.

1.2   Forward and reverse genetic approaches in zebrafish

1.2.1   Forward genetics to discover novel genes involved in haematopoiesis

Simple model organisms, from yeasts to zebrafish, are well suited to the identification of new oncogenes, tumour suppressors, and novel therapeutics important in cancer. This is accomplished using classical (or variations on classical) genetic screens and small molecule screens respectively. Forward genetic screens are based on Mendelian inheritance of genes and the observation of a phenotype in cells or organisms where a gene has been disrupted. The choice of which organism to use will, of course, depend of the goal of an individual study; however, the zebrafish has found a permanent niche as a diploid, vertebrate model organism that is extremely hardy, easy to breed and maintain and is optically transparent.

The first large scale forward genetic screens in zebrafish were undertaken to identify genes that were essential to embryonic development in a vertebrate organism (Driever et al, 1996). Since the embryos developed outside the mother and are transparent for the first few days of life, the zebrafish provides an excellent platform to address developmental biology questions regarding essential genes during embryogenesis. Carried out in Tubingen, Germany and Boston, USA, simultaneous large-scale screens in the early 1990s identified hundreds of mutants including many affecting blood development (Ransom et al, 1996; Stainier et al, 1996). These results demonstrated the potential to discover novel haematopoietic genes and pathways using the zebrafish model. Further, positional cloning of several of these genes showed the power of this model to identify mutants affecting, among others, haematopoietic transcription factors (Lyons et al, 2002) red cell membrane structural proteins (Shafizadeh et al, 2002) and iron transport proteins (Donovan et al, 2002; Donovan et al, 2000; Shaw et al, 2006) relevant to human biology and disease.

Conventional unbiased forward genetic screens generate a series of "mutagenised genomes" by exposing adult male zebrafish to a mutagen, typically the chemical ethyl nitrosourea (ENU). This efficiently induces fixed point mutations in developing spermatogonia. ENU-mutagenised F0 males are bred to wild-type (WT) female fish (after a period of 3–4 weeks to allow for removal of chimeric mature sperm) in order to obtain an F1 generation of fish, each of which has unique mutations at random sites throughout the genome inherited from the mutagenised male. Each F1 fish is then mated to a sibling (or WT) to give rise to an F2 family of fish which will share mutations inherited from the mother and the father. Each F2 family is then bred in a pair-wise manner to identify homozygous mutations that have effects on the system or process of interest, such as defective or aberrant haematopoiesis.

An alternative to chemical mutagenesis is to use a viral insertional mutagenesis strategy. This technique was pioneered in zebrafish in Nancy Hopkins' laboratory where a library of around 300 insertional mutants essential for embryonic development was created (Amsterdam et al, 1999; Amsterdam et al, 2004a; Gaiano et al, 1996; Lin et al, 1994). Insertional mutagenesis is carried out by injecting a murine provirus into embryos at the between 1000–2000 cell developmental stage. Integration of the virus can occur multiple times and pair-

wise crossing of the founder embryos gives rise to F1 progeny that are mosaic for 1 to several insertions. The method used by the Hopkins laboratory then used tailfin DNA from 30 F1 fish from each family to screen for those carrying greater than 3 insertions per fish. These F1 fish were then in crossed to generate F2 families. Progeny from pairwise breeding of F2 families were then screened for developmental defects. This technique has the advantage over chemical mutagenesis as the genomic sequence of the virus is known, so identification of the genes disrupted is considerably easier than using the laborious process of positional cloning techniques to identify point mutations in ENU-mutated animals where the mutation is not known. However, the major disadvantage of viral insertional mutagenesis is the capacity to randomly target all genes and genomic regions. Duplicate alleles with insertions in nearby or identical sites demonstrate that the virus has preference for insertion in some genomic regions. Although this cannot be excluded in the case of chemical mutagenesis, to date this does not appear to be the case, making chemical mutagenesis a more truly unbiased approach.

Most screens rely on the identification of early developmental phenotypes, since this maximises throughput and the number of genomes that can be screened. To analyse haematopoiesis, rapid whole mount cytochemical assays such as *O*-dianisidine staining for haemoglobin or Sudan black or myeloperoxidase staining for granulocytes can be used. Alternatively whole mount in situ hybridisation (WISH) using ribonucleic acid (RNA) antisense probes for genes that are transcribed in a lineage specific manner can be used such as *cmyb* to mark haematopoietic stem cells (HSC) (Burns et al, 2009; Horsfield et al, 2007).

It is known from murine studies that many haematopoietic tumour suppressors are also essential for normal blood development. Based on this knowledge a forward genetic screen was undertaken in the Look laboratory to identify novel genes affecting myelopoiesis. Thus it was hypothesised that a proportion of the genes causing defective myelopoiesis may also serve as tumour suppressors relevant in the development of myeloid malignancies. The format of the screen undertaken is described in Figure 3-1.

1.2.2 Reverse genetic approaches to study haematopoiesis and leukaemogenesis

In contrast to forward genetic screening approaches in the zebrafish, which allow identification of novel genes in an unbiased manner, reverse genetics allows the targeted knockdown of a specific gene or genes and the identification of the functional result of this knockdown. Given the high fecundity and small size of the zebrafish, it is a valuable reverse genetic model system. Since the likely mode of tumorigenesis in human leukaemias is the acquisition of several oncogenic mutations (usually disruption of both proliferation/survival and an additional disturbance of control of differentiation/self-renewal), interrogation of the co-operation of two or more tumour suppressor genes or oncogenic mutations will be greatly facilitated by the ease with which fish carrying the desired alleles (and controls) can be generated.

Transient reverse genetic studies are simple to carry out using morpholinos (MO) or in vitro transcribed RNA. Morpholinos are chemically modified antisense oligonucleotides which are very stable. These can be injected into the one cell stage developing embryo and result in protein knockdown either by blocking translation or disrupting splice donor/acceptor sites. The effects can be observed for up to 5 dpf. Overexpression studies using in vitro transcribed RNA is somewhat more technically challenging since, in general the half-life of injected RNA is far more variable. Knockdown and overexpression studies can be combined with transgenic analysis using the wide range of haematopoietic and vascular transgenic lines available and have resulted in the discovery of a number of key processes in the developmental   biology of haematopoiesis e.g. (Bolli and Payne et al., 2010). Such transient studies have been very informative but are rarely of value beyond 5dpf. Thus the generation of stable lines to examine the effects of loss of function by knockout, or the generation of stable transgenic lines expressing oncogenic proteins, is required for the study of leukaemogenesis.

One problem with reverse genetic studies beyond the first 5 days of life in zebrafish is the difficultly of directing mutations for stable knockout studies to a specific gene of interest within the genome. Until very recently murine models were far more amenable to such reverse genetics via knockout technologies, allowing the alteration of particular genes by manipulation of embryonic stem

cells and homologous recombination. Targeted gene inactivation in the zebrafish has been an extremely time consuming and labour-intensive process, employing random mutagenesis to induce point mutations (as in forward genetics) followed by a search for a mutation in the gene of interest, using a process known as TILLING (Targeting Induced Local Lesions in Genomes), or by using viral insertional mutagenesis strategies. While the latter insertional strategies have the benefit of allowing the rapid identification of disrupted genes by sequencing of regions flanking the insertion site of the virus, this is offset by reduced efficiency and the likely preferential targeting of certain sites within the genome (Amsterdam et al, 1999; Gaiano et al, 1996; Golling et al, 2002).

In a recent advance, three groups have published strategies within the last 18 months that permit the targeting of mutagenesis in zebrafish to specific genetic loci. These groups used chimeric zinc finger nucleases fused to the cleavage portion of the *fokI* endonuclease (Doyon et al, 2008; Foley et al, 2009; Meng et al, 2008). Binding of zinc finger proteins to the forward and reverse DNA strands of a 23–30 base pair (bp) segment within the gene of interest is used to align the 2 *fok1* cleavage domains, which is then able to heterodimerise and cut double stranded DNA in a site-specific fashion (Figure 1-2). Both modular in silico strategies and in vitro bacterial-2-hybrid systems to identify ideal target sequences are now becoming widely available to the zebrafish community, facilitating the development of specific gene knockout models.
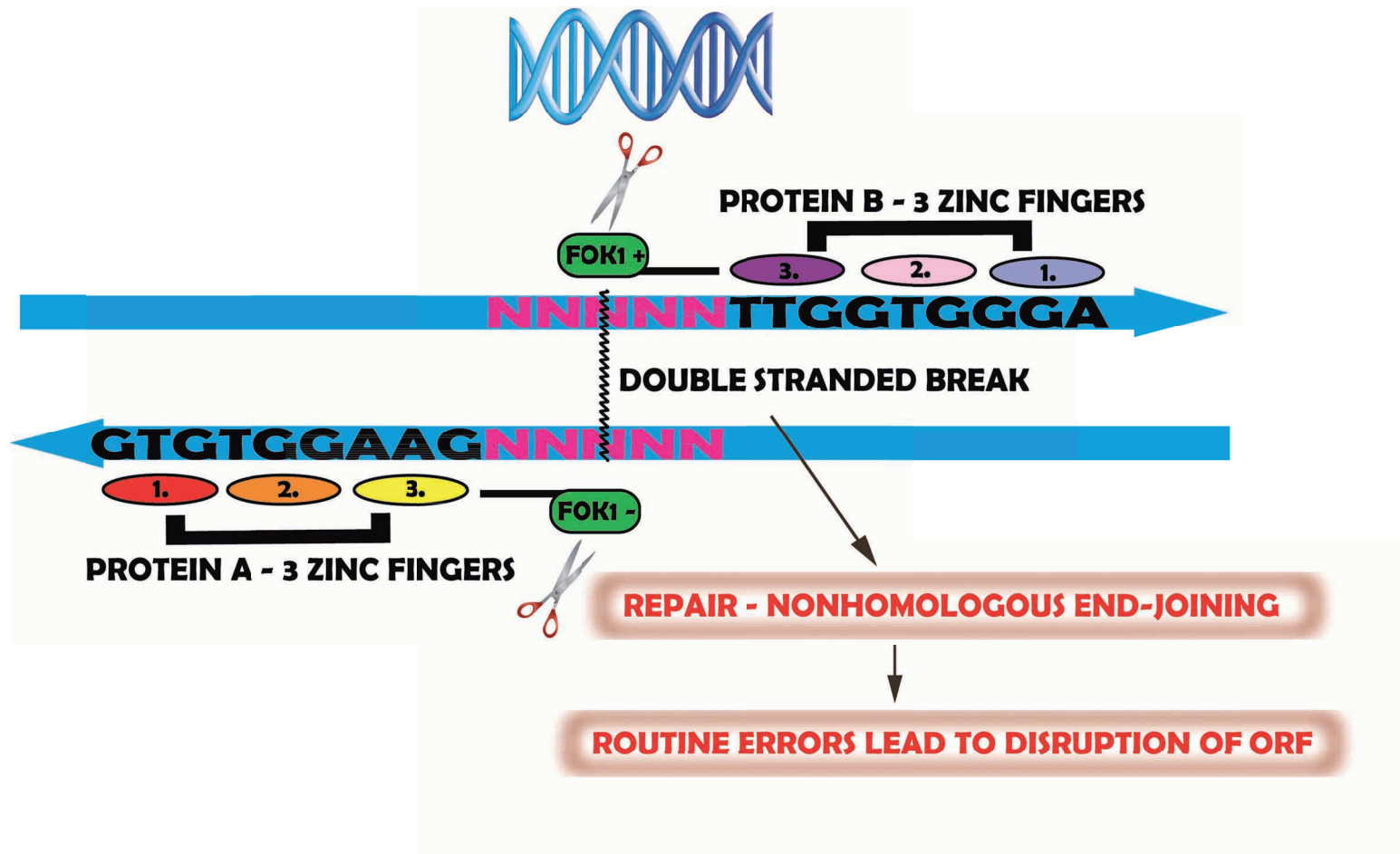
Figure 1-2 : Cartoon of zinc finger nucleases to create zebrafish knockout

Legend Figure 1-2 : RNA from proteins A and B, which each contain 3 zinc fingers that bind the sequence of interest on the forward and reverse strands of genomic DNA are injected into one-cell stage zebrafish. Binding of the protein aligns the cleavage portion of the fokI endonuclease which heterodimerise to cuts the double stranded DNA. Repair of the break by non-homologous end-joining results is error-prone. When the error-prone repair occurs in germ cell DNA, it will be transmitted to the next generation. Repaired products will include frame-shifts and non-sense mutations predicted to disrupt gene function.

Further information about zinc finger strategies can be found at **www.pgfe.umassmed.edu/ZFPsearch.html** and **www.zincfingers.org**

With notable exceptions (such as inherited heterozygosity for *RUNX1* mutations) most mutations in oncogenes or tumour suppressors that result in human leukaemias are somatic rather than germ-line mutations, restricted to haematopoietic tissue. Transgenic models have the benefit that oncogenes can be expressed in particular tissue types by coupling to promoters which are activated by transcription factors in the tissue of interest, e.g. the recombinase activating gene 2 (*rag2*) promoter in T-cell acute lymphoblastic leukaemia (T-ALL) (Langenau et al, 2003). Achieving such tissue-specificity is more complicated when knocking out genes. In murine models, tissue-specificity can be engineered using ex vivo manipulation of embryonic stem cells to generate a "knock-in". Such an approach is not yet available in zebrafish and current zebrafish gene knockouts generated through forward or reverse genetics do not have tissue specificity. This may be disadvantageous when modelling leukaemia, particularly since many tumour suppressor genes are essential for haematopoietic development in both zebrafish and humans.

1.3 Using the zebrafish as a model of human haematopoietic diseases

1.3.1 Zebrafish models of leukaemogenesis

Over the past two decades the zebrafish has become an established model for the study of genetics and developmental biology. In more recent years this organism has also been used to generate cancer models, which, unlike mammalian models, may be amenable to large scale modifier and small molecule

screens. Zebrafish are susceptible to the development of cancer and exhibit a variety of different naturally occurring tumour types similar to those seen in mammals. Human or murine oncogenes driven by tissue-specific promoters in zebrafish have been shown to faithfully develop cancers that closely parallel the human diseases. The first such model was the development of T cell acute lymphoblastic leukaemia (T-ALL) using the murine Myc oncogene driven by the *rag2* promoter (Langenau et al, 2003). The *rag2* promoter has also been utilised to develop T-ALL using the intracellular domain of the *notch1* gene (Chen et al, 2007). Other tumour types have also been modelled in the zebrafish including peripheral nerve sheath tumours (Berghmans et al, 2005), melanoma (Patton et al, 2005) pancreatic cancer, myeloproliferative disorders (Le et al, 2007) and rhabdomyosarcoma (Langenau et al, 2007).

The goal of developing a cancer model in zebrafish is not simply to demonstrate the oncogenicity of mammalian proteins in this system (since this does not necessarily provide additional mechanistic insight above a more complex murine model); it is aimed at harnessing the simplicity and capacity for genetic manipulation and in vivo chemical screens in zebrafish. Thus the challenge for zebrafish researchers is to develop a cancer model that develops the malignancy of choice in a predictable and timely way. This would facilitate using such fish for a modifier screen that would allow detection of mutations that enhance or suppress the cancer phenotype.

An alternative strategy is to retain the focus of study to embryonic (primitive and/or definitive) haematopoiesis and address processes that are known to contribute to the development of cancer such as disrupted cell cycle maintenance, senescence or apoptosis. The relevance to human disease of such an approach derives from murine studies that suggest some haematopoietic oncogenes or tumour suppressors may be essential for not only definitive but sometimes also primitive haematopoiesis, and further that a number of human oncogenes are lethal during embryogenesis when overexpressed in the haematopoietic system. One such oncogene AML1-ETO has been expressed from the ubiquitous and heat-inducible heatshock-70(*hsp70*) promoter in zebrafish to provide a conditional embryonic model and has been successfully used in a small molecule screen (Dayyani et al, 2008; Yeh et al, 2009).

1.3.2 Modelling disorders of erythropoiesis in zebrafish

As evidenced by some of the earliest naturally occurring blood mutants (Stainier et al, 1995), abnormalities of the erythroid lineage are easily studied in the developing transparent embryo over the first days of life with even early non-haemoglobinised erythroid cells being morphologically distinguishable as early as 12hpf, well before the onset of circulation. By 24hpf erythroid cells can be visualised in the developing closed circulatory system and over the next few days increasing quantities of haemoglobinised cells can be observed. The study of erythropoiesis has also been greatly facilitated by the generation of transgenic animals expressing green fluorescent protein (GFP) or dsRED2 from the *gata-1* promoter which is expressed predominantly in erythroid cells.

Zebrafish have several alpha and beta globin genes, which, as in mammalian systems undergo switching from embryonic to adult alpha and beta globins (Chan et al, 1997). They are all encoded on the same chromosome. The primary difference between zebrafish and mammalian erythroid cells is that mature erythroid cells are nucleated in the zebrafish and are ovoid rather than biconcave.

The large-scale forward genetic screens carried out in Boston and Tubingen reported in the early 1990s described mutations affecting all aspects of embryological development. These mutants were examined by brightfield microscopy alone over the first 5 days of development (Haffter et al, 1996). Blood mutants were identified in both screens, 18 mutants with multiple alleles were identified in the Tubingen screen and 9 from the Boston screen (Ransom et al, 1996; Weinstein et al, 1996). A variety of aspects of blood development were affected including cell number, haemoglobin content and photosensitivity. The subsequent characterisation of these mutants and mapping of the causative genes has revealed a staggering 6 of the 7 cloned genes to also be mutated or disrupted in human erythropoietic disorders from porphyria to hereditary elliptocytosis (Brownlie et al, 1998; Childs et al, 2000; Donovan et al, 2002; Donovan et al, 2000; Liao et al, 2000; Paw, 2001; Paw et al, 2003; Shafizadeh et al, 2002). Complementing the forward genetic screens of erythropoiesis are a number of key genetic studies examining the role of haematopoietic transcription factors known to be deregulated in haematological disease (Amigo et al, 2009; Galloway et al, 2005; Rhodes et al, 2005). Reverse genetic studies have also

shed light on the mechanism of some human diseases including Diamond-Blackfan anaemia resulting from ribosomal protein S19 (RPS19) deficiency and Von Hippel Lindau (VHL) (Danilova et al, 2008; Uechi et al, 2008; van Rooijen et al, 2009).

1.3.3 Modelling disorders of myelopoiesis in zebrafish

In contrast to the large number of mutant animals with defects in erythropoiesis, the vast majority of studies of myelopoiesis address the developmental processes governing myelopoiesis and the innate immune system as well as responses to infectious agents such as tuberculosis. In the zebrafish embryo, development of leukocytes commences with the appearance of primitive macrophages from the LPM at 12 hpf. By 18 hpf these cells begin migrating from under the head in the ALPM and over the yolk. These cells express the master regulator of myelopoiesis, transcription factor *pu.1*. At around 18 hpf, expression of *mpx* is first expressed in the anterior LPM and ICM. Some controversy exists over whether *mpx*-expressing (*mpx+*) cells constitute a distinct granulocyte population at this time point since there seems to be some overlap in expression of this and other myeloid genes. However, a population of cells that co-expresses *pu.1* and *mpx* as the expression of *pu.1* begins to wane suggests that these are indeed early neutrophil granulocyte precursors (Bennett et al, 2001; Crowhurst et al, 2002; Lieschke et al, 2002). Between 26 and 30hpf, multipotent HSC are generated in the AGM from the endothelial lining of the aorta. These give rise to the definitive leukocyte lineages, neutrophil granulocytes, monocytes/macrophages, eosinophil granulocytes, mast cells and lymphocytes. Although no basophil equivalent has been identified in the zebrafish, the zebrafish eosinophil granulocytes do appear to share some characteristics usually attributed to basophils in humans. From 96hpf, haematopoietic cells begin to appear in the pronephros, the precursor of the adult haematopoietic organ, the kidney. Over the following weeks, blood production shifts to this site of haematopoiesis. It still remains unclear exactly when the kidney takes over as the site of HSC production but in adult animals all myeloid lineages, eosinophils, granulocytes, monocytes and lymphocytes can be observed.

A large body of work exists utilising the zebrafish to study responses to infectious agents. Their optical transparency and fluorescent transgenic reporter lines have been instrumental in these approaches.(Hegedus et al, 2009; Mathias et al, 2007;

Niethammer et al, 2009; Stockhammer et al, 2009; van der Sar et al, 2009). In addition several groups have modelled myeloid malignancies in zebrafish (Bolli et al; Kramer et al; Le et al, 2008; Le et al, 2007). Although there are some obvious limitations to using embryos to model cancer in adult humans, the evidence that genes necessary for normal blood development are commonly dysregulated or mutated in human cancers argues that this is a valid approach to identify key genetic events that may contribute to leukaemogenesis and dysregulated haematopoiesis in multipotent HSC in adult tissues (McKercher et al, 1996; Robb et al, 1995).

1.4 Ribosomes and haematological disease

1.4.1 Ribosome biogenesis

Ribosomes were so-named in the 1950s following their discovery as the translational machinery of the cell (Palade, 1955). Ribosomes are non-membranous organelles which are composed of a small and large subunit responsible for the recognition and binding of messenger RNA (mRNA) (small) and the catalysis of the addition of individual amino acids supplied by transfer RNA (tRNA) to form the polypeptide chain that will become a protein (large subunit). Components of the ribosome and the various ribosomal subunit precursors are designated by their sedimentation rate (S), which vary considerably between species. The ribosome is composed of central core of ribosomal RNA (rRNA) and around 80 ribosomal proteins (RPs). In addition to the RP at least 200 other protein factors as well as over 70 small nucleolar RNAs (snoRNAs) are required for ribosome biogenesis. Ribosomal RNA in humans is encoded on 5 chromosomes which loop to form ribosomal DNA "clusters" within the nucleolus as shown in the cartoon in Figure 1-3. The nucleolus is a non-membrane bound part of the nucleus which is essentially the ribosome making factory of the cell. rDNA clusters are tandem repeats of rDNA with around 200 copies of the rRNA genes. This is necessary since there is no "amplification step" available for the production of RNA. Contrastingly the protein-making capacity of the ribosome itself can generate large amounts of protein from a single copy of a human gene. Eukaryotic rRNA is composed of 4 different sedimenting components: the 18S giving rise to the small (40S) ribosomal subunit and the 28S, 5.8S, and 5S components that form the large (60S) ribosomal subunit. 28S, 5.8S, 18S are all made from a single initial long rRNA which is then processed

into each component. This rRNA is transcribed in the nucleolus by a polymerase specifically designed for this purpose, RNA polymerase I (PolRI). The 5S component is transcribed by RNA polymerase III (PolRIII) which also transcribes tRNA. Once transcribed, rRNA is heavily modified, mainly by methylation of 2'-OH residues and isomerisation of uridines to pseudouridines. This process is mediated by snoRNAs and associated proteins (collectively termed small nucleolar ribonuclear proteins (snoRNPs)). The product is then cleaved in several steps (denoted by arrows on ribosomal RNA intermediates in Figure 1-3) by endoribonucleases into pre-ribosomal particles. These rRNA species are then assembled in the nucleoplasm into the pre-40S and pre-60S components. Final assembly of the ribosome occurs after transportation of pre-40S and pre-60S into the cytoplasm (Alberts et al, 2008). Ribosomes are found both free in the cytoplasm and bound to the endoplasmic reticulum (ER). Localisation to the ER occurs as a result of the presence of an ER localisation signal in the mRNA sequence being transcribed and thus a given ribosome may be free in the cytoplasm or bound to the ER depending on the mRNA it is transcribing.

Seminal work in the 2000s has revealed that it is the rRNA rather than the associated proteins catalysing the formation of peptide bonds and thus drives the production of peptide chains (Nissen et al, 2000), as reviewed in (Moore & Steitz, 2002). This and related work on the "studies of the structure and function of the ribosome" led to the recent Nobel prize for chemistry in 2009 awarded jointly to Thomas Steitz, Venkatraman Ramikrishnan, and Ada Yonath. In eukaryotes much of what is known about ribosome biogenesis comes from studies in baker's yeast. Figure 1-3 shows some key genes discovered from studies in baker's yeast and where they are required in the generation of rRNA or ribosome biogenesis.
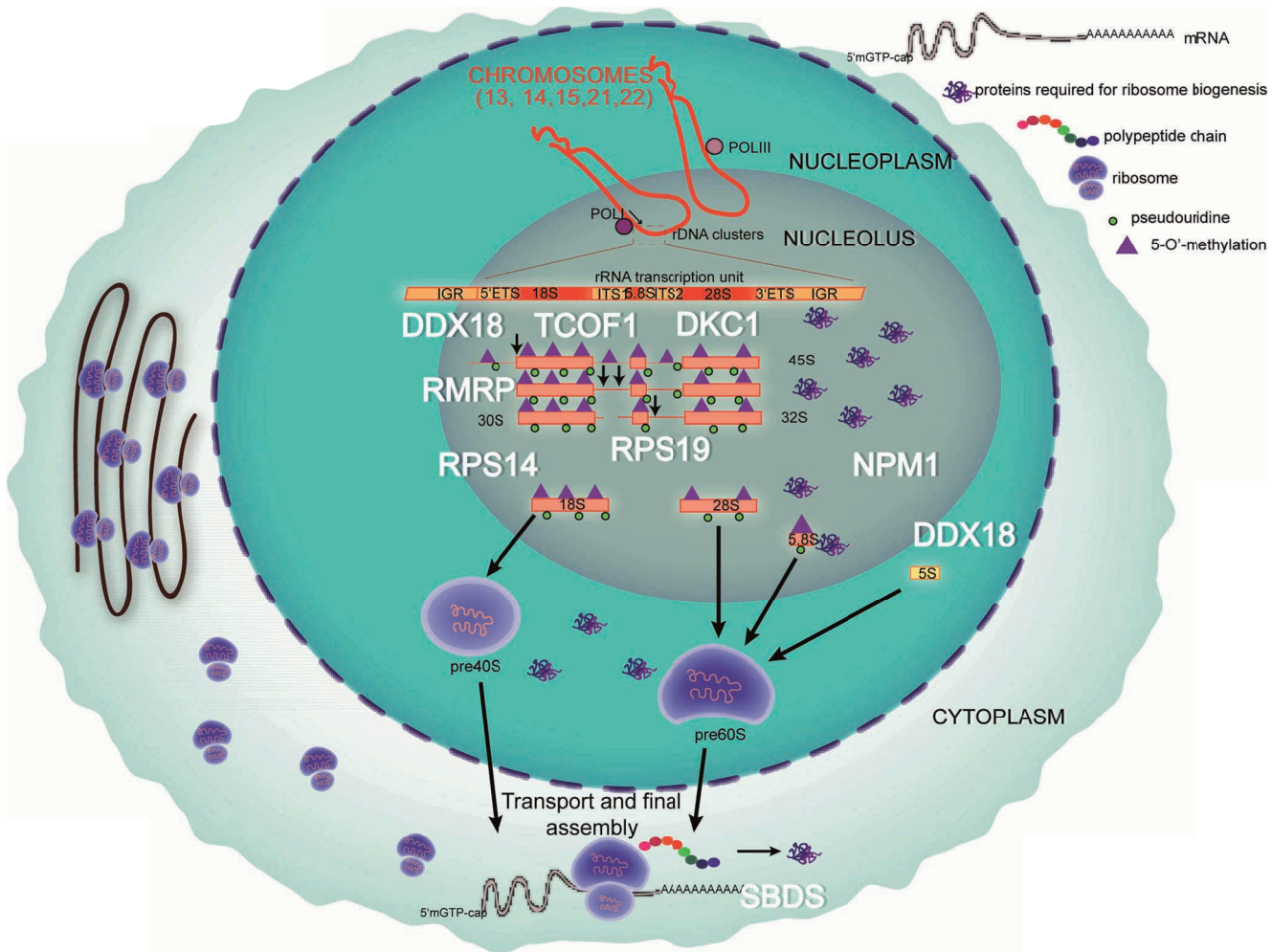
Figure 1-3 : Cartoon of ribosome biogenesis

Legend Figure 1-3: Cartoon of ribosome biogenesis. rRNA is transcribed by PolRI and subsequently processed by endoribonucleic cleavage (small black arrows), pseudouridylation (green circles) and 2-O'-methylation (purple triangles). 5S rRNA is transcribed by PolRIII which is not further processed. Around 80 RPs and over 200 accessory factors including proteins and snoRNAs are also required for ribosome biogenesis. Pre-ribosomal particles are transported from the nucleolus to cytoplasm (dependent on CRM1) before final assembly into active ribosomes. Genes marked in white are required for various aspects of ribosome biogenesis as determined by studies in *Saccharomyces cerevisiae* (adapted from (van Riggelen et al, 2010).

1.4.2 Diamond-Blackfan anaemia

Over the past decade mounting evidence has suggested a function for ribosomes specific to haematopoiesis. The first evidence of this came from the identification of mutation in RP gene of the small ribosomal subunit, *RPS19* as the causative genetic lesion in the congenital red cell aplasia Diamond-Blackfan anaemia (DBA) (Draptchinskaia et al, 1999). It is now known that 50% of cases of DBA arise as a result from of mutations in ribosomal proteins of either the small or large ribosomal subunit (Narla & Ebert, 2010). DBA patients are classically diagnosed with anaemia in the first year of life. In 30–50% of cases there are other associated congenital abnormalities, most commonly midline craniofacial abnormalities such as cleft palate, cardiac malformations (various), renal abnormalities and thumb abnormalities (Ball et al, 1996; Lipton et al, 2006; Ramenghi et al, 1999; Willig et al, 1999). Likewise the severity of anaemia is variable between patients, with some patients showing spontaneous remissions. Most patients are responsive to treatment with corticosteroids. The dose of corticosteroids required to maintain adequate blood counts is often very low although only 60–70% of patients are able to remain transfusion independent. Features of the anaemia include macrocytosis present even when spontaneous remission occurs, as is the persistence of the "i" antigen, elevated adenosine deaminase (ADA) levels and high Haemoglobin F levels (Ball et al, 1996). Bone marrow examination shows a paucity of erythroid precursors with mild lymphocytosis while other lineages are unaffected. Some patients do go on to develop neutropenia over time with rare reported cases of aplastic anaemia. DBA

patients are at an increased risk of malignancy (Janov et al, 1996; Lipton et al, 2006; Willig et al, 1999) and 1.6–6.6% of individuals develop malignancy most commonly AML/MDS and osteosarcoma. The median age at diagnosis is 15 years (compared to 68 years in the non-DBA control group).

The advent of molecular testing has resulted in the new entity of "non-classical" DBA. These are individuals with a DBA mutations presenting in adulthood. In addition to those with a predisposing mutation, individuals with anaemia and high ADA levels have been described who may represent non-classical DBA since only 50% of mutations have been identified (Anur et al, 2009; Vlachos et al, 2008).

1.4.3 5q- syndrome

Myelodysplastic syndrome (MDS) is a heterogeneous disorder of HSCs characterised by peripheral blood cytopenias and a predisposition to develop AML. A subset of MDS patients (around 50%) has abnormalities in their bone marrow karyotype. These abnormalities are almost exclusively gains or losses of large amounts of genetic material (rather than balanced translocation that are frequently observed in de novo AML). The most frequent cytogenetic abnormalities are loss of all or part of the long arm of chromosome 5 (5q) and loss of all or part of chromosome 7. The recurrent nature of these cytogenetic abnormalities has led to the hypothesis that critical tumour suppressor genes (TSGs) required for normal haematopoiesis are located within the deleted segments. Thus over the last three decades several groups have delineated the "critically deleted region(s)" (CDRs) by mapping the region of chromosomal loss in patients with small interstitial deletion of 5q, corresponding to the most likely location of the key TSG(s) whose loss results in the development of MDS (Boultwood et al, 1994; Boultwood et al, 1997; Jaju et al, 1998; Le Beau et al, 1993; Samuels et al, 1988; Van den Berghe & Michaux, 1997; Willman et al, 1993; Xie et al, 2000; Zhao et al, 1997). In the case of MDS with loss of 5q (MDS5q) two critically deleted regions have been identified (Figure 1-4). The clinical phenotype observed with each of the CDRs differs significantly. Those with loss of the proximal CDR have frequent additional cytogenetic abnormalities, a history of previous chemo-radiotherapy and a poor prognosis. Those with loss of the distal region of 5q were associated with the 5q- syndrome. 5q- syndrome constitutes a subset of patients who have isolated loss of 5q, anaemia,

thrombocytosis, a 5:1 female preponderance and a markedly better prognosis than other MDS patients. In 2008 Ebert et al. used an shRNA screen in human cord blood CD34 cells to knockdown all of the genes located in the CDR (Ebert et al, 2008) This landmark study revealed *RPS14* as the most likely gene whose loss results in the anaemia in patients with 5q- syndrome. Both prior and subsequent studies have also shown that 5q- syndrome is associated with reduced expression of many ribosomal protein genes as well as other components of the translational machinery (Pellagatti et al, 2008; Sridhar et al, 2009). Interestingly in one of these studies, investigating the most abundantly upregulated and downregulated genes in the CD34+ cells of MDS patients, found that while 5q- syndrome MDS is associated with downregulation of almost all RPs, patients with a more aggressive disease phenotype show evidence of upregulation of RPs (Sridhar et al, 2009). This supports the data of Lee et al in 2006 who performed Serial (SAGE) analysis in AMLs of various subtypes and observed that numerous ribosomal genes were the most down-regulated group of genes in the t(8;21) patients (Lee et al, 2006).

In addition to *RPS14* several other putative TSGs map to the long arm of chromosome 5. One of these is another gene nucleophosmin 1 *(NPM1)* known to be involved in ribosome biogenesis. Further details of the *NPM1* gene and its role in the development of MDS and AML are discussed in the following sections.

Legend Figure 1-4 : Proximal and distal CDRs located on chromosome 5q. The genes indicated are implicated as haploinsufficient TSGs in MDS and AML with loss of 5q.
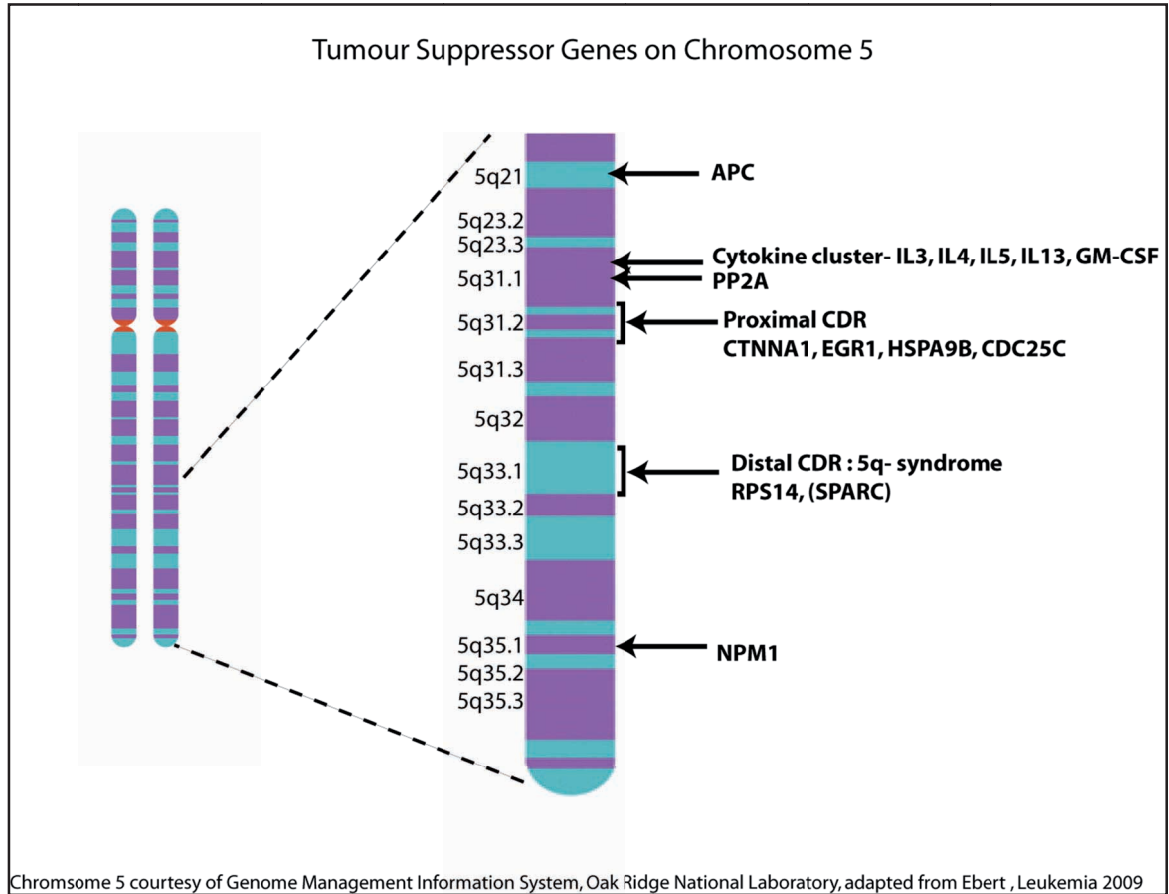
Figure 1-4 : Putative TSGs on chromosome 5

1.4.4 Ribosomes in other haematopoietic and multisystem disorders

Apart from the clear role of RP genes in DBA and MDS5q, several other genes with roles in ribosome biogenesis have been implicated in the pathogenesis of haematopoietic and multisystem disorders.

Schwachman-Bodian-Diamond syndrome (SBDS) is an autosomal recessive congenital disorder that manifests with exocrine pancreatic insufficiency, skeletal abnormalities and neutropenia. There is also an increased incidence of malignancy particularly AML. The genetic lesion causing SBDS was mapped to chromosome 7q. The identified gene which was of unknown function was named *SBDS* after the disease. As a result of gene duplication *SBDS* lies immediately adjacent to a pseudogene *SBDSP* (Boocock et al, 2003). The presence of this pseudo gene is thought to be responsible for the majority of cases arising from uniparental disomy or gene conversion. Investigation into the function of the SBDS protein has suggested a role in RNA binding and ribosome biogenesis (de Oliveira et al; Ganapathi et al, 2007; Menne et al, 2007). Also of note is a recent murine model of MDS and AML which was generated by deletion of Dicer1 in osteoprogenitors. In this non-cell autonomous model of MDS evolution SBDS was noted to be markedly downregulated and subsequent conditional depletion of SBDS from osteoprogenitors recapitulated the MDS phenotype (Raaijmakers et al, 2010). Thus the role of SBDS in the disruption of haematopoiesis may be mediated by its effect on the bone marrow niche than on haematopoietic progenitors per se.

Dyskeratosis congenita (DKC) consists of several variants which can be autosomal dominantly, recessively, X-linked or sporadically inherited (Walne & Dokal, 2009). Mutations causing the disease are found in the telomerase riboprotein complex (including the telomerase reverse transcriptase (TERT) and telomerase RNA component (TERC) genes) and patients are found to have telomere shortening. They have a number of characteristic features including skin and nail lesions, bone marrow failure and propensity to develop MDS and AML. Results from the UK registry of DKC patients suggest that 90% of DKC patients develop bone marrow failure by the age of 30 (Walne & Dokal, 2009). The X-linked form of DKC results from mutations in the *DKC1* gene. This gene is a pseudouridyl synthase which modifies ribosomal RNA during processing prior to ribosome assembly. It also associated with the telomerase complex and thus the

relative role of telomere shortening and ribosomal dysfunction remains an unresolved source of debate (Ruggero et al, 2003; Wong & Collins, 2006; Yoon et al, 2006). It is notable that a portion of these patients have the severe Hoyeraal-Hreidarsson form of DKC possibly indicating that both pathways may be exerting an effect (Ridanpaa et al, 2001).

Cartilage hair hypoplasia (CHH) is an autosomal recessive disease classically described in the Amish. Patients exhibit skeletal abnormalities, short stature, blond hair and hypoplastic anaemia. The gene mutated in CHH patients is the RNA component of ribonuclease mitochondrial RNA processing (RNase MRP) or *RMRP* (Sznajer et al, 2003). This gene has multiple functions including rRNA processing, mitochondrial DNA replication and G2 cell cycle maintenance (Liu & Ellis, 2006).

Treacher Collins syndrome is a rare congenital disorder resulting in severe craniofacial deformities as a result of excessive developmental apoptosis within neural crest cells (Dixon et al, 2006). Mutations in the TCOF gene on chromosome 5q are the causative lesion (Dixon et al, 1997; Wise et al, 1997). Treacle, the protein product of TCOF is required for transcription of ribosomal DNA in vitro. An in vivo mouse model of severe Treacher Collins syndrome revealed a deficit in ribosome biogenesis which correlated to the severity of the phenotype observed in the mice. Unlike other disorders of ribosome biogenesis, no haematopoietic abnormalities are features of this disease. However, it appears that activation of P53 may be responsible for much of the apoptosis observed in neural crest cells, which are responsible for at least a component of the clinical phenotype observed in mice since this can be rescued in a P53 deficient mouse (Jones et al, 2008).

1.5 Dead-box 18

1.5.1 Dead-box proteins

Dead-box proteins are a highly conserved family of RNA helicases that can be involved in all processes involving RNA. These include RNA export, ribosome biogenesis, RNA splicing, microRNA processing, translation and degradation. They belong to the superfamily II (SFII) of helicases/translocases. Members of this large superfamily all possess the capacity for ATP-dependent directional translocation on single or double-stranded nucleic acid, along with, in some

cases the ability to unwind nucleic acid duplexes or protein–nucleic acid complexes (Singleton et al, 2007). This family notably also includes the RecQ-like DNA helicases. Mutations in a number of RecQ-like helicases predisposes to premature aging and cancer such as Werner's and Bloom syndrome (Neveling et al, 2007). DEAD-Box proteins (in common with other helicases), consist of a highly conserved helicase core of around 300 amino acids. This includes nine conserved motifs required for the enzymatic helicase activity including the eponymous DEAD. The carboxy- and amino-termini of these proteins are diverse and presumed to confer substrate specificity. In contrast to DNA helicases (where the primary function is processive unwinding of nucleic acids) it is thought that RNA helicases are more likely to be involved in the process of unwinding short RNA-RNA duplexes or RNA-protein duplexes. Evidence for this comes from recent structural data that the helicase core of DEAD-box proteins forms 2 globular components (RecA domains) with a pocket for ATP or ADP binding (Sengoku et al, 2006). On binding of both ATP and single stranded nucleic acid a conformational change occurs resulting in a "closed" conformation whereby the two globular RecA domains come in close contact (Theissen et al, 2008). In this closed state RNA can only reside in a kinked conformation. It is suggested that this kinked conformation is indicative of an initial step in RNA unwinding (Hilbert et al, 2009) Interestingly the bending and nucleic acid binding appears to be energy neutral and the requirement for ATP is most likely to be for removal of the DEAD-box protein and subsequent recycling (Henn et al; Karow & Klostermeier, 2009).

Several DEAD-box proteins have been implicated as having a role in the pathogenesis of cancer. These include FANC M involved in the Fanconi anaemia complex in response to DNA damage (Sobeck et al, 2009). A summary of the DEAD(H)-box helicases implicated in cancer are shown in Table-1.

RNA is required for the formation of all proteins and thus the cellular processes that require DEAD-box proteins are extremely wide-ranging. These include the DNA damage response (Li et al, 2008; Sobeck et al, 2009), apoptosis (Uhlmann-Schiffler et al, 2009), microRNA processing (Fukuda et al, 2007) DNA methylation (Jost et al, 1999), and proliferation (Botlagunta et al, 2008).

Finally a DEAD-box protein has recently been successfully targeted with a therapeutic agent suggesting that these enzymes could be potential therapeutic targets in the future (Lindqvist et al, 2008).

Table 1-1 : DExH/DEAD-box proteins in cancer

Gene	Evidence for link to cancer
DDX10	Translocated with NUP98 in inv 11(p15q22)
DHX32	Down-regulated in ALL (Abdelhaleem, 2002)
DDX6	Co-amplified in MLL amplified 11q23 AML (Poppe et al, 2004)
FANC M	Fanconi protein involved in DNA damage response (Sobeck et al, 2009)
HAGE (DDX43)	Tumour associated antigen in chronic myeloid leukaemia (Adams et al, 2002)
DDX3	Capable of transforming benign breast cell line to growth factor independence (Botlagunta et al, 2008)

1.5.2 Dead-box 18

Dead-box 18 (*DDX18*) was first described as Myc-related DEAD-box 18 (MrDB) owing to the fact that it was identified as a direct target of Myc-Max heterodimers (Grandori et al, 1996). Since then, several other DEAD-box proteins (as well as many of the ribosomal protein genes and other factors involved in ribosome biogenesis) have also been identified as being direct targets of Myc. Like many members of this family of helicases, DDX18 is highly conserved from fungi to humans (Figure 1-5). Our current knowledge on DDX18 comes predominantly from its budding yeast homologue Has1p. In yeasts there are 26 DEAD-box proteins of which 13 are essential for ribosome biogenesis (Patrick Linder **www.medweb2.unige.ch/~linder/HELICASES_TEXT.html**). This includes Has1p, the yeast orthologue of DDX18. In contrast to the majority of genes involved in ribosome biogenesis, Has1p is required for assembly of both the large ribosomal subunit and the small ribosomal subunit (Bernstein et al, 2006; Emery et al, 2004; Liang & Fournier, 2006; Rocak et al, 2005). In common with other DEAD-box helicases, it appears that Has1p works early in the process of

46

ribosome assembly since it has been shown to sediment with 90S and pre-60S complexes in (Liang & Fournier, 2006). Further delineation of the function of Has1p in ribosome biogenesis shows that it is required for release of U3 snoRNPs from pre-rRNA. The U3 snoRNP is a "processing" ribonucleoprotein complex containing a snoRNA and 4 snoRNPs (Nop1p/fibrillarin, Nop58p, Nop56p, and Snu13p/15.5K). U3 snoRNPs are involved in the endonucleolytic cleavage of preribosomal RNA. The full mechanism of how this occurs has not been elucidated. However, it is known that the snoRNA component of snoRNPs interacts with target rRNA by complementary base-pairing. In the presence of mutated Has1p, U3 snoRNA is unable to dissociate from the rRNA to which it is bound. Furthermore in the same study Has1p was also shown to associated with other snoRNPs and regulate the production of U6 snRNP (Liang & Fournier, 2006). In addition to studies in yeast, a *Drosophila* homologue of *DDX18* named "pitchoune" shows a small phenotype with a defect in cell proliferation (Zaffran et al, 1998). In this study pitchoune mutants were shown to have a defect in incorporation of BRDU and demonstrated an expression pattern that resembled that of *Drosophila* myc (*dmyc*). Studies in human cancer cell lines have also shown that DDX18 is required for proliferation (Dubaele & Chène, 2007).

In keeping with its role in ribosome biogenesis DDX18 has been shown to be localised to the nucleolus (Sekiguchi et al, 2006). In this study DDX18 was identified as a binding partner of nucleolar protein NOP132 by immunoprecipitation (IP) and mass spectrometry. In the reciprocal IP and mass spectrometry of DDX18, several additional proteins involved in ribosome biogenesis were identified as binding to DDX18. Of particular note were a number of RPs, NPM1 and HSPA9B. NPM1 and HSPA9B are notable since they are both located on chromosome 5q and are putative TSGs associated with MDS. DBA-associated RPs or RPS14 were not found as binding partners in this study; however, a more recent study of the RPS19 interactome using GST-tagged RPS19 pull-down and mass spectrometry to identify binding partners did identify DDX18 as an interacting protein (Orrù et al, 2007).

Most recently, the orthologue of Has1p has been identified in *Plasmodium falciparum* (Prakash & Tuteja). These studies confirm the capacity for Has1p to bind and unwind nucleic acids and utilise both ATP and ADP. Importantly, however, this study, using mutational analysis of a truncated protein, also

determines that the N terminal portion of Has1p in addition to its helicase domain is required for its enzymatic activity.

Legend Figure 1-5 : Alignment of human, mouse, chick, xenopus, zebrafish and aspergillus amino acid sequences for DDX18. Grey shading shows identical amino acid sequence. H-human, M-mouse, C-chick, X-xenopus, Z-zebrafish, A- aspergillus. Aligned using Clustal W algorithm
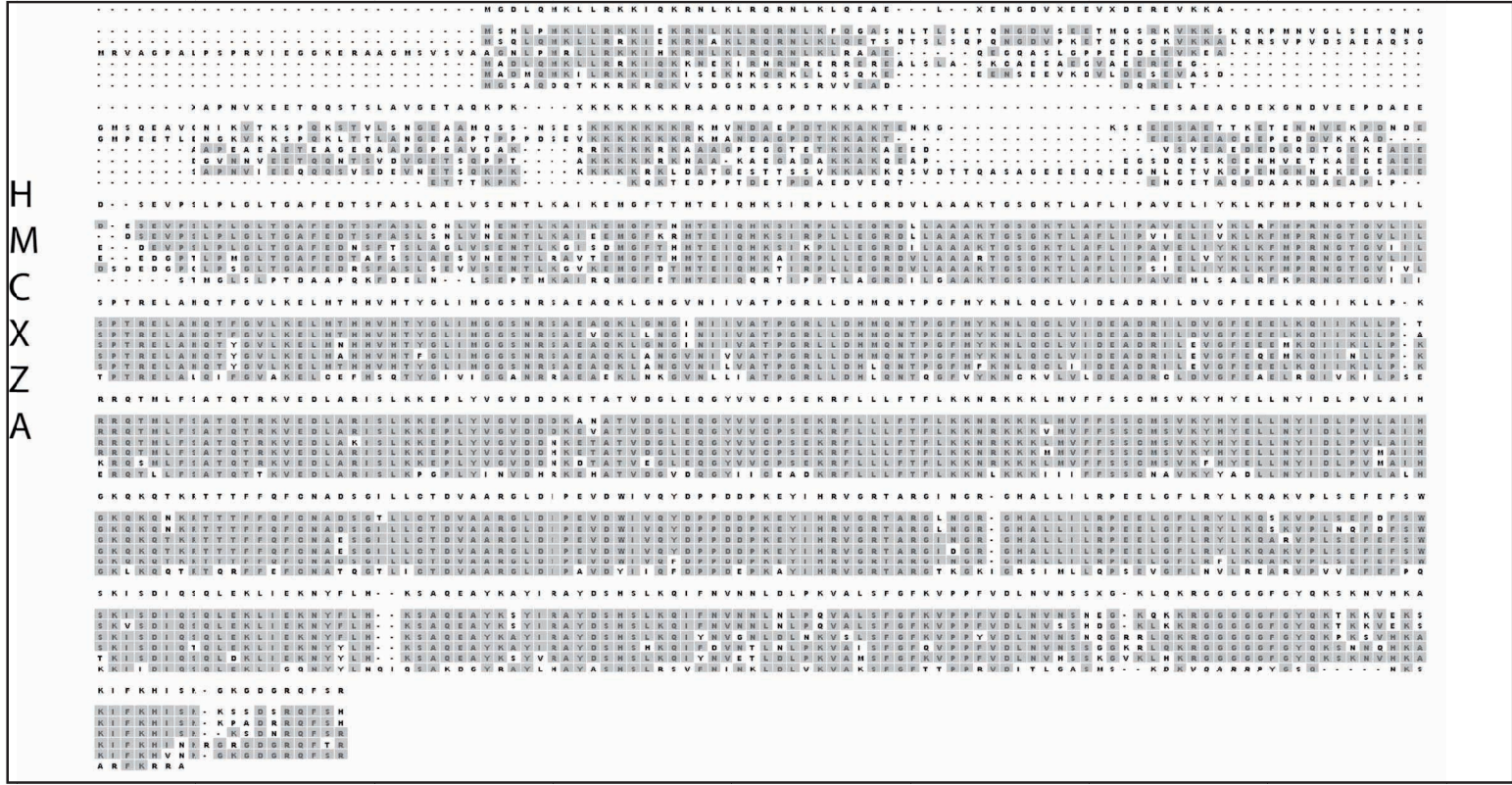
Figure 1-5 : Clustal W alignment of DDX18 orthologues

.

1.6 Nucleophosmin

1.6.1 NPM1 function

Nucleophosmin (NPM1) is a ubiquitous multifunctional phosphoprotein (Grisendi et al, 2006). It is predominantly located in the nucleolus but shuttles between nucleolus-nucleoplasm and cytoplasm. Among its functions, NPM1 is involved in ribosome biogenesis (Herrera et al, 1995; Savkur & Olson, 1998) and control of centrosome duplication (Okuda et al, 2000; Wang et al, 2005). In addition, NPM1 both positively and negatively regulates the tumour suppressors $p14^{ARF}$ (Bertwistle et al, 2004; Korgaonkar et al, 2005) and P53 (Colombo et al, 2002). It is also up-regulated by the occurrence of cellular stresses such as UV or chemically induced DNA damage (Wu & Yung, 2002).

The functional domains of NPM1 can be seen schematically in Figure 1-6. The N terminal part of the protein consists of an oligomerisation domain containing 2 nuclear export signals and a metal binding domain. NPM1 can bind itself (optimally travelling as a pentamer or hexamer) as well as hetero-dimerising or oligomerising with other proteins (Yung & Chan, 1987). The C terminal part of the protein is responsible for DNA/RNA binding and contains a nuclear localisation signal and 2 critical tryptophan residues that are essential for nucleolar localisation. A further nuclear localisation signal is found in the central part of the protein where histone binding occurs.

1.6.2 NPM1 in human haematological disease

The importance of NPM1 in human disease was first recognized when it was mapped as the binding partner of the anaplastic lymphoma kinase (*ALK*) in the t(2;5) translocation in large cell lymphoma (Morris et al, 1995; Morris et al, 1994). Notably it was initially thought that NPM1 was not involved in the development of the lymphoma but merely provided a dimerisation interface allowing autophosphorylation and therefore constitutive activation of ALK.

NPM1 has also been identified as a fusion partner in AML. In the t(5;17) promyelocytic variant of acute promyelocytic leukaemia (APML) the N terminal portion of NPM1 is fused to the retinoic receptor alpha (RARalpha) gene (Redner et al, 1996) and in the rare t(3;5) translocation found in MDS and AML, the N

terminal portion of NPM1 is fused to the myeloid leukaemia factor 1(MLF1) gene (Yoneda-Kato et al, 1996).

The histological observation was made by Brunangelo Falini that, unlike the nucleolar localisation of wild-type NPM1, when NPM1 was part of a balanced translocation, its protein expression was located in the cytoplasm (Falini et al, 2006c). This lead to the search for additional cancers that also showed cytoplasmic positivity and the discovery that NPM1 was cytoplasmic in 1/3 of all AML cases. Sequencing of the NPM1 gene in bone marrow samples from such patients did not reveal novel translocations involving NPM1 but rather revealed heterozygous mutations in exon12 (Falini et al, 2005b). The most common of these mutations (designated mutant A or mA) resulted in a 4bp internal tandem repeat sequence resulting in a frameshift which introduced 4 additional amino acids. The mechanism by which NPM1 mutations result in cytoplasmic positivity has been extensively studied and is the result of the introduction of a new nuclear export signal and the loss of one or both of the two terminal tryptophan residues that mediate nucleolar localisation (Albiero et al, 2007; Bolli et al, 2007; Falini et al, 2006b). Since NPM1 can associate with itself and the mutated NPM1 retains its N terminal oligomerisation domain, residual WT NPM1 is also exported from nucleolus to cytoplasm. Thus the name NPMc+ (for cytoplasmic +) has been given to AML cases where NPM1 is mutated (Falini et al, 2005a).

1.6.3   Animal models of NPM1

NPM1 knockout and hypomorphic murine models have been generated and show unrestricted centrosome duplication and genomic instability (Grisendi et al, 2005). $Npm1^{+/-}$ mice are viable, and show a haematological syndrome similar to human myelodysplastic syndrome (MDS), underscoring the role of NPM1 in haematopoiesis (Grisendi et al, 2005; Sportoletti et al, 2008). $Npm1^{+/-}$ mice also show increased genomic instability and exhibit greater propensity to develop haematological malignancies (Sportoletti et al, 2008). Malignant AML cells resulting from these mice maintain a WT copy of NPM1, implicating NPM1 as a haploinsufficient tumour suppressor (Sportoletti et al, 2008). The majority of these mice had complex karyotypes reflecting genomic instability. This brings into question whether NPMc+ mutations are simply an effect of haploinsufficiency; however, NPMc+ AMLs are almost exclusively of normal karyotypes in contrast to

what would be expected from the murine model implicating genomic instability in haploinsufficient tumorigenesis. Furthermore several lines of evidence suggest that the presence of cytoplasmic NPM1 results in gain of function features that contribute to leukaemogenesis. These include sequestration of the tumour suppressor p14ARF into the nucleoplasm where it is unstable and subjected to proteasomal degradation. This in turn inhibits the tumour suppressive role of P53 as demonstrated by impaired P53-dependent response to G1/S cell cycle check point (Falini et al, 2009). NPMc+ mutants have also been shown to translocate other potential regulators of oncogenesis such as NF kappa B and to stabilise Myc by dislocating its interacting protein FBW7γ into the cytoplasm. A transgenic NPMc+ expressing mouse model has also been generated which results in a relatively mild myeloproliferative phenotype (Cheng et al, 2007). This may be due to the fact that the Mrp8 promoter was used to drive expression of NPMmA in this line. Mrp8 expression occurs specifically in the myeloid and monocytes lineages therefore may be insufficient to induce leukaemogenesis if the target cell is a less differentiated progenitor or stem cell. Gene expression profiling of NPMc+ leukaemic blasts indicate an early stem cell phenotype with upregulate of HOX gene clusters suggesting that this may indeed be the case (Alcalay et al, 2005). Furthermore, detection of the mutated NPMc+ protein in this model was extremely weak as has also been observed in cell culture systems. Thus the dynamic "pull" of the mutated protein compared to the two WT alleles still present in this system may simply be insufficient to exert an oncogenic effect. Our own studies in zebrafish suggest that the HSC is indeed the cell targeted by NPMc+ and paves the way for future chemical screens to modify this effect and generate new therapeutics (Bolli and Payne et al., 2010).
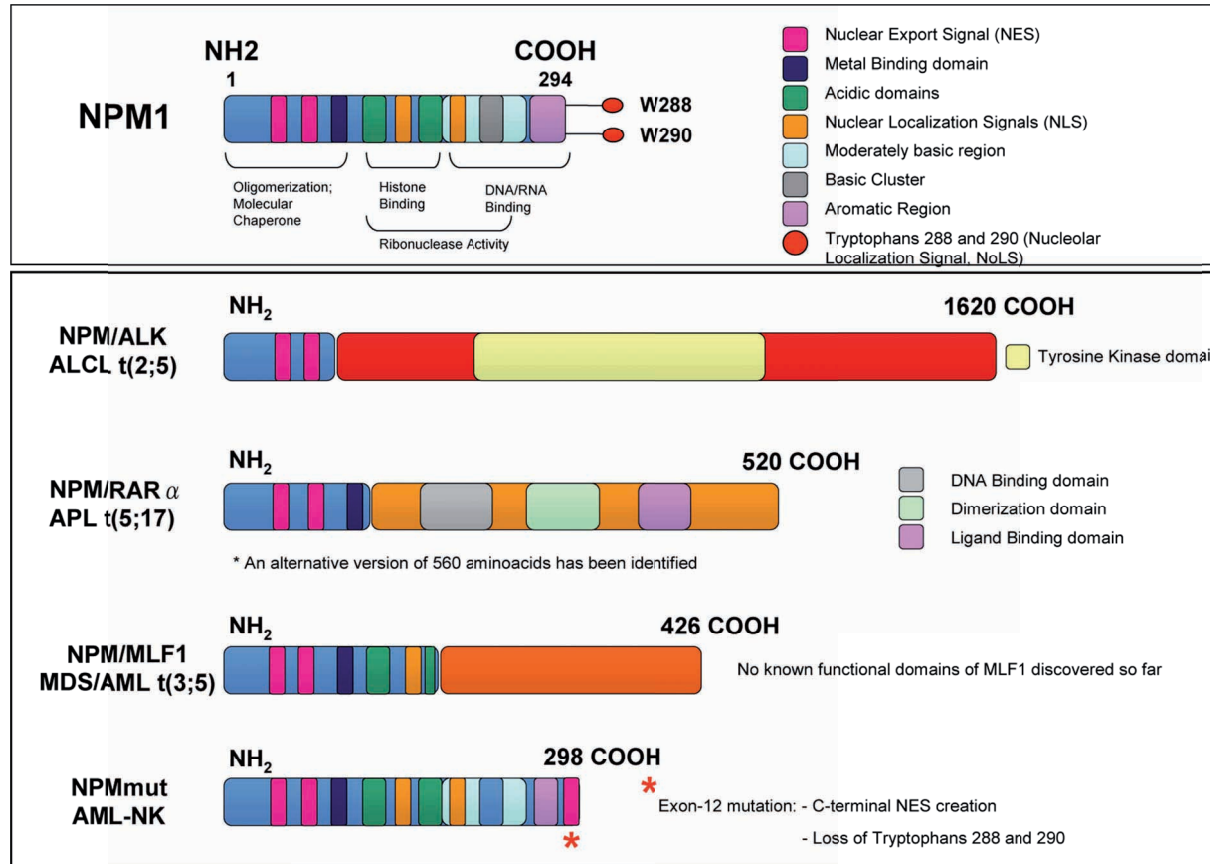
Figure 1-6 - NPM1 structure-function and human leukaemia/lymphoma

1.7   RPS14 and RPS19

Current evidence for the role of RPS14 and RPS19 in MDS and DBA respectively suggest that the effects of ribosomal protein loss are likely to be a class effect rather than gene specific. However, each of the ribosomal genes involved in human diseases discovered to date have additional non-ribosomal functions (reviewed in (Liu & Ellis, 2006), that may contribute to their role in dyserythropoiesis, oncogenesis and developmental abnormalities (in the case of DBA). Alternatively, downstream events triggered by ribosomal disruption may be primed in erythroid cells. It may be that these programmes more explicitly govern the anaemia seen in these disorders and this may explain why only 50% of DBA patients to date have an identified ribosomal protein mutation despite the fact the all ribosomal genes have now been sequenced. Many investigators have shown that the P53-MDM2 regulatory pathway is mediated by a number of ribosomal proteins (Deisenroth & Zhang, 2010; Enomoto et al, 2006; Fumagalli et al, 2009; Ofir-Rosenfeld et al, 2008; Zhu et al, 2009), but, most recently this has been observed in two murine models exhibiting anaemia and/or features of MDS (Barlow et al, 2010; McGowan et al). The mechanism by which RP mutations activate and stabilise P53 to induce apoptosis in thought to be related to an imbalance in large and small ribosomal subunits. Balance of subunit production has recently been shown to be tightly regulated in a post-transcriptional manner since protein levels of other RPs are reduced following reduction of a single RP by shRNA knockdown (Badhai et al, 2009a). Evidence for this also comes indirectly from gene expression profiles in MDS patients with 5q- syndrome (as well as others). Thus "free" ribosomal proteins, with the ability to diffuse from nucleolus to nucleoplasm following defective subunit production can bind Mdm2 and allow P53 stabilisation. This interaction of RP and MDM2 has been demonstrated in murine RPS6 deficiency and with HDM2 in human cells and appears to be predominantly mediated through RPL11 (Fumagalli et al, 2009) (Lohrum et al, 2003).

1.7.1   RPS19

Following its identification as the causative lesion in DBA, on-going studies have focused on demonstrating whether or not the ribosomal or non-ribosomal functions of RPS19 are responsible for the observed phenotype in patients. While evidence now strongly suggests that erythroid cells are sensitive to the effects of

ribosomal protein deficiency in the context of ribosomal function per se, other non-ribosomal functions for RPS19 have been identified. In particular RPS19 directly interacts with and is phosphorylated by the kinase PIM1. This suggests a potential extra-ribosomal link between erythropoietic growth factors and RPS19 (Chiocchetti et al, 2005).

1.7.2 RPS14

A single amino acid substitution has occurred in the RPS14 gene since its evolution from zebrafish to humans attesting its essential role in organismal maintenance of ribosome function. Loss of one allele of the *RPS14* gene was identified by Ebert et al. in 2008 as the most likely causative genetic lesion contributing to MDS in 5q- patients as described above. In this study it was notable that levels of RPS14 were knocked down to around 50% of normal when the phenotype was observed as was the case in patient samples. Since the publication of this work several groups have gone on to confirm that the RPS14 promoter is not methylated in continued support of the function of RPS14 as a haploinsufficient tumour suppressor (Borze et al, 2010; Valencia et al, 2008).

Further definitive evidence that *Rps14* acts as a tumour supressor was identified in 2010 by Barlow, Drynan, Hewitt, and Homes published the results of targeted conditional inactivation of the entire 5q CDR using large-scale chromosomal engineering in a mouse model (Barlow et al, 2010). The loss of a region encoding 8 genes including Rps14 resulted in the development of macrocytic anaemia with features of myelodysplasia. In additional to the RP expression profile observed in 5q- syndrome MDS, several pro-apoptotic mediators are also highly upregulated (Pellagatti et al, 2010a; Pellagatti et al, 2010b). This pro-apoptotic gene expression profile is also seen in other cases of MDS at early stages of the disease that do not have loss of 5q. Over time apoptosis is observed less frequently and escape from apoptosis is likely to represent one of the major features of progression to a more severe disease phenotype.

The long term effects of loss of P53 on the disease phenotype and progression will be informative however since mutation of P53 is commonly observed as a late event associated with poor risk disease and development of AML.

1.8 Aims of the thesis

The overall aims of the thesis are to investigate the effects of genes involved in ribosome biogenesis on the developing haematopoietic system, with a goal of providing mechanistic insight into effects ribosomal disruption has on blood development in human diseases.

1. To investigate the loss of haematopoietic cells in the $ddx18^{hi1727/hi1727}$ mutant by determining a comprehensive blood phenotype

2. To determine the effects of loss on Ddx18 on cell cycle and cell death of zebrafish haematopoietic cells

3. To determine the significance of non-synonymous sequence alterations in $DDX18$ in human AML/MDS

4. Identify and clone the zebrafish nucleophosmin orthologues

5. Investigate the consequences of loss of zebrafish nucleophosmin using transient assay

7. Determine the effects of loss of Rps19 and Rps14 to a haploinsufficient level on developing zebrafish

2. General materials and methods

2.1 Zebrafish husbandry

2.1.1 Egg collection

Male and female zebrafish were set up in pairwise or group mating chambers between 5–8pm each day. Males and females were separated with a divider. At 8am the following morning, dividers were removed and water volume decreased to provide a shallow mating area. Mating chambers allow the eggs to fall through a screen and develop apart from the breeding adults. To collect eggs the adults were transferred to fresh breeding container and eggs poured through a tea-strainer to collect. The mating chamber was rinsed in E3 egg water to ensure all the eggs had been collected. Embryos were allowed to develop in E3 egg water at 28.5°C until required or stored briefly at 19°C until needed for microinjection.

2.1.2 Dechorionation

Embryos were dechorionated between ~12–35hpf embryos where analysis before 12hpf was required were fixed in 4% paraformaldehyde (PFA) for a minimum of 4 hours at 4°C and manually dechorionated with dissecting forceps. Embryos in 100mm Petri dishes were drained of E3 egg water until there was only just sufficient water for the embryos to move in. 400 μl of stock solution (25 mg/ml in ddH$_2$O) of pronase (Roche Applied Science, Indianapolis, USA) was added to each plate and embryos gently swirled around. Embryos were then left at room temperature (RT) for 12–20 minutes (dependant on individual batches of pronase). Embryos were then removed from their chorions by gentle agitation of the plate and rinsed 5 times with egg water. To inhibit pigment development, embryos were placed in 0.003% Phenylthiourea (PTU) where required.

2.1.3 Staging

Embryos were staged according to the system described by Westerfield (Westerfield, 2000). After gastrulation, staging was done by assessing number of somites. Synchronous development at 28.5°C was assumed after staging during somitogenesis.

2.1.4 Fixation

Embryos were fixed in 4% PFA for a minimum of 4 hours. For storage for long periods, embryos were transferred through a series of increasing methanol/PBS concentrations (25, 50, 75, and 100%) and stored at –20°C for up to 6 months.

2.2 Whole mount in situ hybridisation

2.2.1 Cloning of probes

Full-length zebrafish *ddx18*, *npm1a,* and *npm1b* were amplified by a one-step reverse transcription polymerase chain reaction (PCR) (Qiagen, Valencia CA, USA) from RNA pooled from 24–30 hpf embryos. Primers for each gene were designed using Primer3 web-based software (**www.fokker.wi.mit.edu/primer3/**) to include the translation initiation ATG and stop codon to allow subsequent synthesis of RNA from the same clone. For the in vitro transcribed zebrafish *ddx18* probe only a weak signal was detected from in situ hybridisation and therefore a shorter fragment (404bp) was also cloned for subsequent in situ experiments. PCR conditions were determined following the manufacturer's instructions using Tm of 5°C below the lowest Tm of the primers and are shown in Table 2–2. Products were run on an agarose gel (0.8–1.5% depending on product size) and visualised with ethidium bromide on BioRad imager with ChemiDoc software to confirm a single PCR product. 1 μl of PCR product was then directly ligated into the pCRII vector (5 minutes at room temperature) using the TOPO kit (Invitrogen). The ligation product was then transformed into TOP10F' competent cells using heat shock at 42°C for 45 seconds and then returned onto ice. Transformed cells were recovered in 250 μl super optimal broth with catabolite (SOCS) media on a shaking incubator at 37°C for 1 hour. During this time LB agar plates containing ampicillin were coated with beta-galactosidase (X-gal) 40 μl of (40 mg/ml) and 40 μl of isopropyl β-D-1-thiogalactopyranoside (IPTG) (100 mM) to allow blue/white colony screening for ligation products containing the insert. The recovered ligation product was then spread onto the ampicillin/X-gal/IPTG plate using ColiRollers glass beads (EMD Biosciences, Novagen, Madison, WI, USA) and incubated overnight at 37°C. White colonies were then cultured in 5 ml of LB agar 100 μg/ml ampicillin overnight. Plasmid DNA was extracted from the bacterial culture using the Qiaprep spin miniprep kit (Qiagen). This was carried out by centrifuging 2x2 ml aliquots of the bacterial culture in a 2 ml eppendorf tube (sequentially in the same

58

tube) at 10,000G on an Eppendorf 5415D benchtop centrifuge for 2 minutes. The supernatant was discarded and the bacterial pellet lysed in 250 μl of buffer P1 containing RNase A. 250 μl buffer P2 was added and the tube inverted several times. Then 350 μl buffer P3 was added and the tube inverted several times. The resulting mixture was then centrifuged at 17,000G for 10 minutes. The supernatant was then carefully transferred to a Qiaprep spin column and centrifuged at 17,000G for 1 minute. The follow-through liquid was discarded and the column washed with buffer PE 700 μl for 30seconds. Finally the membrane was dried with a further 1 minutes spin. DNA was eluted from the column in 30 μl of ddH$_2$O. This plasmid DNA was digested using EcoR1 (whose restriction sites flank the TA cloning site in pCRII) and run on agarose gel to confirm the presence of an inserted segment of the expected size. Clones containing inserts of the correct size were sequenced by Genewiz (New Jersey, USA).

2.2.2 Plasmid linearisation

Plasmid DNA was linearised with the appropriate restriction enzyme and buffer (from New England Biolabs (NEB)) as shown in Table 2–1. Bovine serum albumin (BSA) was added where specified by NEB. The components of each of the NEB buffers are shown in Table 2. A 40 μl reaction was set up as detailed below

10x Buffer	4 μl
Plasmid DNA	x μl (to give at least 2 g DNA)
(BSA	4 μl)
ddH$_2$O	y μl (32–x with no BSA; 28–x with BSA)
Enzyme	4 μl
TOTAL	40 μl

Digests were carried out at room temperature overnight or at 37°C for 2–4 hours. The linearised plasmid was purified using the QIAquick PCR purification kit (Qiagen). Briefly 5 volumes (200 μl) of buffer PB was added to the digest reaction and applied to the QIAquick spin column. DNA was bound to the column by

centrifuging at 17,000G for 30 seconds. The column was washed using buffer PE 700 μl by centrifuging for 30 seconds at 17,000G. The column was then dried by a further 1 minute centrifugation spin at 17,000G and the DNA eluted in 50 μl ddH$_2$O.

Table 2-1 : In situ hybridisation probes

Probe	Enzyme for antisense probe	NEB buffer (+/- BSA)	Enzyme for antisense probe	Vector
α-E3globin	KpnI or XmaI	Xma 4+BSA	T7	pCRII
band III	BamHI	own buffer	T7	pBK-CMV
cmyb	EcoRI or SpeI	SpeI 2+BSA EcoR1-any	T7	pBK-CMV
coronin	SalI	any	T7	pBK-CMV
fli-1	EcoRI	any	T7	pBS-SK
flk-1	EcoRI	any	T7	pBS-SK
gata1	XbaI	any	T7	pBK-SK
Ikaros	BamHI	own buffer	T7	unknown
krox 20	PstI	3+BSA	T3	unknown
lmo2	EcoRI	any	T7	pBK-CMV
l-plastin	NotI	3+BSA	T7	pBS-SK
lysosyme C	BamHI	own buffer	T3	pBS-SK
mmp13	EcoRI	any	T7	pBK-CMV
mpx	SalI	3+BSA	T7	pBK-CMV
myoD	NcoI	4	Sp6	pEGEMT

nephrosin	SalI	3+BSA	T7	*pBK-CMV*
phox 47	EcoRI	any	T7	*pBK-CMV*
pu.1 (short)	StuI	2	T7	*pBK-CMV*
puma	NcoI	4	Sp6	*pGEM*
runx1	HindIII	2	T7	*pBS-SK*
scl	SalI	3+BSA	T7	*pBK-CMV*
ddx18 (short)	NotI	3+BSA	Sp6	*pCRII*
npm1a	HindIII	2	T7	*pCS2+*
npm1b	HindIII	2	T7	*pCS2+*
cmlc2	NotI	3+BSA	T7	*pCRII*
c-mpl	NotI	3+BSA	Sp6	*pCRII*

Table 2-2 : NEB buffer constituents

Buffer1	Buffer 2	Buffer 3	Buffer 4
10 mM Bis-Tris-Propane-HCl 10 mM $MgCl_2$ 1mM Dithiothreitol pH 7.0 @ 25°C	50 mM NaCl 10 mM Tris-HCl 10 mM $MgCl_2$ 1mM Dithiothreitol pH 7.9 @ 25°C	100 mM NaCl 50 mM Tris-HCl 10 mM $MgCl_2$ 1mM Dithiothreitol pH 7.9 @ 25°C	50 mM K-acetate 20 mM Tris-acetate 10mM Mg Acetate 1mM Dithiothreitol pH 7.9 @ 25°C

1 µl of the linearised plasmid was run on a 0.8% agarose gel to confirm the plasmid had been completely digested.

2.2.3 In vitro transcription of labelled RNA probe

In situ hybridisation probes were in vitro transcribed with the polymerase appropriate to the probe of interest as shown in Table 2-1. To allow secondary detection of hybridized probe nucleotides labelled with either digoxigenin or

fluorescein (Roche) were incorporated into the reaction. The 10x transcription buffer supplied with the polymerase contains (0.4 M Tris-HCl, pH 8.0 (20°C), 60mM MgCl$_2$, 100mM dithiothreitol, 20mM spermidine). The components of the reaction were assembled as shown below and incubated at 37°C for 2 hours.

Linearised plasmid DNA	1–2 µg
RNAse Inhibitor	1 µl
10x DIG RNA labelling mix	2 µl (or FITC)
10x transcription buffer	2 µl
Nuclease Free water	bring to volume of 18 µl
Polymerase (T3, T7 or SP6)	2 µl
Total	20 µl

RNA was purified using the Qiagen RNeasy mini kit and run on 1.5% agarose gel to confirm the expected product. Synthesised probes were then stored in 200µl Hyb(+) at –20°C.

2.2.4 In situ hybridisationprocedure

2.2.4.1 Permeablisation

Embryos for in situ hybridisationwere removed from storage in methanol at -20°C by washing in PBST as follows: one quick wash, 1 for 5 minutes and one further quick wash (room temperature). Embryos older than 22hpf were digested with proteinase K to permeabilise and facilitate access of the probe to all tissues during hybridisation. Proteinase K (ProK) was made as a stock solution at 10 mg/ml and stored in 1.5 ml aliquots at –20°C.

Pro K treatment was carried out depending on the age of the embryos as follows:

Less than 22 hpf	no ProK treatment
22–28 hpf	10 µg/ml for 10 minutes

28–35 hpf	10 μg/ml for 20 minutes
35–52 hpf	20 μg/ml for 20 minutes
52 hpf – 3 days	30 μg/ml for 30 minutes
3–5 dpf	100 μg/ml for 20 minutes
5–10 dpf	100 μg/ml for 30 minutes

Embryos in ProK were incubated at room temperature with very slow rocking to allow fluid to move but not the embryos. After ProK treatment embryos were washed three times in PBST three times for 5 minutes.

Following ProK treatment embryos were either: re-fixed in PFA 4% overnight at 4°C and then stored for days–months at –20°C in methanol, or transferred to Hyb(-) buffer at 65°C to commence in situ hybridisation(see next section).

2.2.4.2 Hybridisation

Hybridisation solutions were preheated to 65–70°C in a hybridisationoven. Embryos in 4% PFA or methanol were washed three times in PBST and then transferred to pre-hybridisation in 1 ml of hyb(-) for 15 minutes in 1.5 ml Eppendorf tubes with gentle rocking at 65–70°C. Hyb(-) was then removed and replaced with Hyb(+) 300 μl for a minimum of 1 hour at 65–70°C. Hyb(+) was then removed and replaced with pre-heated probe at the appropriate concentration (as determined by dose titration for each probe) diluted in preheated hyb(+). For double labelled in situs both probes were added simultaneously. The embryos were incubated in probe overnight at 65–70°C.

Wash solutions were pre-incubated to 65–70°C. The probe was removed (and stored at -20°C to be reused up to 5 times depending on the probe) and embryos washed at 65–70°C with gentle rocking in a series of washes as described below:

2x 15 minutes in 2x SSCT/50%Formamide

1x 15 minutes in 2x SSCT

2x 15 minutes in 0.2x SSCT

The embryos were then washed in maleic acid buffer with 0.1% Tween 20 (MABT) three times for 5 minutes each at room temperature.

2.2.4.3 Blocking and antibody steps

Embryos were then incubated in block (MABT with 2% in-situ blocking solution (Roche) and 10% fetal bovine serum (heat inactivated) (FBS)), at room temperature for a minimum of 1 hour. The block was removed and replaced with 700 μl of 1:5000 solution of anti-DIG FAB fragment antibody (Roche) or anti-FITC FAB fragment antibody (Roche) (depending on which hapten was incorporated into the probe). The embryos in antibody were incubated overnight at 4°C or at room temperature for 4 hours with very gentle rocking. Where two probes were used for double in situ hybridisation, the FITC probe was developed first followed by the DIG probe (after removal of the first antibody as described below).

2.2.4.4 Detection

Embryos were washed at room temp with gentle rocking in MABT for 3x 20 minutes (up to overnight for the last wash). The embryos were then equilibrated in the staining buffer by washing 3 times for 5 minutes each appropriate to the desired stain:

Buffer

Red Stain (Fast Red; Roche)	Blue Stain (NBT/BCIP; Roche)
0.1 M Tris pH8.2	0.1 M Tris pH9.5
	50 mM $MgCl_2$
	100 mM NaCl
	0.1% Tween 20

Staining reagent

1 tablet Fast Red per 2 ml buffer	4.5 μl stock (50 mg/ml) BCIP
	3.5 μl stock (50 mg/ml) NBT

For two-colour in situs the blue colour was developed first.

Once the embryos were equilibrated in staining buffer they were transferred to 12 well plates for developing. Reagents for developing were added to the appropriate buffer (above), applied to the embryos and allowed to develop in the dark at room temperature or 37°C.

The staining procedure was monitored every 30 minutes to achieve the desired level of stain. The embryos were then washed in PBST (three times for 5 minutes each) and embryos developed in blue were rinsed through a series of methanol concentrations (diluted in PBST) (25, 50, 75 and 100%). Each rinse was 10 minutes except for the final rinse which was allowed to proceed for longer; up to overnight at 4°C to ensure all background staining was removed. The embryos were then fixed in 4% PFA and transferred to 80% glycerol for imaging and storage.

2.2.4.5 Two-colour in situ hybridisation

Fluorescein isothiocyanate (FITC)-labelled probes were detected using the blue substrate first where possible. To inactivate the blue staining reaction, embryos were incubated in 1x MAB + 10 mM EDTA at 65°C for 10 minutes. Embryos were then rinsed in a methanol series as described above and then washed in MABT for 2 times for 10 minutes each at room temperature. Following this step embryos were transferred to blocking solution as in step 2.2.4.3. The second (DIG-labelled) probed was developed in Fast Red as described above in step 2.2.4.4.

2.3 Synthesis of RNA

2.3.1 Cloning and subcloning of genes

Full length cDNA coding sequences for zebrafish *ddx18*, *npm1a* and *npm1b* were cloned by PCR into pCRII TOPO vector as described in section 2.2.1. PCR primers were designed to carry unique restriction enzyme recognition sites at their 5' end (that were not repeated within the gene itself) that were located in the pCS2+ plasmid multiple cloning site after the Sp6 phage polymerase promoter and before the polyA adenylation tail signal. After verification of the correct nucleotide sequence in the pCRII vector using DNAStar Lasergene Seqman software (DNAStar Madison, WI, USA), the plasmid was digested using a double digest for the enzymes added as linkers to the primers. The product was run on a

1.5% agarose gel and the resulting band corresponding to the gene of interest was cut from the gel using a scalpel on a UV illuminated box. The DNA from the gel was purified using the QIAquick gel extraction kit (Qiagen). This procedure was identical to the procedure for QIAquick PCR purification kit but used 3 volumes of Buffer QG instead of buffer PB in order to dissolve the DNA from the gel fragment (50°C for 10 minutes). Concurrent with this the pCS2+ plasmid was also digested using the same enzymes, run on a 0.8% gel, excised with a scalpel and gel purified. In order to avoid re-ligation of the plasmid ends the resulting linearised vector was dephosphorylated with shrimp alkaline phosphatase (Roche) (1unit per 50ng vector in supplied 10x buffer). The resulting digested vector and digested insert were then assembled in a ligation reaction:

	Vector:Insert 1:1	Vector:Insert 1:3	No insert control	No ligase control
Vector	x μl (~50ng)	x μl (~50ng)	x μl (~50ng)	x μl (~50ng)
Insert	y μl **	3y μl	none	y μl **
ddH2O	to 10 μl	to 10 μl	to 10 μl	to 10 μl
10x ligation buffer*	1 μl	1 μl	1 μl	1 μl
T4 lgase (Roche)	1 μl	1 μl	1 μl	none

*Components of Roche 10x ligation buffer 660 mM Tris-HCl, 50 mM MgCl$_2$, 10 mM dithiothreitol, 10 mM ATP, pH 7.5.

** Calculation of molar equivalent based on length of insert vs. length of vector, e.g. for 4kb plasmid with 1kb insert, the amount of insert will be ¼ of the amount of plasmid (in ng) for a 1:1 molar ratio.

The ligation was carried out in a thermal cycler at 16°C for 16 hours followed by inactivation of the ligase at 65°C for 10 minutes. The ligation products were then transformed into bacterial competent cells (lab stock from DH5-alpha). This was carried out by gently adding 2 μl of the ligation product to 50 μl of competent cells and mixing by gentle flicking of the tube. This mixture was then incubated on ice

for 20 minutes followed by heat shock at 42°C for 45 seconds. The cells were then returned to ice for 2 minutes and 450 μl SOCS media added. The cells in SOCS media were recovered for 1 hour on a shaking incubator at 37°C. 100 μl of this product was then spread on ampicillin resistant plates using glass beads and incubated overnight at 37°C. If negative controls (no insert and no ligase) plates were confirmed to have no growth after 16 hours then individual colonies were picked from the ligation plates. Colonies were grown in 5 ml LB media with 100 μg/ml of ampicillin overnight at 37°C on a shaking incubator and DNA extracted using the Qiagen-prep spin mini kit as described above in section 2.2.1 The resulting DNA was digested with Bam HI and NotI to confirm the presence of the insert.

2.3.2 RNA synthesis

Full length constructs in pCS2+ were linearised using NotI as described in 2.2.1. The linearised plasmid was purified using the QIAquick PCR purification kit. Linearised plasmid was then in vitro transcribed using the Ambion mMessage mMachine Sp6 kit (Ambion, Austin, TX, USA) as follows:

Nuclease-free water	6–xμl
2x NTP/CAP	10 μl
10x reaction buffer	2 μl
linear template DNA	x μl (1 μg)
Sp6 enzyme mix	2 μl

The transcription reaction was carried out at 37°C for 2–4 hours. 0.5 μl of turbo DNase (Ambion) was then added to the reaction for 15 minutes. Resulting RNA was cleaned up using the Qiagen RNeasy mini kit (2.2.3) and the product run on a 1% agarose gel to confirm effective transcription. The RNA was quantified on a Nanodrop spectrophotometer (Thermo). RNA was stored at –80°C.

2.4 Microinjection

2.4.1 Preparation of microinjection needles

Glass capillary tubes were prepared as microinjection needles using a Flaming Brown Micropipette puller (Sutter Instruments, Novato, CA, USA). The bore of the needle was opened using dissecting forceps (Dumont no. 5) after the injection solution was applied with a microloader pipette tip (Eppendorf).

2.4.2 Preparing agarose mould

Agarose moulds for microinjection were prepared using a 1% agarose in E3 egg water. Hot agarose was allowed to cool to 45°C and then poured into a 10cm culture plate. The injection mould was applied to the plate and allowed to solidify. After removal of the mould the plate was stored with egg water inside wrapped in parafilm at 4°C.

2.4.3 Injections

Injection of zebrafish embryos was carried out using a Narishige Micromanipulator. Nitrogen pressure was turned on to a pressure of 2.7×10^6 Pa. Default injection and balance pressures were set to 6.0 and –0.1 respectively. For morpholino injections, solutions were diluted in phenol red (Sigma) to allow visualisation in the embryo. For injection of in vitro transcribed RNA, DEPC-treated water was used as the diluent. Air bubbles were expelled from microinjection needles by turning the injection time to 99ms. The optimum opening time for the injector was determined for each needle to give a droplet size equivalent to 5–10 picolitres.

2.5 Genotyping

2.5.1 Tailclips

Tupperware tubs were filled with fish water and labelled A1-A12, B1-B12 etc. to correspond to positions on a 96-well plate. A 96-well V-bottom PCR plate was placed on ice and the top left A1 well marked with a black marker pen to maintain the correct orientation. Dissection scissors and tweezers were cleaned with 70% ethanol. Individual fish were collected in a small net and held gently by the body. A small sliver of tailfin was removed with the scissors and the fish immediately placed into a plastic tub. The tailclip was then placed into the corresponding well of the 96-well plate using the tweezers. The scissors and tweezers were wiped

clean between fish. Storage of the fish was performed in plastic tubs until genotyping was complete.

2.5.2 Genomic DNA extraction

Tailclips were pushed to the bottom of each V-bottom well and any residual water removed from them. 40 μl of embryo lysis buffer (ELB) was added to each well.

2.5.3 ELB

10nM Tris pH 8.3

50nM KCl

0.3% Tween 20

0.3% NP40

The tailclips were incubated at 98ºC for 10 minutes to denature the DNA. 10 μl of proteinase K stock solution 10 mg/ml was added to each well and this mixture incubated for 16 hours at 55ºC followed by 10 minutes at 98ºC to inactivate the proteinase K. Genomic DNA was stored at 4ºC. Genotyping was carried out using PCR-based methods depending on the mutant gene and the method of mutation (point mutation or viral insertion).

2.6 PCR

2.6.1 Standard PCR reactions

PCR reactions were carried out using a standard buffer solution (10x buffer contains 100 mM Tris pH 8.3 and 500 mM KCl) supplemented with $MgCl_2$ (final concentration 2 mM) and dNTPs (final concentration 0.24 mM).

A 5x ready mixed stock solution of PCR buffer + dNTPs + $MgCl_2$ was prepared as shown below and stored at –20°C in 1.5 ml aliquots.

10x PCR buffer	600 μl
25 mM $MgCl_2$	480 μl
10 mM dNTPs	150 μl

Standard PCR reactions were set up as follows

5x Buffer+dNTPs+MgCl$_2$	5 µl
Forward primer (10 µM)	1 µl
Reverse primer (10 µM)	1 µl
Taq polymerase (NEB)	0.25 µl
Water	17.75–x
Template DNA	x µl
Total	25 µl

For multiple wells the volumes were scaled accordingly to make a mastermix-template DNA. For each experiment a no template control was run to ensure no contamination of the components had occurred. Cycling conditions were optimised for each primer pair and PCR product as detailed in individual sections.

2.6.2 Long template PCR

For longer templates (for PCR products 0.5–9kb) the Roche Expand Long Template PCR polymerase system was used (a mixture of thermostable, proofreading polymerase) as follows:

ddH$_2$O	20.1–xµl
dNTPs(10 mM)	0.9 µl
Forward primer	0.8 µl (10 µM)
Reverse primer	0.8 µl (10 µM)
10x PCR buffer	2.5 µl
Template DNA	x µl
Total	25 µl

As recommended in the product literature extension times were gradually increased by 20s for each cycle (see individual conditions).

2.6.3 One-step RT-PCR

For one-step PCR directly from RNA, the Qiagen one-step PCR kit was used. This kit uses a combination of reverse transcriptase enzymes (Omniscript Reverse Transcriptase and Sensiscript Reverse Transcriptase) along with HotStarTaq DNA Polymerase to combine reverse transcription and amplification by PCR into a single reaction. QIAGEN OneStep RT-PCR Buffer supplied with the kit was 5x concentrated.

Reactions were set up as follows:

RNase-free water	13.5–x μl
5x QIAGEN OneStep RT-PCR Buffer*	5.0 μl
dNTP Mix (containing 10 of each dNTP)	1.0 μl
Primer A	1.5 μl (10 μM)
Primer B	1.5 μl (10 μM)
QIAGEN OneStep RT-PCR Enzyme Mix	2.0 μl
RNase inhibitor (Roche)	0.5 μl
Template RNA	x μl (100–500ng)
TOTAL	25 μl

Cycling conditions were set up based on the manufacturer's instructions:

Reverse transcription : 30 min 50°C

Initial PCR activation step : 15 min 95°C (activates HotStartTaq inactivates

71

reverse transcription enzymes denatures DNA)

3-step cycling :

Denaturation: 0.5–1 min 94°C

Annealing: 0.5–1 min 50–68°C approximately 5°C below *T*m of primers,

Extension: 1 min 72°C For RT-PCR products of 1–2 kb, increase the extension time by 30–60s

Number of cycles: 25–40

Final extension: 10 min 72°C

2.7 RNA extraction

RNA was extracted where possible on days when no work with DNA (particularly plasmid DNA) was to be carried out to minimise contamination. Bench areas, pipettes and tip boxes were cleaned with 70% ethanol prior to commencing. Barrier tips certified DNase and RNase free were used for RNA extraction.

Live embryos were placed on ice in 1.5 ml Eppendorf tubes and as much egg water as possible was removed. 500 μl of Trizol reagent was applied to the embryos and then dounced with a plastic disposable pestle until all tissue was homogenised (for embryos <24 hpf vortexing for 1–2minutes was substituted here). The trizol homogenate was then left for 10 minutes at room temperature. 100 μl of chloroform was added and the mixture vortexed and allowed to stand at room temperature for 5 minutes. This was then centrifuged at 12,000G at 4°C for 15 minutes. After centrifugation the upper aqueous layer was carefully removed and placed in a fresh 1.5 ml tube (the residual sample in trizol was discarded or stored at 20°C for genomic DNA extraction if required). 1 μl of glycogen was added to the sample and vortexed briefly. 250 μl isopropanol was then added and vortexed briefly. The mixture was then left at room temperature for 10 minutes and centrifuged down at 12,000G at 4°C for 10 minutes. The supernatant was then carefully removed and the pellet washed in 500 μl 75% ethanol (freshly prepared for RNA extraction from 0% ethanol). This was centrifuged at 7500G for 5 minutes at 4°C. The ethanol was then removed and the pellet allowed to air dry. RNA was then eluted into DEPC treated water (10–50 μl depending on number of

starting embryos). RNA was then stored at –80°C.

The same procedure was used for RNA extraction from cells where the cells were centrifuged down at 300G for 3 minutes and the liquid removed prior to adding Trizol. The remainder if the procedure was identical.

2.8 Protein extraction

Embryos (20–100) were pronased and washed in cold magnesium- and calcium-free PBS (–Mg, –Ca). Embryos were then trypsinised in PBS + 0.25% trypsin + 2 mM EDTA at 32°C for 30–60 minutes depending on embryo age in 1.5 ml Eppendorf tubes. The embryos were carefully passed through a 1000 µl pipette tip once during the digestion to aid disaggregation. Once a single cell suspension was obtained the mix was centrifuged at 300G for 3 minutes and the supernatant discarded. The cells were then washed twice in PBS. All the liquid was then removed from the pellet and 100 µl of RIPA buffer (25 mM Tris•HCl pH 7.6, 150 mM NaCl, 1% NP-40, 1% sodium deoxycholate, 0.1% SDS) added directly to cells (including protease inhibitor) and pipetted up and down until no clumps remained. This was then allowed to stand for 20–30 minutes on ice. The solution was then centrifuged down at 4°C at 12,000G for 15 minutes and the supernatant removed and placed in a new tube. The protein concentration of the supernatant was determined using the DC Protein Assay Reagents Package (Bio-Rad, Hercules, CA). Samples were then stored at –80°C.

2.9 Western blotting

20 µg protein was combined with 4x denaturing Laemmli buffer, heated at 90°C for 5 minutes. Samples were loaded onto precast 4–12% NuPAGE Novex Bis-Tris Mini Gels (Invitrogen) and separated in Tris-glycine-SDS buffer. Samples were run at 20–25 milliamps (mA) for 20 minutes until the tracer dye was past the stacking gel, the current was then increased to 60mA. Once the tracer dye reached the bottom of the gel the current was removed. To transfer to a nitrocellulose membrane (Thermo Fisher Scientific, Pittsburgh, PA), the gel was excised, and placed in a "sandwich" as shown in Figure 2–1 below. The corner of the gel and membrane were notched in order to maintain the orientation of the gel. The sandwich was enclosed between 2 glass plates within the transfer apparatus in transfer buffer (Bio-Rad, Hercules, CA) (1x transfer buffer consisted

of 2.5 mM Tris, 19.2 mM Glycine, pH8.2 in 20% methanol). Transfer was run at 500mA for 1 hour with the apparatus sitting in an ice bath.
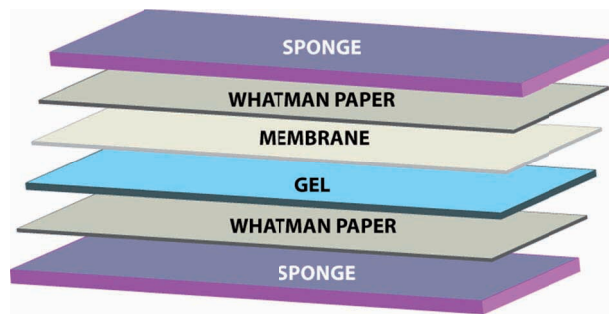
Figure 2-1 Western blot transfer "sandwich"

Legend Figure 2-1: Cartoon of Western blot transfer sandwich. The layered components are then sandwiched between 2 glass plates within the transfer apparatus.

The membrane was washed 1 x 10 minutes and 3 x 5 minutes in Tris buffered saline with Tween (0.1%) (TBST) and rinsed in Ponceau red to confirm the presence of protein. The membrane was then blocked with 5% milk powder in TBST and probed with primary antibody overnight at 4°C. Membranes were then washed in TBST and probed with anti-rabbit, or anti-mouse-horse radish peroxidase (HRP)-coupled secondary antibodies; 1:5000 (GE Life Science, Piscataway, NJ) for 1 hour. After washing in TBST proteins were detected by ECL (Pierce-Thermo Fisher Scientific).

2.10 Morpholino design and validation

Morpholinos were designed by Genetools LLC to target 5' UTRs or splice donor sites of the desired gene. Morpholino sequences are shown in Appendix 1. Specificity of morpholinos for their target was determined by obtaining the same phenotype with two morpholinos and by confirmation of knockdown of the RNA/protein of interest was confirmed where possible in one of the following ways.

2.10.1 Validation of a cross-reacting antibody

Since few zebrafish antibodies are available commercially available human and murine antibodies were screened to determine whether the epitopes used to generate these antibodies were conserved with zebrafish. Polyclonal antibodies were favoured over monoclonals based on the assumption that more than one

amino acid sequence could potentially be targeted by the antibody. To ascertain whether a given antibody could detect endogenous zebrafish proteins, morpholino knockdown and RNA overexpression of the gene of interest was performed, as shown below, and protein extracted from a minimum of 30 embryos per condition. As controls, human cells known to express the gene of interest and forced RNA expression of the human RNA were also used to confirm antibody function (assuming the antibody was raised to a human protein or peptide):

1. human cells known to express protein of interest

2. morpholino knockdown 1 mM

3. morpholino knockdown 500 mM

4. morpholino knockdown 100 mM

5. uninjected control

6. 100 pg in vitro transcribed RNA

7. RNA forced expression at maximum concentration of in vitro transcribed RNA (usually 400 pg)

8. human RNA overexpression in zebrafish embryos

Protein was extracted as described in section 2.8 and Western blot carried out using 2 dilutions of the primary antibody (depending on the manufacturers recommended dilution initial studies were carried out at the lowest and highest recommended concentrations) Antibodies were confirmed as cross-reactive when over-expression resulted in an increase in the observed band and knockdown resulted in a loss of observed band size, as illustrated in Figure 2–2
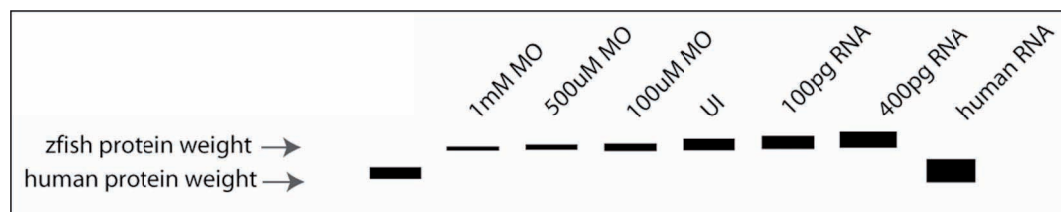
Figure 2-2 : Cartoon showing Western blot of cross-reactive antibody

Legend Figure 2-2: Scheme of Western blotting optimisation for zebrafish proteins cross-reacting with a human antibody. Knockdown and overexpression of the gene using MO and RNA respectively for the desired gene identify whether there is a band of the predicted molecular weight (or other) that represents the zebrafish isoform.

While the utility of having a cross-reactive antibody was greatest for 5'UTR morpholinos (where morpholino function could not be assessed by the method described below), where possible a known functional splice site morpholino was used to initially test the antibody.

2.10.2 Validation of knockdown with splice-site morpholinos

Using splice-site morpholinos has the advantage over 5'UTR morpholinos in that when the morpholino effectively disrupts normal splicing, the alternate splice products can usually be detected and a concurrent reduction in the WT correctly spliced product can always be detected. Detection of aberrant splice products was undertaken by injecting a range of concentrations of morpholino. For each dose 1–20 embryos were pooled for RNA extraction in trizol (see above). Following RNA extraction one-step PCR was carried out using primers that covered the full coding region of the gene. Aberrant splice products were visible as PCR products of different sizes to the wild-type band seen in the control injected embryos when run on an agarose gel. All the PCR bands were cut from the gel using a razor blade and DNA extracted using the QIAquick gel extraction kit as described in 2.3.1. The gel extracted fragment was cloned into the pCRII topo vector and each product sent for sequencing to confirm that the alternate spliced products introduced a premature stop codon.

2.11 Flow cytometry

2.11.1 Embryo dissociation

Embryos (20–100) were pronased and washed in cold PBS without magnesium or calcium. Embryos were then digested in a 1 in 200 dilution of liberase blendzyme III in PBS (–Mg, –Ca) at 32°C for 30–60 minutes depending on embryo age in 1.5 ml Eppendorf tubes. The embryos were carefully passed through a 1000 µl pipette tip once during the digestion to aid disaggregation. Once a single cell suspension was obtained the mix was centrifuged at 300G for 3 minutes and the supernatant discarded. The cells were then washed x2 in PBS.

Cells were filtered through a 40μm mesh filter and the final wash was resuspended in PBS + 5% FBS + heparin 1 unit/ml

2.11.2 Propidium iodide staining for cell cycle analysis

Dissociated embryos were prepared as described above. After the last wash cells were fixed in 1 ml 70% ice-cold ethanol for 1 hour on ice. Cells were then centrifuged down at 300G and washed twice in PBS. Cells were then resuspended in 500 μl (per 100 embryos) of PBS + propidium iodide 50 μg/ml + RNase A 50 μg/ml for 15 minutes at room temperature in the dark. Cells were analysed for DNA content using the FL2 area parameter on a FACS Caliber or FACS Canto flow cytometers (Becton Dickinson).

2.11.3 Analysis of transgenic lines and flow sorting

Zebrafish carrying the transgene of interest were set up with the necessary controls as in the following example

1. CONDITION

male (promoter-GFP) x female (promoter-dsRED) – progeny rfp/gfp

2. GFP control

male of female (promoter-GFP) x wild-type

3. RFP control

male of female (promoter-dsRED) x wild-type

4. No fluorochrome control

wild-type cross

At the necessary time point embryos were dissociated as described above. Flow cytometric sorting was carried out on FACSAria or MoFLO cell sorters. Assisted set-up of flow cytometry parameters included doublet discrimination to exclude coincident events and compensation of between channels to minimise spectral overlap between fluorochromes. Cells were collected into PBS with 3% FBS and 1U/ml heparin (when thrombocytes were contained within cell populations being collected). Collected cells were centrifuged at low speed (400G) and the

supernatant removed. Subsequent use of the cells depended on the downstream application (RNA extraction, cytospin, cell cycle analysis, TUNEL).

3. Ddx18 loss and abnormal haematopoiesis

3.1 Introduction

3.1.1 Rationale for forward genetic screens to define genes required for blood development

Early screens performed using zebrafish were initially designed to identify genes essential for early vertebrate development. In addition, systematic study of the transparent embryos demonstrated the potential of this model for the identification of mutants deficient in embryonic red blood cell production (Ransom et al, 1996). The study of erythroid development formed part of the developmental screens as erythroid cells can easily be visualised with the naked eye, even prior to the onset of circulation. Other screens have provided more focused examination of embryonic blood development by using simple benzidine derivatives such as *O*-dianisidine which can be used to detect haemoglobin in live zebrafish by virtue of their conversion of it to an oxidised red precipitate in the presence of haemoglobin. Screens to determine abnormalities in other components of the developing haematopoietic system require more labour intensive techniques such as in situ hybridisation. In situ hybridisation screens have been carried out to determine mutants with defective HSC production (using cmyb ISH) as well as those with abnormalities in primitive myelopoiesis using *pu.1* and *runx1* ISH during somitogenesis (Hogan et al, 2006; Horsfield et al, 2007). The primary goal for all of these screens has been to determine genes required for developmental haematopoiesis.

3.1.2 Rationale for doing a new screen

While several screens have used markers of primitive myelopoiesis to determine developmental genes involved in this process screens assessing the production of mature myeloid cells had not been performed. Several oncogenes or tumour suppressors known to play a role in the pathogenesis of human leukaemias have been shown to disrupt haematopoiesis during murine development (Anderson et al, 1998; McKercher et al, 1996; Robb et al, 1995; Scott et al, 1994; Zhang et al, 1997). Therefore it was reasoned that by using a forward genetic screen which identified zebrafish mutants with abnormal numbers of myeloid cells not only would novel genes involved in myelopoiesis be identified but potentially genes that could function as oncogenes or tumour suppressors relevant to human leukaemias.

3.1.3 Methods of screening

With the above hypothesis in mind a forward genetic screen to identify zebrafish mutants with abnormal numbers of myeloid cells was designed. The screen was carried out in two components.

3.1.3.1 An early pressure screen of ENU mutants generated in the Look laboratory

Early pressure (EP) screening takes advantage of the fact that eggs squeezed from the female can be "pseudo-fertilised" with UV inactivated sperm from males. The females are then literally put under pressure using a French press resulting in duplication of the female chromosome (and therefore homozygosing any mutations). Since males and females carrying the *same* mutations are not required for breeding, this method has the advantage of cutting out an entire generation, saving significantly on time and space for breeding and growing fish. Zebrafish embryos derived from EP were analysed using ISH for the myeloid-specific gene *mpx* at 2 dpf and 4.5 dpf. 28 potential mutants (putants) were identified in this screen for further study.

3.1.3.2 Viral insertional screen

A library of 276 insertionally mutated lines (identified as recessive genes essential for embryonic development) was generated in the laboratory of Dr Nancy Hopkins laboratory at MIT (Amsterdam et al, 2004a; Golling et al, 2002). Collaboration with the Hopkins laboratory was established to screen this library for recessive mutations that effected myeloid blood development. The major advantage of the viral insertional screen is that since the sequence of the virus is known, identifying the gene disrupted is relatively straight forward and since the library had been previously annotated, all the genes disrupted in each of the lines was already known. The viral insertional screen, performed by Dr Jennifer Rhodes in Dr Look's laboratory identified 14 zebrafish lines with quantitatively abnormal myelopoiesis (either increased or decreased *mpx* expression) (Rhodes et al, 2009). A scheme for this viral insertional screen design is shown in Figure 3-1.

Legend Figure 3-1: Scheme of the genetic screen to identify mutant zebrafish with aberrant developmental myelopoiesis.
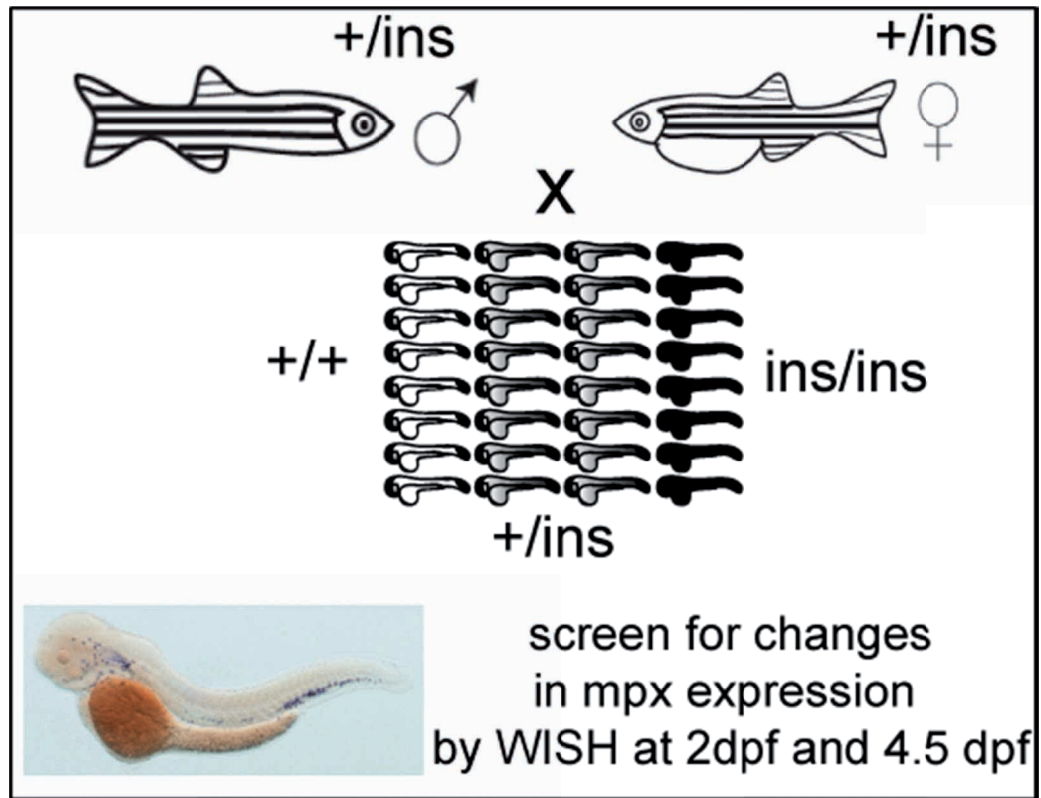
Figure 3-1 : Scheme of forward genetic screen to identify novel genes involved in myelopoiesis

3.1.4 Prioritisation of mutants identified in the new screen

Mutants identified from the viral insertional screen were prioritised for further study rather than ENU mutants. This is both because of the technical challenges associated with the EP screen and because the genes disrupted in the viral insertional screen were already identified (thus eliminating the necessity for time-consuming positional cloning). EP screens are confounded by several factors. The first is that, depending on how close to the telomere the mutation occurs, the likelihood of homozygosing varies, so that anywhere from 20–100% of the clutch may be affected. This is because more telomeric lesions are likely to undergo crossing over at meiosis I and therefore exhibit a heterozygous phenotype whereas mutations closer to the centromere are less likely to undergo crossing over and thus are homozygosed (Cheng et al, 1997; Streisinger, 1984). Secondly, squeezing of females can result in death or damage to the founder fish or difficulty in subsequent breeding. Thirdly, confirmation of the observed phenotypes requires an entire generation of fish. Fourthly, as the screened fish have only undergone a single outcross from the F0 mutagenised male, they are more likely to carry several mutations potentially resulting in a compound effect. Finally, mapping of the affected gene is dependent at least in part on the sequenced coverage of the genome in the affected region and the degree of polymorphism in that region between the two mutated and mapping strain. Overall the viral insertional mutants, despite potential confounding variables presented a better and clearer route of study.

3.1.4.1 Choice of $ddx18^{hi1727/hi1727}$ for further study

Prioritisation of genes within the pool of 14 mutants identified was made on several factors:

1. known functions of the mutated genes pertinent to the development of cancer (e.g. cell cycle regulation, control of apoptosis)

2. location of the human orthologue within a region known to be associated with recurrent cytogenetic abnormalities

3. degree of aberrant phenotype observed

The $ddx18^{hi1727}$ allele carries a viral insertion within the first intron of the Myc-associated DEAD-box 18 gene ($ddx18$). It was prioritised for further study based

on it having one of the most marked reductions in the number of myeloid cells. In humans, *DDX18* is located on 2q14.1, a region not previously identified for recurrent cytogenetic abnormalities in human leukaemia. *DDX18* was included in a focal constitutional region of UPD identified in a pair of twins that developed ALL arising from the same clone carrying t(12;21). At the time, Ddx18 was given priority for further study, the role of ribosome biogenesis in the pathogenesis of DBA and other haematopoietic disorders was only just becoming fully realised, thus the *ddx18* mutant apparently represented a totally novel mechanism of impaired myelopoiesis.

3.2   Aims of the experiments described in this chapter

1. To clarify by rescreening the reduction in myeloid cells observed in *ddx18^{hi1727}* mutants

2. To determine the endogenous expression pattern of *ddx18* in WT zebrafish

3. To determine the haematopoietic phenotype in *ddx18$^{hi1727/hi1727}$* mutants

4. To determine whether the phenotype of *ddx18$^{hi1727/hi1727}$* mutants is specific haematopoietic cells

5. To use morpholino knockdown to confirm that loss of Ddx18 is responsible for the observed haematopoietic phenotype

3.3 Methods

3.3.1 Screen design

The screen was undertaken by Dr Jennifer Rhodes using RNA in situ hybridisation for the pan-granulocyte peroxidase, myeloid peroxidase (*mpx*). 276 viral insertionally mutated lines were analysed at 2dpf and 4.5dpf for deficient or abnormal expression of *mpx*. Since the mutations are embryonic lethal this was a recessive screen where clutches of embryos derived from crossing heterozygous adults together resulted in a phenotype observed in 25% of the embryos. Several novel genes that have not previously been associated with myelopoiesis were identified (Dodd et al, 2009; Mathias et al, 2007). A cartoon of the screen design is shown above in Figure 3-1. I performed all the subsequent experiments and analysis related to the *ddx18*$^{hi1727/hi1727}$ mutant.

3.3.2 PCR genotyping for *ddx18* WT and *ddx18*^{hi1727} mutant alleles

Genotyping of adult zebrafish to identify *ddx18*$^{hi1727/+}$ heterozygotes was performed using a viral primer and a DNA primer in the first exon of the *ddx18* gene as shown in Figure 3-2. This method is sufficient to detect heterozygotes since no homozygous animals survive to adulthood. In embryos, to distinguish between heterozygous and homozygous animals (both show a product from PCR with the above primer pair) an additional primer 3' to the viral primer was used. A PCR reaction with all 3 primers; viral primer (designated nltr3), 5' *ddx18* primer (*ddx18*-forward) and 3' *ddx18* genomic primer (*ddx18*-WT reverse) gave two PCR products. The first is a viral/5' *ddx18* band in the presence of a mutant allele. The second is a 5' *ddx18*/3' *ddx18* band, when a wild-type allele is present. This is shown in Figure 3-2. This complexed PCR allowed distinction of WT/heterozygous and homozygous mutants in a single reaction.

3.3.3 Subcloning of human *DDX18* into pCS2+

The full length cDNA for human *DDX18* was purchased from Open Biosystems. The clone was supplied in the pCMV-SPORT6 expression vector. After confirmation of the correct sequence in pCMV-SPORT6, the *DDX18* fragment was excised by restriction enzyme digest with EcoRI and XbaI. The pCS2+ vector was digested with the same enzymes and both products run on 0.8% agarose gel, excised with a razor blade and gel-purified using the Qiagen kit. Overnight ligation at 16°C was carried out (Chapter 2) using 1:1 and 1:3 vector: insert molar

ratios. Transformed ligation products were incubated overnight at 37°C and 6 colonies grown in 5 ml LB broth with 100 μg/ml of ampicillin added. Plasmid DNA extracted from the 6 preps was digested to confirm the insert and sequences of 6 individual clones analysed using Seqman software (DNASTAR Inc., WI, USA). RNA synthesis was carried out as described in Chapter 2.3.2.

3.3.4 Statistical analysis

An unpaired two-tailed student's t test was used to determine whether or not the reduction of haematopoietic cells observed in $ddx18^{hi1727/hi1727}$ mutants was statistically significant. A p value of 0.05 was used to reject the null hypothesis. The F test was used to compare variance between data sets and Welch's correction was used whenever datasets under comparison had significantly different variances. For each condition a minimum of 10 embryos were assessed. Analysis was performed using GraphPad Prism Version IV Software.

Legend Figure 3-2: Upper panel shows a cartoon depicting the coding exons of *ddx18* and schematic location of the viral insertion within the first intron. The lower panel shows the scheme for genotyping embryos to determine all three possible genotypes (homozygous WT, heterozygote, or homozygous *ddx18*^{hi1727/hi1727})

Figure 3-2 : Scheme of genotyping to identify $ddx18^{hi1727/hi1727}$, WT/ heterozygous and homozygous embryos

3.4 Results

3.4.1 Confirmation of screen result

Zebrafish embryos homozygous for *ddx18*^{hi1727} were identified in the primary screen as having reduced numbers of myeloid cells at 4.5 dpf. To confirm this result, during rescreening expression of *mpx* was assessed from 27 hpf until 4 dpf. *ddx18*^{hi1727/hi1727} mutants were found to have reduced numbers of *mpx*+ myeloid cells from 27 hpf and also showed reduced *slc4a1* (*band3*), a marker of erythroid cells from this time point onwards (Figure 3-3). A reduction in myeloid cells in zebrafish embryos homozygous for *ddx18*^{hi1727} was also seen using the marker *l-plastin* which may mark an overlapping but distinct population of monocytic cells. (Le Guyader et al, 2008; Herbomel et al.,1999)

Numbers of *mpx*+ myeloid cells, *slc4a1*+ erythroid cells and *l-plastin*+ monocytoid cells per embryo in zebrafish embryos homozygous for *ddx18*^{hi1727} was statistically significantly lower than numbers of corresponding cells in WT siblings (Figure 3-4).

These results indicate that at least two haematopoietic cell lineages are reduced in *ddx18*^{hi1727/hi1727} zebrafish embryos at 27 hpf. This time point corresponds to the latter stages of primitive zebrafish haematopoiesis. Some definitive haematopoietic cells have begun to emerge by this time point including the transient erythro-myeloid population (see Figure 1-1) (Bertrand et al, 2008) and some HSCs (Jin et al, 2007; Warga et al, 2009b); however, the majority of cells remain of primitive origin.
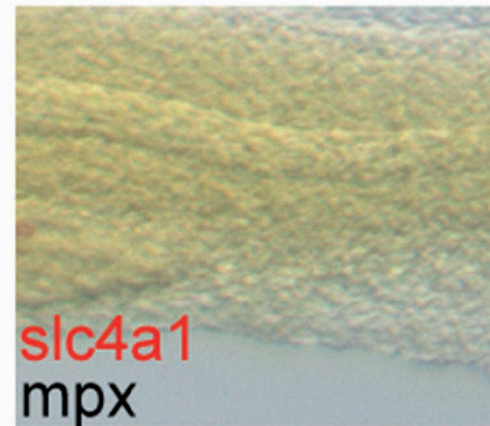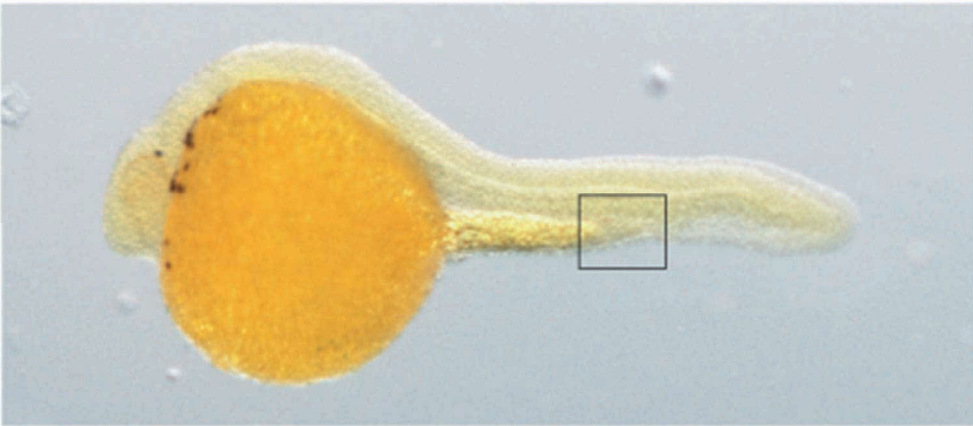
Figure 3-3 : Loss of Ddx18 in *ddx18*^{hi1727/hi1727} mutants leads to loss of erythroid and myeloid cells
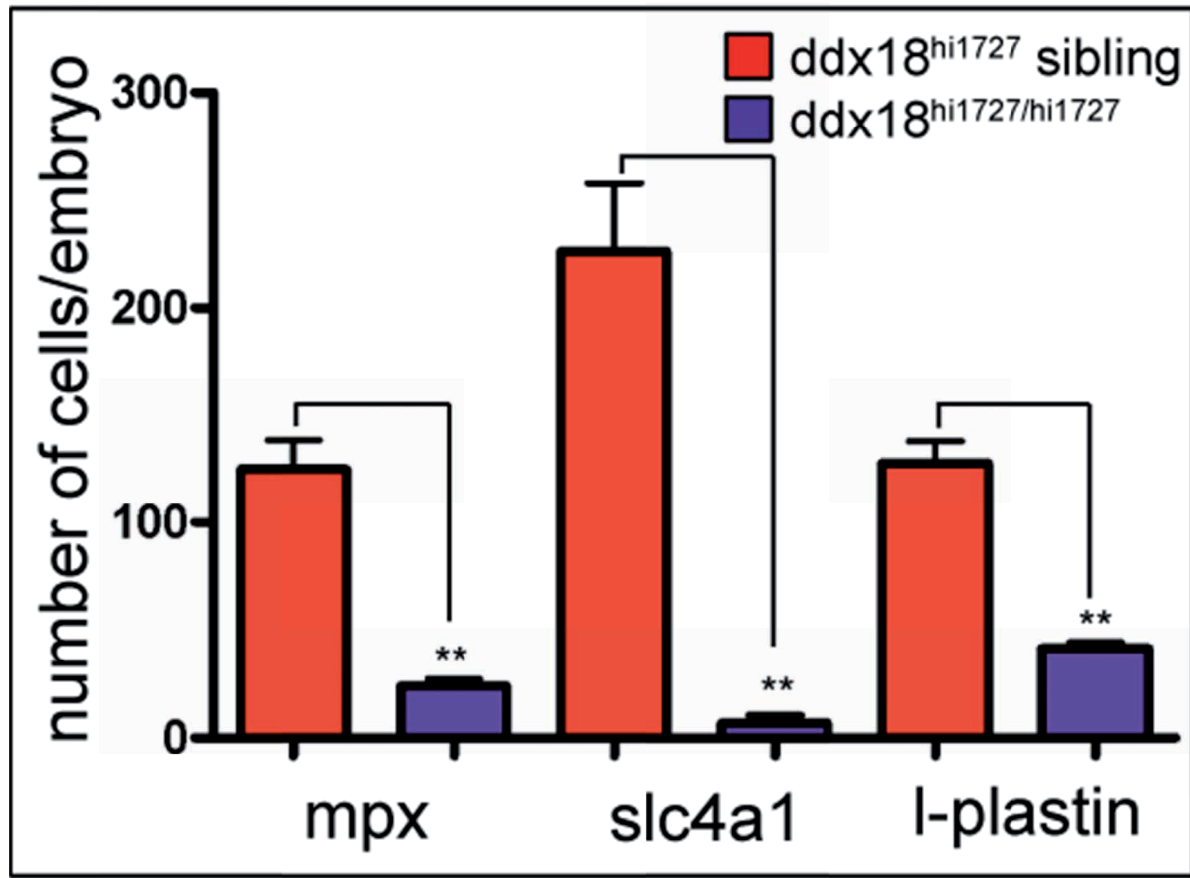
Figure 3-4 : Quantification of *mpx+* (myeloid), erythroid (*slc4a1+*) and monocytoid (l-*plastin+*) cell numbers in WT/sib (red) and *ddx18*[hi1727/hi1727] (blue) mutants

Legend Figure 3-3: WISH for *scl4a1 (band3)* (red) and *mpx* (black) showing *ddx18*^{hi1727/hi1727} mutants below and siblings above. Embryos are 27hpf and were staged using somite number. Embryos are oriented with dorsal towards the top of the page and head to the left. Close-up views on the right are indicated by the grey box, highlighting the posterior blood island.

Legend Figure 3-4: Quantification of *mpx+* (myeloid), erythroid (*slc4a1+*) and monocytoid (*l-plastin+*) cell numbers in 48 hpf embryos. Columns represent mean numbers of cells per embryo, Error bars show standard error of the mean. **p<0.01 (two-tailed unpaired students t test). Data is aggregate of 10 embryos per condition assessed.

ddx18$^{hi1727/hi1727}$ mutants were easily identified macroscopically as they also showed developmental defects visible from around 16–18 hpf. These included a small head with cerebral oedema and later, brain necrosis, a foreshortened yolk extension and small size (live images shown in Figure 3-5). In addition, from 24 hpf there was a reduction in developing red blood cells visible to the naked eye in the posterior ICM (yellow arrows Figure 3-5) and this was even more apparent at 48 hpf when red blood cells could be seen in the heart and over the yolk extension in the WT/siblings but not in the mutant animals (red arrow Figure 3-5) At 24 hpf I was able to correctly identify all *ddx18*$^{hi1727/hi1727}$ mutants from their WT or heterozygous siblings as determined by genotyping for WT and mutant alleles.

Legend Figure 3-5 : Brightfield images of *ddx18*^{hi1727/hi1727} mutants and siblings using Nomarski optics. The left panels show embryos at 24 hpf. Mutants could be distinguished from their siblings by their small heads, shortened and narrowed yolk extension, cerebral oedema and necrosis. Yellow arrowheads denote erythroid cells in the posterior blood island where mutants showed a reduction in the number of erythroid cells developing. Right panels show *ddx18*^{hi1727/hi1727} mutants and siblings at 52 hpf. Red arrow shows absence of red circulating blood in the ducts of Cuvier over the yolk extension in *ddx18*^{hi1727/hi1727} mutants.
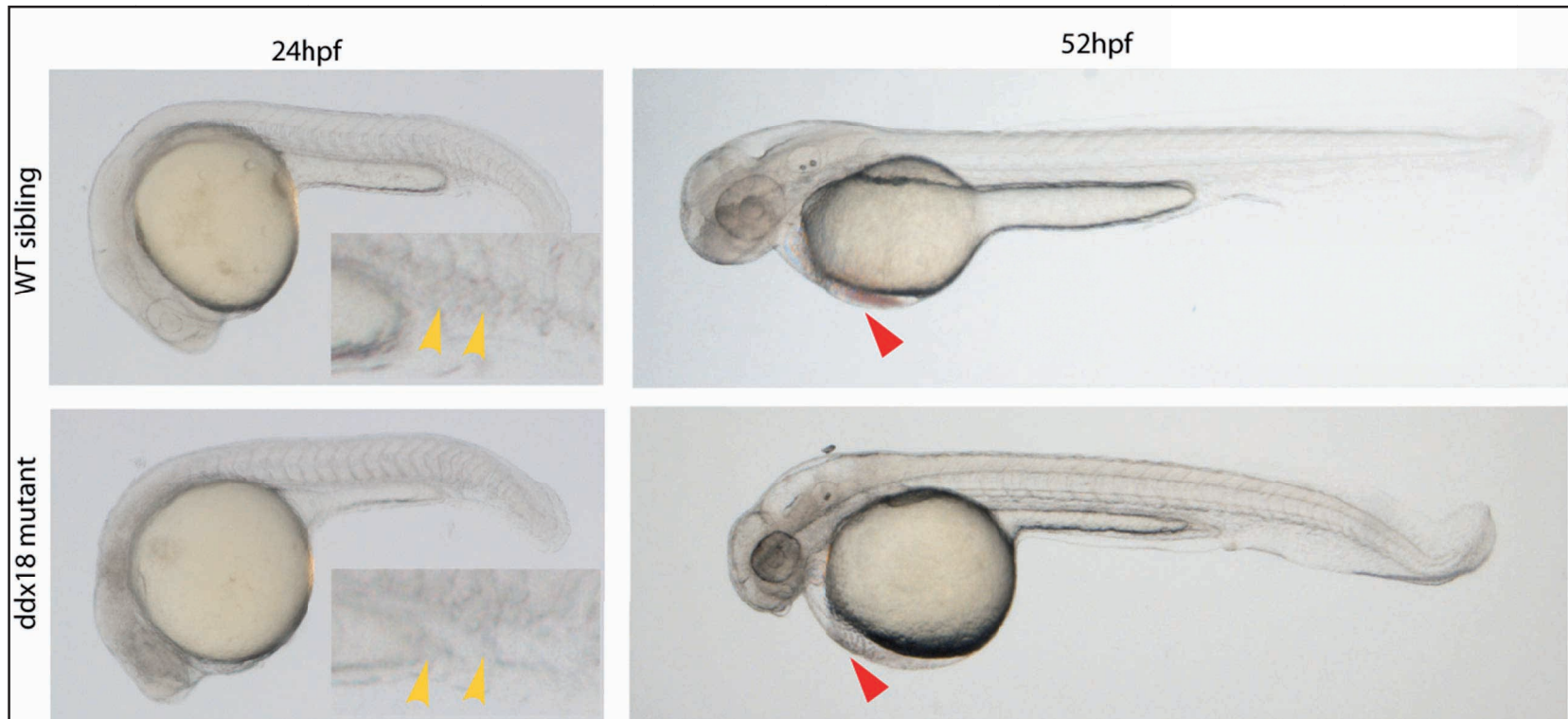
Figure 3-5 : Brightfield images of *ddx18*^{hi1727/hi1727} embryos shows reduced numbers of red blood cells

3.4.2 Expression pattern of endogenous *ddx18* in WT animals

To determine the endogenous expression pattern of *ddx18* in zebrafish, a digoxigenin labelled *ddx18* probe for RNA in situ hybridisation was synthesised. The initial probe was generated from the full length coding sequence that was cloned for the purposes of rescue experiments. This probe was 2167bp in length and resulted in a very weak signal in whole mount in situ hybridisation experiments. Therefore a smaller fragment containing only 404bp of the zebrafish *ddx18* gene was designed. This probe yielded a more distinct signal and notably *ddx18*$^{hi1727/hi1727}$ mutants showed very little expression of the *ddx18* transcript using this probe. Expression of *ddx18* was seen in one-cell stage WT embryos indicating transfer of maternal RNA. By 12 somites more distinct expression was seen in the developing brain and eye of WT animals (Figure 3-6 A [flat mount] and B). By 24 hpf this pattern of expression continued and was more pronounced. *ddx18* was also strongly expressed in the posterior blood island and ICM shown in Figure 3-6 C and D (marked with the yellow arrow). At 40 and 48 hpf individual cells showed expression in the region of the dorsal aorta (yellow arrows Figure 3-6 E) and caudal haematopoietic tissue (yellow arrows Figure 3-6 F). At 48 hpf expression was observed in presumed circulating blood cells appearing over the yolk in the ducts of Cuvier (Figure 3–6 G and yellow arrow Figure 3-6 H) and heart (red arrow Figure 3-6 H).

Legend Figure 3-6: Developmental expression of *ddx18* in WT zebrafish using in situ hybridisation. A and B – expression pattern at 12 somites is ubiquitous, with more focal expression seen in the developing somites, brain and eye. C and D – expression at 24 hpf begins to show clear expression in developing blood in the posterior blood island (yellow arrows) E and F – expression at 40 hpf is in the head, brain and individual cells along the blood vessels, where definitive HSCs are located (yellow arrowheads). G and H – at 48 hpf expression can be seen in erythroid cells over the yolk (yellow arrowhead) and in the heart (red arrow). Cardiac expression is notable since cardiac abnormalities are observed in *ddx18*$^{hi1727/hi1727}$ mutants.
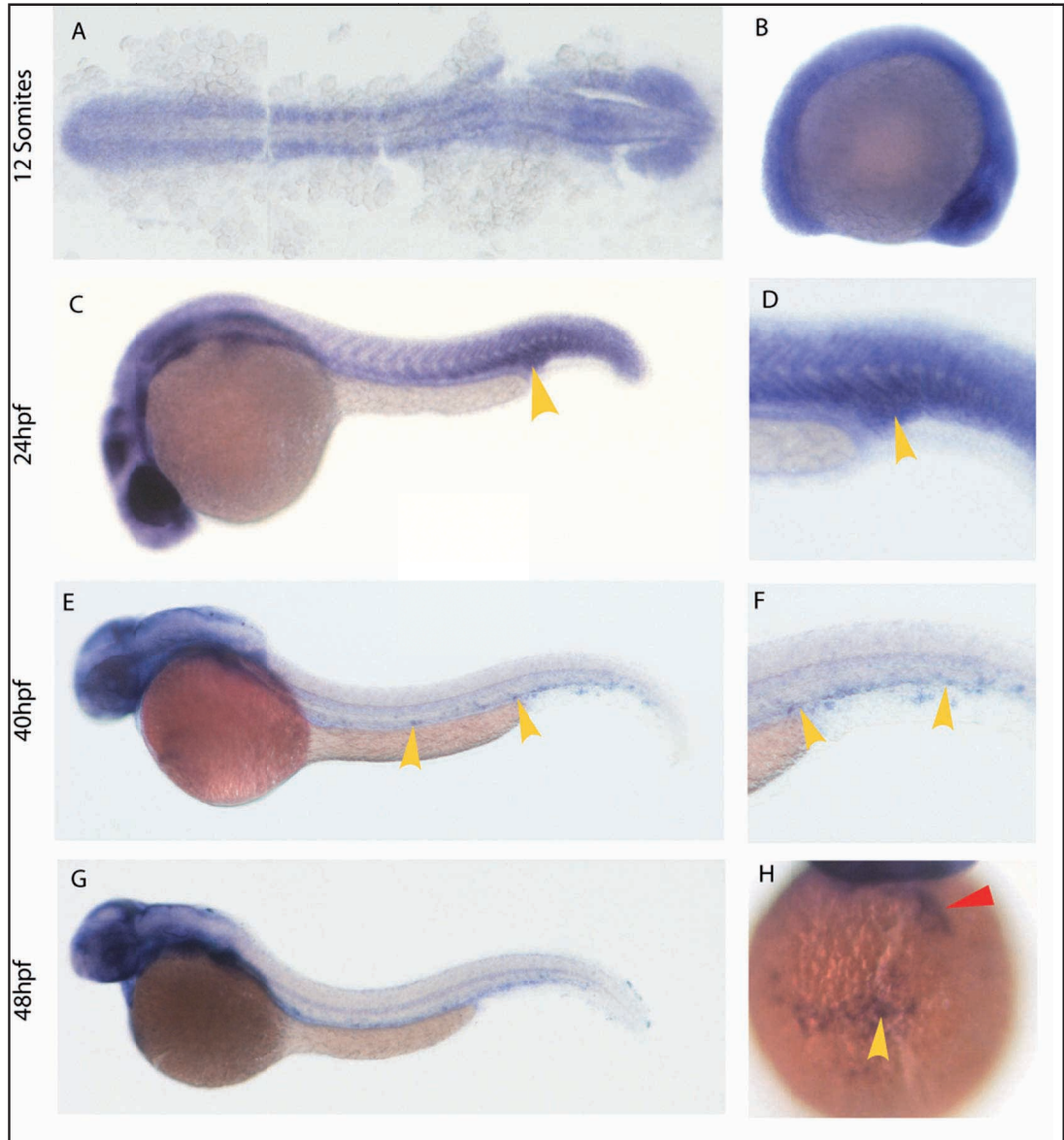
Figure 3-6 : Expression of *ddx18* by WISH in WT zebrafish

3.4.3 Whole mount in situ hybridisation for lineage-specific blood markers

To determine the earliest time point at which Ddx18 affects the development of blood in *ddx18$^{hi1727/hi1727}$* mutants, in situ hybridisation was performed with a range of markers delineating erythroid, myeloid and haemangioblast precursors. Figure 3-7 shows that prior to the onset of circulation the distribution and quantity of these markers was similar in *ddx18$^{hi1727/hi1727}$* mutant embryos and in WT embryos. At such an early developmental stage mutants were not reliably distinguishable from siblings by morphology alone, thus 12 embryos per gene were imaged and genotyped to confirm the findings. Although no clear difference in cell numbers was detectable at 14 somites (16 hpf), *ddx18$^{hi1727/hi1727}$* mutant embryos exhibited abnormal migration and a non-significant reduction in number of cells positive for the early myeloid marker *pu.1* at 24 hpf. This finding was confirmed when *ddx18$^{hi1727/hi1727}$* embryos were crossed to transgenic (Tg) fish expressing EGFP from the *pu.1* promoter, *Tg(pu.1:EGFP)* fish (Tg [promoter:expression construct] for all future references to transgenics) shown in Figure 3-8. In addition to other markers of primitive haematopoiesis, *ddx18$^{hi1727/hi1727}$* mutants and WT siblings were assessed for defects specific to definitive HSCs. The markers *runx1* and *cmyb* were used as markers of zebrafish HSC development (Burns et al, 2002; Thompson et al, 1998). Since the runx1 probe has variable efficacy in our hands, cmyb ISH alone was used as a marker of HSC. *c-myb* RNA was markedly reduced in the dorsal aorta and caudal haematopoietic tissue of *ddx18$^{hi1727/hi1727}$* mutants compared to WT siblings indicating that mutants possessed reduced numbers of HSCs (Figure 3-9).
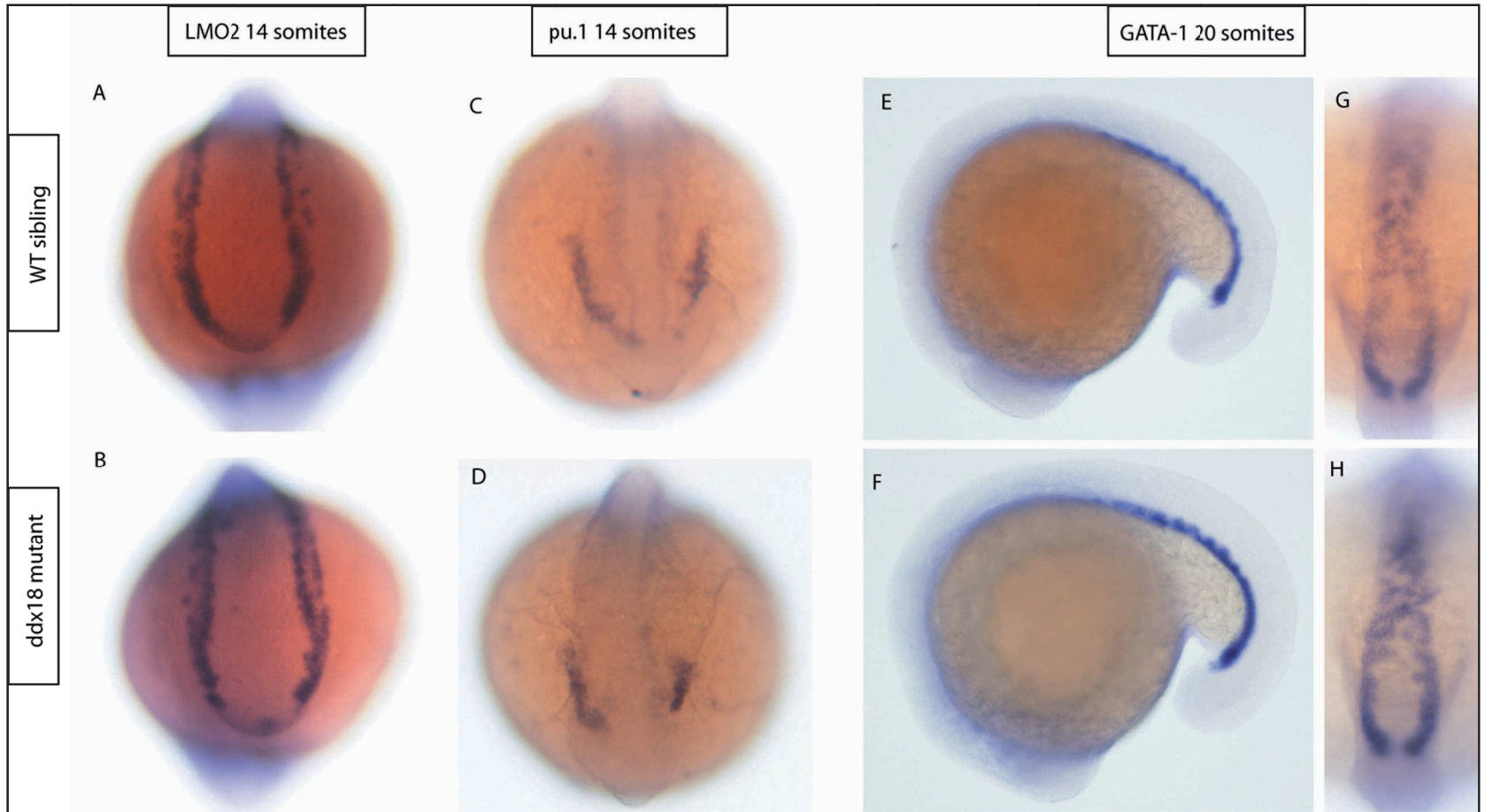
Figure 3-7 : Expression of blood markers using WISH in *ddx18^{hi1727/hi1727}* mutants and siblings
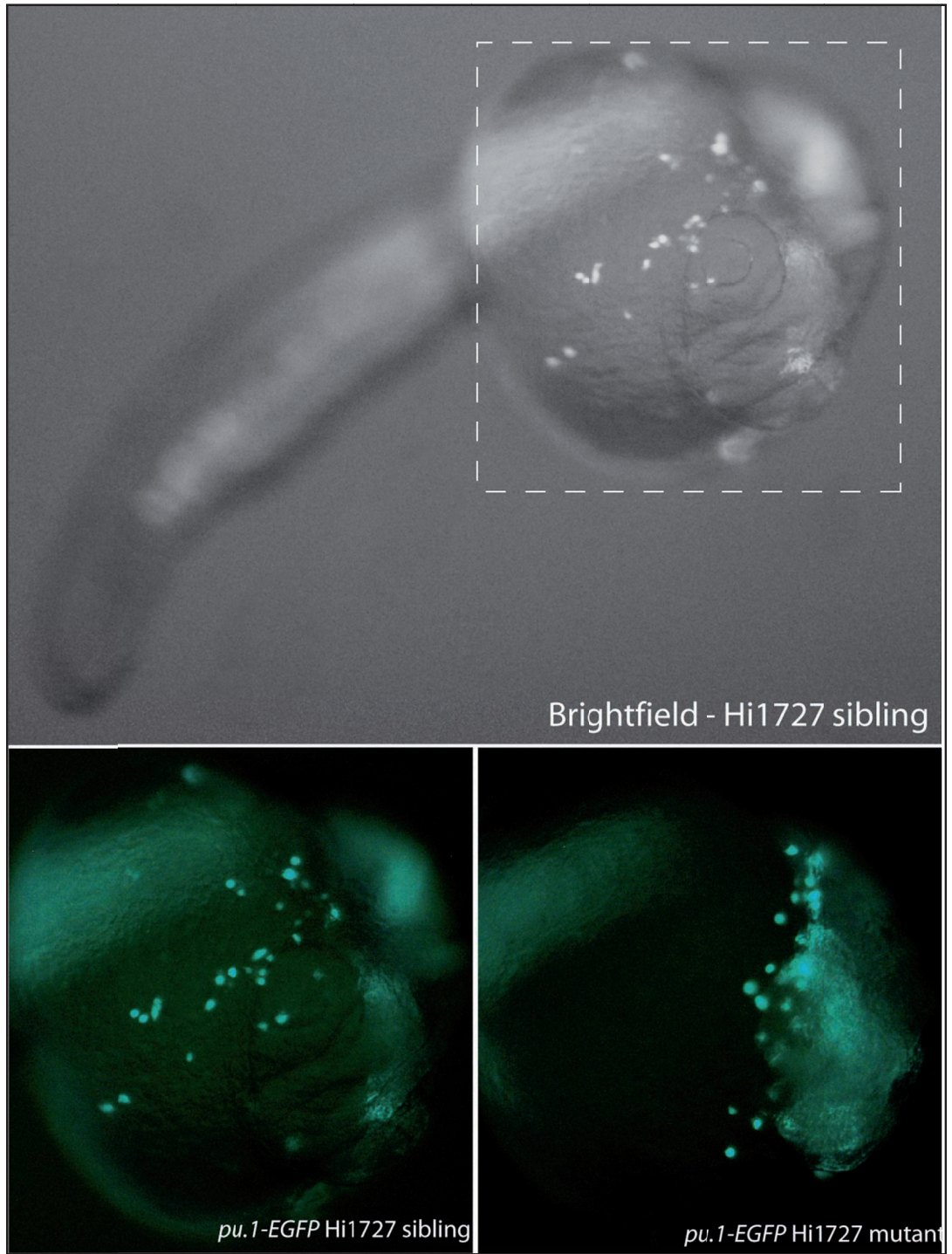
Figure 3-8 : Abnormal migration of EGFP+ pu.1-early myeloid cells in $ddx18^{hi1727/hi1727}$; *Tg(pu.1:EGFP)* embryos

WISH for c-myb at 32hpf
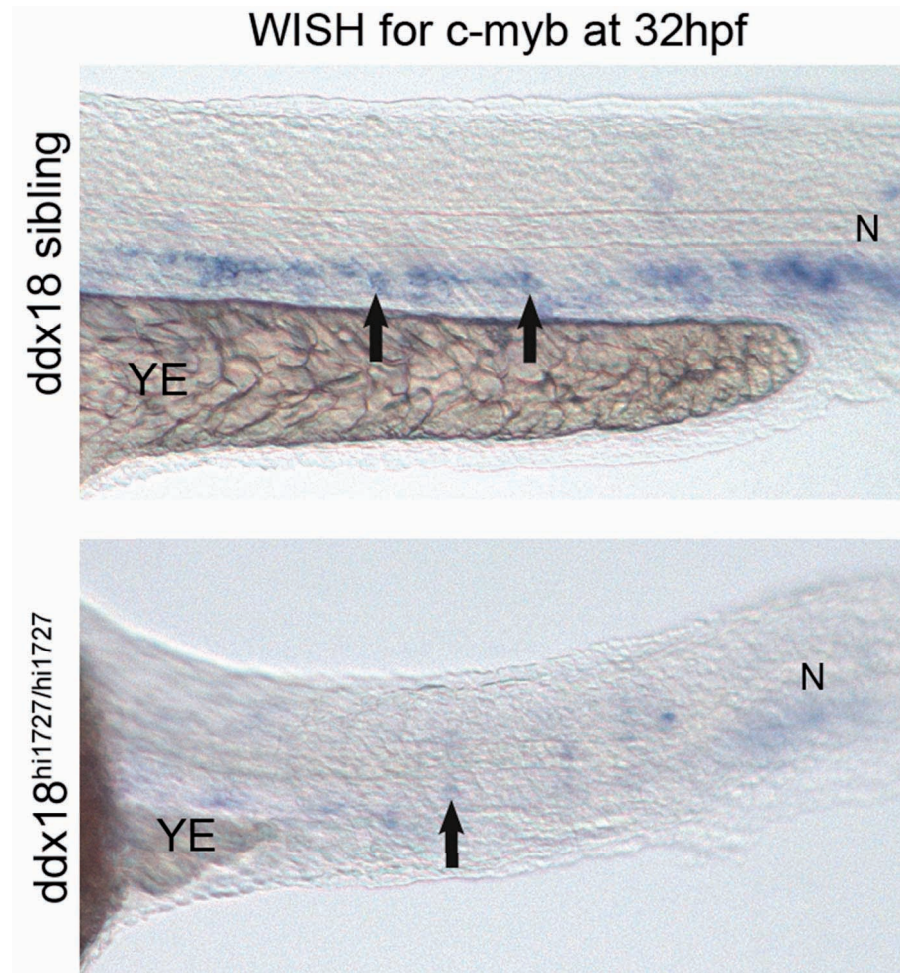
Figure 3-9 : *ddx18*[hi1727/hi1727] mutants have lower expression of *c-myb* indicating reduced HSC

Legend Figure 3-7 : Whole mount in situ hybridisation for lmo2, pu.1 and gata.1 in *ddx18^hi1727/hi1727* mutants and siblings. No difference in expression was observed between WT siblings and *ddx18^hi1727/hi1727* mutants. Individual embryos were imaged and genotyped to confirm the genotype.

Legend Figure 3-8: Upper panel : brightfield image of WT/sibling embryo from *ddx18^hi1727* clutch at 24 hpf showing orientation of embryos in oblique ventral view. Lower panels: epifluorescent images of WT sibling (left) and *ddx18^hi1727/hi1727* mutant embryos (right) crossed to Tg(pu.1:EGFP) expressing embryos. Numbers of GFP expressing cells were modestly reduced in mutants compared to siblings and EGFP-expressing cells exhibited markedly less migration over the yolk in mutants compared to WT siblings.

Legend Figure 3-9: Whole mount in situ hybridisation using probe for cmyb. Cells in the dorsal aorta and caudal haematopoietic tissue are presumed HSC. A marked reduction in expression *cmyb* was observed in *ddx18^hi1727/hi1727* mutants compared to WT siblings. N = notochord; YE = yolk extension; arrows indicate presumed HSC in dorsal aorta.

3.4.4 Expression of non-haematopoietic markers are unaffected

Given the prominent developmental phenotype observed in *ddx18^hi1727/hi1727* mutants, in situ hybridisation was performed using the *krox20* (*egr2*) probe to determine if loss of Ddx18 simply led to reduction of expression of all genes in all tissues. The *krox20* probe was chosen because the major developmental defect observed in *ddx18^hi1727/hi1727* mutants was abnormal brain development, and *krox20* is expressed in developing rhombomeres 3 and 5. Expression of krox20 in *ddx18^hi1727/hi1727* mutants showed a slightly different distribution pattern since the brain anatomy is disrupted. However, as shown in Figure 3-10 *krox20* expression (shown in red, marked by black arrows) was not reduced in *ddx18^hi1727/hi1727* mutants. Embryos in Figure 3-10 were co-stained for *mpx* (black) showing reduced myeloid cells in *ddx18^hi1727/hi1727* mutants.

Legend Figure 3-10 : Double in situ hybridisation for *krox20* and *mpx* showing reduced numbers of *mpx* expressing cells (black) with retained level of *krox20* staining in rhombomeres 3 and 5 (red).
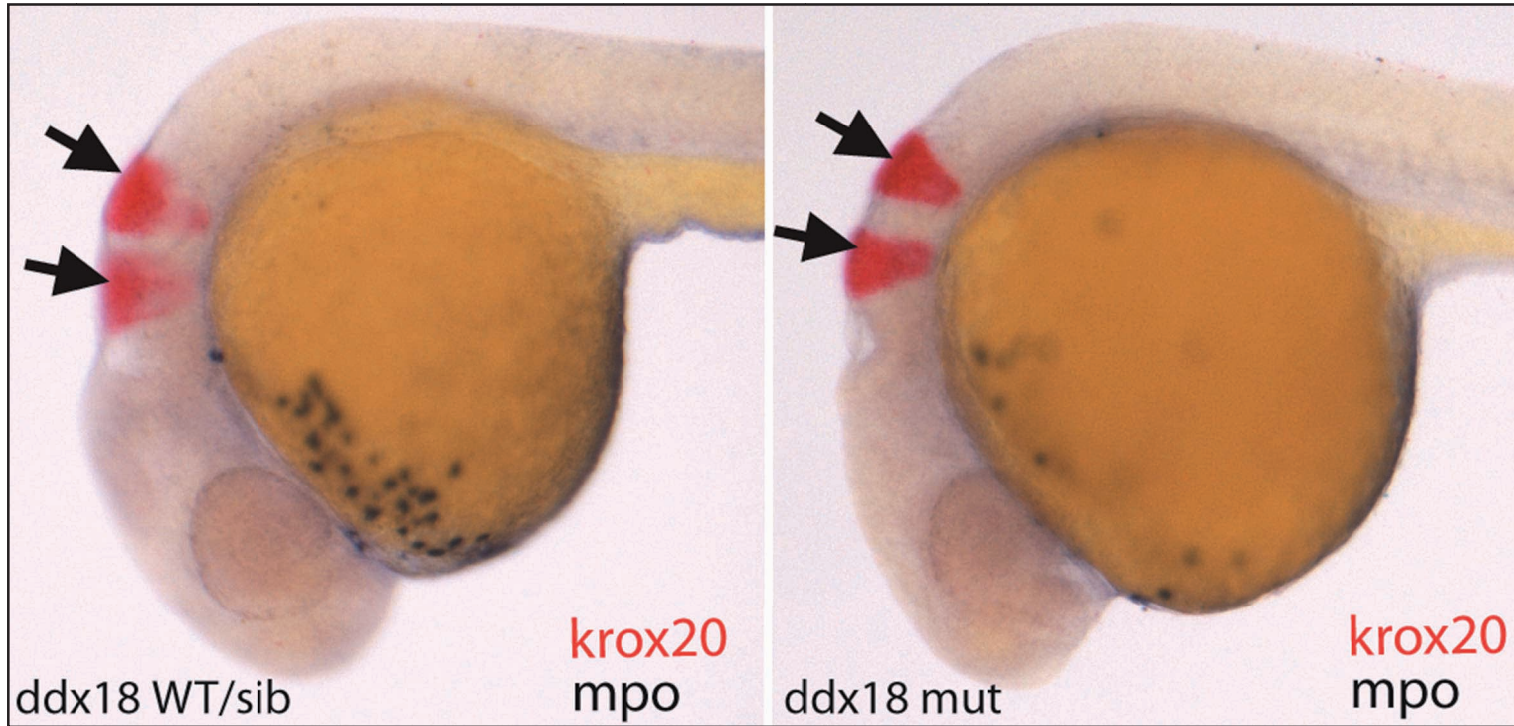
Figure 3-10 : *ddx18*^{hi1727/hi1727} mutants have reduced *mpx* (black) and other blood markers while retaining normal *krox20* (*egr2*) (red)

3.4.5 Knockdown of Ddx18 with using morpholinos phenocopies the *ddx18*^{hi1727/hi1727} mutant

Three morpholinos were designed to target the *ddx18* gene. One was directed against the 5'UTR, the other two were directed against the splice donor sites of exon1-intron1 (E1-I1) and exon2-intron2 (E2-I2) respectively. Morpholinos were designed by Genetools LLC. All three morpholinos phenocopied the developmental effects of Ddx18 loss in *ddx18*$^{hi1727/hi1727}$ mutants, shown in Figure 3-11.

The effects observed with the 5'UTR morpholino were markedly more severe than those of the splice morpholino where 0.16ng (20μM) was lethal due to gross developmental defects within 3 dpf. This is compared to the 0.8–4ng (100–500μM) doses of the E2-I2 giving a significantly less potent effect where embryos are able to survive to 4.5 dpf. Since the E2-I2 phenotype most closely resembled the developmental effects observed in *ddx18*$^{hi1727/hi1727}$ mutants these morpholinos were selected for use in additional studies. The effects of the splice blocking morpholinos were determined using the Qiagen one-step RT-PCR kit (Figure 3-11; bottom right). In situ hybridisation for mpx was performed on embryos at 27 hpf injected with a range of different morpholino concentrations (Figure 3-11; left panels quantified in top right graph). These resulted indicated that injection of E2-I2 splice-blocking morpholino resulted in developmental and myeloid defects similar to those observed in *ddx18*$^{hi1727/hi1727}$ mutants in a dose-dependent manner.

Legend Figure 3-11: Left panels show embryos at 27 hpf with head to the left and dorsal upwards. Embryos are stained by in situ hybridisation for mpx. Cell numbers are quantified in the panel on the upper right and error bars shown are standard error of the mean. The lower right panel shows one-step PCR from RNA derived from pooled whole embryos at 27hpf. Aberrant splicing from occurred as a result of the morpholino and showed a larger band than WT when amplified using full length primers.
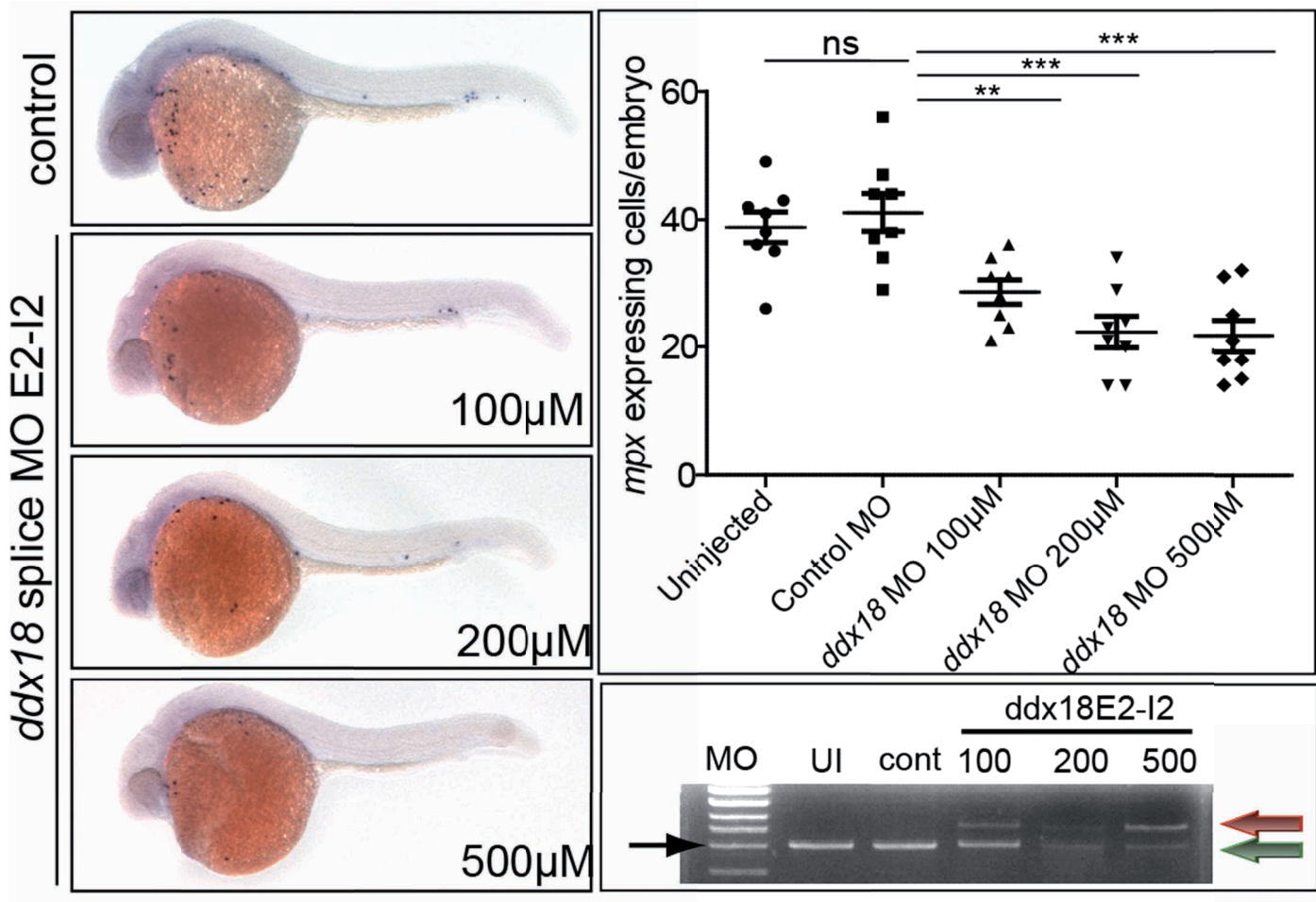
Figure 3-11 : Morpholino knockdown of *ddx18* phenocopies the *ddx18*[hi1727/hi1727] mutant

3.4.6 RNA encoding human DDX18 rescues the haematopoietic defect seen in *ddx18^{hi1727/hi1727}* mutants

In vitro transcribed RNA from human *DDX18* subcloned into *pCS2+* was injected into one-cell stage embryos from *ddx18^{hi1727/+}* heterozygous incrossed clutches. Doses of RNA were titrated from 10–400ng/µl. As the dose of RNA increased fewer embryos with mutant phenotype were visible in the clutch at 24–72 hpf. In addition a range of "monsters" were seen ranging from mild-severe dorsalised body phenotype to Cyclops. The number of monsters increased with increasing doses of RNA presumably representing an overexpression phenotype. Genotyping of all "normal" looking embryos confirmed that at least 30% of *ddx18^{hi1727/hi1727}* mutants showed a normal phenotype at 3 dpf confirming the human RNA was able to rescue the mutant developmental phenotype (shown in the pie chart 3–12). Genotyping of "monsters" showed around a third were WT, a third were heterozygous and a third were *ddx18^{hi1727/hi1727}* mutants (Figure 3–12).
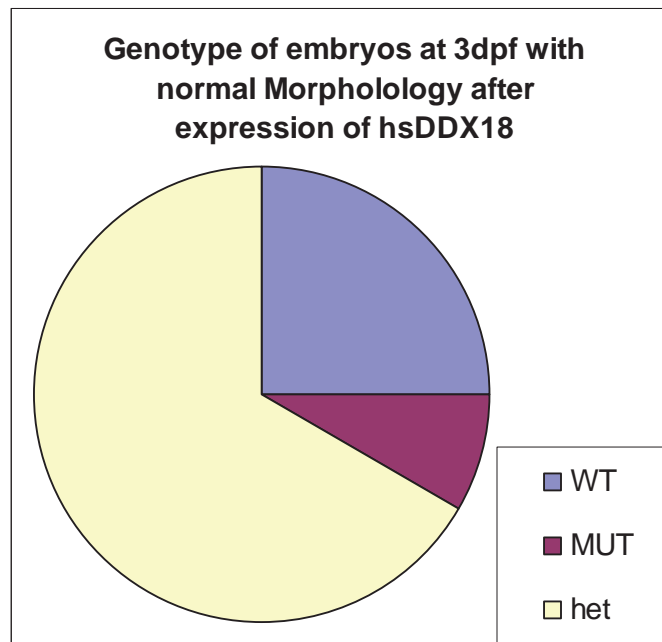
Figure 3-12 : Pie chart showing genotype:phenotype in *ddx18^{hi1727/hi1727}* injected with RNA encoding DDX18

Legend Figure 3-12 : Pie chart showing the genotype of embryos with normal developmental morphology at 3 dpf. 50 embryos were screened. The dark pink area shows that nearly half of the number of expected *ddx18^{hi1727/hi1727}* homozygous mutants were phenotypically WT at 3 dpf

following DDX18 overexpression.

In order to determine whether DDX18 could rescue the haematopoietic defects associated with Ddx18 loss, embryos were injected with *DDX18* RNA or control (mcherry-encoding) RNA, fixed at 27 hpf and ISH for *mpx* performed. Since the developmental phenotype was corrected in the majority of mutant embryos, the number of myeloid cells was recorded from each embryo, which were then photographed and DNA extracted to determine their genotype. The results are shown in Figure 3-13. Overexpression of human *DDX18* RNA is able to rescue both the developmental and myeloid effects associated with loss of Ddx18 in *ddx18*[hi1727/hi1727] mutants. This result indicates that the phenotype of *ddx18*[hi1727/hi1727] mutants can be attributed to loss of Ddx18 and that the human and zebrafish DDX18 are functionally conserved.

Legend Figure 3-13: Haematopoietic cell loss observed in *ddx18*[hi1727/hi1727] mutants can be rescued by overexpression of human DDX18. DDX18-encoding RNA was injected at the one cell stage into and embryos staged and fixed at 27 hpf. ISH for mpx was then performed. Individual embryos were photographed and myeloid cell numbers counted. The embryos were then genotyped. Panels A and C show representative sibling embryos. Embryo C is a *ddx18*[hi1727/hi1727] embryo injected with 100pg of human *DDX18*. Myeloid and developmental defects are clearly improved compared to embryo D which is also a *ddx18*[hi1727] embryo, but injected with mCherry encoding RNA. The scatter plot shows cell numbers per embryo for genotyped embryos (rescues only). Statistical analysis was performed with GraphPad Prism Version IV Software using an unpaired student's t test. The F test was used to confirm normal distribution of the variables.
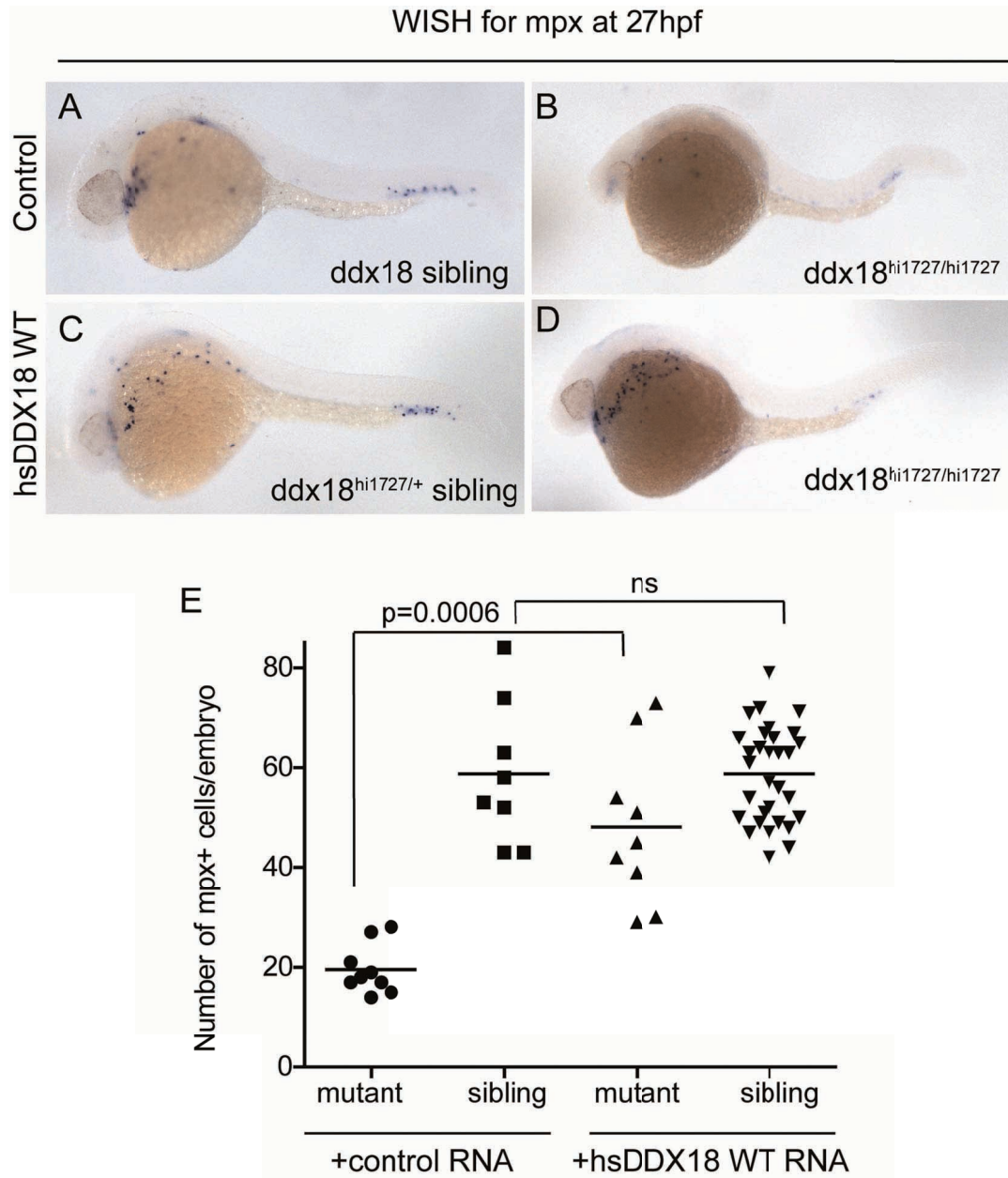
Figure 3-13 : DDX18-encoding mRNA rescues the blood defects of *ddx18^hi1727/hi1727* mutants

3.5 Chapter discussion

The initial analysis of *ddx18*^{hi1727/hi1727} mutants confirmed the result suggested in the primary screen, namely that there were reduced numbers of myeloid cells in *ddx18*^{hi1727/hi1727} mutants. The primary screen was carried out at 2 and 4.5 dpf and the phenotype of *ddx18*^{hi1727/hi1727} mutants was only assessed at 4.5 dpf. Re-screening demonstrated for the first time that there was a reduction in the number of erythroid and myeloid cells in *ddx18*^{hi1727/hi1727} mutants as early as 27 hpf. *ddx18* is an essential gene for development in zebrafish resulting in embryonic lethality by 5 dpf. My studies suggest a specific role for Ddx18 in primitive and definitive blood development in zebrafish embryos.

In order to address whether or not loss of *ddx18* was likely to result from cell-autonomous or non-cell autonomous effects on blood development in situ hybridisation was performed over a time course to determine the expression of *ddx18* during development. It was reasoned that the expression of *ddx18* in haematopoietic tissues would indicate that it is more likely to have a cell autonomous effect when disrupted in these tissues. At early time points the expression pattern of *ddx18* was ubiquitous, but, by 24hpf there was clear evidence of expression of *ddx18* within the primitive erythroid forming region of the embryo, the posterior blood island and ICM. At later time points (40 and 48 hpf) expression was seen in the aorta and the ducts of Cuvier suggesting expression in HSC and circulating red blood cells respectively. It is also noteworthy that at the 48hpf time point *ddx18* was expressed in the heart, since *ddx18*^{hi1727/hi1727} mutants show evidence of abberant cardiac contractility from this timepoint.

The effects of loss of Ddx18 on blood development did not appear to occur earlier than 14 somites since expression of the early haemangioblast marker *lmo2* and early myeloid marker *pu.1* appeared normal at this time. In contrast by 24hpf reduced red blood cells could be seen by light microscopy and evidence of abnormal localisation of early myeloid precursors expression GFP from the *pu.1*-promoter suggested that the onset of defective blood development occurs at some time between 16 hpf (14 somites) and 24hpf.

Since production of definitive red and white blood cells appeared to be reduced by loss of Ddx18 and the expression pattern of *ddx18* was seen in the aorta when

HSCs are generated, I addressed whether this could be the result of loss of definitive HSCs arising in the wall of the aorta from around 26 hpf (Bertrand et al, 2008; Jin et al, 2007; Kissa et al, 2008). Several groups have used transgenic animals and fate-mapping studies by injecting embryos with caged rhodamine dextran. This caged red (or green) fluorophore can be activated by laser and thus single cells can be targeted for uncaging using a confocal microscope. Three groups have defined the presence of HSCs in the zebrafish arising from cells that express GFP from the promoters of the *fli1, cd41 or cmyb* genes (Bertrand et al, 2008; Jin et al, 2007; Kissa et al, 2008) by following the fates of GFP-expressing cells from those promoters which had been uncaged. Other investigators have utilised *runx1* as a primary marker of HSC based on the knowledge of its role in mammalian HSC development (Burns et al, 2002; Gering & Patient, 2005). For the experiments described in this chapter, in situ hybridisation for *cmyb* was included (Burns et al, 2009). However, WISH for *runx1* in $ddx18^{hi1727/hi1727}$ clutches was unsuccessful. As an alternative strategy delineation of expression patterns of *cd41* in $ddx18^{hi1727/hi1727}$ mutants was attempted. This has proven to be a major technical challenge. HSCs expressing low levels of *cd41* may fall below the limit of detection for in situ hybridisation probes. However, *cd41* is also expressed at high levels in developing thrombocytes. It was not possible to detect expression of *cd41* in mutants or control siblings using the probe published in (Lin et al, 2005). This probe is a large >3kb probe that required hydrolysis to reduce it to smaller fragments. Despite successful fragmentation (determined by agarose gel electrophoresis) no signal was obtained. To further attempt to determine the expression pattern of *cd41*, the full length of the gene was re-cloned into three fragments and in situ hybridisation was performed using all three fragments. This approach also failed to show any signal in mutants or controls of various stages. Thus studies looking at HSC RNA expression have been limited to *cmyb*.

Studies were restricted to development of HSCs and erythroid and myeloid lineages in $ddx18^{hi1727/hi1727}$ mutants. In an attempt to extend observations to the megakayocyte/thrombocyte lineage, an antisense probe directed against the thrombopoietin receptor (*tpo-R, c-mpl*) was designed to identify thrombocytes. However, the utility of this strategy is severely limited because analysis of $ddx18^{hi1727/hi1727}$ mutants was restricted to the first 48 hours of development (because of profound developmental abnormalities) and the thrombocyte lineage is challenging to detect before 3dpf.

One potential concern about the observed phenotype is that *ddx18*^{hi1727/hi1727} mutants possess marked developmental abnormalities in non-haematopoietic tissues and become progressively more dysmorphic over the 2–4 day period until death. It was therefore critical to determine whether the loss of Ddx18 resulted in defects specific to blood development, To achieve this expression of *krox20 (egr2)* was examined, revealing expression in rhombomeres 3 and 5 in *ddx18*^{hi1727/hi1727} mutants. Ddx18 was expressed in this region of the brain at 27hpf in *ddx18*^{hi1727/hi1727} mutants and siblings to a similar level. This suggests that blood development was more sensitive to the effects of Ddx18 loss, at this time point. Nonetheless, the evaluation of definitive haematopoiesis i.e. after 36hpf–4dpf is severely impeded by the potential impact of the severe abnormal developmental effect. Thus I have chosen to focus on analysis of *ddx18*^{hi1727/hi1727} mutants to the first 2 days of life.

It was essential to consider the possibility that other viral insertions or mutations may exist in the *ddx18*^{hi1727} line. The likelihood of this was minimised by outcrossing the mutant line by more than 10 generations. However, to determine whether or not loss of Ddx18 is the specific gene causing the reduction in myeloid cells and developmental defects observed Ddx18 was knocked down using morpholino antisense oligonucleotides. Initially a morpholino was used targeting the 5'UTR/translation initiation site of *ddx18*. Such morpholinos anecdotally are more "effective" at knocking down their targets or at least in producing a phenotype (Eisen & Smith, 2008; Len Zon personal communication). Although difficult to demonstrate definitively as this would require the availability of an antibody, this observation is most likely to be related to the blocking of all RNA transcripts including maternal RNA using a morpholino of this type. In keeping with this concept, knockdown of Ddx18 using a translation blocking morpholino proved very potent, with embryos showing gross developmental abnormalities (similar to but more severe than those observed in the *ddx18*^{hi1727/hi1727} mutants) even at very low doses. *ddx18* is expressed maternally and loss of maternal *ddx18* is the most likely explanation for this observed phenotype. Another possible explanation is that since the viral insertion is in the 1st intron of the *ddx18* gene, it is possible some normal splicing may occur with the resulting mutant being hypomorphic rather than completely null for Ddx18. This is likely for *ddx18*^{hi1727/hi1727} mutants given the intronic location of the virus and the potency of the 5'UTR morpholino. To obtain a phenotype more closely resembling

ddx18^{hi1727/hi1727}, splice-blocking morpholinos were used to block the exon2-intron2 splice boundary of *ddx18.* The major benefit of this type of morpholino is that it allows semi-quantitative measurement of the degree of knockdown by looking at the amount of WT transcript remaining.   Even with the amount of WT protein apparently remaining at greater than 50%, reduced numbers of myeloid cells were seen in the morphants. Myeloid numbers and developmental effects were dose-dependent, with the maximal reduction in myeloid cells occurring where around 20% WT transcript was present. Taken together these data strongly argue that the *ddx18^{hi1727}* allele is hypomorphic. In particular, no reduction in myeloid cells was observed in heterozygous mutants. While off-target effects of the morpholino cannot be excluded, a likely explanation is that heterozygous animals have greater than 50% levels of Ddx18.

Given that the morpholino photocopied the effects of the *ddx18^{hi1727/hi1727}* mutant it is possible to be confident that this gene indeed was the cause of the blood phenotype seen in *ddx18^{hi1727/hi1727}* mutants. However, it remained possible that the viral insertion disrupted a *cis*-regulatory region located in the intron of *ddx18* affecting the expression of one or more alternate genes. Thus to confirm that *ddx18* was the gene responsible for the phenotypes observed rescue experiments were performed using human *DDX18* in vitro transcribed RNA. Human *DDX18* is highly expressed in many cell lines therefore initially it was attempted to clone it from RNA derived from K562 cells. Several attempts at cloning the 2.5kb cDNA including the use of a high fidelity long-range PCR kit were unable to obtain an error-free fragment in the pCRII-topo vector. (I later became aware that the high fidelity Taq used in these kits does not leave the TA ends necessary for TOPO cloning, thus explaining the lack of colonies). To circumvent this issue the full length clone for *DDX18* was purchased from Open Biosystems and subcloned into the pCS2+ vector. Injection of in vitro transcribed RNA into *ddx18^{hi1727}* clutches at different doses showed rescue of the developmental phenotypes of *ddx18^{hi1727/hi1727}* mutants in 30–60% of mutants. In addition, an overexpression phenotype was observed. Overexpression resulted in dorsalisation of the embryo with loss of the tail region and marked disruption of somites. In the most severe cases cyclops was observed. While the number of overexpression "monsters" correlated with the increasing doses of *DDX18* RNA injected, genotyping revealed that even some mutants were exhibiting this phenotype. This suggests that *DDX18* RNA expression is mosaic and/or variable

in expression level within the embryos injected and may have specific toxic effects on the Nodal signalling pathway disrupted in the Cyclops zebrafish mutant (Dougan et al., 2003). Overexpression studies were also used to determine whether the expression of human DDX18 could rescue myeloid defects observed in $ddx18^{hi1727/hi1727}$ mutants. In this instance a lower dose (100pg) of RNA was used to limit overexpression artefacts. Myeloid cell numbers could be rescued using human DDX18 indicating that the function of DDX18 in haematopoiesis is conserved from zebrafish to humans.

In summary, this chapter defines that Ddx18 loss results in abnormal haematopoiesis commencing between 16 somites (17hpf) and 24hpf. The affect is on primitive erythroid and myeloid development as well as the generation of definitive HSCs. It was further established that while other developmental abnormalities are clear, $ddx18^{hi1727/hi1727}$ mutants appear to show increased sensitivity to effects on the developing haematopoietic system.

4. Effects of Ddx18 loss on cell death and cell cycle arrest

4.1 Introduction

4.1.1 Potential mechanisms for reduced numbers of myeloid cells in $ddx18^{hi1727/hi1727}$ mutant zebrafish

In Chapter 3 of this thesis, experimental evidence was presented that demonstrates that loss of Ddx18 leads to reduced numbers of haematopoietic cells in zebrafish embryos. This chapter describes work performed to identify the mechanisms underlying this reduction in myeloid cells. Candidate mechanisms include: (i) a reduction in haematopoietic cell proliferation, (ii) an increase in cell death or cellular senescence and (iii) aberrant cell cycle progression.

Dead-box proteins have the potential to carry out a broad range of cellular functions owing to their ability to function as modifiers of RNA-associated structures. Accordingly, some dead-box proteins are extremely promiscuous in their functions. For example, DDX5 can act as a transcriptional co-regulator with P53 (a key regulator of cell death), as a micro-RNA unwinder, as a nucleo-cytoplasmic shuttle protein and as a putative tumour suppressor in breast and colon cancer (Fuller-Pace, 2006). Other identified functions of dead-box proteins include; participation in the DNA damage response (DDX1 dissociates RNA–DNA duplexes at the site of irradiation induced DNA damage) dependent on ATM (Li et al, 2008); and protection from the pro-apoptotic effects of P53 target gene ASPP2 (via direct interaction with the C terminal domain of DDX47) (Uhlmann-Schiffler et al, 2009). The functional promiscuity of dead box proteins makes it difficult to predict cellular pathway(s) that will be affected by dead-box protein loss.

Studies in both flies and in cell culture have suggested that loss of Ddx18 results in aberrant cellular proliferation (Dubaele & Chène, 2007; Zaffran et al, 1998). In a study of the drosophila mutants "pitchoune" (the orthologous gene to *ddx18*), mutants are small and over expression of *ddx18* resulted in increased cellular proliferation (measured by incorporation of BRDU and increased mitoses (measured by phosphohistone H3 staining) (Zaffran et al, 1998). A study using an in vitro cell culture model demonstrated that shRNA knockdown of *DDX18* or forced expression of a mutant form of *DDX18* unable to bind nucleic acids resulted in reduced cell numbers. In the latter study, disruption of DDX18 did not result in cell cycle disturbance or apoptosis (Dubaele & Chène, 2007).

In contrast, studies have shown that the yeast homologue of Ddx18, Has1p, is required for ribosome biogenesis (Emery et al, 2004), providing evidence that Ddx18 is involved with ribosomal function, suggesting a putative pathway linking Ddx18 to the control of cell death or cell cycle regulation. Ribosome production is a tightly regulated process designed to maintain the necessary supply of protein-producing organelles required for the growth and survival of the cell. Ribosomes are known to interact with P53, a key regulator of cell death and cell cycle progression. Loss of either small or large ribosomal subunit proteins or defects in processing of pre-rRNA subunits can result in stabilisation of p53 with resulting apoptosis or cell cycle arrest (Chakraborty et al, 2009; Fumagalli et al, 2009; Hölzel et al, 2010; McGowan et al, 2008). There is evidence that this effect is primarily mediated by a protein component of the large ribosomal subunit, RPL11 (Fumagalli et al, 2009). While it has been known for some time that RPL11 and several other ribosomal proteins can bind MDM2 resulting in P53-stabilisation, this was thought to occur as a result of disruption of the nucleolus (Rubbi & Milner, 2003). More recent evidence suggests that RPL11 is able to mediate sequestration of MDM2 and subsequent p53 stabilisation independent of nucleolar disruption. Proposed mechanisms by which this process can occur depend on which of the two ribosomal subunits is being disrupted. Small ribosomal subunit disruption secondary to reduced small ribosomal subunit proteins led to selective upregulation of RPL11 in a post-transcriptional manner. This occurred as a result of the presence of a polypyrimidine tract near the RPL11 translation initiation site (known as 5'TOP mRNAs). In contrast, disruption of large ribosomal subunit production (from loss of large ribosomal subunit proteins) leads to an increase in free cytoplasmic Rpl11 which in turn inhibits Mdm2, allowing P53 stabilisation.

As ribosomes have a central role in the control of P53-mediated apoptosis and/or cell cycle arrest and Ddx18 may be involved with ribosomal function, it can be reasoned that Ddx18-deficiency might result in reduced numbers of myeloid cells in zebrafish by disruption of ribosomal integrity and/or induction of ribosomal stress leading to increased cell death and/or cell cycle arrest. Therefore the focus was placed on investigation of the contribution of these two mechanisms to the reduced haematopoiesis seen in $ddx18^{hi1727/hi1727}$ mutant zebrafish embryos and the potential contribution of stabilisation of P53, a critical mediator of cell death

and cell cycle regulation to the haematopoietic and developmental phenotypes of *ddx18^{hi1727/hi1727}* mutant zebrafish.

4.2 Aims of the experiments described in this chapter

1. To determine if Ddx18 loss increases cell death
2. To determine the effects of Ddx18 loss on cell cycle progression
3. To determine if the apoptotic and myeloid phenotype seen in *ddx18^{hi1727/hi1727}* mutant zebrafish can be rescued by loss of p53
4. To determine if cell death or cell cycle arrest represents the dominant mechanism for loss of haematopoietic cells in *ddx18^{hi1727/hi1727}*

4.3 Methods

4.3.1 Acridine orange staining for detection of cell death

Acridine orange is a supravital dye that stains dead and dying cells regardless of the mechanism death. Live embryos were placed in 12 well plates (Nunc) in 1 ml of egg water. 10μl of stock acridine orange (AO, 1 mg/ml, Sigma Aldrich) was added to the egg water to make a final concentration of 10 μg/ml. The plate was swirled to ensure all the AO was mixed. Embryos were then incubated at 28°C for 30 minutes in the dark, transferred to mesh wells and washed 3 times for 10 minutes in egg water at room temperature with gentle rocking in the dark (covered in aluminium foil). Embryos were then immediately visualised using a fluorescent microscope.

4.3.2 Whole mount terminal deoxynucleotidyl transferase dUTP nick end labelling (TUNEL) assay for detecting apoptosis-related DNA fragmentation

This assay uses the terminal deoxynucleotidyl transferase enzyme to detect nicks in DNA that occur during apoptosis attaching a dUTP (exogenously supplied) and labelled such that it can be detected with an antibody colourimetrically or fluorescently. Whole mount staining for TUNEL was performed using the Bioscience Research (formerly Chemicon) ApopTag Fluorescein Direct *In Situ* Apoptosis Detection Kit. Zebrafish were fixed at the desired time point (up to 48 hpf) in 4% PFA overnight. Embryos were then washed 3 times in PBST for 5 minutes with gentle rocking at RT and then stored in 100% methanol overnight. The following day the embryos were rehydrated by washing 3 times for 5 minutes in PBST, followed by 15 minute digestion in μg/ml proteinase K in PBST for 15

minutes. Embryos were then re-fixed in 4% PFA for 20 minutes at RT and then washed again 3 times in PBST for 5 minutes. For the final PBST wash, embryos were transferred to round-bottom polypropylene tubes (Becton Dickenson). PBST was completely aspirated and replaced with 75 μl of equilibration buffer and incubated at RT for 1 hour. Working strength TdT reaction mix as follows was prepared and mixed thoroughly as follows:

Reaction buffer	77 μl
TdT enzyme	33 μl
Total	110 μl

55 μl of TdT reaction mix was applied to each sample, tubes were covered in parafilm, and placed inside a 50 ml Falcon tube containing 5 ml distilled water and incubated overnight at 37°C.

The following day the embryos were washed in 150 μl of the working strength stop/wash buffer supplied in the kit (1 ml stock + 34 ml dH$_2$O).

Working strength fluorescein antibody solution was prepared as follows, vortexed and stored on ice:

Blocking solution	68 μl
Anti-digoxigenin antibody conjugate	62 μl
Total	130 μl

Embryos were then incubated overnight at 4°C in tubes wrapped in parafilm in the presence of 65 μl fluorescein antibody solution per tube.

The next day, embryos were washed in 3 times for 5 minutes in PBST and mounted in 80% glycerol for imaging.

4.3.3 Whole mount immunofluorescence for activated caspase-3 and phosphorylated histone H3 (serine 10)

Embryos were fixed overnight in 4% PFA and then transferred to 100% methanol for 4 hours at −20°C. Embryos were washed 3 times for 10 minutes in 1.5 ml

Eppendorf tubes at RT in PBST, 0.3% Triton-X and 1% DMSO (PDT). Embryos were blocked with 300 μl caspase antibody block (CAB) (10% HI-FBS, 2% BSA in PBST) for 1 hour at RT with gentle rocking. Anti-activated-human-caspase-3 antibody (BD Biosciences) or anti-phospho(serine10)-histone H3 (Santa Cruz) was diluted 1 in 500 in CAB and 100 μl incubated with the embryos overnight at 4°C. The following day embryos were washed 3 times for 20 minutes in PDT and blocked for a further 1 hour in CAB. Embryos were then incubated with secondary antibodies (goat anti-rabbit Alexa 488 (green) or Alexa 568 (red, both Molecular Probes) diluted 1 in 200 in CAB) at RT for 4 hours in the dark. Embryos were then washed 3 times for 20 minutes in PDT and then equilibrated in 70% glycerol overnight before imaging.

4.3.4 DNA content analysis

Cell cycle was assessed with propidium iodide (PI) staining. $ddx18^{hi1727/hi1727}$ mutants (or siblings) were sorted at 24 hpf, pooled and dissociated into single cell suspension. The cells were washed in PBS and lysed in a hypotonic solution of 50 μg/ml PI, 0.1% sodium citrate and 0.1% tritonX-100. Cells were then analysed for DNA content using a FACS caliber or FACS canto flow cytometer. The data was analysed using Modfit software.

4.4 Results

4.4.1 Acridine orange staining to assess dead and dying cells in $ddx18^{hi1727hi1727}$ mutants

$ddx18^{hi1727/hi172}$ mutants showed clear evidence of brain necrosis at 24 hpf by brightfield microscopy. This prompted the hypothesis that loss of Ddx18 may result in an increase in cell death. Therefore to determine the contribution of increased cell death to the reduced numbers of myeloid cells observed in $ddx18^{hi1727/hi1727}$ mutants' acridine orange staining was performed on live $ddx18^{hi1727/hi1727}$ mutants and siblings at 24hpf. A marked increase in the number of acridine orange positive cells was observed in $ddx18^{hi1727/hi1727}$ mutants compared to control siblings (Figure 4–1), indicating an increased number of dying and/or dead cells. The acridine orange positive cells in $ddx18^{hi1727/hi1727}$ mutants were located predominantly in the head and spinal cord. No clear expression of cells in the regions where haematopoiesis was developing was observed at this time point.

4.4.2 TUNEL staining to assess apoptosis-cell death *ddx18*^{hi1727hi1727} mutants

To determine if the increase in cell death observed using acridine orange staining in *ddx18*^{hi1727/hi1727} mutants was a result of increased apoptosis resulting in nuclear fragmentation, the embryos were stained at the same stage (24 hpf) using TUNEL assay. TUNEL staining using anti-FITC antibody to detect labelled dUTP demonstrated a marked increase in TUNEL positive cells in *ddx18*^{hi1727/hi1727} mutants compared to their siblings (Figure 4–2). Distribution of TUNEL positive cells was similar to the acridine orange positive cells in *ddx18*^{hi1727/hi1727} mutants.

Figure 4-1 : Acridine orange staining shows increased cell death in *ddx18*$^{hi1727/hi1727}$ mutants

Legend Figure 4-1 : Acridine orange (AO) staining of *ddx18*^{hi1727hi1727} mutants (lower panel) and WT/siblings (upper panel) at 24 hpf. There is a marked increase in AO positive cells in *ddx18*^{hi1727hi1727} mutants compared to siblings. Staining is most prominent in the head and spinal cord regions. Note green background fluorescence in the yolk.
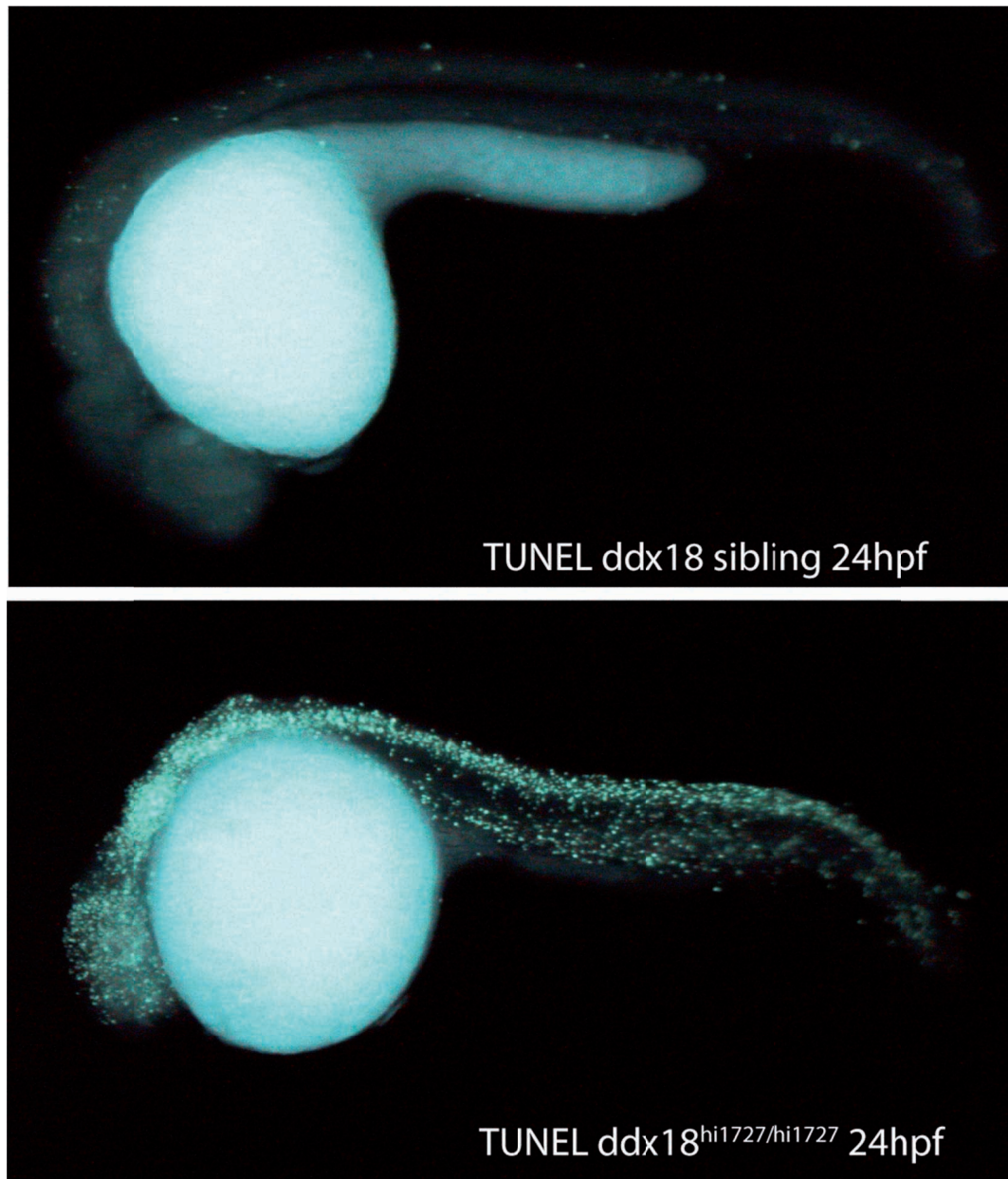
Figure 4-2 : Increased TUNEL staining in *ddx18*$^{hi1727/hi1727}$ mutants

Legend Figure 4-2 : TUNEL staining of *ddx18*^{hi1727hi1727} mutants (lower panel) and WT/siblings (upper panel). *ddx18*^{hi1727hi1727} mutants show a marked increase in TUNEL positive cells. Background fluorescence is observed in the yolk.

4.4.3 Confirmation of apoptosis using activated caspase-3 immunofluorescent staining showed localisation to the site of haematopoiesis

Activation of caspases occurs following initiation of apoptosis as a result of mitochondrial outer membrane permeablisation (MOMP). Activated caspase-3 is a heterodimer of the 12kD and 17kD fragments that result from the cleavage of pro-caspase-3 during apoptosis. Thus active anti-caspase-3 antibody staining represents a marker of active apoptosis.

Consistent with our observations using AO staining and TUNEL assay, activated caspase-3 staining was markedly increased in the $ddx18^{hi1727/hi1727}$ mutants compared to that of WT/siblings (Figure 4.3). In contrast to AO staining and TUNEL assay results, activated caspase-3 staining was preferentially localised in the posterior blood island/CHT where blood cells (particularly erythroid cells) are developing (Figure 4.3, yellow arrows) as well as in the head and spinal cord regions. However, activated caspase-3 staining is less specific for apoptosis than TUNEL staining, as non-apoptotic roles for caspase-3 have been described (Ribeil et al, 2007), and might explain why localisation of increased cell death or apoptosis identified by acridine orange staining or TUNEL assay was not observed in this area. In view of these findings, the TUNEL assay was chosen as the preferred method for detection of apoptotic cells in mutant zebrafish in subsequent experiments.
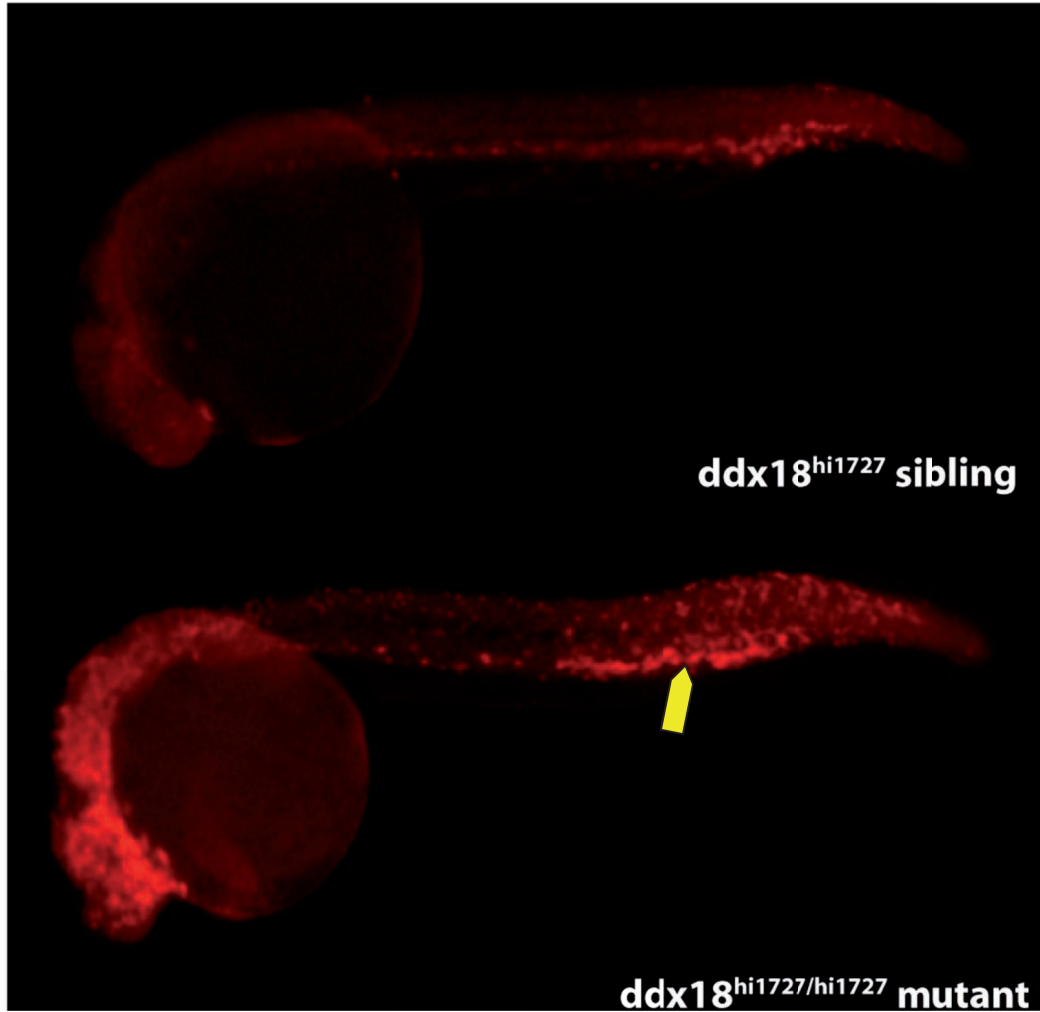
Figure 4-3 : Increased activated caspase-3 in *ddx18*^{hi1727/hi1727} mutants

Legend Figure 4-3: Activated caspase-3 antibody staining in *ddx18*^{hi1727hi1727} mutants (lower panel) and WT/siblings (upper panel) at 27 hpf . There is an increase in the amount of activated caspase-3 positive cells in the *ddx18*^{hi1727hi1727} mutants with localisation of caspase positive cells in the posterior blood island (yellow arrow).

4.4.4 *ddx18^{hi1727hi1727}* mutants show G1 cell cycle arrest

The effect of loss of Ddx18 on the cell cycle was chosen next for examination. DNA content analysis showed cells from *ddx18$^{hi1727/hi1727}$* mutants were blocked in the G1 phase of the cell cycle with a concurrent reduction of cells in S phase and G2/M phases. (Figure 4–4, left hand panels). To confirm that this disruption of cell cycling occurred in myeloid lineage haematopoietic cells of *ddx18$^{hi1727/hi1727}$* mutants, the experiment was also performed using *ddx18$^{hi1727/hi1727}$* mutant and WT/sibling embryos derived from the transgenic zebrafish line *Tg(pu.1:EGFP)* after purification of myeloid haematopoietic cells using flow-cytometric sorting of GFP-positive cells. A marked increase in the proportion of myeloid haematopoietic cells in G1 phase (with 2N complement of DNA) with a concomitant reduction in the portion of myeloid haematopoietic cells in S and G2 phases was seen in *ddx18$^{hi1727/hi1727}$* mutant myeloid cells compared with myeloid cells from WT/sibling embryos (Figure 4–4, right hand panels). The degree of G1 cell cycle arrest, determined by the increase in the proportion of cells in G1 seen in *ddx18$^{hi1727/hi1727}$* mutants compared to WT/sibling embryos, was similar in cells from whole embryos and purified myeloid cells from *Tg(pu.1:EGFP).* To examine cell cycle disturbance in *ddx18$^{hi1727/hi1727}$* mutants immunofluorescence was performed using an antibody directed against phosphorylated histone H3 at serine 10 (pH3). This phosphorylation event is specific to cells in mitosis occurring in late prophase. Thus the expression pattern of pH3 gives an indicator of cells undergoing mitotic division. As shown in Figure 4–5 *ddx18$^{hi1727/hi1727}$* mutants have a marked reduction in pH3 positive cells compared with siblings, confirming the reduction in G2/M phase observed by DNA content analysis.

Legend Figure 4-4 : Cell cycle analysis determined by measurement of DNA content using propidium iodide. Left panels show whole embryo lysates at 24 hpf and right panels show purified myeloid haematopoietic cells from *Tg(pu.1:EGFP);ddx18^{hi1727hi1727}* mutant or WT/sibling embryos at the same time point. *ddx18^{hi1727hi1727}* mutant embryos show a marked increase in the proportion of cells in G1 phase and a reduction in the proportion of cells in S-G2/M consistent with G1 cell cycle arrest.

Whole embryo suspensions

Hi1727 Siblings 24hpf

G1: 52.77 %
G2: 7.98 %
S: 39.25 %

Hi1727 Mutants 24hpf

G1: 77.84 %
G2: 3.54 %
S: 18.62 %
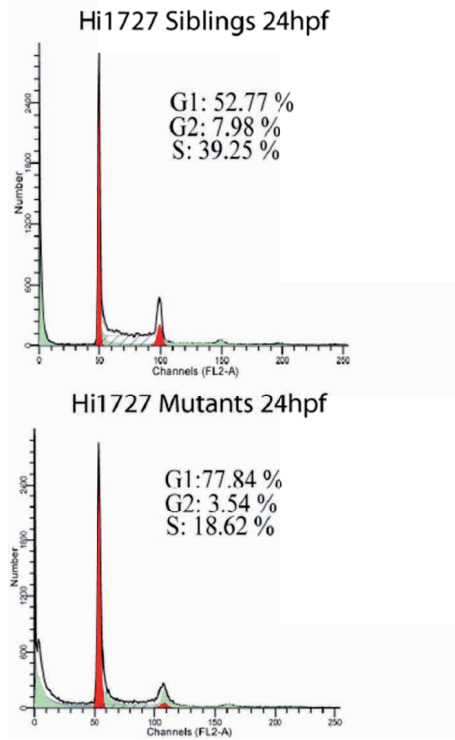
FACS-sorted pu.1-EGFP-expressing cells

SIBLINGS
G1:48.4%
G2:4.7%
S: 46%

MUTANTS
G1:73.4%
G2:2.3%
S: 24.4%
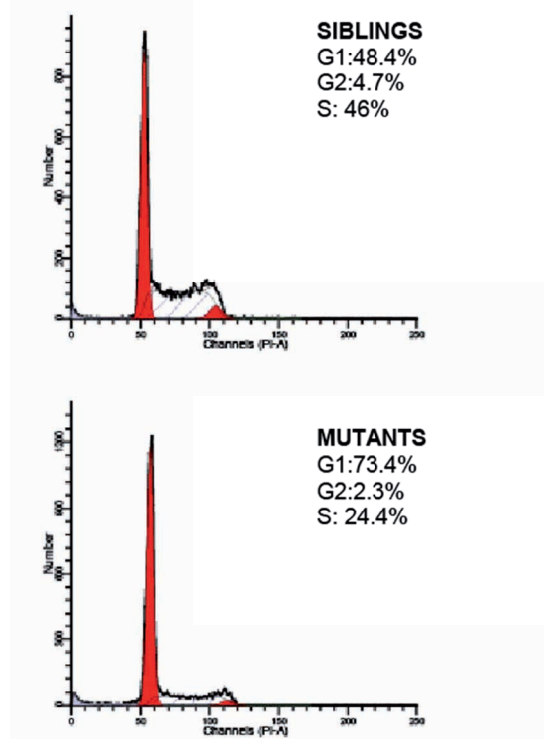
Figure 4-4 : *ddx18*[hi1727/hi1727] mutant zebrafish have G1 cell cycle arrest
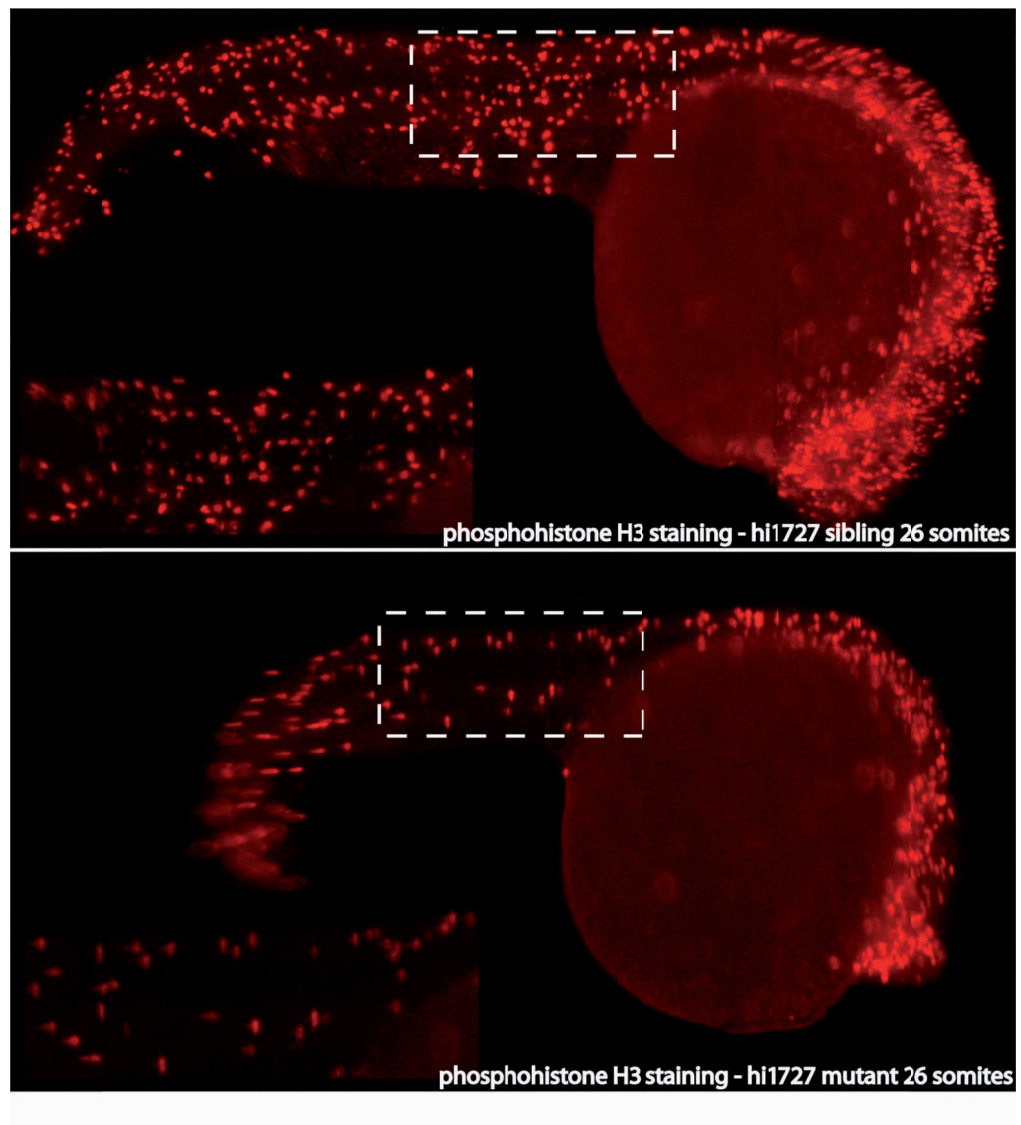
Figure 4-5 : Phosphohistone H3 serine 10 immunofluorescence

Legend Figure 4-5 : Immunofluorescence for phosphorylated histone H3 (serine 10) at 26 somites (22 hpf) shows a reduced number of pH3 positive cells (indicating fewer cells in M phase of the cell cycle) in *ddx18^{hi1727hi1727}* mutants compared to WT/siblings.

4.4.5   Knockdown of p53 resulted in rescue of *ddx18^{hi1727hi1727}* mutant phenotypes

The function of p53 in regulation of cellular integrity in response to ribosomal stress and the likely conserved role of Ddx18 in ribosome biogenesis led to the hypothesis that loss of Ddx18 may activate and/or stabilise the *p53* tumour suppressor gene. p53 plays a central role in apoptosis and both the G1 and G2 phases of the cell cycle although the specific cues to activate transcriptional targets to induce one or other (or both) responses are not fully understood.

To test whether the increased apoptosis or the cell cycle arrest observed in *ddx18$^{hi1727/hi1727}$* mutants was dependent on p53 function, *p53* was knocked down in *ddx18$^{hi1727/hi1727}$* mutants using morpholinos to address whether this would alter the phenotype of the *ddx18$^{hi1727/hi1727}$* mutants.   A *p53* morpholino blocking the 5'UTR (Langheinrich et al, 2002) was injected into the one-cell stage of embryos obtained from *ddx18$^{hi1727/+}$* heterozygous in-crosses.

Morpholino knockdown of p53 rescued developmental defects associated with *ddx18$^{hi1727/hi1727}$* mutants during the first 48 hpf, such that mutant embryos could not be distinguished from their siblings. Only after 48 hpf did occasional mutant embryos became apparent consistent the transient biological effect of morpholinos.   Figure 4–6 shows genotyping of embryos injected with *p53* morpholino with normal morphology, along-side "monsters" (presumed injection artefacts) and uninjected embryos showing mutant morphology. The genotyping confirmed that some of the embryos with WT morphology are mutants, and "monsters" contain embryos of all genotypes while all the mutants in the uninjected clutch were all correctly identified. This result shows that p53 loss rescued *ddx18$^{hi1727/hi1727}$* mutants from early developmental effects.

To determine if *p53* knockdown also rescued the myeloid phenotype of *ddx18$^{hi1727/hi1727}$* mutants, myeloid cell numbers were quantified using ISH for *mpx* in *p53* MO-injected and uninjected clutches of *ddx18$^{hi1727/hi1727}$* mutants and WT/siblings at 48 hpf (Figure 4–7). Knock-down of p53 in *ddx18$^{hi1727/hi1727}$* mutants resulted in a statistically significantly greater number of myeloid cells when compared to uninjected mutants (p<0.0001), such that numbers of myeloid

cells in p53 knocked-down $ddx18^{hi1727/hi1727}$ mutants were not statistically significantly different from the numbers seen in WT animals (Figure 4–8).

Legend Figure 4-6: Genotyping of individual embryos based on morphological developmental phenotype injected with *p53* morpholino or no morpholino. Embryos were visualised using brightfield microscopy at 30 hpf and phenotype characterised as WT, "monsters" or mutants. There were no phenotypic mutants seen in the embryos injected with *p53* morpholino. "Monsters" were deemed to be associated with injection artefact since they contained *ddx18^{hi1727hi1727}* mutants, heterozygotes and WT siblings (middle panel). Phenotypically WT embryos injected with p53 MO included *ddx18^{hi1727hi1727}* mutants (top panel) while all *ddx18^{hi1727hi1727}* mutants identified from uninjected siblings were confirmed as mutants (lower panel), thus confirming rescue of the developmental phenotype of *ddx18^{hi1727hi1727}* mutants with loss of p53.

Legend Figure 4-7: *ddx18^{hi1727}* embryos at 48 hpf injected with *p53* morpholino (top panel) or uninjected (lower panels). Mutants are clearly identifiable by morphology and reduced myeloid cell number (lower pane) compared to siblings (middle panel). Embryos injected with p53 morpholino could not distinguish between mutants and siblings (top panel).

Legend Figure 4-8: Quantification of myeloid cell numbers by ISH for *mpx* from the embryos in Figure 4-7. p values are for unpaired students t-tests.
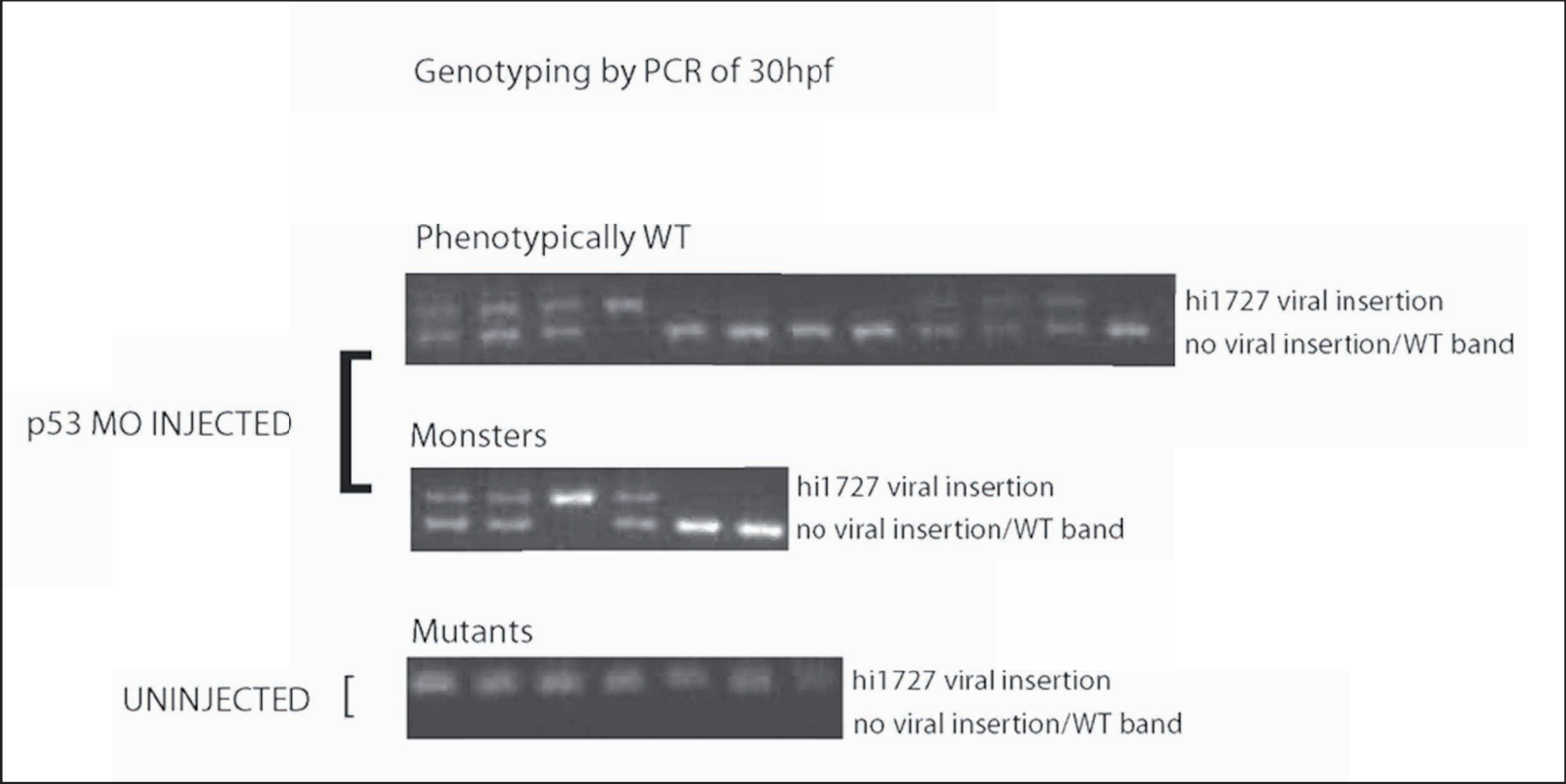
Figure 4-6 : *p53* morpholino rescues the developmental defects of *ddx18*$^{hi1727/hi1727}$ mutants
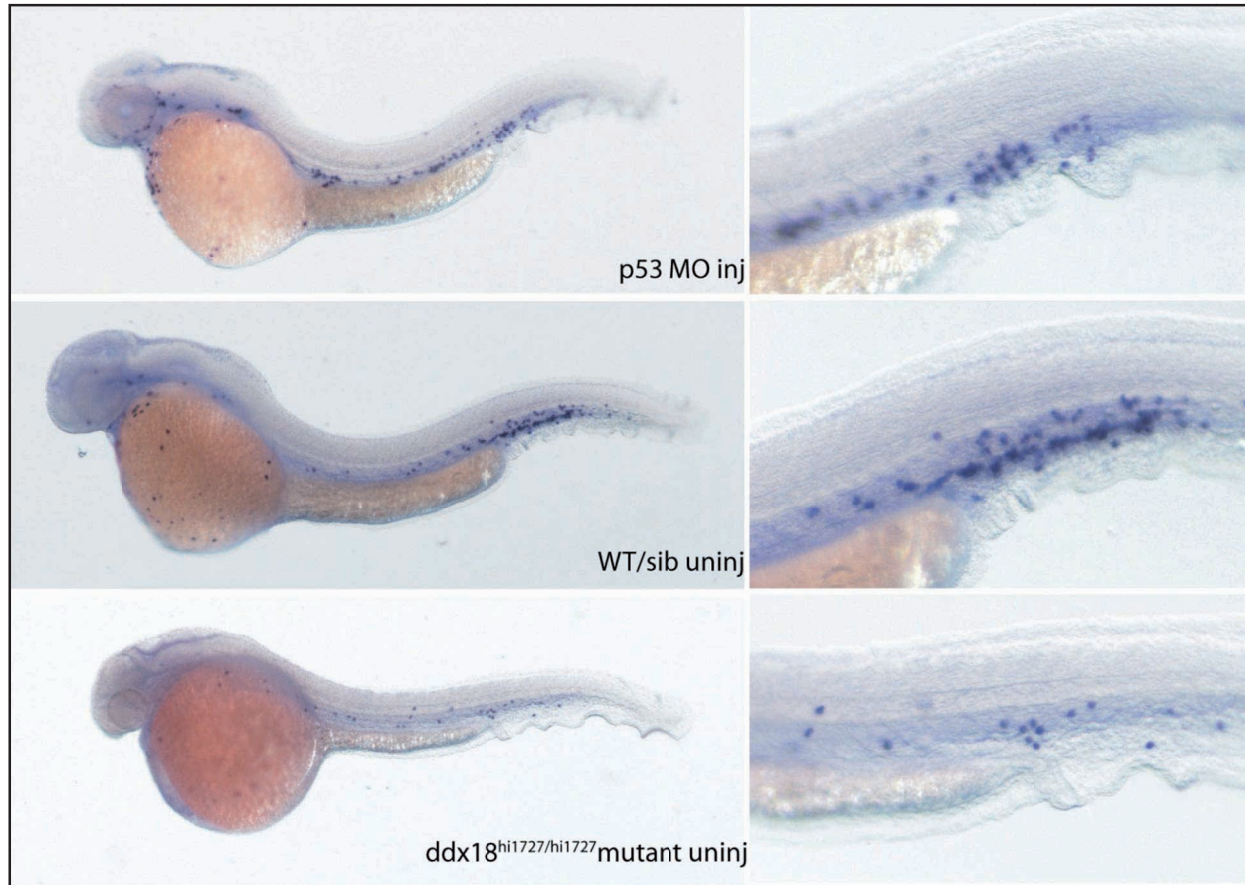
Figure 4-7 : *p53* morpholino rescues myeloid cell number in *ddx18*^hi1727/hi1727^ mutants
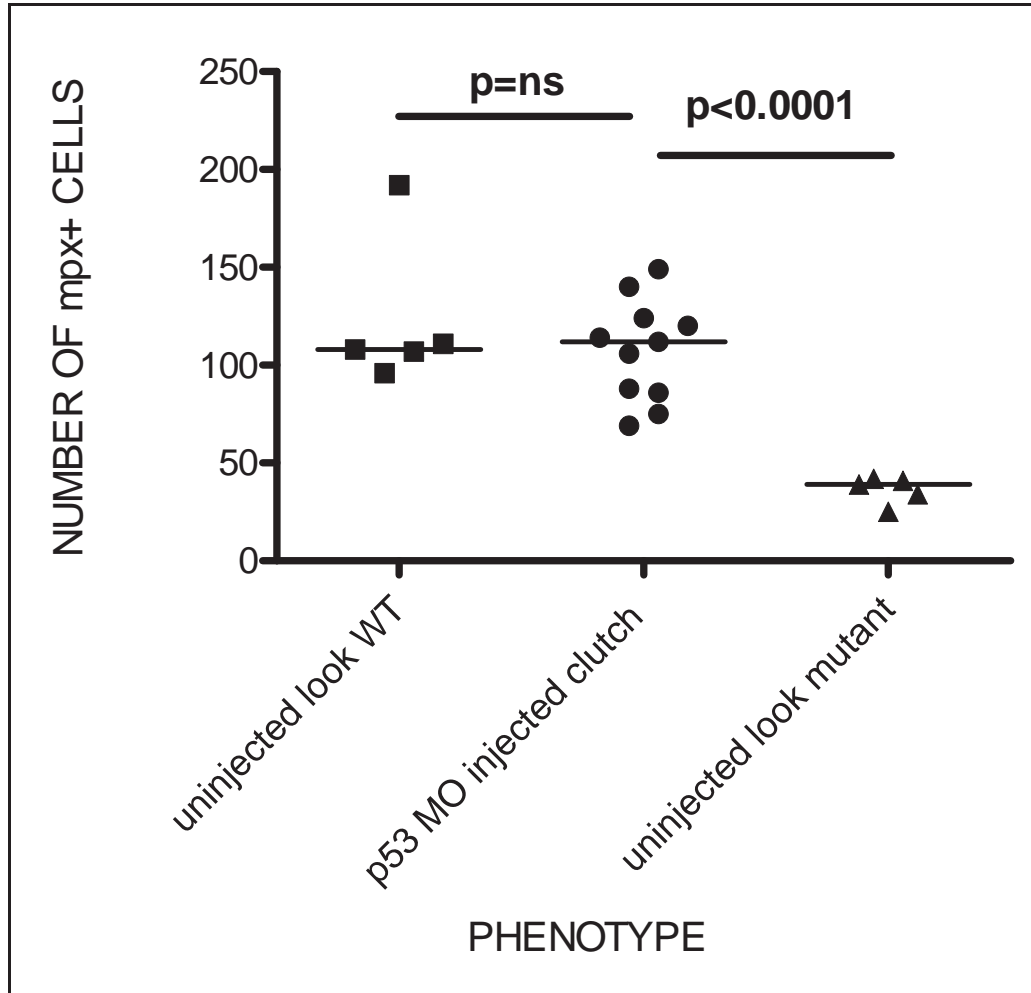
Figure 4-8 : Number of *mpx*+ cells in uninjected WT, *p53* knockdown *ddx18*^{hi1727/hi1727} and siblings and uninjected *ddx18*^{hi1727/hi1727} clutches

I next chose to investigate whether stable loss of p53 function might rescue *ddx18*^{hi1727/hi1727} mutants from lethal developmental defects. I therefore used a *p53* mutant zebrafish line which carries a mutation within the DNA binding domain of the *p53* gene in exon 7 ($p53^{e7/e7}$ or $p53^{m/m}$). This line has been characterised and results in resistance to irradiation-induced cell death and cell cycle arrest in response to irradiation suggesting that this allele is functionally null (Berghmans et al, 2005). In addition this line is prone to development of malignancy, predominantly peripheral nerve sheath tumours. I crossed *ddx18*^{hi1727/+} adults into the $p53^{e7/e7}$ and assessed whether the progeny of *ddx18*^{hi1727/+} ;$p53^{e7/e7}$ were able to survive. The clutches were monitored for gross developmental abnormalities daily. By 2 dpf some embryos began to demonstrate features of *ddx18*^{hi1727/hi1727} mutants similar to what was observed in *p53* MO injected *ddx18*^{hi1727/hi1727} clutches (Figure 4–9). In particular the cardiac chambers appeared to lack normal folding and contractility (see attached movies). In addition at 2 weeks of age 20 larvae were randomly genotyped to determine whether any *ddx18*^{hi1727/hi1727} homozygous mutant fish could survive in the *p53* mutant background, but no mutants were recovered. Thus while both developmental and haematopoietic defects in *ddx18*^{hi1727/hi1727} mutant zebrafish were transiently rescued by loss of p53, p53 loss was insufficient to rescue *ddx18*^{hi1727/hi1727} mutants from lethality by 5 dpf. Morphologic examination of the embryos indicated cardiovascular failure was the likely cause of death.
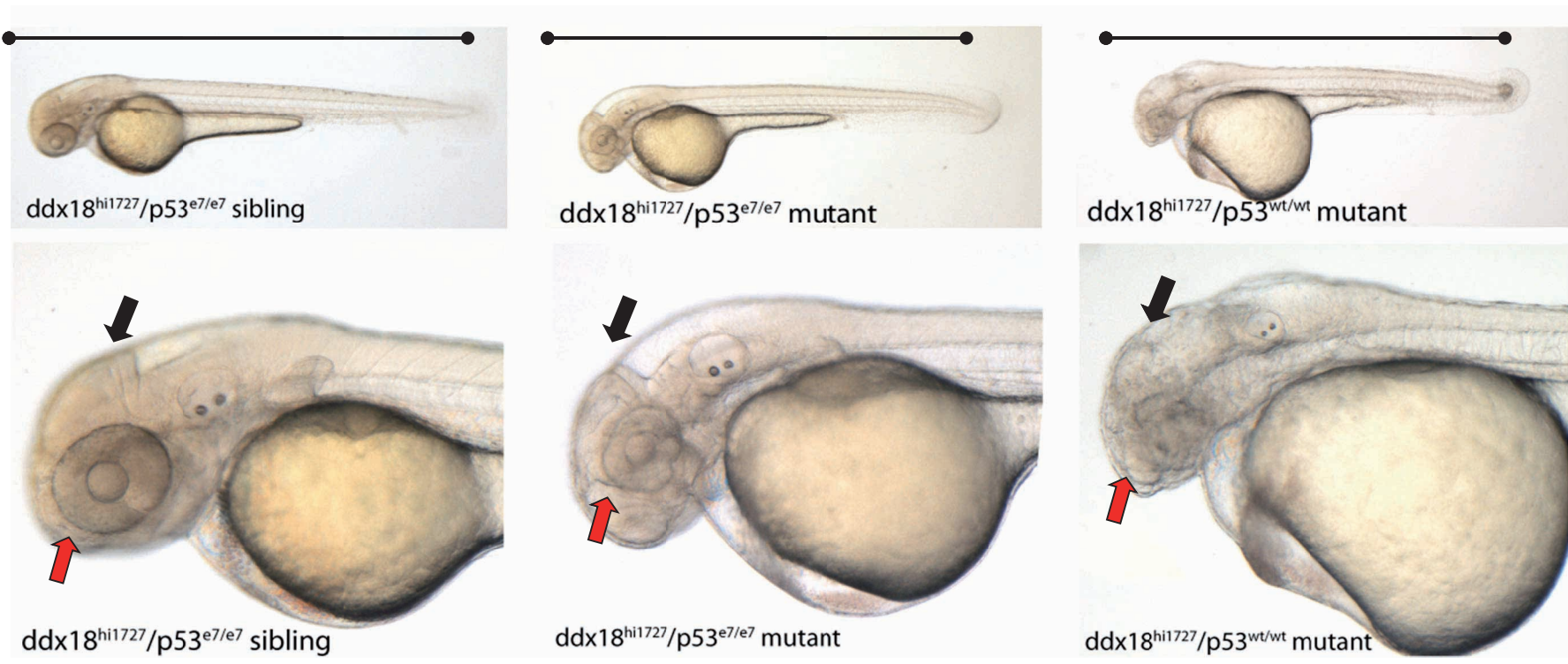
Figure 4-9 : Developmental morphology of *ddx18*^{hi1727/hi1727} mutants and siblings +/- *p53*^{e7/e7}

Legend Figure 4-9: *ddx18$^{hi1727/+}$;p53$^{e7/e7}$* siblings (left) and double mutants (middle) and *ddx18$^{hi1727/hi1727}$; p53$^{WT/WT}$* (right panel) at 48 hpf. Many developmental defects are rescued by the loss of p53 (*ddx18$^{hi1727/hi1727}$; p53$^{e7/e7}$* (middle) compared with *ddx18$^{hi1727/hi1727}$; p53$^{WT/WT}$* (right panel); however, *ddx18^{hi1727hi1727}; p53$^{e7/e7}$* double mutants show smaller eyes (red arrow), mild cerebral oedema (black arrow) and shorter body axis (black bar-belled line) than *ddx18^{hi1727}; p53$^{e7/e7}$* siblings (left).

4.4.6 *p53*-dependent G1 cell cycle arrest resulted in loss of myeloid cells in *ddx18$^{hi1727/hi1727}$* mutants while apoptosis does not.

Since p53 stabilisation can result in both disruption of the cell cycle and in increased apoptosis, and *ddx18^{hi1727}* mutants showed evidence of both these processes, I sought to determine the relative contributions of G1 cell cycle arrest and apoptosis to the myeloid and developmental phenotypes observed in *ddx18^{hi1727}* mutants. To do this, the finding that over expression of the Bcl2-family member Bcl-xl is able to rescue cell death induced by irradiation in zebrafish embryos was utilised (Sidi et al, 2008). Bcl-xl acts by inhibiting pro-apoptotic proteins such as BH3 only proteins Puma, Noxa and Bid, therefore protecting mitochondria from MOMP, cytochrome C release and activation of executioner caspases. Critically, the effects of Bcl-xl occur downstream of p53 stabilisation and have little or no effect on cell cycle. Therefore phenotypes rescued by p53 loss and Bcl-xl overexpression are likely to be related to apoptosis whereas phenotypes rescued by p53 loss but not Bcl-xl are likely to be as result of p53-dependent effects on the cell cycle.

Both the developmental defects and the reduced number of myeloid cells observed in *ddx18$^{hi1727/hi1727}$* mutants were rescued by knockdown of *p53* but not by Bcl-xl overexpression at 27 hpf (Figure 4–10). For this experiment, *ddx18$^{hi1727/hi1727}$* mutants were identified based on the expression of *ddx18* RNA by ISH (red) which is virtually absent in *ddx18$^{hi1727/hi1727}$* mutants.
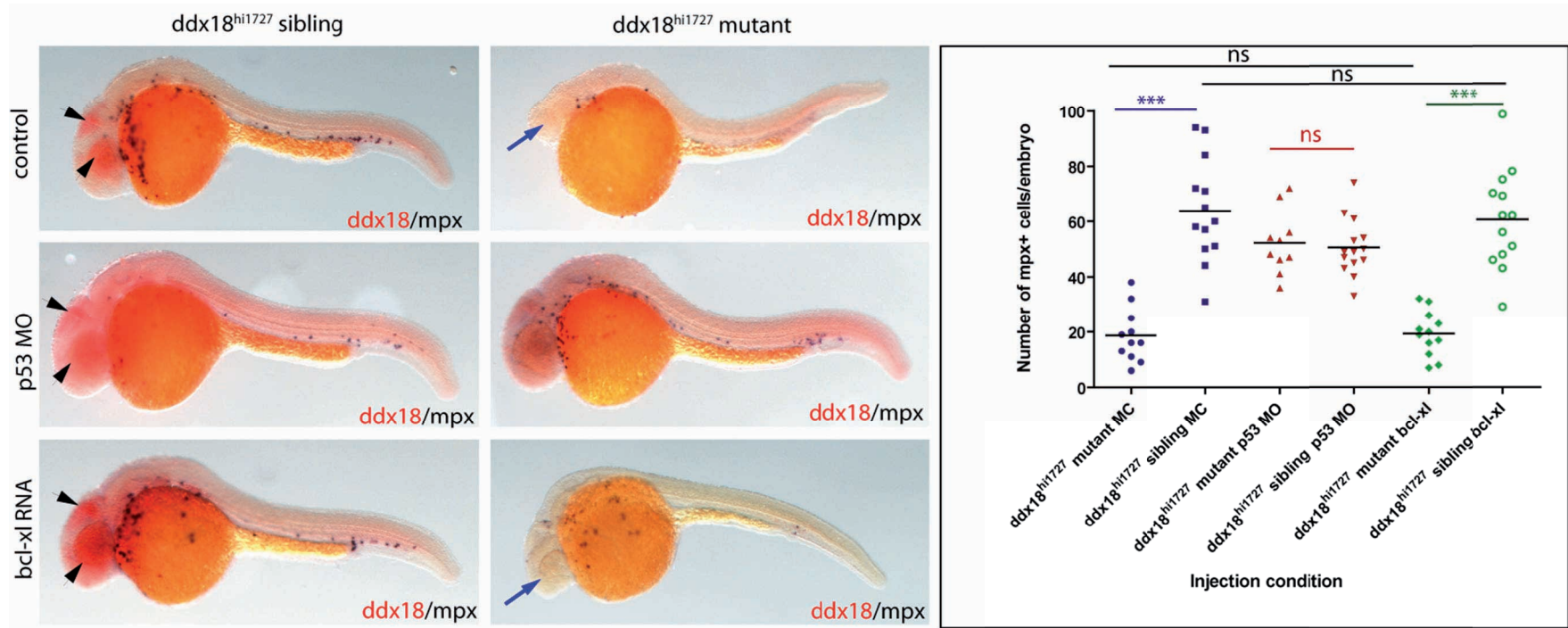
Figure 4-10 : *p53* morpholino but not Bcl-xl RNA rescues *ddx18*^{hi1727/hi1727} mutants

Legend Figure 4-10 : Left panels show double in situ hybridisation for *mpx* (black/blue) and *ddx18* red) siblings on the left and *ddx18^hi1727/hi1727* mutants on the right. Controls are shown on the top injected with mCherry (MC)-encoding RNA (10pg). Middle row shows *p53* MO (200μM) injected embryos and bottom row shows Bcl-xl (10pg) injected embryos. Expression of *ddx18* is seen mainly in the head in the ventricles and eye (black arrowheads) absent or minimal in the *ddx18^hi1727/hi1727* mutants. Bcl-xl injected *ddx18^hi1727/hi1727* mutants show reduced brain necrosis by brightfield microscopy (not shown), evident by clearer delineation of head structures compared to controls as highlighted in the eye (blue arrow). The graph on the right shows individual *mpx*-cell counts per embryo for each condition. ***p<0.0001 (students t test). ns= not significant.
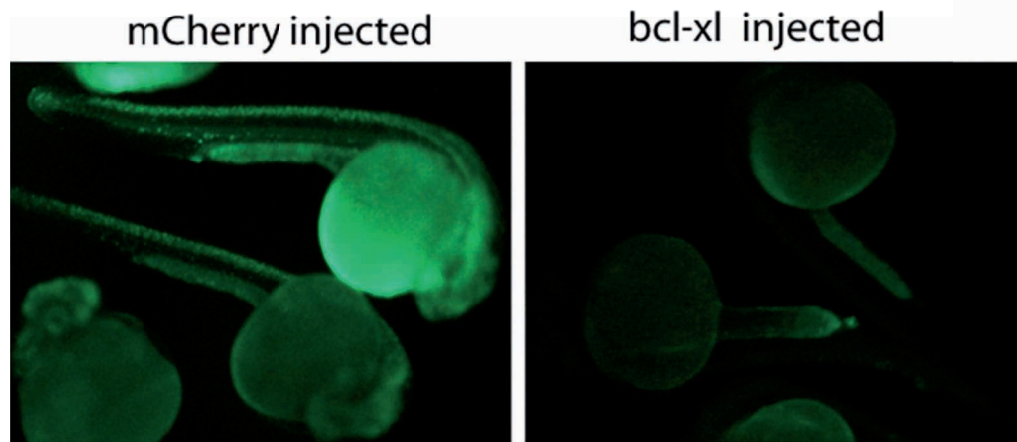
Figure 4-11 : Bcl-xl-encoding RNA prevents irradiation induced apoptosis

Legend Figure 4-11: Acridine orange staining to identify cell death in embryos irradiated with 12Gy of gamma irradiation. AO staining was performed on live embryos 6 hours pos irradiation. *bcl-xl* injected embryos show an absence of dead/dying (green fluorescent) (right panel) cells compared to control (mCherry) (left panel) injected cells. Mild auto-fluorescence is noted in the yolk in both control and *bcl-xl* injected embryos.

While injection of Bcl-xl clearly did not rescue the developmental defects or the reduction in myeloid cell numbers observed in *ddx18*$^{hi1727/hi1727}$ mutant zebrafish, clearer delineation of head structures in embryos injected with Bcl-xl suggested that these animals has less necrosis in this region (Figure 4–10) giving a surrogate indication that the injected Bcl-xl indeed prevented apoptosis in injected embryos. However, to conclusively demonstrate that the overexpression of Bcl-xl was able to prevent cell death in *ddx18*$^{hi1727/hi1727}$ mutant zebrafish, a portion of the clutch of Bcl-xl-injected or control-(mCherry) injected *ddx18*$^{hi1727/hi1727}$ mutant zebrafish were removed and irradiated at 24 hpf with 12Gy of gamma irradiation. Six hours post irradiation embryos were stained with acridine orange. Control injected embryos showed widespread acridine orange positive cells in the spinal cord, head and scattered through the rest of the body while virtually no positive cells are seen in the Bcl-xl injected embryos (Figure 4–11) demonstrating that Bcl-xl injection was able to rescued cell death in *ddx18* mutant zebrafish and siblings.

4.5 Chapter discussion

The primary aim in this chapter was to delineate the relative contributions of cell death and cell cycle arrest to the reduced numbers of haematopoietic cells observed in *ddx18*$^{hi1727/hi1727}$ mutants. The evidence presented suggests that there is an increase in cell death in *ddx18*$^{hi1727/hi1727}$ mutants compared to siblings based on acridine orange, activated caspase-3 and TUNEL staining. There was however discordance between the localisation of dying cells using different assays, with an increase in activated caspase-3 staining in the blood-forming regions of the embryos, but no clear increase in TUNEL staining in the same region. This observation may reflect the different sensitivity and specificities of the assays. Another potential explanation for these findings is the existence of a specific time window during which cell death in haematopoietic cells is most prominent. However, this possibility was excluded by performing the TUNEL assay at multiple time points in WT/sibling and *ddx18*$^{hi1727/hi1727}$ mutant zebrafish. The number and location of cells dying did not change over time from 18 somites to 48 hpf cell death was not localised to haematopoietic areas at any time point. The increased activated caspase-3 antibody staining seen in the posterior blood island could therefore be explained by non-apoptotic related staining. Activated caspase-3 is known to be highly expressed during erythroid differentiation. This is

thought to be associated with the enucleation of erythroid cells (which requires the DNA fragmentation associated with caspases and is also seen during enucleation of cells in other tissues such as the lens). It is not clear if this represents a non-apoptotic role of capase-3 or if other factors allow the cell to survive while caspase-3 "apoptoses" the nucleus (reviewed in Yi & Yuan, 2009). The latter hypothesis is favoured by the observation that in the absence of the chaperone heat-shock protein 70 (Hsp70), cleavage of the transcription factor *Gata-1* occurs and the cell dies (Ribeil et al, 2007). This role of capsase-3 in erythroid cells is insufficient in itself to explain the presence of activated caspase-3 in the zebrafish posterior blood island since mature erythroid cells retain their nuclei in teleost fish. Nonetheless, taken together with the observation that cell death was not observed in this region using acridine orange staining it seems unlikely that the activated caspase-3 staining seen in *ddx18*$^{hi1727/hi1727}$ mutants was reflective of haematopoietic cells undergoing increased apoptosis.

ddx18$^{hi1727/hi1727}$ mutants showed an increase in cells in the G1 phase of the cell cycle, with reduction of cells in S phase and G2. There was also a corresponding reduction in mitotic cells in *ddx18*$^{hi1727/hi1727}$ mutants compared to siblings using whole mount staining for phosphorylated histone H3 on serine 10. To confirm whether this effect was observed in haematopoietic cells, the transgenic line *Tg(pu.1:GFP)* crossed to *ddx18*$^{hi1727/+}$ was used. PI analysis of DNA content was carried out on GFP positive cells sorted from *Tg(pu.1:GFP)* ;*ddx18*^{hi1727} mutants and siblings and a G1 cell cycle arrest was observed in GFP positive cells. There are several lines of evidence to support the findings that Ddx18 loss disrupts cell cycle. Ddx18 is a highly conserved protein whose yeast orthologue is required for several components of ribosome biogenesis (Emery et al, 2004; Liang & Fournier, 2006). Ribosomal function is closely linked with cell cycle regulation. rRNA transcription by RNA pol I is tightly regulated throughout the cell cycle, with levels of rRNA increasing during G1, remaining high during S and G2 and dropping markedly during M phase reflecting preparation to divide (G1 phase) and protein producing capacity (in the form of ribosomes) to adequately synthesise the protein components (S phase) to facilitate cell division. The major regulator of rRNA transcription is transcription factor upstream binding factor 1 (UBF1) which binds rDNA regions dependent on phosphorylation status. Further evidence linking cell cycle control and ribosome biogenesis is provided by the observation that many genetic mutants resulting in small cell size are associated

134

with disruption of cell cycle regulatory factors or ribosome biogenesis factors (Jorgensen et al, 2002; Jorgensen & Tyers, 2004; Lambertsson, 1998; Liang & Fournier, 2006). It is well established that a critical cell size is required for entry into the cell cycle in yeasts (Nurse et al, 1998). It is not however clear whether or not there is a direct mechanism whereby cell cycle progression is affected by ribosome production per se or if aberrant ribosome biogenesis simply reduces cell growth and size secondary to reduced global protein production, thus limiting entry into the cell cycle. Finally it is clear that the P53 tumour suppressor and its major negative regulator, the E3 ubiquitin ligase MDM2 (HDM2 in humans) are responsible for the maintenance of deregulated ribosomal protein production. This occurs via MDM2 sequestration by free RPL11 or degradation by other means in turn leading to cell death and or cell cycle arrest in a p53–dependent manner.

The experiments described in this chapter suggest that both cell death and cell cycle arrest are increased in $ddx18^{hi1727/hi1727}$ mutants. Both these mechanisms appear to occur throughout the whole embryo, suggesting that Ddx18 is an essential gene for development of a both haematopoietic and non-haematopoietic tissues. Although the data herein conclusively show that myeloid cells in $ddx18^{hi1727/hi1727}$ mutants have disrupted cell cycling, albeit it has not been possible to demonstrate that increased apoptosis seen in $ddx18^{hi1727/hi1727}$ mutants occurs specifically within haematopoietic tissues.

Since Ddx18 has been linked to ribosomal function, and activation of the p53 pathway has been described in association with ribosomal stress, experiments were performed to determine if the phenotype observed in $ddx18^{hi1727}$ mutants was dependent on p53. Loss of P53 rescued the majority of developmental defects in $ddx18^{hi1727/hi1727}$ mutants until around 2 dpf. Beyond 2 dpf p53-deficient $ddx18^{hi1727/hi1727}$ mutants become distinguishable from their siblings by exhibiting some of the features of p53-replete counterparts, including small size, small eyes and mild brain oedema. By 5 dpf $ddx18^{hi1727/hi1727}$ mutants account for 25% of the clutch of embryos based on morphological phenotype. They show cardiac abnormalities in folding and contractility.

To shed light on whether cell cycle arrest or apoptosis was the dominant mechanism effecting $ddx18^{hi1727/hi1727}$ mutants a rescue experiment was

performed using either *p53* morpholino or Bcl-xl RNA. Over expression of Bcl-xl was not able to rescue *ddx18*$^{hi1727/hi1727}$ mutant developmental or myeloid phenotypes while morpholino-mediated knockdown of p53 resulted in rescue of both developmental and myeloid phenotypes. Bcl-xl is a pro-survival protein of the Bcl2 family that sequesters pro-apoptotic proteins to inhibit MOMP and cytochrome c release from the mitochondrion. MOMP is downstream of p53 stabilisation in the process of apoptosis and is the major stimulus for activation of caspases resulting in formation of the apoptosome and subsequent apoptosis. Although there is some evidence that Bcl-xl is regulated in a cell cycle-dependent manner, by far its major role is as an anti-apoptotic protein. It was confirmed that Bcl-xl protected the injected embryos from apoptosis by irradiating them with 12Gy and subjecting them to AO 6 hours post irradiation. Thus since the *ddx18*$^{hi1727/hi1727}$ mutants are not rescued by Bcl-xl over expression, but are rescued by p53 loss, this suggests the p53-dependent cell cycle arrest rather than apoptosis is the dominant mechanism by which *ddx18*$^{hi1727/hi1727}$ developmental and haematopoietic defects arise.

In summary the loss of Ddx18 results in both increased apoptosis and p53-dependent cell cycle arrest, with the latter representing the dominant mechanism underlying the abnormal phenotype observed in *ddx18*$^{hi1727/hi1727}$ mutants. Further studies in this area could address which precise mediators of the cell cycle machinery result in G1 arrest. The most likely mechanism based on the current literature for ribosomal protein loss-mediated ribosomal stress is via Mdm2. Future studies could investigate whether or not over expression of MDM2 can rescue the observed phenotype.

5. *DDX18* sequence variants in human haematopoietic diseases

5.1 Introduction

Knockout murine models have shown that several tumour suppressors known to be disrupted in human AML patients also have a role in developmental myelopoiesis (McKercher et al, 1996; Zhang et al, 1997). These observations have led to the hypothesis that genes required for embryonic myelopoiesis will not only further our understanding of developmental haematopoiesis but may also act as tumour suppressors in human myeloid malignancies including AML and MDS. There is increasing evidence that genes involved in ribosome biogenesis play a specific role in maintenance of haematopoiesis (Narla & Ebert, 2010). Therefore ribosomal genes, including *DDX18*, are candidate tumour suppressors that could be disrupted or mutated in human AML/MDS. To test this hypothesis, 78 peripheral blood/BM samples were sequenced from adult patients with AML and MDS for mutations in the coding regions of the *DDX18* gene. This sequencing identified non-synonymous single nucleotide sequence variants (nsSNSV) in two of these samples. Therefore, a further cohort of 98 AML and 98 MDS patient samples were sequenced in collaboration with Dr Ross Levine at Memorial Sloane Kettering (New York, USA). This resulted in the identification of a further sequence variant, a 3bp deletion resulting in deletion of a single glutamic acid residue at position 76.

In addition, given its essential role in ribosome biogenesis, haematopoietic phenotype and the fact that all RP genes have now been sequenced *DDX18* is a good potential candidate gene involved in the pathogenesis of Diamond-Blackfan anaemia. Therefore, a further collaboration was established with Dr Hanna Gazda at Children's Hospital Boston, to sequence the coding regions of *DDX18* in 117 Diamond-Blackfan anaemia probands.

5.2 Aims of the experiments described in this chapter

1. To determine if *DDX18* is mutated in patients with AML/MDS
2. To determine if *DDX18* is mutated in patients with Diamond Blackfan anaemia
3. To determine functional consequences of *DDX18* nsSNSVs identified in AML patients

5.3 Materials and methods

5.3.1 Sequencing

Sequencing was performed exon by exon using gDNA bone marrow samples from adults with AML or MDS obtained from the Dana Farber Cancer Institute and also on 22 human AML cell lines. The sequencing was carried out by Agencourt Bioscience Corporation (Beverley, MA, USA). Traces were analysed using Mutation Surveyor software (Softgenetics LLC, PA, USA) Additional sequencing of larger cohort of samples from AML and MDS patients was carried out in collaboration with Dr Ross Levine at Memorial Sloane Kettering by Genewiz Inc. (South Plainfield, New Jersey) and DBA patient samples in collaboration with Dr Hanna Gazda (Children's Hospital Boston).

5.3.2 Bioinformatics assessment of nsSNSVs

Single nucleotide sequence variants were assessed for their potential to result in deleterious effects using three on-line software analysis tools – PANTHER 7 cSNP analysis, Polyphen and Polyphen-2 (Adzhubei et al; Brunham et al, 2005; Ramensky et al respectively) . More information can be found at www.pantherdb.org/tools and www.genetics.bwh.harvard.edu.

The computational methods applied by these software tools differ slightly. PANTHER applies a probability score of potentially deleterious nsSNSVs based on the evolutionary variability of amino acids at the given position. In contrast, Polyphen assesses the likelihood of a nsSNSV being damaging based on three main parameters: (i) the sequence based characteristics of the substitution (i.e. is it in a known defined domain of the protein), (ii) the position specific independent counts (PCIS) profile score which applies a logarithmic score to the probability of the amino acid substitution being deleterious based on blast searches for the altered sequence, (Sunyaev et al, 1997) and (iii) a calculation of structural parameters and contacts. Finally, Polyphen-2 updates this latter analysis to also include a broader assessment of evolutionary diversity based on multiple different sequence alignment strategies. This version of the software outputs information on the likelihood a nsSNSV is damaging in two formats. The first, HumDiv, is an assessment of the likelihood that a nsSNSV is damaging when inherited constitutionally. The second, HumVar, is the likelihood a nsSNSV is damaging where it is assumed to be an acquired mutation.

5.3.3 PCR-cloning of *hsDDX18-WT* into *pEGFP-C1*

Human *DDX18* was PCR-amplified from *pCMVSport* using a forward primer carrying 5' EcoR1 adapter and a reverse primer carrying a BamH1 adapter. The PCR product was run on a 0.8% agarose gel, excised and cloned into pCRII-TOPO. The sequence was confirmed using Sp6, T7 and internal *DDX18* primers. *pCRII-TOPO-EcoR1-hsDDX18-BamH1* and *pEGFP-C1* were digested with EcoR1 and BamH1, gel-purified and ligated together using overnight ligation at 1:3 molar ration at 16°C using T4 ligase (Roche) (Chapter 2.3.1).

5.3.4 Site-directed mutagenesis

Site-directed mutagenesis was carried out using the Stratagene quikchange PCR mutagenesis kit (Agilent Technologies Inc, CA, USA). Primers were designed using the the QuikChange® Primer Design Program (sequences can be found in Appendix 2) : More information can be found at

www.genomics.agilent.com/CollectionSubpage.aspx?PageType=Tool&SubPage Type=ToolQCPD&PageID=15.

Using the mutation-specific primers, the *pCS2+DDX18-WT* plasmid generated in Chapter 3, and *pEGFP-DDX18-WT* were amplified using PFUTurbo DNA polymerase (supplied in the kit) and then subjected to Dpn1 digestion. Since Dpn1 only can only digest plasmid DNA which has been methylated and almost all Escherichia Coli strains are Dam-methylated, any residual parental plasmid should be digested. Therefore following digestion the resultant DNA product should only contain the new mutated sequence-specific product. This was then transformed into XL1-Blue competent cells (also supplied with the kit) and single colonies selected, cultured and sequenced.

5.3.5 Cell culture

250,000 293T cells were seeded on glass coverslips in 35mm wells in 2ml of DMEM medium with 10% FBS, 1% penicillin/streptomycin and 1% glutamine. At the same time, 1µg of plasmid DNA was transfected using Fugene 6 (Roche Applied Science, Mannheim Germany) following manufacturer's instructions. 24 hours post transfection, cells were fixed in 4% paraformaldehyde (10 min) and rinsed twice in PBS in the well. Coverslips were then air-dried, flipped and

mounted on glass slides with 20μl of ProLong Gold anti-fade kit with DAPI (Molecular Probes, Carlsbad, CA).

Cells were visualised with a Zeiss Axio imager Z1 microscope using a Zeiss 63x/1.4 NA Apochromat Oil lens (Carl Zeiss, Thornwood, NY). Images were acquired with Openlab software (Perkin Elmer, Waltham, MA).

5.3.6 Co-immunoprecipitation

Cells were transfected as described above with 1μg of plasmid DNA, and then lysed in ice-cold RIPA buffer with protease inhibitors 24 hours post-transfection. 50 out of 500μg of protein lysate where used as input. The remaining was first immunoprecipitated with 2μg of a control unrelated IgG and 30μl of Protein G PLUS-Agarose (Santa Cruz Biotechnology, INC., Santa Cruz, CA) for 3 hrs rocking at 4° C, then the supernatant was immunoprecipitated with anti-GFP (Roche Applied Science) and 30μl of Protein G PLUS-Agarose (Santa Cruz Biotechnology, INC.) as above. Beads from the control IP and the anti-GFP IP where then washed in RIPA 4 times and finally suspended in lithium dodecyl sulphate (LDS) Sample Loading buffer (Invitrogen, Carlsbad, CA). Input and IP proteins were loaded and separated on a 4–12% NuPage Bis-Tris Gel (Invitrogen) and then transferred on a nitrocellulose membrane using standard protocols. The membrane was blocked 1 hour at room temperature with TBST-milk 5%, then incubated either of the following primary antibodies at 4°C overnight: anti-GFP Roche, 1:1000; anti-NPM1 mAb 376 (a kind gift from Prof. B. Falini, University of Perugia, Italy) 1:2; anti *DDX18* from Bethyl Laboratories, Montgomery, TX, 1:500). Following 4 washes in TBST, membranes were probed with secondary anti-mouse (1:30000, Pierce, Rockford IL) or anti-rabbit (1:10000, Cell Signaling Technology INC., Danvers, MA) HRP-conjugated antibodies. Following 4 washes in TBST the signal was detected using the SuperSignal West Pico Chemiluminescent Substrate (Pierce).

5.4 Results

5.4.1 Sequencing trace file analysis

5.4.1.1 AML/MDS patient cohort 1

78 patient samples and 22 cell lines were sequenced. All traces were inspected manually as well as computationally by Mutation Surveyor. nsSNSVs were

identified in two patients (3% of the cohort, Patient 33 and Patient 44) within the *DDX18* gene. Bidirectional sequencing was undertaken to confirm the presence of the variants. Figure 5-1 shows the sequencing traces analysed using Mutation Surveyor. Patient 33 had 2 distinct nsSNSVs, a heterozygous G to A substitution resulting in C183Y, and heterozygous G to A substitution resulting in V341I. Patient 40 had a single nsSNSV, a heterozygous G to A substitution resulting in V621I. Search of the dbSNP database and HapMap database did not identify these nsSNSVs as previously recorded SNPs.

5.4.1.2 AML/MDS patient cohort 2

Following identification of the three *DDX18* sequence variants in AML patients detailed above, a further cohort of 98 AML and 98 MDS patient samples were sequenced by Genewiz Inc in collaboration with Dr Ross Levine at MSK. This identified a further AML patient with an out of frame 3bp AAG deletion resulting in the deletion of glutamic acid at position 76 within the DDX18 amino acid sequence (Figure 5–1).

5.4.1.3 DBA patient cohort

Sequencing of *DDX18* in 117 DBA patients did not identify any mutations or nsSNSVs in the *DDX18* gene.

Legend Figure 5-1: DNA sequencing trace from Mutation Surveyor identifying 4 sequence variants within the *DDX18* gene in 3 patients with AML.
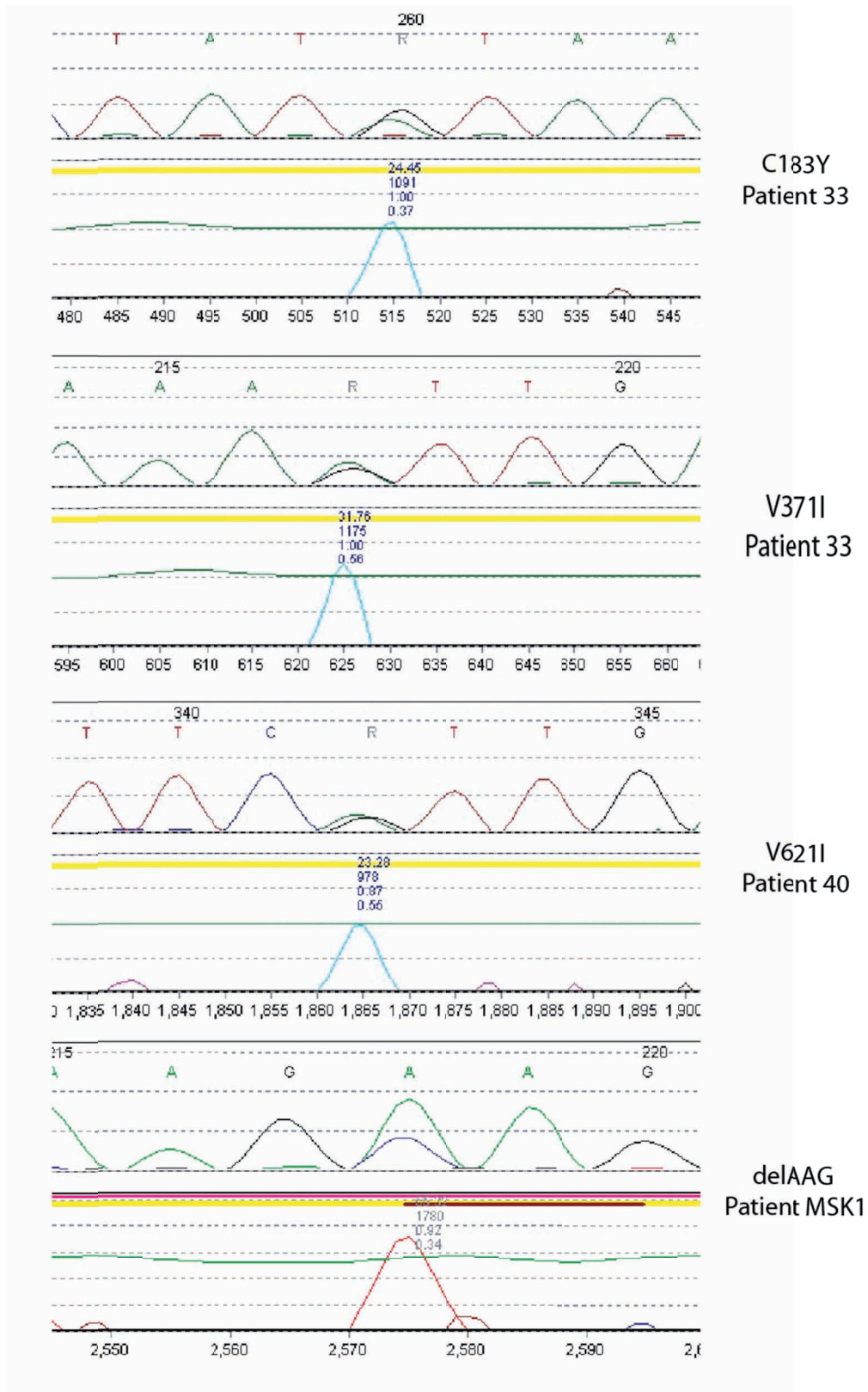
Figure 5-1 : Trace sequence plots showing nsSNSVs and deletion identified from AML patient samples

5.4.2 Patient demographics and disease characteristics

The characteristics of the 3 AML/MDS patients with sequence variants are shown in Table 5-1. All 3 patients had normal karyotype by conventional G-banding. MSK1 had sequence data available for all common AML and MDS–associated mutations. This patient was also found to carry an activating mutation in the IDH1 gene R132C. Unfortunately information regarding the natural history and/or clinical course of the disease in these patients was unavailable.

Table 5-1 : Patient demographics and disease characteristics

	AGE (YEARS)	GENDER	DIAGNOSIS/WHO CLASSIFICATION	CYTOGENETICS	MOLECULAR CHARACTERISTICS	BLAST CELL IMMUNOPHENOTYPE
PT33	81	Male	RELAPSED AML M6	46XY	Not available	CD45$^+$,CD13$^+$, CD33$^+$,CD34$^+$,CD117$^+$
PT40	20	Male	DE NOVO AML	46XY	Not available	CD34$^+$,CD13$^+$, CD33$^+$,CD7$^+$
MSK1	72	Female	AML EVOLVED FROM MDS	46XX	Wild Type (TET2, ASXL1, IDH2, FLT3, NPM1, CEBPA) R132C IDH1	Not available

Legend Table 5-1: Patient demographics and disease characteristics of 3 AML patients with *DDX18* sequence variants
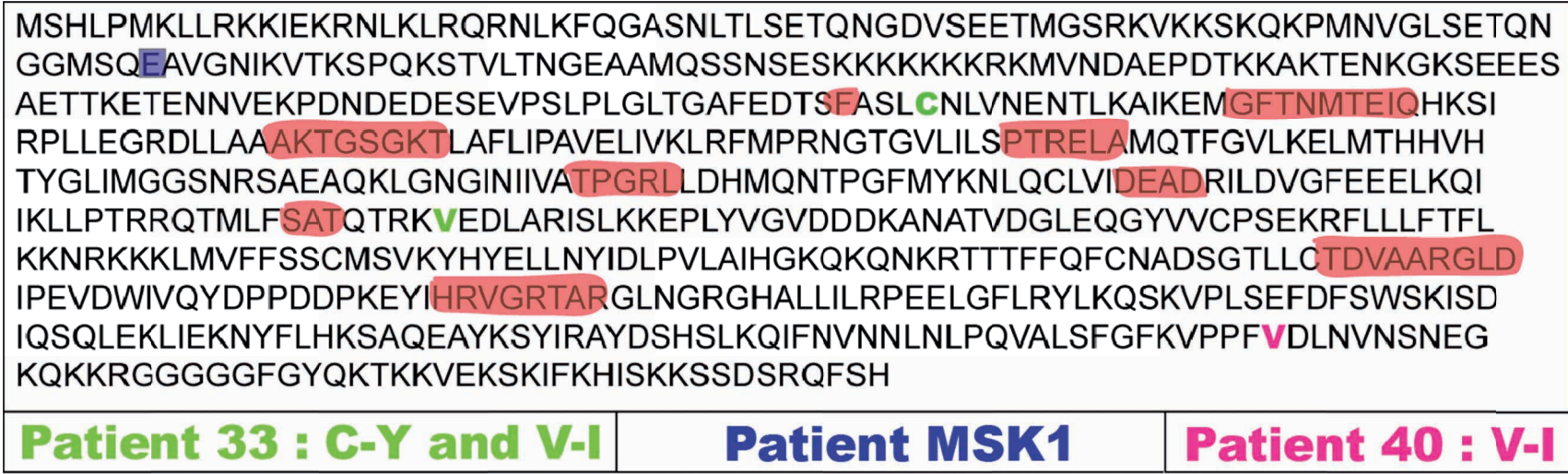
Figure 5-2 : Amino acid sequence, functional domains and location of mutations within human *DDX18*

Legend Figure 5-2: Human DDX18 amino acid sequence. Pink highlighted regions denote conserved motifs found in all dead box proteins. nsSNSVs are highlighted in green and bright pink and the deleted amino acid in patient MSK1 is boxed over in blue.

5.4.3 In silico assessment of significance of *DDX18* nsSNSVs

Following identification of the nsSNSVs, the National Center for Biotechnology Information (NCBI) SNP database was searched to determine if any of the variants were previously annotated as SNPs (www.ncbi.nlm.nih.gov/snp).

None of the nsSNSVs within the *DDX18* gene identified in AML/MDS patients were annotated SNPs in any species on the database. Following this, three different web-based bioinformatics programs were used to assess the likelihood that the nsSNSVs were predicted to disrupt protein function. Unfortunately, in the case of the in-frame deletion in patient MSK1 there are no bioinformatics approaches available to address whether or not loss of this amino acid would alter protein function; therefore no in silico data is presented for this mutation.

Interestingly, the three bioinformatics approaches gave conflicting results for the potential damaging potential of the *DDX18* nsSNSVs I had identified in patients 33 and 44. PANTHER7 software did not predict that any of the sequence variants were likely to be damaging (Table 5-2). POLYPHEN predicted that C183Y was probably damaging (Table 5-2) while POLYPHEN2 suggested this was likely to be totally benign (Figure 5-3). POLYPHEN2 also predicted that V621I was a possibly damaging mutation unlike the other two programs. Thus from this computational data set it is difficult to predict with certainty the likelihood of any of the nsSNSVs being damaging since there is little concordance between programs. Thus definitive functional studies are required to conclusively demonstrate whether these nsSNSVs are damaging or benign.

Table 5-2 : In silico assessment of SNP function

PATIENT	SNP	PANTHER7*	POLYPHEN	POLYPHEN2
PT33	C183Y	−1.12214 (NOT DAMAGING)	PROBABLY DAMAGING	BENIGN
PT33	V371I	−1.76136 (NOT DAMAGING)	BENIGN	BENIGN
PT40	V621I	−2.09951 (NOT DAMAGING)	BENIGN	POSSIBLY DAMAGING
MSK1	DEL-E76	N/A	N/A	N/A

Legend Table 5-2: Scores for PANTHER7 and POLYPHEN show that for PANTHER none of the sequence variants reach a significant level as predicted to be deleterious but C183Y is predicted to be probably damaging by POLYPHEN. *scores ≤ –3 ARE SIGNIFICANT

5.4.4 Functional assessment of DDX18 interaction with NPM1 using nsSNSVs from patients with AML/MDS

Wild type DDX18 is a nucleolar protein binding the nucleolar shuttling phosphoprotein NPM1. Aberrant subcellular localisation of NPM1 results in the development of myeloid malignancies, therefore I initially chose to determine the subcellular localisation of DDX18 variants and if they were able to bind NPM1. As viable blast cells from the AML/MDS patients were not available, 293T cells were transfected with constructs harbouring each of the nsSNSVs. Each of the nsSNSVs was cloned into the pEGFP vector and transfected into 293T cells. Figure 5-4 shows that GFP-fused DDX18 protein for all three nsSNSVs was expressed in the nucleolus and that DDX18 protein was made at a similar level independent of the sequence variant or WT construct transfected (Western blot left panel Figure 5-4). In addition, immunoprecipitation using anti-GFP antibody and blotting for NPM1 showed that DDX18 protein with all three nsSNSVs was still able to bind NPM1 (Western blot right panel Figure 5-4).

Legend Figure 5-3: Transfection of *GFP-DDX18* nsSNSV fusion contructs into 293T cells. Left panel shows epifluorescent images of transfected cells. Green fluorescence denotes that all GFP-DDX18 protein constructs are expressed in the nucleolus. Right panels show input and anti-GFP immunoprecipitation indicating all nsSNSV-carrying DDX18 proteins are expressed is this cell culture system and can bind NPM1.

Legend Figure 5-4 : Rescue experiment using RNA encoding human DDX18 sequence variants identified from AML patient bone marrow. All embryos show WISH for mpx at 27 hpf. Left panels show the whole embryo. Head to the left and dorsal upwards. Right panels show zoom view of tail denoted by boxed region in left panel. RNA and morpholino injected is indicated on the far left. RNA encoding DDX18-WT, C183Y, V371I, and V621I at 100pg resulted in rescue of developmental and myeloid phenotypes (Panels D–K compared to A, B (control) and C, D (*ddx18* morphant), while DDX18△76E could not rescue either (panels L and M compared to panels A–D).
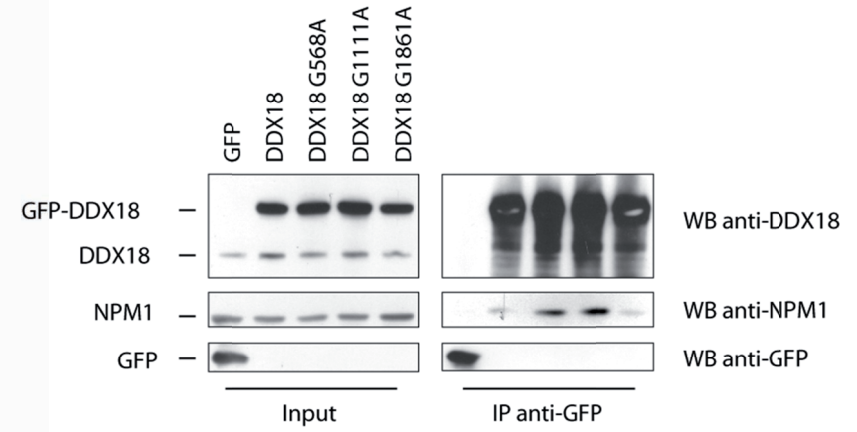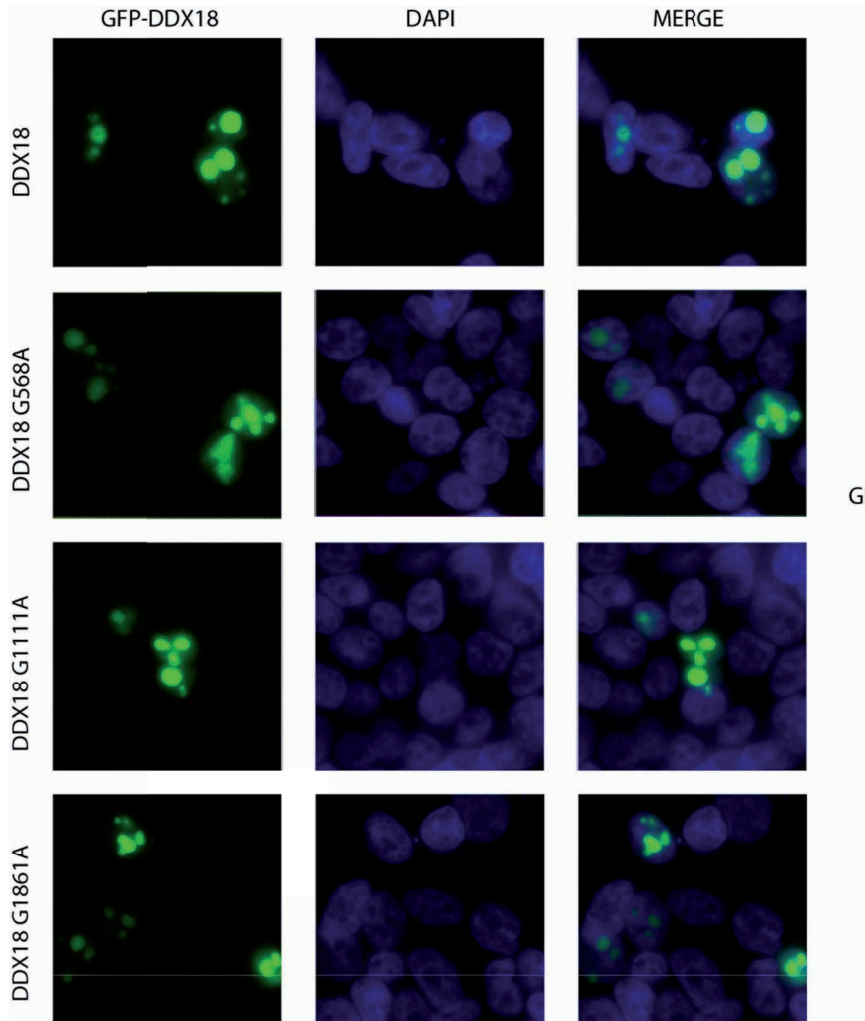
Figure 5-3 : nsSNSV-carrying DDX18 proteins are localised to the nucleolus and can bind NPM1 protein

5.4.1 In vivo rescue experiments to identify functionally null sequence variants

Since WT *DDX18* mRNA can rescue the myeloid and developmental defects (as shown in Chapter 3) mRNAs encoding the nsSNSVs C183Y, V371I, V621I and △76E variants of DDX18 were generated by in vitro transcription. Mutant, WT *DDX18* or control mRNAs were injected into one cell stage embryos with either control morpholino or *ddx18* morpholino. Embryos were fixed at 27 hpf and stained by WISH for mpx. The numbers of *mpx+* cells/embryo were counted and demonstrated nsSNSVs C183Y, V371I, and V621I-encoding mRNAs could rescue developmental and myeloid phenotypes of *ddx18* morphants. In contrast DDX18△76E variant could not rescue either the developmental or myeloid phenotype (Figure 5-5). This suggested that this variant was functionally null. Myeloid cell numbers were quantified per embryo to highlight this (Figure 5-6). To ascertain the DDX18 protein levels were similar for all injection conditions Western blotting was performed (Figure 5-6). This data also shows that nsSNSVs C183Y, V371I, and V621I are likely to represent private or low frequency SNPs or inconsequential passenger mutations.

Legend Figure 5-5: Quantification of myeloid cell numbers is shown per embryo in the scatter plot. All myeloid cell counts reached statistical significance over the *ddx18* morphants with control RNA injection except DDX18-C183Y, and DDX18△76E. DDX18△76E, however, shows no developmental or myeloid improvement at all in contrast to DDX18-C183Y which showed clear rescue of developmental effects and partial rescue of myeloid numbers. The right panel shows a Western blot to address whether the variant-encoding RNAs were being expressed. Notably the DDX18-C183Y is expressed at the lowest level which is most likely to account for the discrepancy in the myeloid cell numbers observed.
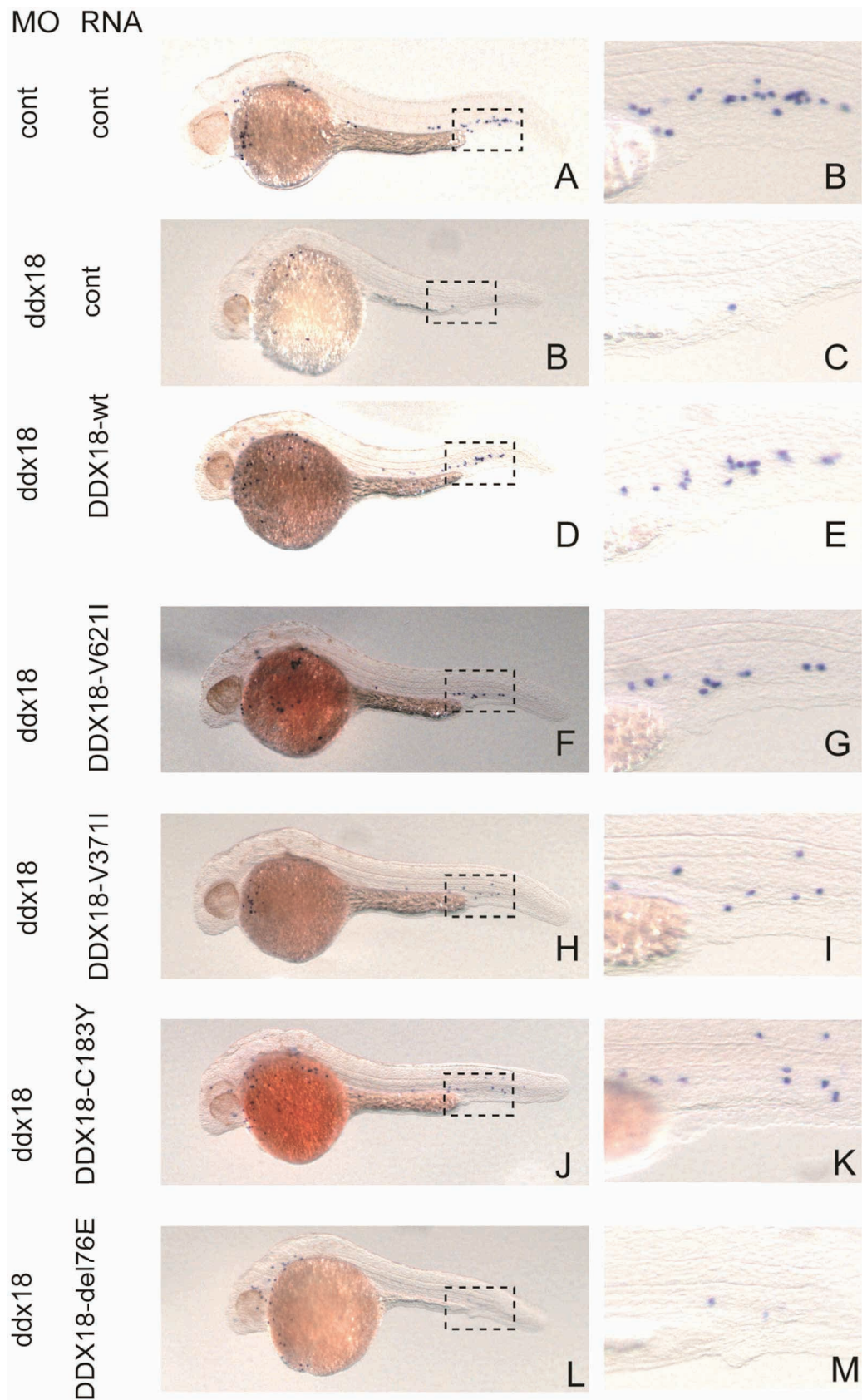
Figure 5-4 : Identification of DDX18-del76E as functionally null allele of human DDX18
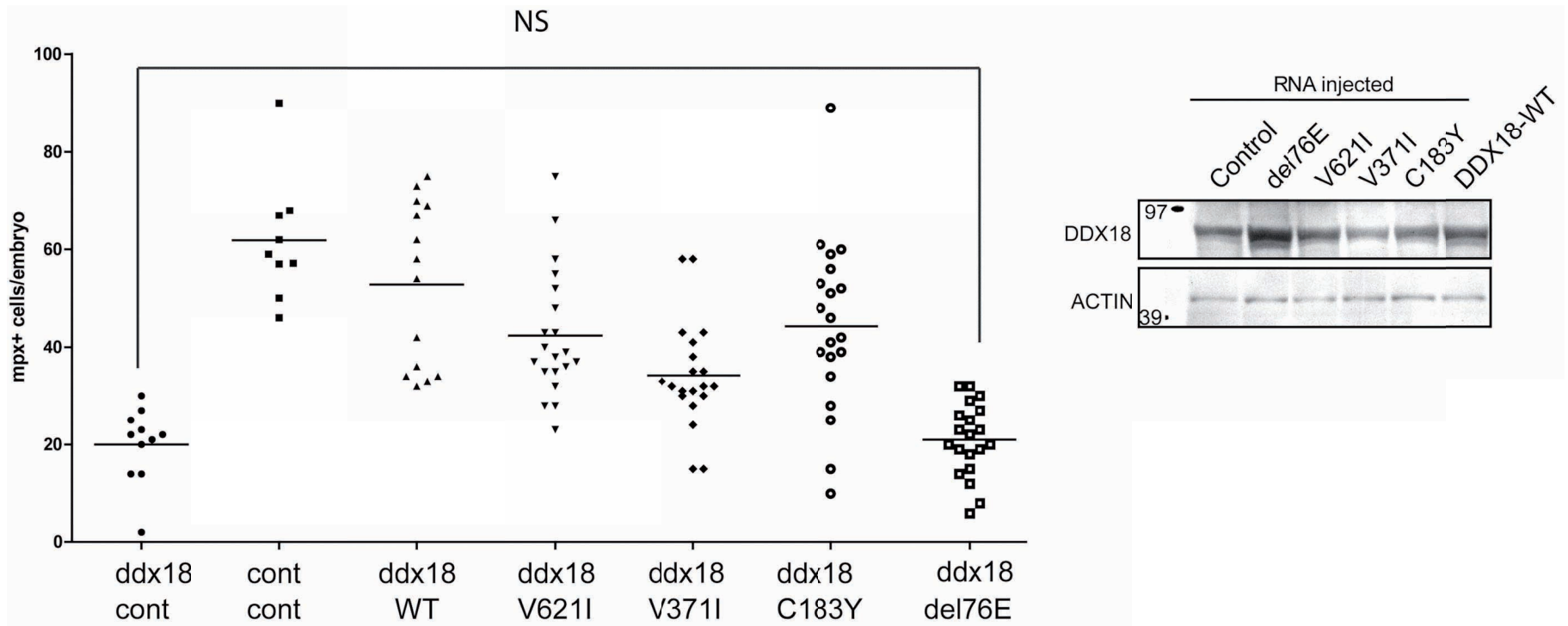
Figure 5-5 : *mpx+* quantification and protein expression of human DDX18 in sequence variant overexpression

5.5 Chapter discussion

Sequence variants in human *DDX18* were detected in a low proportion of AML patients (3% of patients in cohort 1, 1% of patients in cohort 2, and 2% of patients in both cohorts). No *DDX18* variants were identified in any patients with MDS or DBA. Three of the four *DDX18* variants identified were nsSNSVs. None are known annotated single nucleotide polymorphisms (SNPs). Unfortunately none of the patients had matched germ line or remission samples available to allow assessment of these abnormalities to determine if they were constitutional or acquired. This data suggests that *DDX18* mutations are an uncommon event in adult AML patients and do not occur with any meaningful frequency in patients with MDS or DBA. In view of the low frequency of DDX18 abnormalities in AML patients it was essential to consider if such mutations could contribute to the pathogenesis of disease in these patients or if *DDX18* mutations are passenger events with little or no functional sequelae in this context.

To address this issue, I considered first whether the *DDX18* sequence alterations identified in AML patients were likely to have resulted in damage to protein function using bioinformatics-based approaches applicable only to the nsSNSV *DDX18* abnormalities. It seems unlikely that the V371I mutation is damaging to protein function given it was predicted to be benign by all 3 computational methods employed. In contrast, both the C183Y and the V621I nsSNSVs were predicted to be probably or possibly damaging in 1 of 3 bioinformatics approached used. The functional significance of these data is unclear and these results may have arisen from the different computational algorithms used by the different biometric approaches. Another limitation of such approaches is that they can only consider the functional significance of individual nsSNSVs in isolation. It is possible to imagine that multiple nsSNSVs, although individually not detrimental to protein function, could act in combination to adversely affect protein function.

In view of the conflicting results predicting nsSNSV-carrying DDX18 protein dysfunction, it was important to assess DDX18 protein localisation and function in the presence of these nsSNSVs. Functional analysis would also shed light on DDX18 protein function in the presence of the amino acid deletion arising from out of frame deletion, which was not amenable to the in silico predictive approach

described above. Ideally DDX18 protein function would be studied in primary leukaemic blasts and germ line cells from patients with DDX18 abnormalities. Unfortunately this material was not available, so a cell culture-transfection approach was used. The cell culture experiments were designed to address three specific functional questions: (i) are *DDX18* nsSNSVs expressed at the protein level, (ii) is the subcellular localisation of nsSNSV-carrying DDX18 protein disrupted and (iii) can nsSNSV-carrying DDX18 protein bind NPM1? These experiments demonstrated preservation of normal subcellular localisation and NPM1 binding function in nsSNSV-carrying DDX18 protein. Based on these criteria there does not appear to be functional sequelae of the *DDX18* nsSNSVs. It is of course possible that there are other functional abnormalities associated with these *DDX18* nsSNSVs and these may alter the function of DDX18. At the time of this experiment only the 3 nsSNSVs were known of as sequence variant from the Dana-Farber patient cohort, thus this data for DDX18△76E is not available.

To definitively address whether *DDX18* mutations were fully functional, RNAs encoding each of the sequence variants were injected into WT embryos, along with a specific morpholino targeting the ATG/5'UTR of the *ddx18* gene, or a control morpholino. The results show that RNAs encoding DDX18 sequence variants V621I, C183Y and V371I were able to rescue the developmental and myeloid effects of Ddx18 loss; however, the RNA encoding DDX18△76E was unable to rescue the effects of Ddx18 loss, indicating that this mutation disrupts the function of DDX18. Furthermore, RNAs encoding the DDX18 sequence variants V621I, C183Y and V371I did not induce developmental defects or alteration in myeloid cell numbers when injected into WT embryos, suggesting that these mutations did not result in dominant negative or gain of function changes in DDX18. The mechanism whereby loss of DDX18 function might contribute to leukaemogenesis is not clear. DDX18 was prioritised for further study following the discovery that DDX18 is able to bind NPM1 and HSPA9B (Sekiguchi et al, 2006), two putative tumour suppressor genes in AML/MDS located on chromosome 5q (Craven et al, 2005; Grisendi et al, 2005; Sportoletti et al, 2008) as well as a *RPS14* and *RPS19* genes. The deleted glutamic acid residue in the DDX18△76E variant, resides within a conserved consensus SQE motif, which is a binding motif for phosphatidylinositol-3-OH kinase related kinases (PIKKs). Binding of PIKKs (such as DNA damage proteins ATM and

ATR) to their target binding sites is thought to be required for kinase activation (Downs et al, 2000). This may be one explanation why loss of this residue results in loss of protein function. Furthermore, a recent study of the plasmodium falciparum orthologue of DDX18 showed that, in addition to the 9 conserved DEAD-box helicase motifs the N terminus of the protein is also required for its helicase activity (Prakash & Tuteja, 2010). The patient with DDX18△76E mutation had a normal karyotype AML which had evolved from prior MDS. This patient also had the IDH1-R132C mutation. IDH1 mutations, particularly those affecting the R132 residue have been described in MDS patients early in the course of disease as well as secondary AML (although not in matches cases) (Kosmider et al, 2010). Thus it is possible that the driver genetic lesion in this case is IDH1-R132C. Loss of functional DDX18 may occur as a secondary event during disease evolution leading to further deregulation of myeloid and erythroid maturation. Importantly, functional Ddx18 loss may also impose a selective pressure to lose functional p53. Such a selective pressure is observed in both human patients with ribosomopathies, who are susceptible to Li-Fraumeni spectrum of malignancies; and in zebrafish models with RP deficiencies (MacInnes et al, 2008; Narla & Ebert, 2010).

In the era of whole genome sequencing, an increasing number of nsSNSVs are being identified in small proportions of patients with myeloid malignancies. There is currently an unmet need for a simple model in which to determine the functional significance of these novel nsSNSVs in order to prioritise new mutations that may represent potential therapeutic targets for further study. Here we have successfully used the zebrafish to determine the functional significance of nsSNSVs in human patients in a single gene. However the model could be applied to multiple novel gene nsSNSVs which would facilitate the rational investigation of new mutations found in human disease.

6. Identification, cloning and functional analysis of zebrafish *npm1* genes

6.1 Introduction

6.1.1 NPM1 in human leukaemia

NPM1 is the most commonly mutated gene in human AML. These NPM1 mutations, occurring almost exclusively in AML are heterozygous gain-of-function mutations that result in aberrant displacement of the normally nucleolar NPM1 to the cytoplasm. The presence of such mutations are defined in the revised WHO classification as a sub-category of AML called NPMc+ (for cytoplasmic positive) AML (Vardiman, 2010). Human *NPM1* is located on the long arm of chromosome 5 (5q). In addition to the gain-of-function mutations observed in AML, NPM1 is also deleted in greater than one third of cases of AML/MDS associated with loss of 5q (5q– AML/MDS) (Heinrichs et al, 2009). Loss of NPM1 in murine models results in embryonic lethality by embryonic day 9.5. $NPM1^{-/-}$ mice die as a result of profound anaemia but, also exhibit defective telencephalic and ocular development (Grisendi et al, 2005). Mice that are heterozygous for NPM1 survive to adulthood but go on to develop a syndrome resembling human MDS and subsequently many die from myeloid or lymphoid leukaemia or myeloproliferative disorders (Sportoletti et al, 2008). However, there are important phenotypic differences between the leukaemias seen in $NPM^{+/-}$ mice and human NPMc+ leukaemias. NPMc+ mutations occur almost exclusively in normal karyotype AML whereas chromosomal aberrations with multiple centrosomes are common in the AMLs that develop in $NPM^{+/-}$ mice. The latter is likely to reflect the function of NPM1 in maintenance of centrosome duplication.

The gain-of–function associated with mutated NPMc+ alleles in human AML results from the creation of a new nuclear export signal at the expense of a nucleolar localisation signal, resulting in displacement of the protein into the cytoplasm. The presence of a heterozygous NPMc+ mutation also disrupts the normal function of remaining NPM1 WT allele, displacing WT NPM1 protein into the cytoplasm. This occurs because NPMc retains its oligomerisation domain at the N terminus.

NPM1 is a chaperone protein that can shuttle nucleic acids and proteins to and from the nucleolus. However, the specific mechanisms governing its oncogenicity

are largely unknown (Bolli et al, 2009; Bolli et al, 2007). In addition, WT NPM1 is known to play a role in centrosome duplication (Okuda, 2002; Okuda et al, 2000). Therefore, it is possible that heterozygosity for WT NPM1 results in leukaemia because of genomic instability. The normal karyotypes observed in NPMc+ leukaemias make it is unlikely that this is the dominant mechanism for leukaemogenesis in this situation. Since aberrant cytoplasmic localisation of NPM1 protein is also observed in cases of AML with chromosomal translocations involving *NPM1*, it is probable that the cytoplasmic localisation of NPMc+ (and NPM1) provides a survival advantage specific to haematopoietic cells that contributes to leukaemogenesis.

6.1.2 Modelling NPM1-mediated haematopoietic disease in zebrafish

Many outstanding questions remain about the role of NPM1, most notably how disruption of such an apparently promiscuous protein with a broad range of functions and binding partners results in a lineage-specific disorder such as AML. In particular the differential effects observed between haploinsufficiency for NPM1 and heterozygous gain-of-function mutations are intriguing, suggesting a specific role for this ubiquitous protein in haematopoietic cell maintenance, potentially through one or more mechanisms. A rapid genetic model amenable to analysis of NPM1 gain or loss would be a powerful tool to dissect these potential mechanisms.

The experiments described in this chapter were designed to determine whether the zebrafish could be used to examine the role of *npm1* in haematopoietic development and disease. First I sought to identify and clone the zebrafish orthologue(s) of NPM1. Following identification of zebrafish *npm1* orthologues their potential role in developing zebrafish haematopoiesis was explored. Finally functional orthology between zebrafish and human NPM1 was addressed to discover if they do demonstrate that zebrafish provide a viable model to study the genetic effects of loss of *npm1* or the effects of the human mutated NPMc allele.

6.2 Aims of the experiments described in this chapter

1. To identify the orthologues of human NPM1 in zebrafish
2. To clone the zebrafish Npm1 genes
3. To determine the expression pattern of the zebrafish *Npm1* genes

4. To determine the haematopoietic effects of loss of Npm1a and Npm1b alone or in combination

5. To determine the effects of loss of p53 on this phenotype

6. To determine if human NPM1 can rescue the phenotype observed with loss of zebrafish Npm1

6.3 Methods

6.3.1 Comparative analysis of zebrafish and human NPM1

Putative zebrafish orthologues for NPM1 were identified using a "reciprocal best-hit" analysis (Barbazuk et al, 2000). TBLASTN (compares a protein query sequence against a nucleotide sequence database dynamically translated in all reading frames) searches were applied for human NPM1 and BLASTX (compares a nucleotide query sequence translated in all reading frames against a protein sequence database) or TBLASTN searches for zebrafish cDNA sequences or proteins (respectively) annotated in Ensembl Zv7. Searches were carried out on the Ensembl, UCSC and NCBI platforms. Comparative analysis between the human and the two zebrafish protein sequences was carried out using the Clustal W algorithm (www.ebi.ac.uk/Tools/clustalw2/index.html). Other genes located in the human 5q35.1–5q35.2 region were identified using NCBI Mapviewer (www.ncbi.nlm.nih.gov.ezp-prod1.hul.harvard.edu/mapview/).

Reciprocal blast searching was carried out for each of the 5q genes in this region to determine syntenic relationships between human and zebrafish chromosomes.

6.3.2 PCR cloning of zebrafish *npm1a* and *npm1b*

Full length cDNA of the two zebrafish *NPM1* orthologues *npm1a* and *npm1b* were RT-PCR-amplified from 30 hpf AB embryos. Primers for full-length *npm1a* amplification were designed based on the published NCBI sequence (NM_199428). Since the full length sequence for *npm1b* was not annotated, a selection primers were designed to span the multiple EST's on chromosome 14 and each was PCR amplified form genomic DNA of 30 hpf, 5 dpf and adult kidney.

6.3.3 Subcloning of human NPM1 cDNA

Full length human NPM1 cDNA was sub-cloned from pGEM-T-easy-NPM1 (provided by Dr Niccolo Bolli) into the pCS2+ vector as shown in Figure 6.1.

Plasmid DNA was cut sequentially with SpeI, cleaned and run on a 0.8% agarose gel to confirm linearisation and then cut with EcoRI. This strategy was used to prevent interference with the efficiency of cutting the SpeI site arising from the presence of a second EcoRI immediately adjacent to the SpeI site in the multiple cloning site of the pGEM vector. Following EcoRI digestion the digest was cleaned up and the entire product run on a 0.8% agarose gel. The digested band was excised and gel extracted using the Qiagen gel extraction kit. The pCS2+ vector was cut with EcoRI and XbaI (which has compatible ends with SpeI), cleaned and run on a 0.8% gel and extracted using the Qiagen kit. The cut pCS2+ was incubated with shrimp alkaline phosphatase to dephosphorylate the ends as described in 2.3.2. The ligation reaction was set up as described in 2.3.2 in 1:1 and 1:3 molar ratios of vector: insert. Colonies obtained from the ligation reaction transformation were screened for the NPM1 insert by digest with EcoRI and NotI. Colonies containing the insert were then sequenced using Sp6 and T7 primers.

Legend Figure 6-1: Subcloning strategy for human *NPM1*-WT from p-GEM-T Easy to pCS2+. *NPM*-WT was digested from p-GEM-T-Easy using EcoR1 and Spe1. pCS2+ was digested with EcoR1 and XbaI. SpeI and XbaI have compatible sticky ends and ligation was carried out as described in 2.3.1.
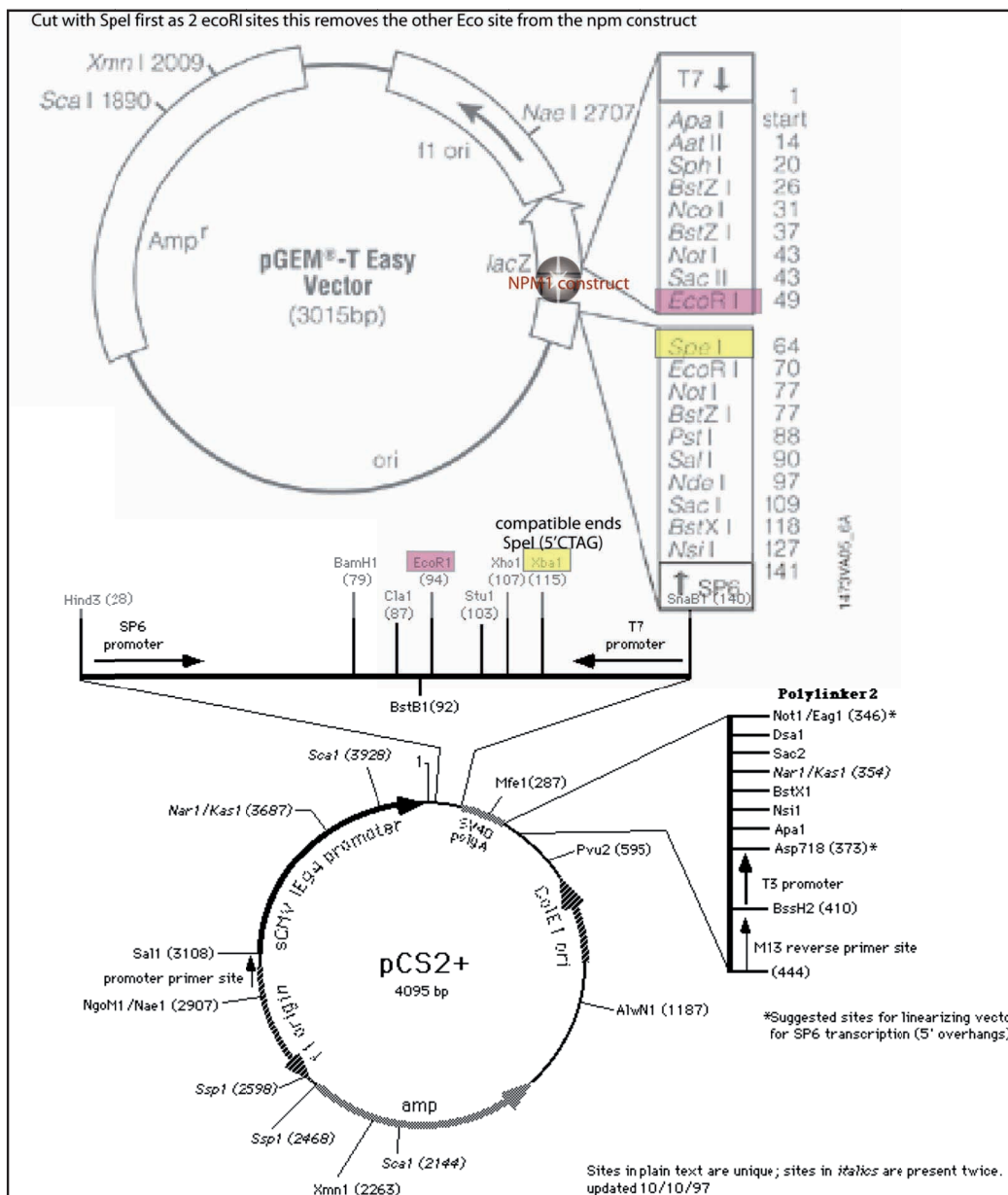
Figure 6-1 : Subcloning strategy NPM1

6.4 Results

6.4.1 In silico analysis

6.4.1.1 Identification of two zebrafish *npm1* genes by TBLASTN

Two loci were identified by TBLASTN, including an annotated zebrafish *npm1* gene on chromosome 10 whose protein product exhibits 51% identity to NPM1, and multiple overlapping expressed sequence tags (ESTs) on chromosome 14, corresponding to a gene with 48% identity to NPM1 (Figure 6-2). Initial studies utilised the Zv6 assembly of the zebrafish genome and later studies Zv7. The finding of two *npm1* genes within the zebrafish genome was not unexpected as zebrafish often have two copies of genes orthologous to a single mammalian gene as a result of genomic duplication during teleost evolution (Gates et al, 1999).

6.4.1.2 Assessment of synteny with human chromosome 5q

The genomic regions surrounding the two zebrafish *npm1* genes were subjected to BLAST searches as described in materials and methods and showed high degrees of synteny with human 5q35.1, the locus of human *NPM1* (Figure 6-3). Thus, by syntenic relationship each of these genes is orthologous to *NPM1* and were designated (and are referred to herein) as *npm1a* (chromosome 10) and *npm1b* (chromosome 14).

Detailed analysis of the 5'UTR Clustal W alignment of the proteins encoded by the two genes showed that critical NPM1 functional domains are conserved in both Npm1 zebrafish proteins (Figure 6-4). Such domains include the C terminal tryptophan residues required for nucleolar localisation which are necessarily lost in NPMc myeloid leukaemia mutants (Falini et al, 2006a).

Legend Figure 6-2: Schematic representation of multiple zebrafish expressed sequence tags identified from TBLASTN search of human NPM1. Each black arrow (or dotted arrow) is a single EST blast hit sequence in Ensembl, NCBI or UCSC genome servers. The level of coverage is indicated by the thickness of the blue/green line and the level of conflict between overlapping sequences is colour-coded as shown in the key where black is identical. Sequences were aligned using the DNAStar Seqman software.
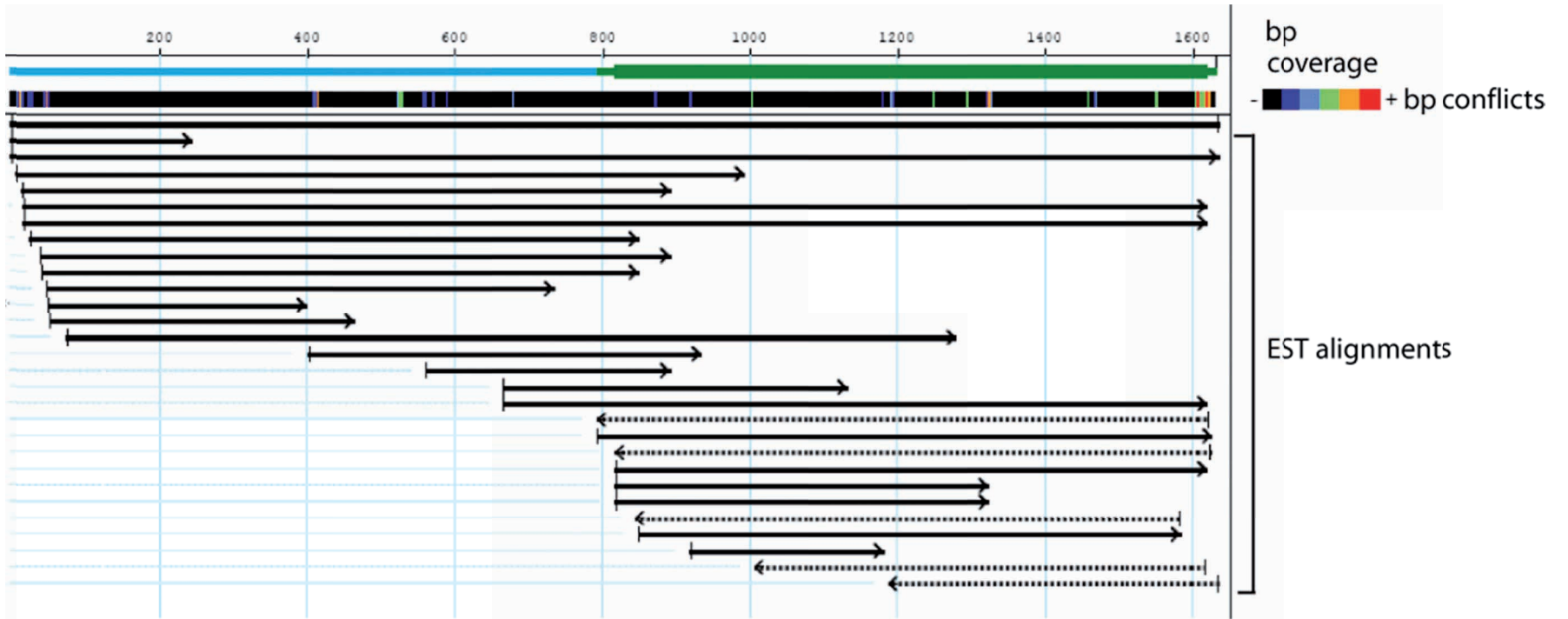
Figure 6-2 : Multiple ESTs and predicated protein coding regions overlap to form *npm1b*
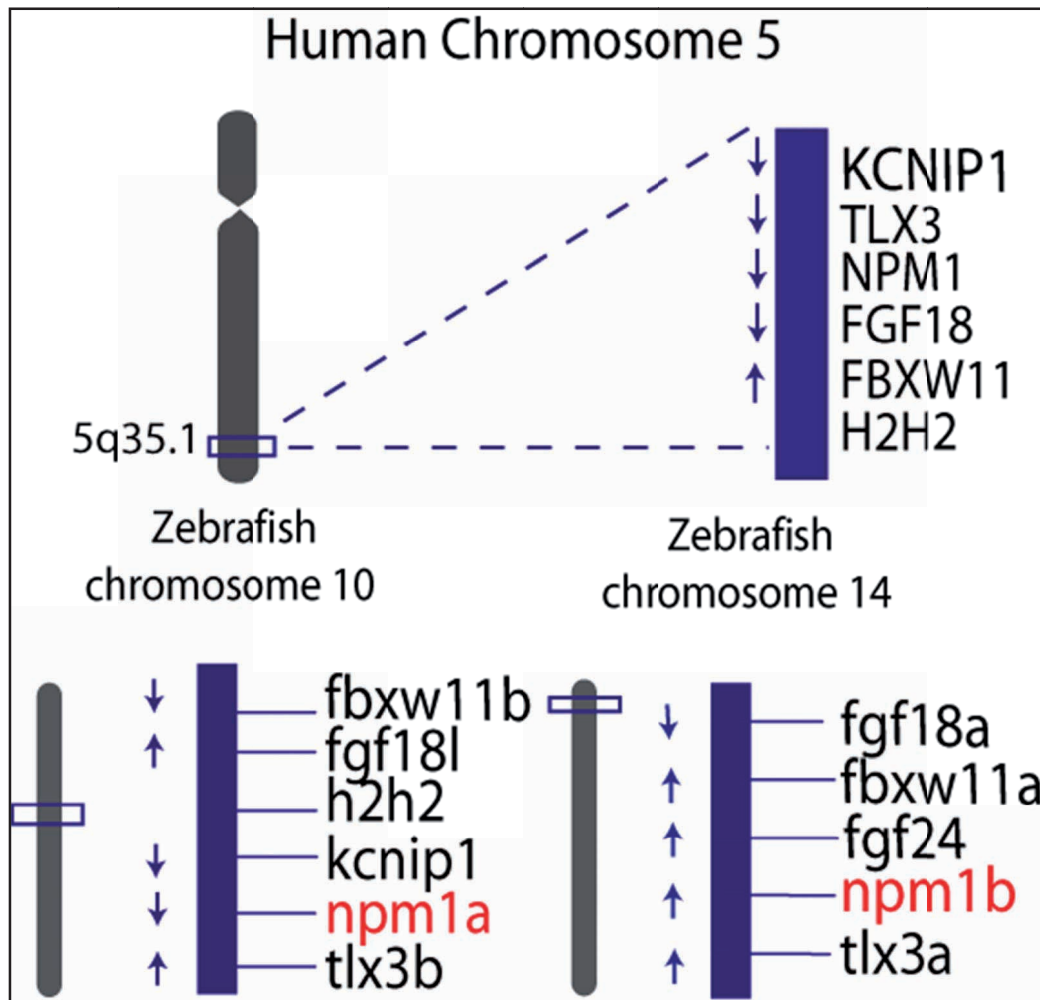
Figure 6-3 : Human chromosome 5q in the region of *NPM1* is syntenic with zebrafish chromosome 10 (*npm1a*) and zebrafish chromosome 14 (*npm1b*)

Legend Figure 6-3: Synteny between human chromosome 5q and zebrafish chromosomes 10 and 14 indicates both *npm1a* and *npm1b* are true orthologues to human *NPM1*. Analysis carried out using Ensembl Zv7 (zebrafish genes) and NCBI Mapviewer for human chromosome 5 gene annotation.

```
h-NPM1     MEDSMDMDMSPLR-PQNYLFGCELKAD-KDYHFKVDNDENEHQLSLRTVSLGAGAKD
z-npm1a    ------MDLEQMG-PQTFLYGCELKAG-KDITFNPEDDDYDHQLSVRMACVDPSTKD
z-npm1b    ----MEDNIKDLSRPQMYLFGCSLKGDKKEHKVDLDDDEAEHQLSLKSVCLGAEAED
           ::. :   **  :*:**.**..  *:    .. ::*: :****:: ..:.. ::*

ELHIVEAEAMNYEGSPIKVTLATLKMSVQPTVSLGGFEITPPVVLRLKCGSGPVHISGQHLVAVEE
ELNVVEIEGQDSEGQKVKAVLATLKPSTLPSVCLGGFEITPPVVFRLRTGSGPVHISGQHLVIMGG
KFHTVETEGLTYDGKTTKITLAVLKPSVLPSLSLGGFEVTPPVSFRLQSGGGPVYISGQHFVSVK-
:::  ** *.     :*.   *  .**.** *.  *::.*****:**** :**: *.***:*****:* :

DAESEDEEEEDVKLLSISGKRSAPGGGSKVPQKKVKLAADEDDDDDDEEDDDEDDDDDDDFDDEEAE
DQSFDEEEEEEEEEETVMTSKKRPALSTPKPSKKMKMDE-EDDDDDDEDDDDEDDDEE----DESE
--ESDDEDEEEEENNTSPVKRPSNMTLAKVPQKKLKMDSDEDEDSDDDDDDDDDDDDDEEDDDKQE
  . ::*:**: :   :     .:       :   *.**:*:    **:*.**::***.***:: :: *

E---KAPVKKSIRDTPAKNAQKSNQNG----KDSKPSSTPRSKGQESFKKQEKTP--KTPKGPSSV
E---ESPVKE--KKAPAK-PKTPTQNG----KGPKPSTPAKQTPQK--GKKEQTP--KTPQTPRTL
KPAVKSPVKS-TQKTPEKKKSADKQNGSPDKKAGTSGKPQTQTPQKVKDKSAAGPSGKTPSIP-SL
:     ::***.  :.:* *   .  .*** *  ..... .. *:   *.    *  ***. * ::

EDIKAKMQASIEKGGSLPKVEAKFINYVKNCFRMTDQEAIQDLWQWRKSL--
ADIKSKMMESVAKGVSLPKVQLKFENYVNNCFKGTDPKVVEELWKWRQTVK-
SEVKSKLTSAAKEGKPFPKTEQKFENFARSSFKISDKQVIKDLWNFVQSLKK
::*:*:   :   :* .:**.: ** *:....*: :*  :.:::**:: :::
```

Figure 6-4 : Clustal W alignment of human and zebrafish amino acid sequences

Legend Figure 6-4: Clustal W alignment of zebrafish Npm1a and Npm1b amino acid sequences with human NPM1 amino acid sequence. * marks identical amino acids, : are similar and . less similar. Boxed region shows conserved tryptophan residues essential for NPM1 nucleolar localisation and are mutants in human AML.

6.4.2 Cloning of zebrafish *npm* genes

As shown in Figure 6-5 each of the predicted amplicons was obtained at the correct size at all time points. Full length *npm1a* and *npm1b* primers were designed with restriction enzyme linkers (EcoRI and ClaI for *npm1a* and BamHI and XhoI for *npm1b*) and were cloned in pCRII topo vector (Invitrogen, Carlsbad, CA) and then subcloned in pCS2+ using restriction enzyme digest and gel purification of the fragment. Clones carrying the correct sequence were determined by sequencing the pCRII clones using M13 forward and reverse primers (Genewiz) .
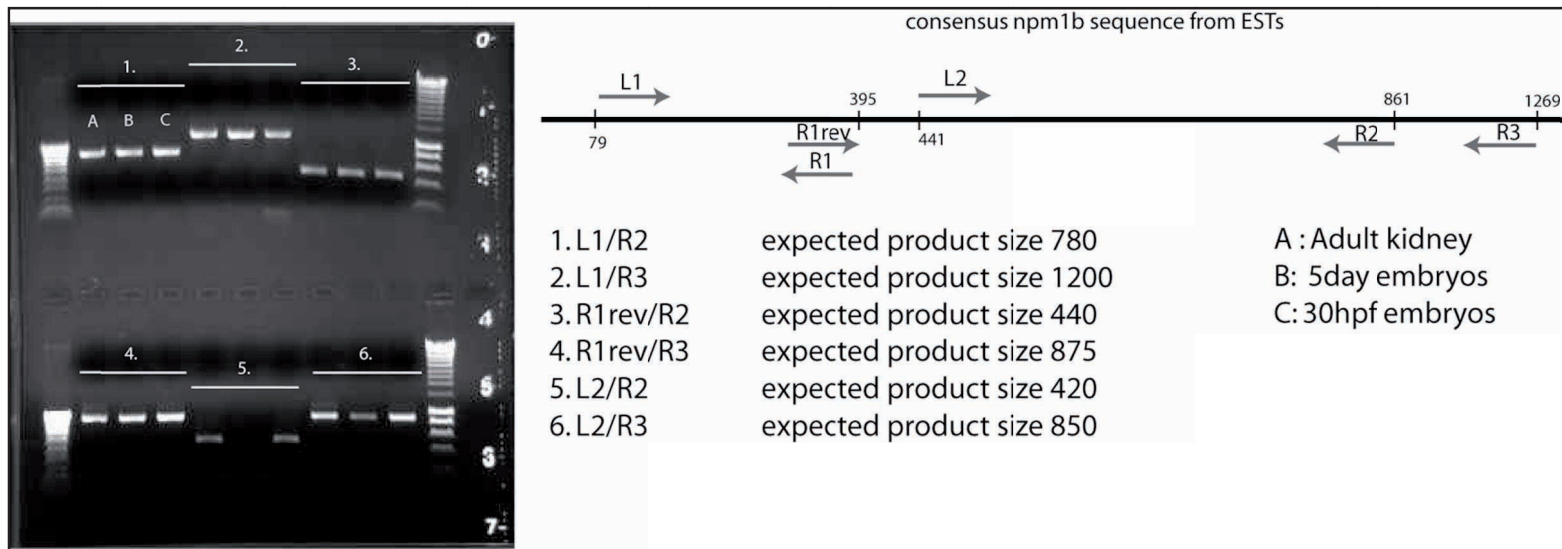
Figure 6-5 : Cloning of *npm1b* from overlapping EST consensus sequence

Legend Figure 6-5: Cloning of *npm1b* based on overlapping EST sequences (Figure 6-1). 5 primers spanning the overlapping regions of the ESTs were designed based on the consensus sequence. PCR fragments were amplified using 6 different combinations of primers as shown. cDNA from adult kidney marrow, 5 day old embryos and 30 hpf embryos was used for each primer pair. As shown the expected size of PCR products was generated for each reaction (right DNA ladder is 10kb – middle gap region is between 1kb and 1.5kb; left ladder is 1kb ladder, each division is 100bp). Primer sequences are shown in Appendix 2.

6.4.3 Expression pattern of zebrafish *npm1* genes

Digoxigenin-labelled in situ hybridisation probes were generated for *npm1a* and *npm1b* the full length cDNA clones in pCS2+ as described in 2.2.4. The results for 3 time points are shown in Figure 6-7. The expression pattern of *npm1a* and *npm1b* were examined over time from 12 somites to 3 dpf.

Early in development both *npm1a* and *npm1b* were expressed ubiquitously, by 24 hpf expression of *npm1a* was localised to the developing eye, brain and somites. By 2 and 3 dpf expression was found in the brain and in the aortic and caudal haematopoietic regions respectively, consistent with expression in HSCs. Npm1b expression was less distinct at all time points and remained at higher levels in the brain. No clear expression of either Npm1a or Npm1b was seen in blood forming regions. To confirm that both *npm1a* and *npmb* RNA was expressed in blood cells, PCR was performed using full length primers for each gene (and beta actin control) on whole kidney marrow which had been sorted (using forward and side scatter characteristics Traver et al, 2003); into the following cell subsets; progenitors, erythroid cells, myeloid and lymphoid compartments (RNA, a gift from Dr Clemens Grabher). As shown in Figure 6-6 this confirmed that both genes were expressed in all haematopoietic cell compartments. *npm1a* and *npm1b* were expressed at similar levels within each cell subset, with the lowest expression seen in the lymphoid compartment. This was in keeping with expression patterns of *NPM* human haematopoietic cell subsets, where the lowest levels of expression occur in lymphoid cells (N Bolli and B Fallini personal communication).
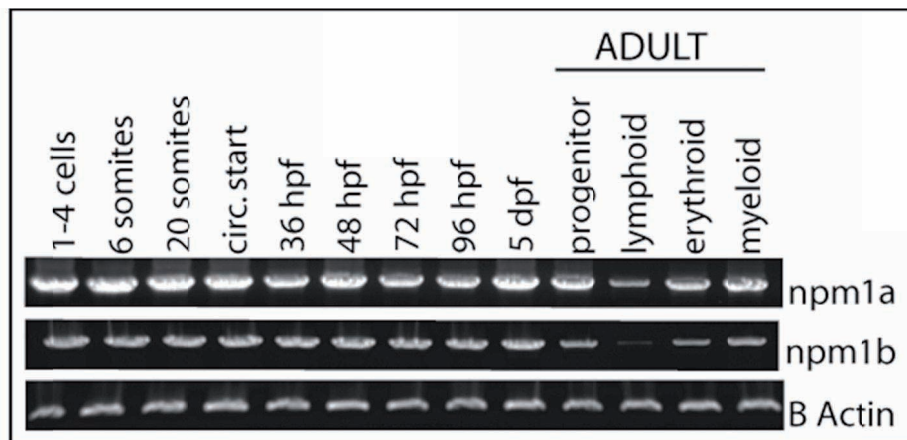
Figure 6-6 : *npm1a* and *npm1b* are expressed in developing embryos and haematopoietic tissue
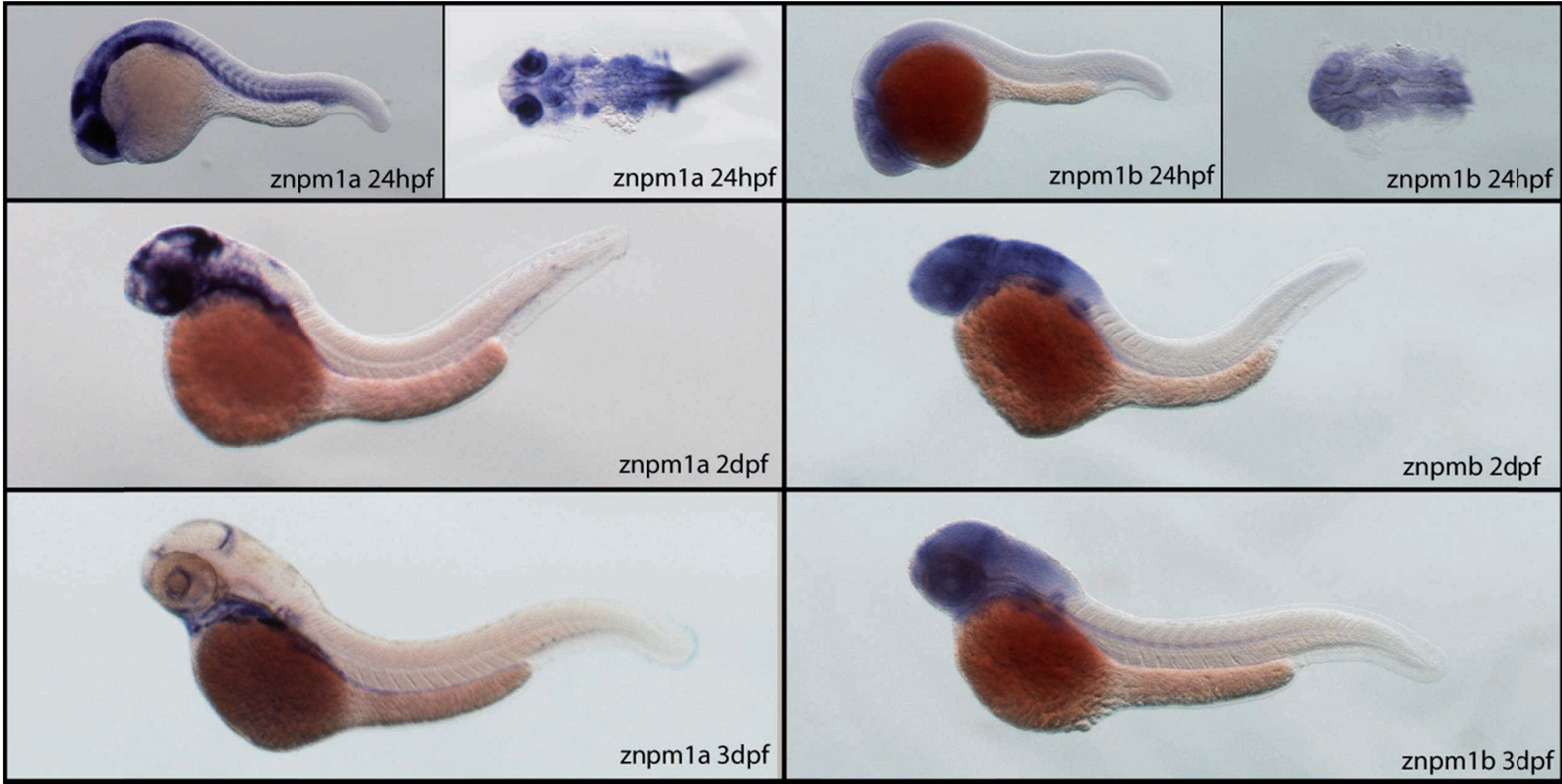
Figure 6-7 : Expression pattern of *npm1a* and *npm1b*

Legend Figure 6–6 : RT-PCR showing *npm1a* (top row) and *npm1b* (middle row) expression at the indicated time points. Beta-actin expression levels are used as a loading control (bottom row). Right, RT-PCR from precursor, lymphoid, myeloid and erythroid cells sorted from adult kidney marrow (gating strategy based on forward and side scatter plots; Traver et al, 2003).

Legend Figure 6–7: *npm1a* or *npm1b* RNA expression by WISH in 24 hpf (upper), 2 dpf (middle) and 3 dpf (lower) embryos. Embryos are all shown in lateral view, anterior to the left, dorsal upwards except 24 hpf also shown in dorsal view of head and anterior trunk flat-mounted and de-yolked.

6.4.4 Loss of *npm1* genes resulted in reduced numbers of white blood cells

To determine if the zebrafish *npm1* genes played a role in haematopoiesis, each gene was knocked down using antisense morpholinos directed at the 5'UTR/ATG codon or splice donor sites. The initial studies were carried out using 5'UTR/ATG codon morpholinos. Embryos were analysed for *mpx* expression by WISH at 2 dpf. Knockdown of each gene individually lead to a significant reduction in the number of *mpx*-expressing cell (Figure 6-8). When *npm1a* and *npm1b* were knocked down simultaneously, the effect on *mpx*-expressing cell numbers was greater and appeared to be at least doubled (Figure 6-8). Embryos injected with both morpholinos together also showed developmental abnormalities, with a smaller body size, smaller head and eyes and a shortened yolk extension.

Morpholinos can have off-target effects. Validation of protein knockdown requires an antibody directed against the protein being knocked down. Unfortunately there are very few such antibodies available with specificities for zebrafish proteins. Several antibodies against conserved epitopes in human NPM1 were tested but none were cross-reactive with either of the zebrafish Npm1a or Npm1b proteins. Therefore to further validate the specificity of the phenotype observed in *npm1a+b* morphants, several morpholinos directed at splice donor sites of *npm1a* and *npm1b* were tested. Knockdown of each gene was confirmed by RT-PCR and sequencing of the products to demonstrate the introduction of a premature stop codon in aberrantly spliced products (Figure 6-10). Combined knockdown of *npm1a* and *npm1b* using the splice donor site morpholinos led to the same myeloid phenotype in these morphants as that induced by the 5'UTR/ATG-targeted double morphants (Figure 6-9)

168
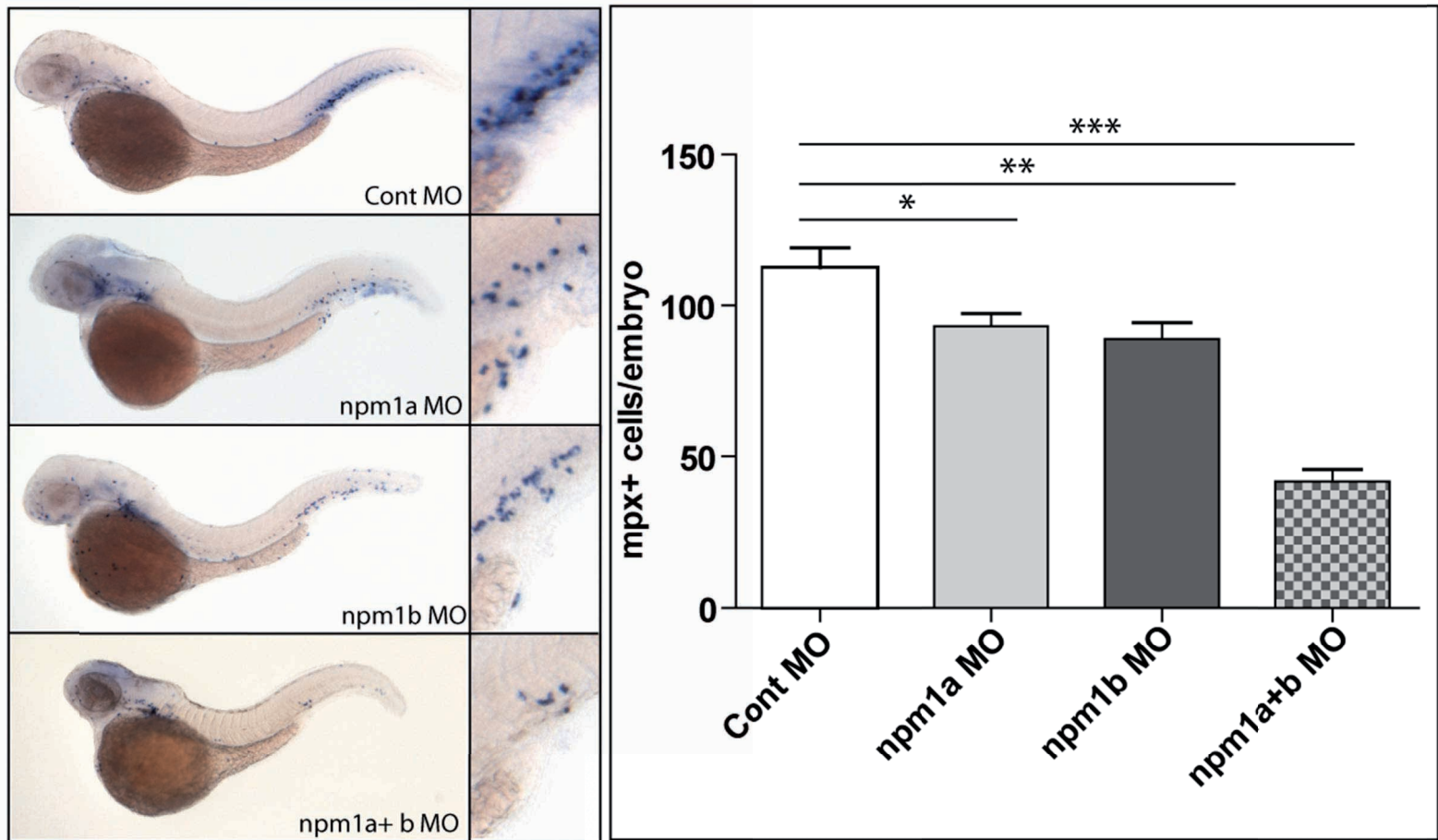
Figure 6-8 : Loss of Npm1 in zebrafish leads to reduced numbers of *mpx*-expressing cells
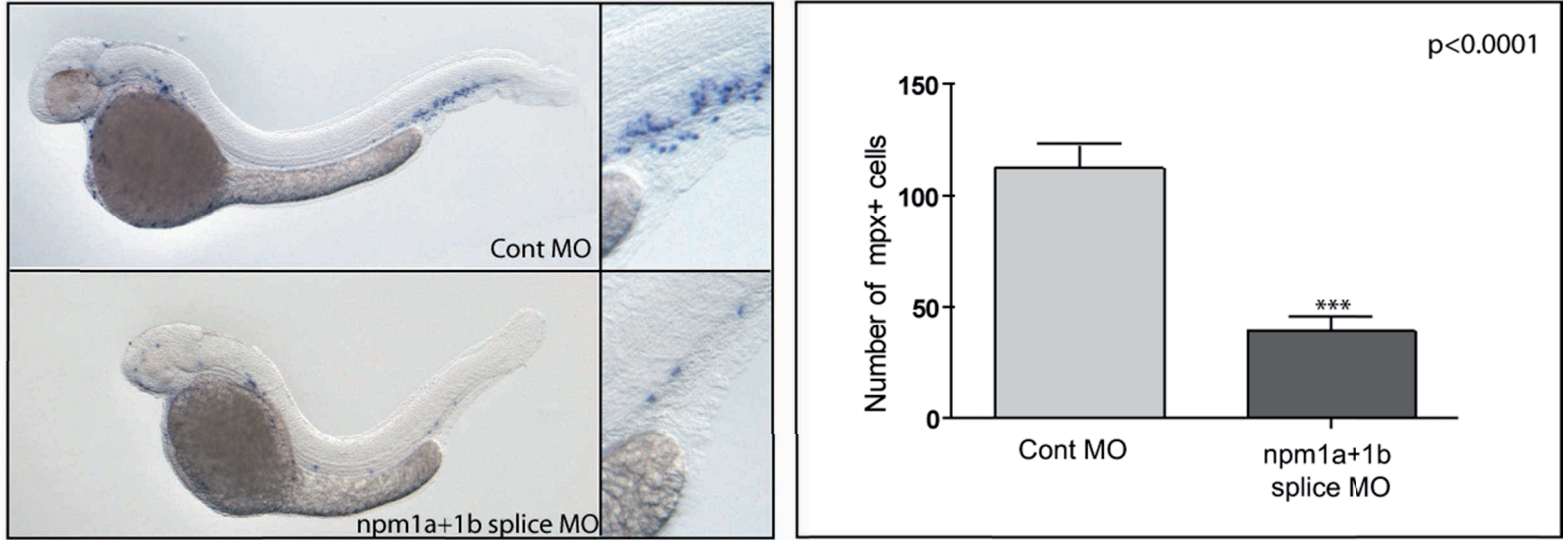
Figure 6-9 : Npm1 splice morphants show loss of *mpx* expression
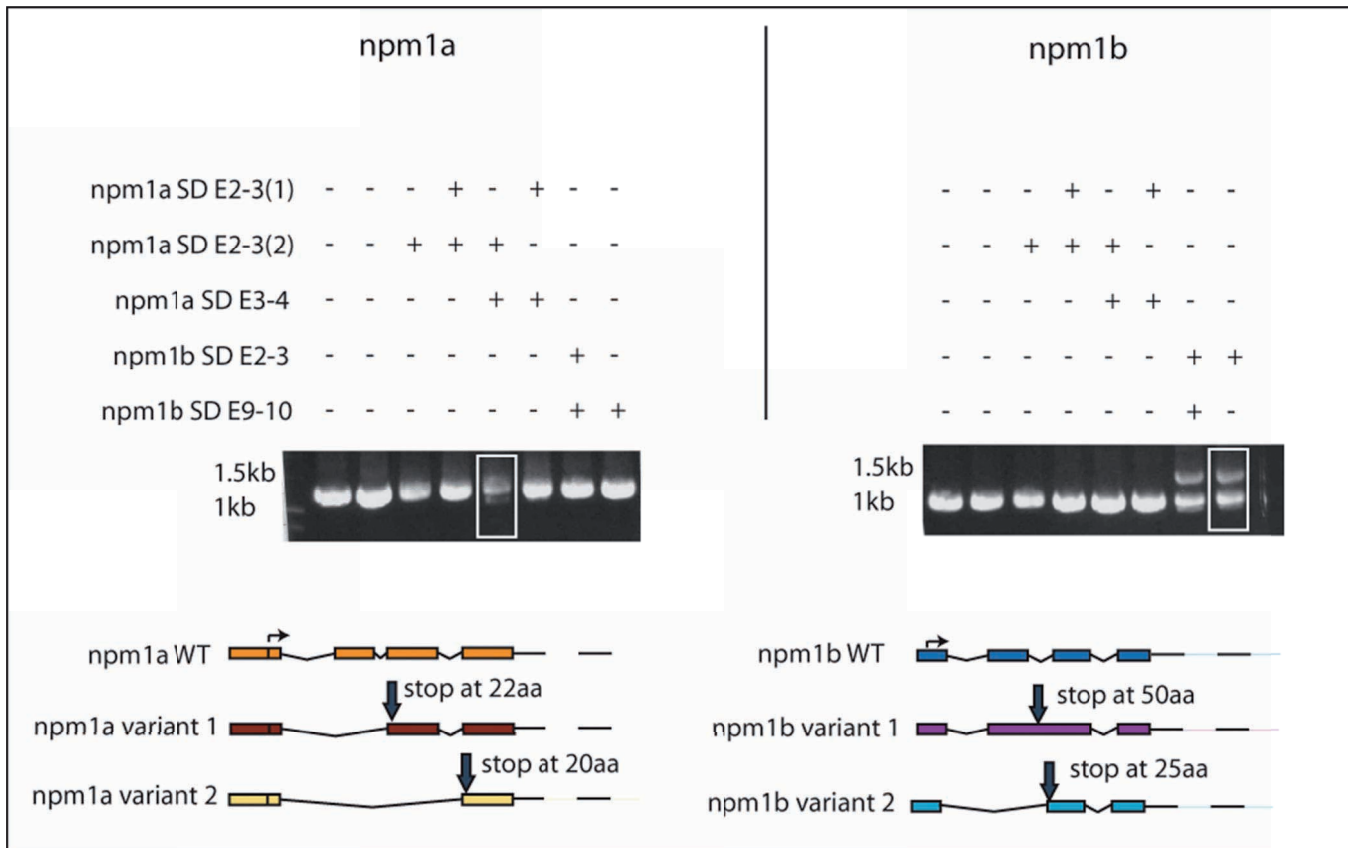
Figure 6-10 : Npm1 splice morphants have aberrant splice products

Legend Figure 6-8: WISH for *mpx* in 48hpf embryos, lateral view, anterior to the left, dorsal upwards. Knockdown of *npm1* genes results in loss of *mpx*-expressing myeloid cells. A significant reduction was seen in myeloid cell numbers when each gene (*npm1a* and *npm1b*) is knocked down when compared to controls. This was significant when each was knocked down individually and was at least additive in the double knockdown experiments (*npm1a* + *npm1b*). Myeloid cell numbers were quantified by counting number of myeloid cells/embryo in the bar chart (right) for a 10–20 embryos per condition. *npm1a*MO = 5'UTR MO (1.4 ng). *npm1b*MO = 5'UTR MO (1.4 ng). *npm1(a+b)* = *npm1a* MO + *npm1b* MO (1.4 ng each). Control MO = *npm1a* 5bp mismatch and npm1b 5bp mismatch at 1.4 ng each. Error bars represent standard error of the mean. *p<0.02; **p=<0.01; ***p<0.0001 (unpaired two-tailed Student's t-Test).

Legend Figure 6-9: Left panels show lateral views of 48 hpf embryos. WISH assays for *mpx* in control injected (16ng) and *npm1a*+*npm1b* splice MO injected (*npm1a* E2-I2(2), 8ng +, *npm1a* E3-I3, 4ng + *npm1b* E2-I2, 4ng) embryos showing reduced *mpx*-expressing cells in the latter. Right panel shows bar chart of mpx+ myeloid cell numbers in 15 pooled embryos per condition; ***p<0.0001 (unpaired two-tailed Student's t-Test).

Legend Figure 6-10: RT-PCR genotyping using full length primers for *npm1a* (left) and *npm1b* (right) coding sequences. Sequencing of aberrant splice products (delineated by the white boxed lane) demonstrated truncating splice products at the sites indicated by arrows.

6.4.5 The reduction of *mpx*-expressing myeloid cell numbers after morpholino knockdown of *npm1 a* and/or *b* was partially rescued by *p53* loss

Some morpholinos are capable of activating the *p53*-pathway resulting in cell death (Robu et al, 2007). To ensure that the phenotype observed in *npm1a* and *npm1b* morphants was not a result of *p53*-mediated morpholino toxicity, the morpholinos directed against npm1a and npm1b were injected into the $p53^{e7/e7}$ line (harbouring a mutation in the DNA-binding domain, rendering it resistant to radiation induced cell death (Berghmans et al, 2005)) and analysed by WISH for *mpx* expression at 2 dpf. Compared to wild-type AB embryos, $p53^{e7/e7}$ injected embryos also showed a significant reduction of *mpx* expression (Figure 6-11).

172

While this experiment demonstrates that the loss of myeloid cells is not a result of morpholino-associated toxicity, there is clearly some increase in the number of myeloid cells observed in the *p53* mutant background. Given that NPM1 is known to interact with p53 it is possible that loss of myeloid cells occurred in part due to *bona fide* p53-dependant mechanisms. Given the current limitations of the assay it is difficult to be clear about the role of p53 in this setting.

6.4.6 Human NPM1 RNA rescued the reduction in *mpx+* myeloid cells in *npm1a+b* morphants

To functionally validate *npm1a* and *npm1b* as true orthologues of human *NPM1*, human NPM1 RNA was in vitro transcribed and injected into *npm1a+b* morphants at the one-cell stage, immediately after injection of the morpholinos. Injection of *NPM1* mRNA (10 pg) rescued both the myeloid and developmental defects when injected into *npma+b* double morphants, but, had no effect when injected along with the control MO (Figure 6-12). Complete rescue (defined as *mpx*-expressing cells/embryos greater than the lower limit of the 95% confidence interval of the control RNA/control MO injected embryos) was observed in 10% of embryos and partial rescue (defined as *mpx*-expressing cells/embryos greater than the upper limit of the 95% confidence interval of the *npm1a+b* MO, but, below the 95% confidence interval of the control RNA/control MO injected embryos) was seen in 50% of embryos. This data demonstrated that *npm1a* and *npm1b* are true functional orthologues of *NPM1*.
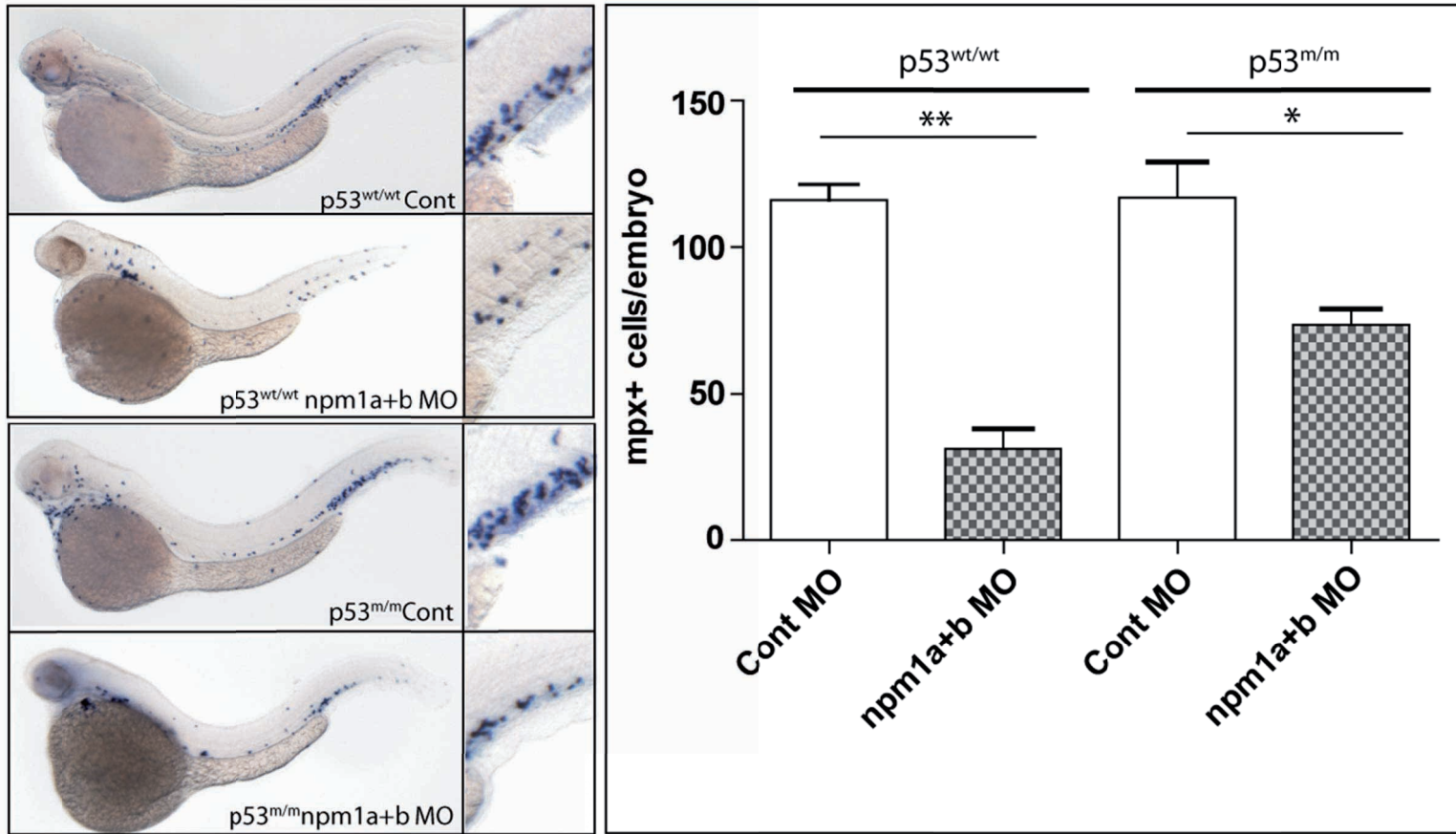
Figure 6-11 : $p53^{e7/e7}$ mutants partially rescued reduced numbers of *mpx+* myeloid cells in Npm1 morphants
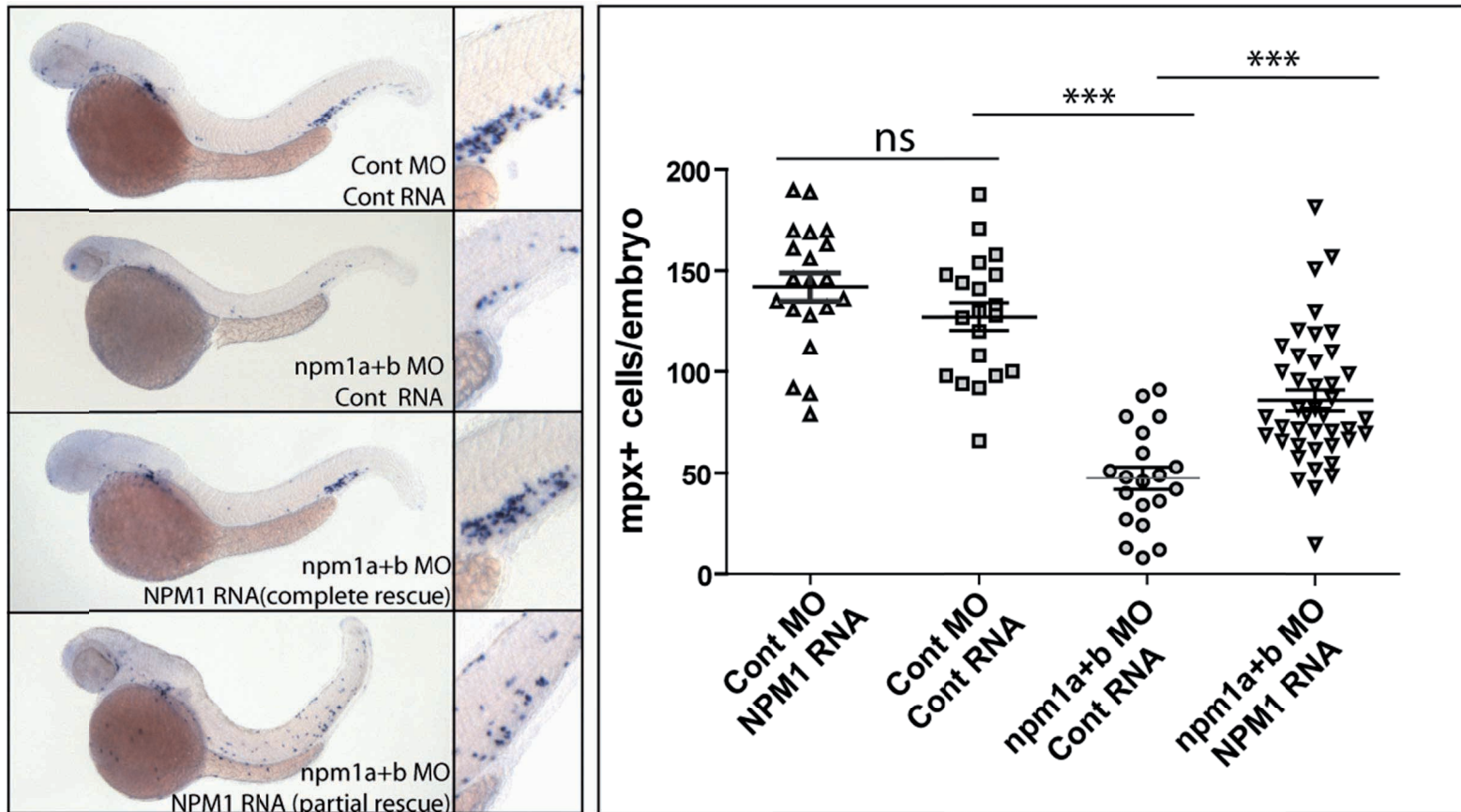
Figure 6-12 : Human NPM1 rescued reduced numbers of *mpx*+ myeloid cells in zebrafish Npm1 morphants

Legend Figure 6-11: Left panels; WISH for mpx in 48 hpf embryos showing reduced expression of *mpx* upon *npm1* knockdown in both the *p53^{WT/WT}* and *p53^{e7/e7}* backgrounds. Right panels: Bar charts shows numbers of mpx+ myeloid cells from 10–20 pooled embryos per condition. Error bars represent standard error of the mean. *p<0.02; **p=<0.01 (unpaired, two-tailed Students t-Test).

Legend Figure 6-12: Left panels show WISH for mpx at 48 hpf. Loss of *mpx* expression by knockdown of *npm1* could be rescued completely or partially by NPM1 RNA injection (10pg). No differential expression of *mpx* was observed when 10 pg. NPM1 or 10 pg. control (mCherry-encoding) RNA were injected with a control morpholino. Cell numbers were quantified as *mpx*-expressing cells/embryo on the scatterplot on the right which shows numbers of myeloid cells for individual embryos for clarity. *npm1a+b = npm1a* MO + *npm1b* MO (1.4 ng each). Control MO = npm1a 5bp mismatch and npm1b 5bp mismatch at 1.4 ng each. Error bars represent standard error of the mean. ***p<0.0005 (Unpaired two-tailed Student's t-Test).

6.5 Chapter discussion

Previous studies in our laboratory using morpholinos to knockdown the gene annotated as zebrafish *npm1* in NCBI did not result in a clearly abnormal phenotype, suggesting that additional orthologues of human NPM1 may exist in the zebrafish. Thus when I began my studies on zebrafish *npm1,* bioinformatics was used first to address whether or not there may be additional copies of the *npm1* gene. Gene duplication is common in teleost fish and can result in redundancy between duplicated genes. Bioinformatics BLAST searching revealed another putative copy of the *npm1* gene on chromosome 14. It was then demonstrated that both copies were syntenic with human chromosome 5 suggesting both *npm1a* and *npm1b* genes are true orthologues of human *NPM1*. In the case of nucleophosmin this is particularly important since even in the human genome there are a number of NPM1 pseudogenes as well as other nucleoplasmin family members that exhibit some homology with NPM1.

The expression pattern of endogenous zebrafish *npm1* genes was next addressed since gene duplication can sometimes result in differential expression patterns and 'split' functions between duplicated genes. WISH showed no

evidence of *npm1b* expression in haematopoietic tissues in contrast to *npm1a,* where a small amount if expression was evident in the PBI. This suggested that *npm1a* may play the dominant role in haematopoietic tissue in zebrafish. However, RNA ISH probes can be variable in terms of hybridisation efficiency based on their length and sequence and therefore to obtain more accurate information on expression in haematopoietic tissue RT-PCR was performed on cells sorted from adult kidney marrow into the major sub-populations of haematopoietic cells in zebrafish. This data showed that relatively high levels of expression of *npm1a* and *npm1b* were found in all zebrafish adult blood cell subsets. The lowest expression level was observed in *npm1b* in lymphoid cells. This observation has also been made in human immunohistochemical studies (of normal lymphoid cells) for NPM1 in patient samples (N Bolli and B Fallini personal communication).

To address the function of the zebrafish *npm1* genes *npm1a* and *npm1b* were knocked down both genes, alone and in combination. This demonstrated that loss of *npm1* genes resulted in reduced numbers of *mpx*-expressing myeloid cells. This phenotype was seen when each gene was knocked down individually, but, was more marked (at least additive) when both genes were knocked down together suggesting there is some redundancy between the two genes. Double knockdown also resulted in pronounced developmental phenotypes including small size, small head, small eye and shortened yolk extension. These features are in keeping with the murine Npm1 knockout where knockout mice are non-viable and show aberrant brain and eye development (as well as haematopoietic defects) (Grisendi et al, 2005).

Initial studies were carried out using morpholinos targeting the 5'UTR/ATG translation initiation sites of Npm1a and Npm1b. Despite testing several mouse and human antibodies for cross-reactivity it was not possible to identify an antibody that recognised either Npm1a or Npm1b. Therefore, to address the possibility of off-target effects causing the reduction in myeloid cells a selection of splice-blocking morpholinos where used and blocked splice donor sites in each gene. Several splice-blocking morpholinos tested did not result in any phenotype; however, "morphotyping" to detect for induction of aberrant splice products showed only WT transcripts suggesting the morpholinos were non-functional (Figure 6-10). Three morpholinos resulted in the production of aberrant splice

products (2 for *npm1a* and 1 for *npm1b*). A reduction in myeloid cell numbers was observed in splice morphants, but, the effect was more variable than that observed in the 5'UTR/ATG morpholinos, only apparent in the double knockdown, and lacked the developmental effects. The most likely explanation for this is that significant WT transcript was still present for both *npm1a* and *npm1b* (as shown in Figure 6-10). This could either be maternally derived (since maternal RNA is already spliced and is not blocked by splice morpholinos) or simply reflect incomplete blocking of WT splicing by the morpholinos. In either scenario WT Npm1 protein was likely to be present in these embryos, particularly since NPM1 (and Npm1 in mice) is known to have an extremely long half-life (in the order of days) (P Pandolfi personal communication). Thus the milder phenotype seen in splice morphants is likely due to less effective knockdown of Npm1 than in 5'UTR/ATG morphants. Because of this bias all subsequent experiments were carried out using the 5'UTR/ATG morpholinos.

To be certain the observed effects did not result from morpholino-induced toxicity known to activate the *p53* pathway, knockdown of Npm1a and Npm1b was carried out in *p53$^{e7/e7}$* mutants. A significant decrease in myeloid cells was observed in *npm1a+b* double morphants regardless of *p53* status. There was also a significant increase in the number of *mpx*-expressing cells in p53$^{e7/e7}$ mutants compared to *p53$^{WT/WT}$* in *npm1a+b* morphants (but not controls) suggesting that loss of *p53* may have partially rescued the *npm1a+b* phenotype. Published data describing the interaction of NPM1 and T53 are complex and at times contradictory (Colombo et al, 2002; Cuomo et al 2008; Kurki et al, 2004; Lambert & Buckle 2006; Li et al, 2006). NPM1 is known to directly bind P53 via the free loop of its DNA binding domain and the tetramerisation domain of P53 carrying a nuclear export signal (NES) (Lambert & Buckle, 2006). In this regard it has been proposed that NPM1 protects P53 from exposing its tetramerisation domain (necessary for activation) and NES and maintains a nuclear/nucleolar reservoir of P53, protected from nucleoplasmic degradation HDM2. NPM1 also interacts directly with HDM2 in response to ultraviolet damage or viral stress. Upon exposure to such stressors NPM1 is translocated from nucleolus to nucleoplasm where it competes with P53 for HDM2 at its N terminus. In cells exposed to UV irradiation or viral stressors, this NPM1–HDM2 interaction preceded P53-stabilisation (Kurki et al, 2004). In keeping with this, overexpression of NPM1 in mouse embryonic fibroblasts resulted in p53-

dependent senescence response showing co-localisation of NPM1 and p53 in the nucleolus (P53 is usually nucleoplasmic). Paradoxically, loss of NPM1 in a murine knockout model showed p53-dependent tetraploid cell cycle arrest (post-mitotic) in Npm1 null and hypomorphic cells and reduced growth in Npm+/-MEFs. The growths of these cells could be rescued by loss of *p53* (Grisendi et al, 2005). A potential explanation for these observations is that p53 stability and maintenance is likely to depend on NPM1 level, subcellular localisation, tissue specificity and genetic background.

To determine conclusively that NPM1 was the true orthologue of Npm1a and Npm1b, rescue experiments were performed using *in vitro* transcribed human NPM1 RNA injection. Overexpression of human NPM1 resulted in rescue of myeloid cell numbers seen at 48 hpf showing zebrafish Npm genes were the true orthologues of NPM1. Human RNA was chosen for study and not the individual zebrafish gene RNA for two reasons. Firstly, future project plans included the generation of a transgenic zebrafish model of AML using the mutated human NPM1 and therefore it was necessary to ascertain that *npm1a and npm1b* were functional orthologues of NPM1. Secondly, the phenotype seen using *npm1a* and *npm1b* 5'UTR morpholinos was far more robust than the splice morpholinos phenotype. Rescue with zebrafish *npm1a* and *npm1b* RNA in the 5'UTR/ATG morphants would require site-directed mutagenesis to introduce silent mutations' in the 5'UTR/ATG coded by the morpholinos, otherwise the morpholinos would simply bind and prevent translation of the in vitro transcribed RNA.

The data generated in this chapter confirmed that *npm1a* and *npm1b* have an essential role in zebrafish haematopoiesis and suggest that the zebrafish could be used to model NPMc leukaemias. In addition to the work described in this chapter, in collaboration with Dr Niccolo Bolli, I have demonstrated that over-expression of the human NPMc+ mutant results in aberrant production of haematopoietic stem cells in developing zebrafish indicating a putative role for NPMc+ in leukaemogenesis (Bolli and Payne et al, 2010) (original manuscript attached).

7. RPS14 and RPS19 in zebrafish haematopoiesis

7.1 Introduction

A decade ago haploinsufficiency for RPS19 was identified as the genetic event responsible for DBA in 25% of patients with this disease (Draptchinskaia et al, 1999). More recently, investigators have tried to elucidate the mechanisms responsible for the haematopoietic tissue-specific effects of disruption of RPS19 in such patients, despite the ubiquitous expression of RPS19. Several studies have identified non-ribosomal functions of RPS19, such as a putative phospho-dependent function following phosphorylation by haematopoietic associated kinase PIM1 (Chiocchetti et al, 2005). However, the identification of mutations affecting other ribosomal protein genes (coding for both small and large ribosomal subunits) in DBA patients, along with the delineation of the pivotal role of RPS14 in the anaemia associated with 5q- syndrome MDS, has led to the paradigm that it is ribosome dysfunction per se that plays a dominant role in the pathogenesis of these diseases (Narla & Ebert, 2010). Several years before ribosome dysfunction had been implicated in DBA, it was established that increased apoptosis of erythroid progenitors occurred in erythroid cells from DBA patients (Perdahl et al, 1994). Subsequently p53-mediated apoptosis has been proposed as a mechanism by which loss of RPS19 might adversely affect erythroid development (Danilova et al, 2008; Narla & Ebert, 2010). This is consistent with the model that ribosomal stress results in p53 stabilisation in an MDM2-dependent manner (Deisenroth & Zhang, 2010).

In 2008 Ebert *et al.* demonstrated that RPS14 haploinsufficiency was a major mechanism contributing to anaemia in 5q- syndrome MDS (Ebert et al, 2008). Subsequently a knockout mouse carrying conditional deletion of 7 genes including RPS14 has been generated resulting in an MDS-like disease that can at least partially be rescued by loss of p53. Bone marrow progenitors from these RPS14-deficient mice show increased apoptosis (Barlow et al, 2010). Evidence of increased P53 protein expression has also been observed in patient samples from 5q- syndrome trephine biopsies suggesting that P53 plays a role in the pathogenesis of this disorder (Pellagatti et al, 2010b).

Since DBA is an inherited disease, the role of apoptosis as a primary pathogenic mechanism for anaemia is a very plausible. This is because all cells will carry the

mutation and affected erythroid or haematopoietic progenitor cells do not require a selective survival advantage to maintain a pathological clone. In addition, DBA patients are at increased risk of a range of solid tumours with similar tissue distributions to those occurring in patients with Li Fraumeni syndrome; where patient inherit heterozygous *P53*-inactivating mutations. This latter observation suggests a selective pressure for clones with mutated or reduced P53 occurs in tumorigenesis in DBA patients. By contrast, in the case of 5q- MDS, where only somatic haematopoietic cells have haploinsufficiency for RPS14, erythroid cells primed to die as a result of P53 stabilisation and apoptosis would be unlikely to have a survival advantage and clones carrying such deficiencies should be eliminated in the presence of a functional P53 response. Furthermore, non-5q-syndrome MDS with loss of 5q (i.e. those with other cytogenetic abnormalities) are frequently associated with loss of P53 and appears to confer a poor prognosis (Merlat et al, 1999). Furthermore, regardless of the mechanistic role of P53 in the apoptosis in the pathogenesis of anaemia in RP-deficient states, P53 loss is inherently tumorigenic, and thus manipulation of this pathway for therapeutic purposes is not appropriate. Therefore two key questions remain unanswered:

1. If loss of RPS14 in haematopoietic stem cells is an initiating event in the development of MDS, what mechanism gives these cells a survival advantage?

2. Are there *p53*-independent mechanisms contributing to MDS and DBA with ribosomal protein deficiencies and might be amenable to therapeutic manipulation?

The zebrafish is an excellent model system to study the effects of ribosomal protein loss on erythropoiesis. Ribosomal proteins are highly conserved between zebrafish and humans (Rps14 has a single amino acid difference in zebrafish compared to humans). Furthermore, cross-reactive antibodies are readily available. In this chapter the zebrafish is used to model the anaemia observed in DBA and MDS using morpholinos. Importantly, a p53-independent component to the anaemia observed in Rps14 and Rps19 knockdown zebrafish is identified and has the potential to lead to the identification of a new therapeutic target in Rps14 deficient DBA patients.

7.2 Aims of the experiments described in this chapter

1. To determine the effects of Rps14 and Rps19 knockdown on zebrafish erythropoiesis
2. To identify key features of p53-dependent and independent anaemias in Rps14 and Rps19 morphants
3. To identify p53-independent mechanisms that contribute to anaemia in Rps14 and Rps19 morphants

7.3 Methods

7.3.1 Morpholino knockdown and RNA rescue experiments

Morpholinos for Rps19 knockdown were designed by Gene-tools LLC (splice morpholinos) or from published research ((Uechi et al, 2008) (5'UTR/ATG morpholinos). Rps14 morpholinos were designed to block E2-I2 boundary. Standard Gene-tools control morpholinos were used (MO sequences are annotated in full in Appendix 1).

Western blotting was performed to demonstrate knockdown of Rps19 and Rps14 respectively using goat anti-human RPS19 (Santa Cruz) at a dilution of 1:5000 and rabbit anti-human RPS14 (Santa Cruz).

Rps14 cDNA was cloned into pCS2+ using one-step PCR from RNA obtained from 2 dpf embryos (Qiagen) as described in 2.3.1. *Rps19* cDNA in pCS2+ carrying silent mutations within the binding site for the 5'UTR/ATG morpholino was a gift from Naoya Kenmochi and Tamayo Uechi from the University of Miazaki. *rps14* and modified *RPS19* were in vitro transcribed as described in section 2.3.2. Rescue experiments were carried out with a range of RNA quantities from 10–400pg.

7.3.2 *O*-Dianisidine staining for haemoglobin content

Dechorionated embryos were placed in a 12-well plate and stained with 1 ml of freshly made *O*-dianisidine staining solution (below) for 15 minutes at RT in the dark. Stock *O*-diansidine (1.4 mg/ml in 100% ethanol) solution was kept in the dark at RT for 1 month.

<u>O-dianisidine staining solution</u>

O-dianisidine stock	2 ml
1 M Sodium acetate buffer (pH4.7)	50 μl
Deionised water	2 ml
Hydrogen peroxide (30%)	100μl

Embryos were then washed 3 times in PBST for 5 minutes each, fixed for 1 hour with 4% PFA, washed again in PBST and equilibrated in 90% glycerol overnight before imaging on a DIC dissecting microscope.

7.3.3 Flow cytometric cell sorting

Sorting of dsRED2-expressing cells from whole embryo lysates was performed on a FACSAria flow cytometric cell sorter as described in 2.11.

7.3.4 May-Grunwald-Giemsa (MGG) staining

dsRED2-Flow cytometrically sorted cells were cytospun onto poly-D-lysine coated slides in a Thermo Scientific Cytospin 4 cytocentrifuge at 350rpm for 4 minutes. Following air-drying overnight, they were fixed in 100% methanol for 5 minutes in a Coplin jar. Slides were then stained for 10 minutes in May-Grunwald (Fluka), rinsed with distilled water briefly and then stained for 20 minutes in freshly diluted Giemsa (10ml Giemsa (Fluka) + 40 ml distilled H_2O). Slides were rinsed for 5 minutes in distilled water and allow to air-dry overnight. Dry slides were mounted with a coverslip using perimount and visualised on a Zeiss Axio imager Z1 compound microscope (Zeiss).

7.4 Results

7.4.1 Morpholino knockdown of Rps19 results in both p53-dependent and p53-independent anaemia and developmental defects

Rps19 was knocked down in zebrafish using anti-sense morpholinos. To account for possible morpholino-associated toxicity from the *p53* pathway, *p53*$^{e7/e7}$ mutant embryos were injected alongside *p53*$^{WT/WT}$ embryos. *rps19* MO-injected p53$^{WT/WT}$ embryos exhibited reduced haemoglobin levels and developmental abnormalities including small body, small head and short yolk extension when compared to control MO injected *p53*$^{WT/WT}$ embryos (Figure 7-1, left panels). These findings

are on keeping with published data on the effects of Rps19 knockdown in zebrafish embryos (Danilova et al, 2008; Uechi et al, 2008). In contrast, $p53^{e7/e7}$ mutant embryos injected with *rps19* MO had much less marked developmental defects and a more modest, but persistent reduction in haemoglobin when compared to control MO-injected $p53^{e7/e7}$ mutant embryos (Figure 7-1 right panels).

To determine if the protein levels of Rps19 in morphants were in the haploinsufficient range a Western blot was performed using anti-human Rps19 antibody (Santa Cruz) at 1:5000 and secondary anti-goat HRP conjugate. Quantitation performed using Image J software showed around 40% knockdown in Rps19 morphants relative to controls (normalised to beta actin). Overexpression of *rps19* increased the Rps19 protein levels to 1.8 fold and 1.2 fold in the rescue experiment (Figure 7-2).

To determine whether the amelioration of Rps19 knockdown-related developmental phenotype and anaemia observed in $p53^{e7/e7}$ mutants was the result of off-target *p53* pathway activation by the *rps19* morpholino, rescue experiments were performed using *rps19* RNA. Since the *rps19* MO was a 5'UTR/ATG morpholino, RNA was modified to contain silent mutations in the regions of morpholino binding. Expression of the *rps19* RNA in combination with *rps19* MO was able to rescue the anaemia and developmental effects of Rsp19 knockdown to normal levels in 60% of cases (Figure 7-3). Rescued *rps19* morphants demonstrated either completely normal haemoglobin level with no developmental effects or remained phenotypically similar to non-rescued morphants, suggesting a threshold Rps19 level may be required for normal development (Figure 7-3). The RNA dose for *rps19* was titrated from 10pg to 400pg. No difference was observed in the level of rescue or toxic effects from the different doses injected.

Figure 7-1 : Morpholino knockdown of Rps19 in $p53^{WT/WT}$ and $p53^{e7/e7}$ mutated zebrafish

Legend Figure 7-1 : Haemoglobin staining with O-dianisidine at 48 hpf. Knockdown of Rps19 using a morpholino targeting the 5'UTR/ATG (lower panels) in $p53^{WT/WT}$ (left panels) and $p53^{e7/e7}$ (right panels) results in anaemia. Both embryos also show developmental abnormalities (small size and head, shorter yolk in $p53^{WT/WT}$, small head in $p53^{e7/e7}$). Partial amelioration of both developmental abnormalities and anaemia is observed in the $p53^{e7/e7}$ mutant background.
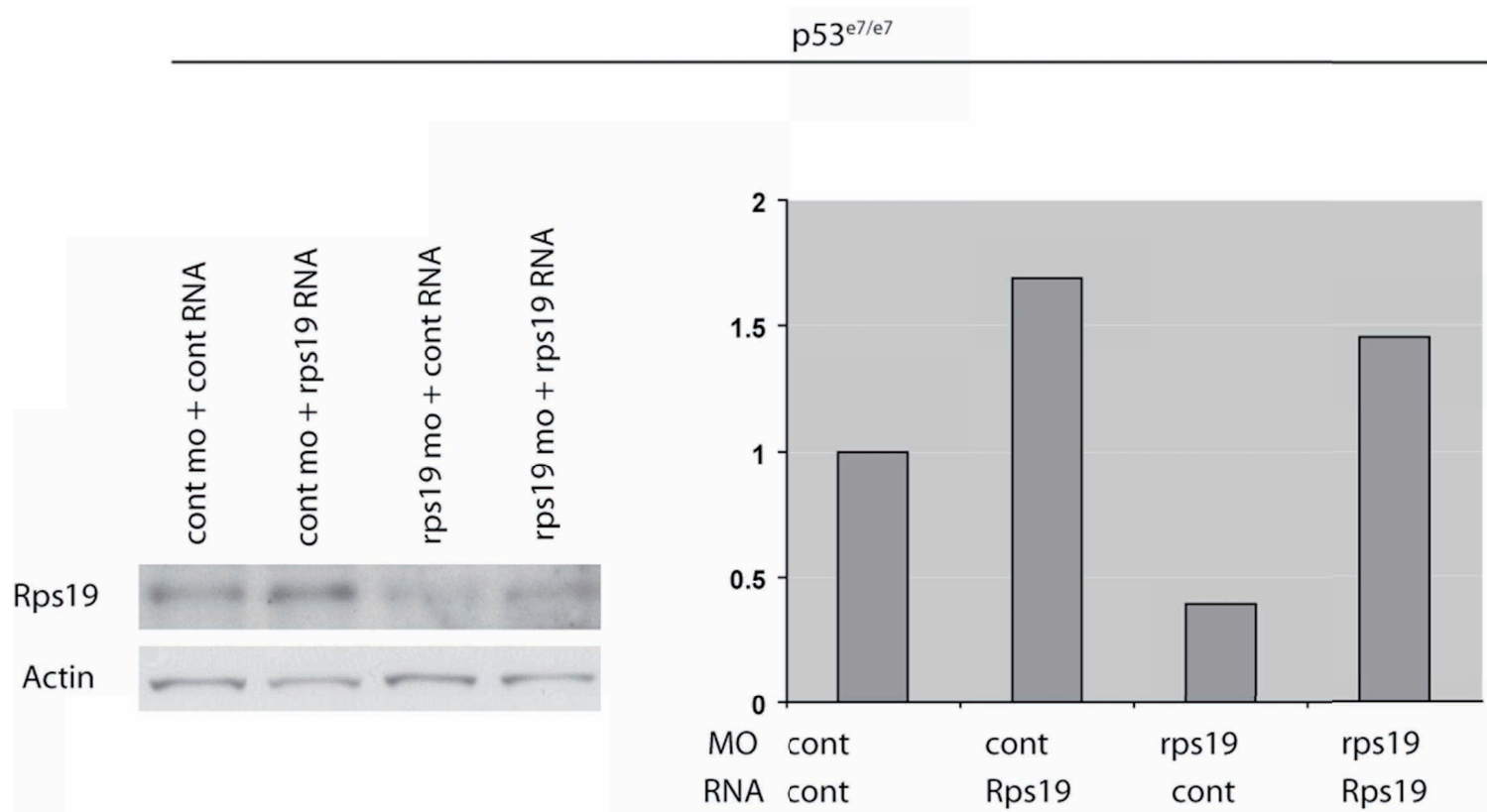
Figure 7-2 : Rps19 protein levels after MO knockdown are approximately 50% of levels seen in control zebrafish, approximating haploinsufficiency
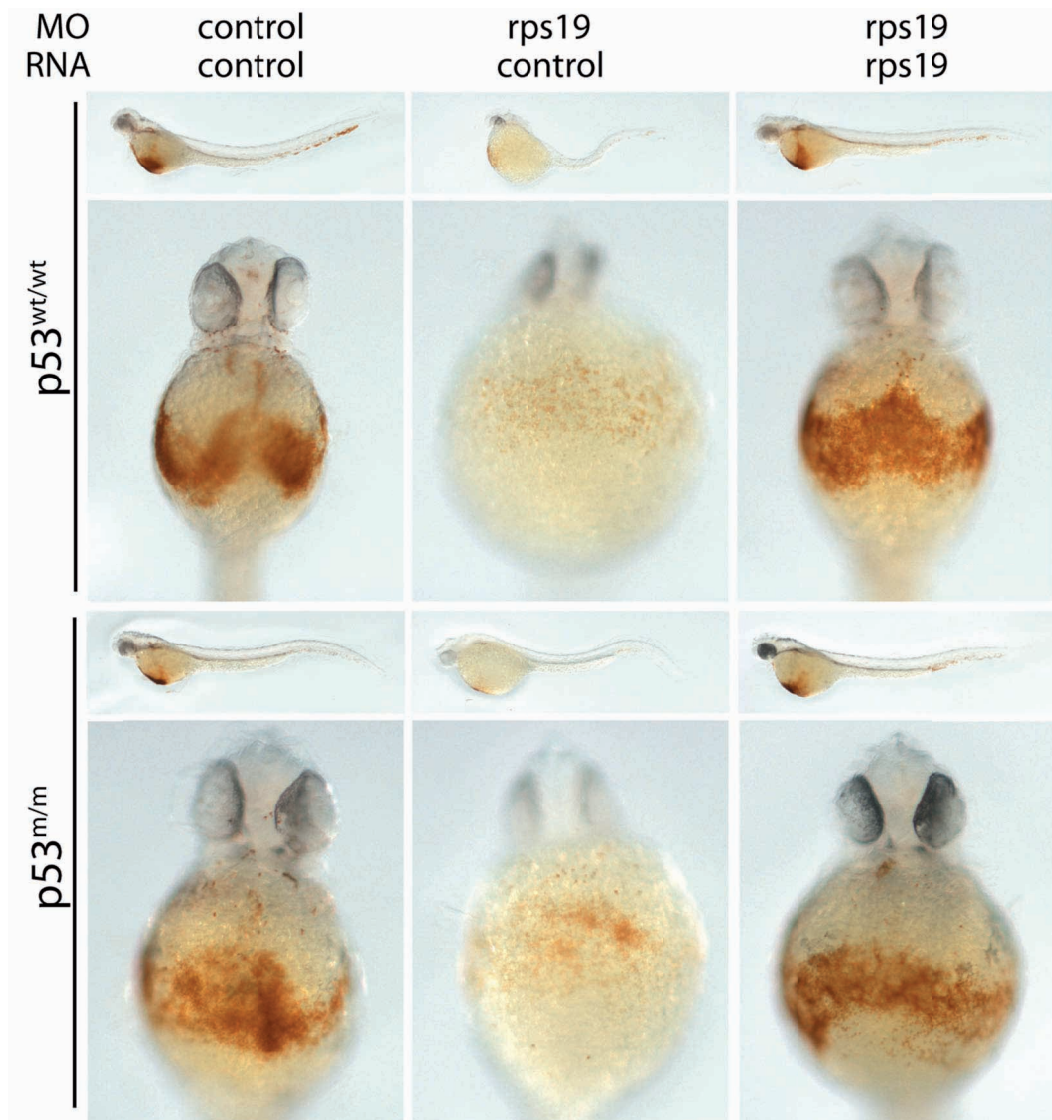
Figure 7-3 : Modified *rps19* RNA rescues both anaemia and developmental defects in *rps19* morphants

Legend Figure 7-2: Polyacrylamide gel electrophoresis immunoblot (left) and Image J quantification (right) demonstrate the level of MO knockdown of Rps19 protein (shown for this Western blot). Blots are derived from whole embryo extracts at 48 hpf. Relative quantification of Rps19 in embryos injected with 0.16ng *rps19* MO show 45% of the levels of Rps19 protein seen in control MO-treated animals. Overexpression using 100pg of *rps19* modified RNA with control MO shows increased expression to ~1.7 fold control. Rescue of *rps19* MO injected embryos with modified *rps19* RNA show the Rps19 protein level at 1.4 fold of control.

Legend Figure 7-3: *O*-dianisidine staining for haemoglobin at 48 hpf, injected with *rps19* morpholino or controls along with modified Rps19 RNA or Control (mCherry-encoding) RNA. Upper panels $p53^{WT/WT}$, lower panels $p53^{e7/e7}$. Expression of modified RNA for r*ps19* (carrying 5 silent mutations at the morpholino binding site) rescues the developmental defects and anaemia observed in *rps19* morphants.

7.4.2 Loss of Rps14 also results in p53-independent anaemia.

The question of p53-independent anaemia observed in *rps19* morphants being specific to Rps19 or also occurred with loss of other RPs known to play a role in human disease was next addressed. A splice-blocking morpholino was used to knockdown Rps14. In common with my findings for Rps19, anaemia and developmental defects were apparent in the *rps14* morphants compared to controls and this effect could not be almost completely rescued with loss of p53 (Figure 7-4 upper panels). The anaemia and developmental effects could also be rescued by co-injection of *rps14* in vitro transcribed RNA along with the *rps14* MO. Since the *rps14* morpholino was designed to block normal splicing, *rps14* levels were initially titrated and quantified at the RNA level using one-step RT-PCR on whole embryo lysates from 2 dpf embryos (Figure 7-4 bottom left). The approximate 50% knockdown in transcript was confirmed at the protein level using a rabbit anti-human RPS14 antibody (Figure 7-4 bottom right). Thus a knockdown level of around 50% was observed in *rps14* morphants using both RNA and protein readouts.
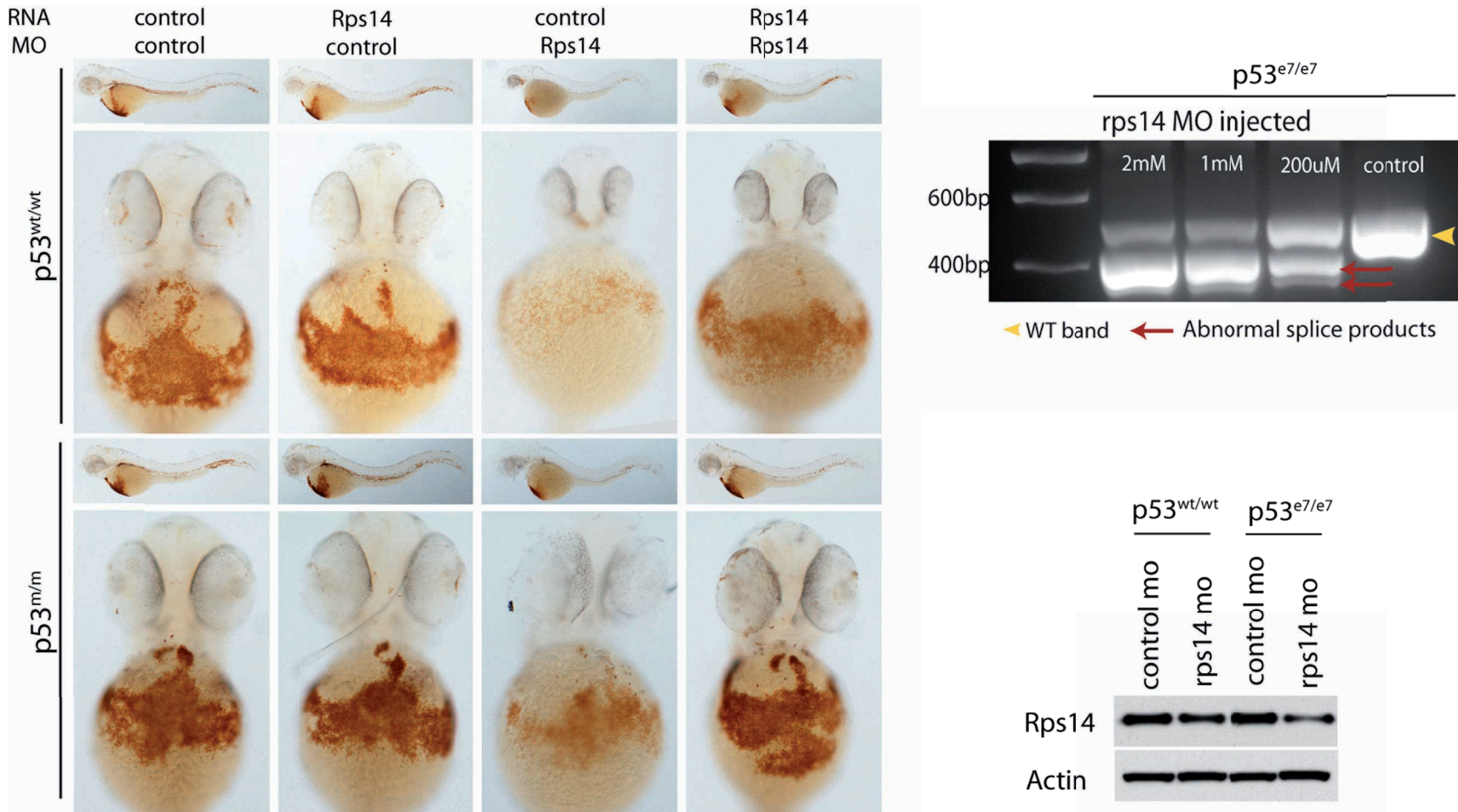
Figure 7-4 : Haploinsufficient loss of Rps14 also results in p53-independent anaemia

Legend Figure 7-4: Loss of Rps14 by morpholino knockdown results in p53-dependent and p53-independent anaemia (top panels). Levels of *rps14* RNA by "morphotyping" with full length primers at 2 dpf showed fish treated with 200μM (1.6ng) of *rps14* morpholino had approximately 50% of the level of *rps14* transcript seen in control MO-treated fish.

7.4.3 Loss of Rps19 results in macrocytic erythropoiesis

One cardinal feature of DBA patients, also seen in most MDS patients, is the presence of macrocytosis. Interestingly, macrocytosis persists in DBA patients who have undergone spontaneous remission of anaemia and are independent of transfusion and/or steroid therapy. The question of loss of Rps19 resulting in macrocytic anaemia in zebrafish was asked. The transgenic zebrafish line Tg(gata-1: dsRED2) was injected with *rps19* morpholino or control MO. Gata-1 is a master erythroid transcription factor and *Tg(gata-1:dsRed2)* zebrafish express dsRed in their erythroid cells from 30 hpf through to adulthood (Traver et al, 2003). For loss of p53 in this line I used a *p53* MO (Berghmans et al, 2005) *Tg(gata-1:dsRed2)* injected embryos were dissociated and sorted on a FACSAria. As shown in Figure 7-5, *rps19* MO-injected embryos had less erythroid cells than control MO-injected cells. This effect was also seen when *p53* MO was injected along with *rps19* or control MOs. In addition, cells gated on dsRED2 expression were macrocytic when compared to control MO-injected morphant cells. The *rps19* MO-associated macrocytosis was not apparent in embryos also injected with *p53* MO. Flow cytometry-sorted dsRED expressing (erythroid) cells were also cytospun and stained with MGG (Figure 7-6). *rps19*-MO-injected embryos showed features suggestive of a more primitive erythroid cell development (erythroid macrocytosis, a high nuclear: cytoplasmic ratio, open chromatin pattern) compared to control injected embryos (mature erythroid cells are nucleated in zebrafish). In cells from embryos injected with both *rps19*- and *p53*-MOs the erythroid cell development was still abnormal, although morphologically more mature and normocytic than erythropoiesis in fish treated with *rps19*-MO alone (Figure 7-6, far right panel). These data demonstrate that loss of Rps19 results in macrocytic anaemia as a result of reduced cell numbers and that the macrocytosis but not the anaemia is p53 dependent.
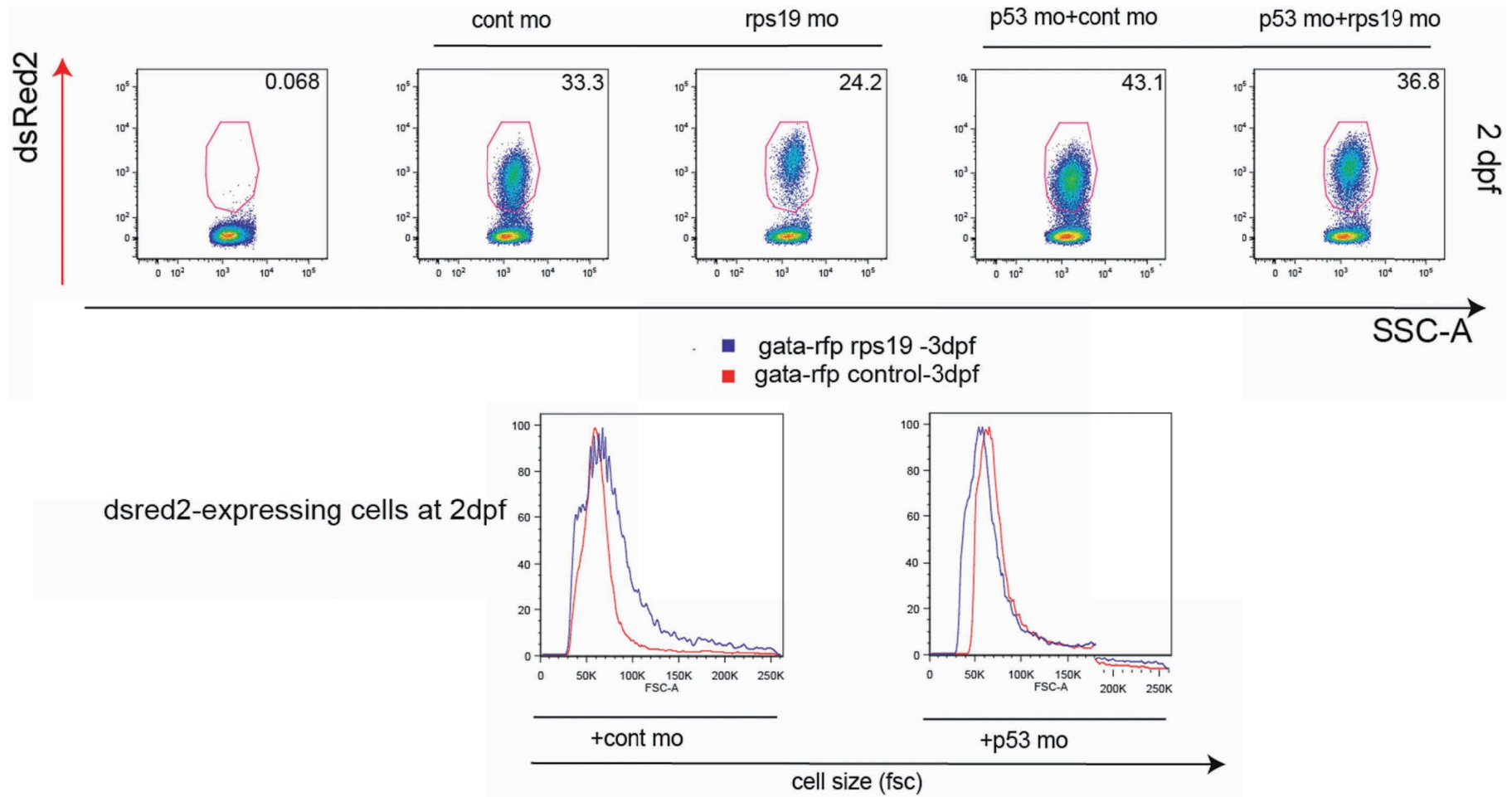
Figure 7-5 : Rps19 loss results in a reduction in proportion of erythroid cells which persists despite *p53* knockdown, and an erythroid macrocytosis which is corrected by *p53* knockdown
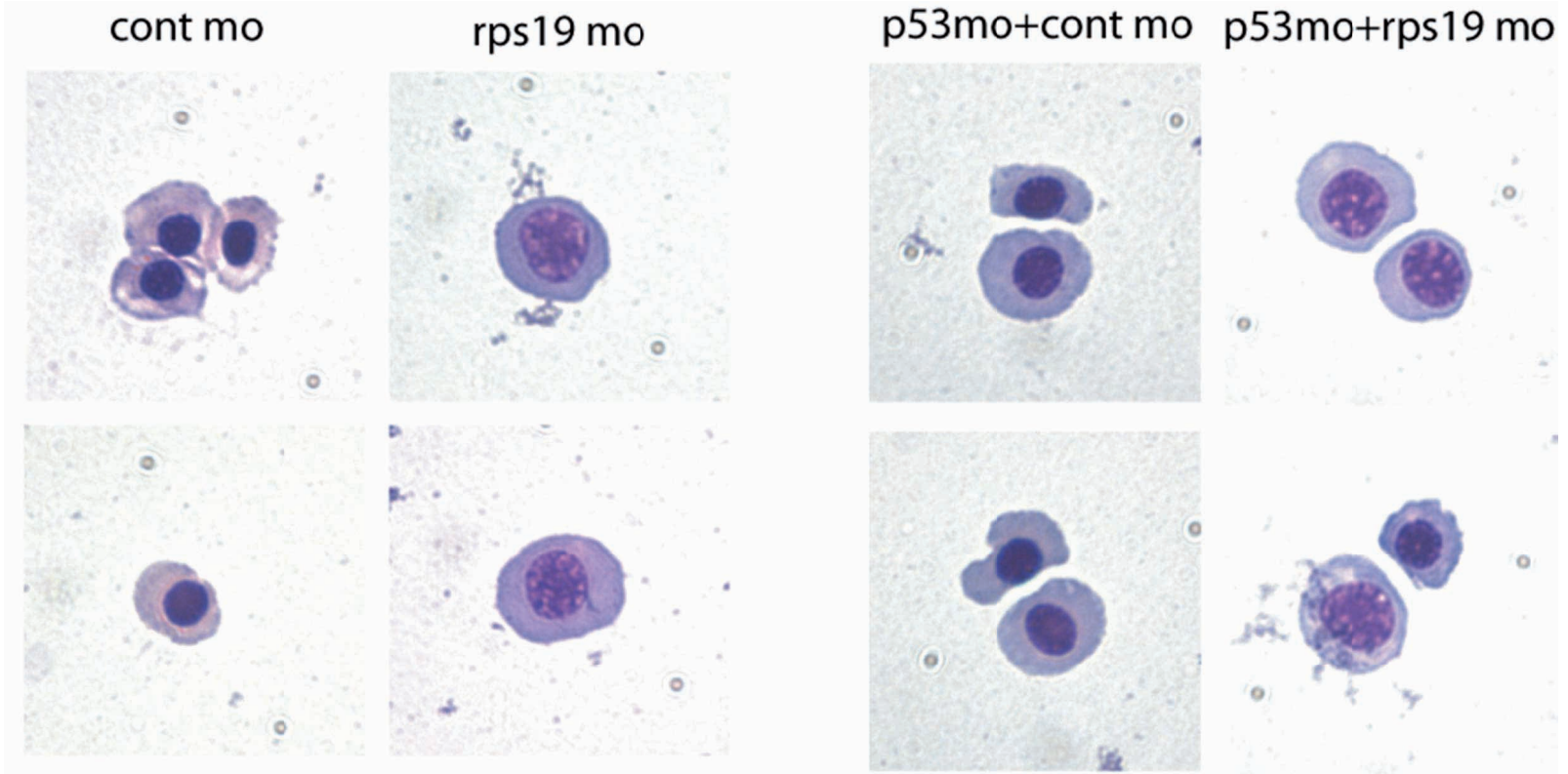
Figure 7-6 : Morphology of Rps19-deficient cells without and with additional *p53* knockdown, by MGG staining

Legend Figure 7-5: Rps19 loss results in a reduction in the proportion of erythroid cells which persists despite p53 knockdown and an erythroid macrocytosis corrected by p53 knock-down.

Upper panels; representative dot plots at 3 dpf showing erythroid cells (dsRED, y axis) and forward scatter (x axis) in conditions 1, 2, 3, 4 and 5. Numbers in upper right corner of dot plots represent percentage of erythroid cells.

Lower panel; *rps19* morphants have macrocytic dsRED2-expressing erythroid cells corrected on injection of *p53* MO (Lower histograms gated on dsRED2 positive cells show control in red, *rps19* morphants in blue with FSC indicating cell size on the x-axis).

Legend Figure 7-6: Morphology of Rps19-deficient cells without and with additional *p53* knockdown, by MGG staining Cytospins of dsRED2 expressing cells from *rps19* morphants and controls with and without additional *p53* MO knockdown (3 dpf). *rps19* morphant erythroid cells are macrocytic with a high nuclear: cytoplasmic ratio and open chromatin pattern suggestive of a block in differentiation (left panels). The addition of *p53* morpholino normalises the size of erythroid cells and partially corrects in the nuclear morphology (right panels).

7.4.4 Loss of Rps19 in zebrafish embryos resulted in p53-independent apoptosis

Previous work by Danilova and colleagues in 2008 has shown that loss of Rps19 in zebrafish embryos results in activation of p53 family members and apoptosis. Embryos in their study were examined at 24 hpf. It can be reasoned that the loss of erythroid cells observed in *rps19* morphants independent of p53 observed at later timepoints may have been the result of apoptosis programmed to have effect later in development, thus preferentially affecting definitive erythroid development (not established until after 24 hpf). A whole mount TUNEL assay was therefore performed on *rps19* morphants and controls in $p53^{WT/WT}$ and $p53^{e7/e7}$ embryos at both 3 and 4 dpf. At 3 dpf it was observed that there was an increase in apoptotic cells in $p53^{e7/e7}$ embryos injected with *rps19* MO similar to that observed in the $p53^{WT/WT}$ embryos injected with *rps19* MO (Figure 7-7). However, the location of the TUNEL positive cells did not appear to correspond to

the blood-forming regions of the embryo. Therefore, although p53-independent cell death is clearly observed in *rps19* morphants, it is unclear whether this could account for the anaemia observed in *p53^{e7/e7}* *rps19* morphants.

Figure 7-7 : Whole mount TUNEL stain show p53-independent cell death in *rps19* morphants at 3 dpf

Legend Figure 7-7 : Whole mount TUNEL stain of 3 dpf *rps19* morphants in *p53$^{WT/WT}$* (left) or *p53$^{e7/e7}$* mutants (right). *p53$^{e7/e7}$* mutants injected with *rps19* morpholino show an increase in TUNEL positive cells compared to controls (right panels) and at a similar level as the *p53$^{WT/WT}$* embryos injected with *rps19* morpholino (left panels).

7.4.5 Loss of p63 or p73, either alone or in combination with p53, did not rescue the anaemia in Rps19 morphants

Danilova has also observed that in *rps19* morphants several p53-related family members were transcriptionally activated (Danilova et al, 2008). They specifically noted an increase in expression of the p63 isoform deltaNp63. p63 isoforms are derived from one of two promoters with the deltaN forms lacking the N terminus transactivating (TA) domain. This isoform is the most abundantly expressed p63 isoform in zebrafish during early development. DeltaN forms of p63 are thought to function as repressors rather than activators of transcription, since they lack the TA domain (Ghioni et al, 2002). Paradoxically, Danilova and colleagues observed an additive improvement in developmental defects with loss of both p53 and p63 in *rps19* morphants. Thus, p63 was knocked down alone and in combination with p53 in *rps19* morphants to determine if p63 was contributing to the anaemia. Loss of p63 alone resulted in a very mild anaemia in control injected embryos in both $p53^{WT/WT}$ and $p53^{e7/e7}$ embryos. No improvement in the anaemia of *rps19* morphants was observed either with p63 loss alone or in combination with $p53^{e7/e7}$ compared to the relevant controls (Figure 7-8 and Figure 7-9).

Since there are several isoforms of p63, the p63 splice-blocking morpholino was designed to remove all isoforms. This can be seen by the RT-PCR morphotyping (Figure 7-10, left panel) where there was no residual WT transcript.

To address whether the p53 family member p73 could contribute to cell death and anaemia in *rps19* morphants, p63 and p73 alone or in combination were knocked down, in both $p53^{WT/WT}$ and $p53^{e7/e7}$ fish (Figures7-8 and 7-9).

No improvement in the anaemia of RPs19 morphants was observed with loss of p73. In fact p73 morphants exhibited a p53-independent anaemia which was also independent of Rps19 (Figures 7-8 and 7-9). This effect may have been consequent on the fact that p73 has been shown to regulate the major erythroid regulator Gata-1. The *p73* morpholino was a 5'UTR/ATG translation blocking morpholino and therefore its functional effects were demonstrated using Alcian blue, an immunohistochemical stain marking cartilage. p73 has a known function in development of the branchial arch cartilage, thus Alcian blue serves as a positive control for the *p73* morpholino (Rentzsch et al, 2003).
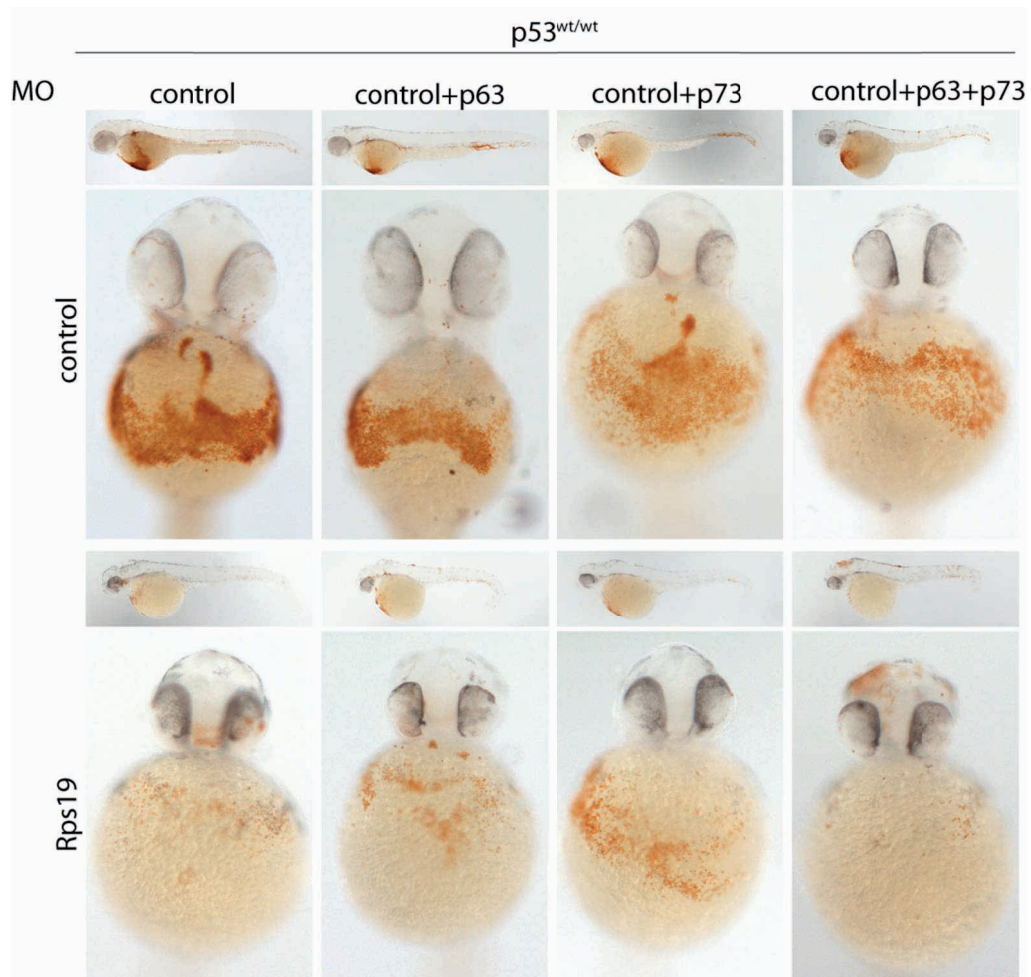
Figure 7-8 : Loss of *p63* or *p73* alone or in combination does not rescue anaemia in *rps19* morphants
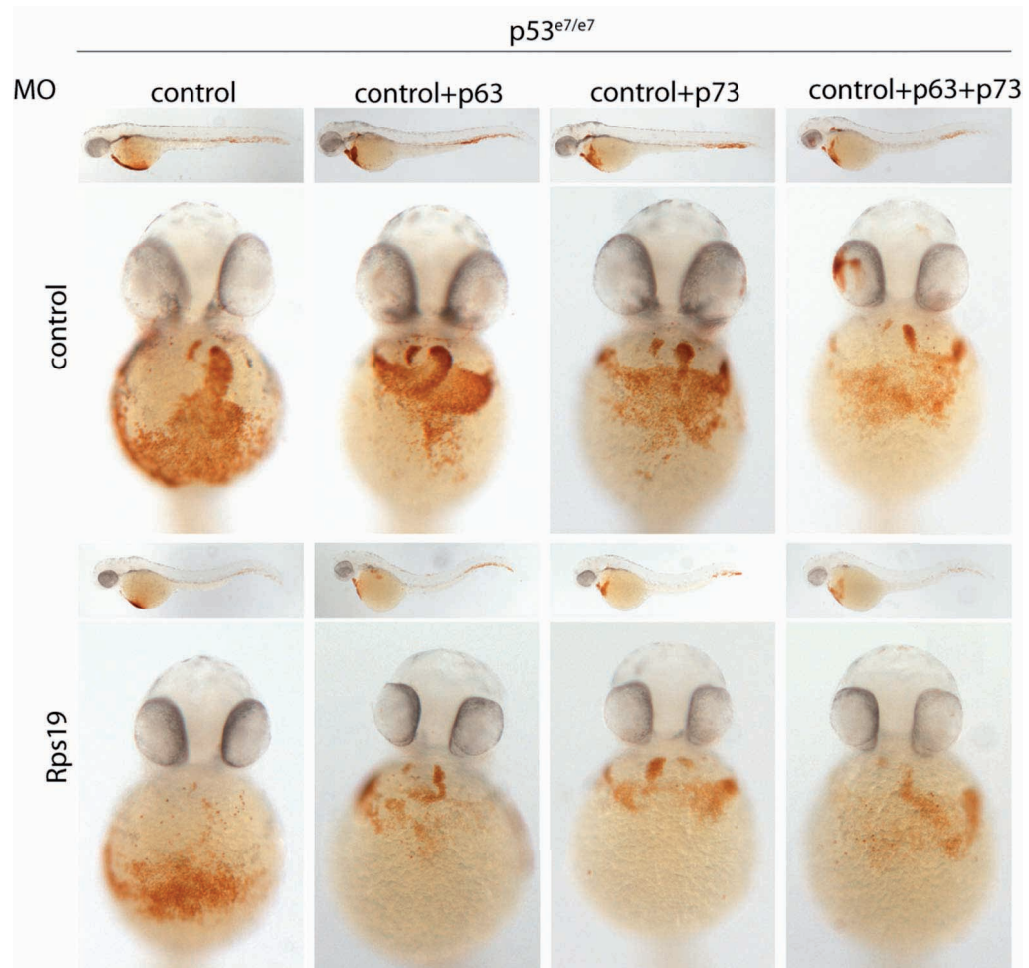
Figure 7-9 : Loss of *p53*, *p63* or *p73* alone or in combination does not rescue anaemia in *rps19* morphants
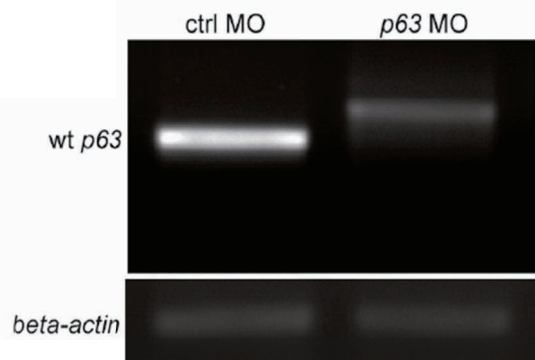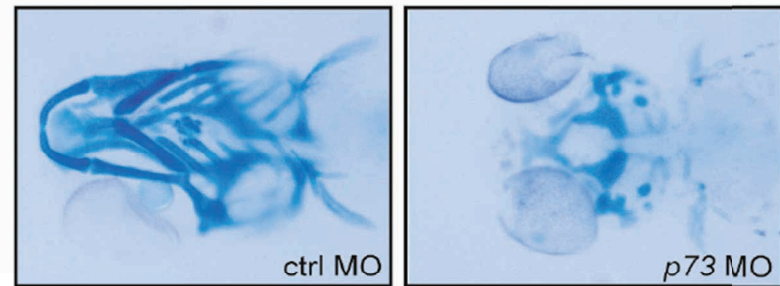
Figure 7-10 : *p63* and *p73* morpholinos are functional (Pictures courtesy of Dr. Ujwal Pyati and Dr. Sam Sidi)

Legend Figure 7-8: Loss of p63 or p73 alone or in combination does not rescue the anaemia in *rps19* morphants. Injection conditions are as indicated. *p63* MO dose is 5ng.

Legend Figure 7-9: Loss of p53, p63 or p73 alone or in combination does not rescue the anaemia in *rps19* morphants. *p63* and *p73* MO doses are 5ng each. Loss of p73 alone results in anaemia independent of the *rps19* morpholino.

Legend Figure 7-10 : Splice-morphotyping confirms effective knockdown of all WT *p63* transcripts (left gel, red arrow indicates WT transcript, blue arrow indicates aberrant splicing resulting in intron retention and premature stop codon) at 24 hpf. Right panels show alcian blue stain for cartilage in control and *p73* MO (5ng) Loss of p73 results in aberrant jaw development, a known developmental function of p73 (shown at 4 dpf) (Rentzsch et al, 2003). Morphotyping and Alcian blue staining courtesy of Ujwal Pyati.

7.4.6 Stress response is activated following knockdown of Rps19

The observation that p53 and p63 loss could not rescue the anaemia induced by loss of Rps19 suggests that an alternate pathway is activated in *rsp19* morphants leading to apoptosis also accounting for the presence of TUNEL positive cells in $p53^{e7/e7}$ 3 dpf morphants. Another possibility is that the dominant mechanism leading to anaemia in the absence of p53 is not cell death, but, another process such as cell cycle arrest or senescence. Addressing the first hypothesis, one pathway known to result in p53-independent apoptosis is the integrated stress response pathway. This can be activated by various stressors such as amino acid deprivation, double stranded RNA viruses, endoplasmic reticulum (ER) stress or haem deficiency. Activation of apoptosis in response to stress is mediated by phosphorylation of the eukaryotic initiation factor 2 subunit 1 alpha (EIF-2alpha or EIF2S1) at serine 51. Depending on the type of stress signal, one (or more) of four kinases are known to autophosphorylate, leading to phosphorylation of EIF-2alpha. Through interaction with EIF2B, EIF-2alpha is required for recycling of inactive GDP-EIF2B to active GTP-EIF2B allowing initiation of translation. In the presence of phosphorylated EIF-2alpha, this recycling cannot occur and thus translation is shut off for most mRNAs. A few

mRNAs possessing multiple short upstream open reading frames (uORFs) are capable of bypassing this shutdown and become translationally unregulated. These include the transcription factor ATF4, which in turn upregulates response genes to initiate repair or death. Since EIF-2alpha is required for assembling the 43S pre-initiation complex of the ribosome it is reasoned that loss of Rps19 might result in ribosomal stress leading to phosphorylation of Eif-2alpha via one of the above kinases. Western blots were therefore performed using pooled whole embryo lysates to assess whether Eif-2alpha was phosphorylated in *rps19* morphants. The results showed that loss of Rps19 led to an increase in phosphorylated Eif-2alpha compared to controls. This effect was observed in both $p53^{WT/WT}$ and $p53^{e7/e7}$ backgrounds (Figure 7-11).
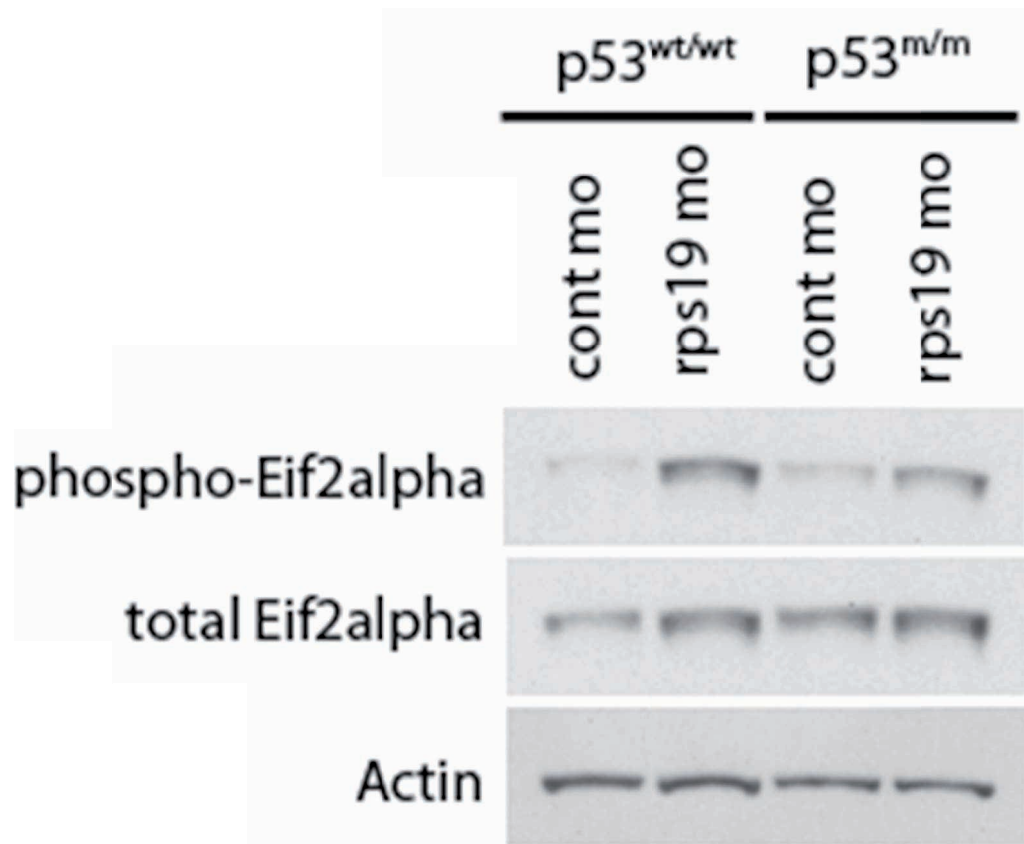
Figure 7-11 : Eif-2alpha is phosphorylated following Rps19 knockdown.

Legend Figure 7-11: Western blot for phosphorylated and total eIF2alpha (Eif2s1) and actin loading control at 2 dpf.

7.4.7 The transcription factor C/EBP homologous protein 10 (CHOP) does not mediate anaemia in *rps19* morphants

Following activation of transcriptional targets by ATF4 in response to EIF-2alpha phosphorylation, cells make a decision whether to recover or die. While the events governing this decision are not well studied, evidence suggests that the transcription factor C/EBP homologous protein 10 (CHOP), itself a transcriptional target of ATF4, is the main mediator of death as a result of activation of this pathway. CHOP is thought to function through activation of mitochondrial-mediated death pathways. Thus to determine if the p53-independent anaemia seen in *rps19* morphants could be a result of Chop-mediated death I knocked down Chop in *rps19* morphants in $p53^{WT/WT}$ and $p53^{e7/e7}$ embryos. Loss of Chop did not rescue the anaemia observed in *rps19* morphants (Figure 7-12). Morphotyping has confirmed knockdown of *chop* by RT-PCR for this batch of morpholino at this concentration (U Pyati personal communication).

Legend Figure 7-12: Injection of *chop* morpholino does not rescue the anaemia seen in *rps19* morphants. Upper panels show injections in $p53^{WT/WT}$ embryos, lower panels show injections into $p53^{e7/e7}$ mutants. Injection conditions are annotated across the top.
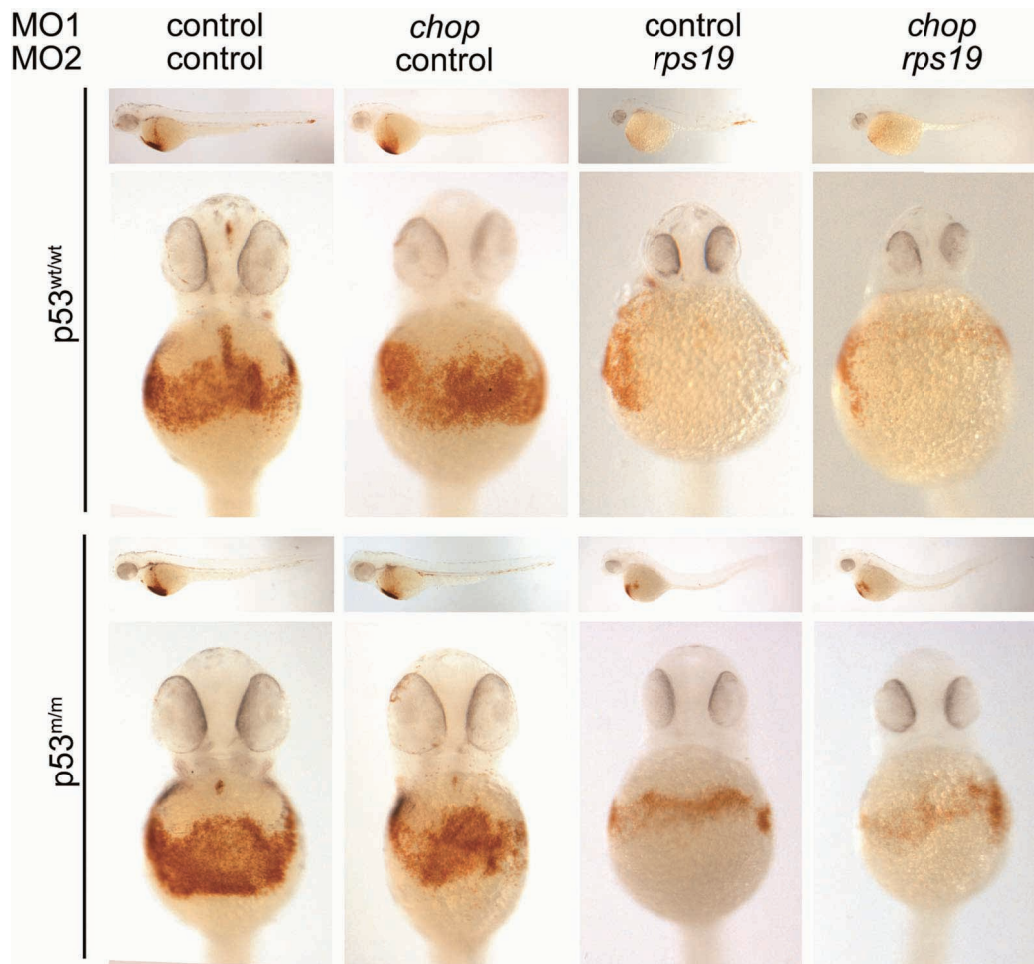
Figure 7-12 : Loss of Chop does not rescue the anaemia in *rps19* morphants

7.5 Chapter discussion

This data described in this chapter shows that reduction of the ribosomal proteins Rps19 and Rps14 to haploinsufficient levels results in anaemia for zebrafish. While some improvement in the anaemia was observed in $p53^{e7/e7}$ mutants, suggesting a p53-dependent component to the anaemia, embryos remained anaemic in the presence of mutated p53 indicating that there was also a p53-independent component to the anaemia. This is important for two main reasons: (i) modulation of the p53 pathway is an unattractive choice for development of therapeutics for any disease given its potent tumour suppressor function, and (ii) many patients with loss of 5q (although not 5q- syndrome patients) already carry p53 mutations indicating that concomitant loss of p53 is (not surprisingly) associated with disease progression in MDS clones with loss of 5q.

Importantly, the specificity of the anaemia observed in both *rps19* and *rps14* morphants was demonstrated with RNA rescue experiments. Around 60% of embryos could be rescued with RNA in both cases. Such rescue experiments in zebrafish embryos are technically challenging. Partial phenotypic or small numbers of embryos being rescued are the norm, therefore, it is notable that not only were large numbers of embryos rescued, but, the observed phenotypes were binary. That is, either the embryos were completely rescued both developmentally and from anaemia, or not at all. This observation is consistent with the current hypothesis that the precise level of Rps19 (or other ribosomal protein) is critical in mediating the anaemia in DBA patients (Narla & Ebert, 2010). One notable feature of the rescued embryos is that they were not able to survive past 5 days. The Western blot data (Figure 7-2) suggests that the level of knockdown in *rps19* morphants is around 40% with rescued embryos achieving levels of 120% and is consistent at 2 dpf and 3 dpf. These data indicate that the half-life of the morpholino is likely to be longer than that of the injected RNA, and that it is possible that the developing zebrafish embryos are more sensitive to haploinsufficient loss of Rps19 than humans. In addition, the data also suggest that a level of Rps19 reduced to 40% of normal levels is simply insufficient for viability in zebrafish embryos. This again suggests that there may be a tight window of Rps19 levels required for viable development as well as for anaemia.

Based on flow cytometric data (Figure 7-5) and morphology (Figure 7-6), loss of Rps19 recapitulated the macrocytic erythropoiesis observed in DBA patients.

Interestingly, loss of p53 appeared to correct the macrocytosis while having only a small effect on the anaemia in *rps19* morphants. This is especially noteworthy given that a recent mouse model of MDS associated with Rps14 loss suggested that macrocytosis could be rescued by loss of p53. Unfortunately, the authors of this study were only able to speculate about whether loss of p53 could rescue the anaemia since the lmo2-*cre* conditional allele they used resulted in anaemia in control animals similar to that seen in knockouts (Barlow et al, 2010).

Since loss of p53 was not able to correct the anaemia in *rps19* morphants, I addressed whether there was on-going cell death in the absence of p53 in these animals. TUNEL staining indicated that p53-independent death was occurring but not clearly localised to areas of in haematopoiesis. The most likely mediators of apoptotic cell death in the absence of p53 are other p53 family members and therefore both p63 and p73 alone and in combination were knocked down with p53. None of the morpholino combinations could rescue the anaemia observed in *rps19* morphants. p63 is known to be required for developmental cell death in the epidermis of zebrafish morphants and this is where it is most abundantly expressed (Rentzsch et al, 2004). p63 is expressed at much lower levels in other tissues including haematopoietic tissue, providing a possible explanation for why it was less likely p63 would have an effect on cell death in blood cells.

It can be reasoned that cell death might be mediated by another pathway. An ideal candidate is the integrated stress pathway. The precise events governing stress pathway activation depend on the type of stress and linked to this which kinase catalyses subsequent phosphorylation. Regardless of the kinase, Eif-2alpha phosphorylation occurs and translation of most mRNAs into proteins is impaired. Eif-2alpha phosphorylation was observed in both $p53^{WT/WT}$ and $p53^{e7/e7}$ embryo lysates at 2 and 3 dpf. Notably there also appeared to be an increase in total eIF2alpha relative to the control injected embryos. The explanation for this is unclear since eIF2alpha is not thought to be regulated and is usually considered a housekeeping gene. Most studies addressing the phosphorylation of EIf2alpha assess this quantitatively by using a ratio of phosphorylated: total eIF2alpha. Using such quantitations, the increase in phospho-eIF2alpha in *rps19* morphants was much less marked compared to that of phospho-Eif-2alpha: actin. The interpretation of the increase in phospho-Eif-2alpha is also potentially limited by the fact that the Western blot results were derived from whole embryo lysates

and therefore not tissue specific to erythroid cells. Obtaining sufficient erythroid cell numbers for Western blot by flow cytometric cell sorting from embryo suspensions is technically challenging since it would require several hundred embryos per condition. Another option would be to determine whether the phospho-Eif-2alpha antibody functions in whole mount immunofluorescence or immunohistochemistry to ascertain tissue specificity of this response. In contrast to protein, only tiny numbers of cells are required to obtain sufficient RNA for analysis. Therefore in order to derive some tissue-specific information RNA was studied from flow cytometrically-sorted erythroid cells from *rps19* morphants and controls. The initial downstream effects of eIF2alpha phosphorylation are mediated by translation dependent activation transcription factor ATF4 (Jiang et al, 2007; Vattem & Wek, 2004). Detection of Atf4 protein in zebrafish is also subject to similar constraints of limited cell numbers and tissue specificity. In addition detection of Atf4 may also be hampered by the fact that *atf4* is duplicated in the zebrafish genome, thus an antibody to human or murine ATF4 may detect none, one or two of the zebrafish Atf4 copies. It may also be that one of the *atf4* genes is dominant in the response to stress. To date there is no published literature on the zebrafish *atf4* genes, although, their expression pattern in early embryogenesis is observed to ubiquitous on the zebrafish model organism database (www.zfin.org/cgi-bin/webdriver?MIval=aa-ZDB_home.apg). Thus to detect the downstream effects of Eif-2alpha phosphorylation quantitative RT-PCR was used for genes known to be direct targets of Atf4:- *chop, atf3* and *c/ebp beta*. Unfortunately, the results from these experiments were extremely variable and did not consistently demonstrate an increase in Chop target genes. This may have reflected the fact that the cells had undergone significant manipulation prior to being collected resulting in death of cells expressing Chop, or other pathways negatively regulating the expression of Atf4 targets were already activated (Kim et al, 2006). Finally minor technical differences between experiments may also have contributed to gene expression levels given the large number of steps required prior to qPCR analysis.

The cues determining the fate of cells that have phosphorylated EIF-2alpha are not fully understood. It is known that stressed cells that cannot be repaired undergo programmed cell death. Evidence suggests that the apoptosis of cells undergoing such stress responses is mediated by the transcription factor CHOP (Kim et al, 2006; Oyadomari & Mori, 2003). Activation of CHOP results in the

initiation of mitochondrial cell death and caspase activation (Oyadomari & Mori, 2003) . A least a proportion of this is independent of p53. To determine if Chop could be mediating p53-independent cell death and anaemia in *rps19* morphants I knocked down Chop using a splice-blocking morpholino. Loss of Chop was not able to rescue *rps19* morphants from anaemia. A mild degree of anaemia was observed in the Chop knockdown embryos consistent with data in mice that Chop knockout mice have a developmental anaemia.

Depending on the "stress" inducing the phosphorylation of Eif-2alpha, other response pathways may be activated in tandem. In the case of ER stress, the accumulation of excess unfolded proteins in the ER leads to activation of the pancreatic endoplasmic reticulum kinase (PERK) which phosphorylates eIF2alpha. In addition, mobilisation of the ER chaperone protein HspA5 (also known as BiP) also occurs by detachment from protein IRE1. The detached IRE1 is able to homodimerise resulting in activation of intrinsic endoribonuclease activity. Phosphorylated IRE1 can then catalyse an unconventional splicing reaction (independent of the splicosome) of the *XBP1* gene. This unconventional splicing event results in removal of an additional 26bps of the 1st exon to generate an alternate reading frame. The translated protein product of this alternatively spliced isoform (XBP1s) acts as a transcription factor to upregulate many target genes involved in recovery from ER stress. In mammals ER stress also results in activation of transcription factor ATF6 by proteolytic cleavage. Other stress responses that result in the phosphorylation of eIF2alpha also result in activation of other pathways both known and potentially unknown potentially contributing to the anaemia in *rps19* morphants. Future studies will aim to address which kinase is responsible for the activation of phosphorylation of eIF2alpha in *rps19* morphants and thus the component or components of the stress response pathway(s) contributing to anaemia in this setting.

There are a number of outstanding questions regarding the results in this chapter. Firstly, while there is clearly evidence of p53-independent cell death in *rps19* morphants, this is not localised to erythroid cells or regions of production of blood cells. Therefore it is possible (or even likely) that the anaemia observed is not wholly a result of apoptosis. It would be informative to investigate the cell cycle and proliferative characteristics of *rps19* morphants compared to controls to identify alternative mechanisms contributing to the anaemia. Evidence from cell

culture experiments suggests that loss of ribosomal proteins does result in disruption of the cell cycle (Badhai et al, 2009b) although it is unknown if this is p53-dependent or not. Secondly, P53-independent senescence is another possible mechanism, although the assessment of senescence using SA-beta galactosidase assays has only been used successfully in embryos 4 dpf and older (Kishi et al, 2008). It is also difficult to reconcile the hypothesis that the primary mode of anaemia in p53$^{e7/e7}$ embryos is cell death with observations made by Danilova and colleagues (2008) showing that all cell death was rescued in *rps19* morphants at 24 hpf (by AO and TUNEL). My experimental results have also confirmed these observations. In addition, a robust increase in TUNEL positive cells was not observed in *p53$^{e7/e7}$ rps19* morphants until 3 dpf. While 3 dpf is coincident with the timing when the majority of erythropoiesis is thought to be of definitive origin, this does not explain the presence of anaemia in *p53$^{e7/e7}$* morphants at 2 dpf. It is attractive to speculate that the phosphorylation of Eif-2alpha is the most likely initiator of whatever mechanism leads to the anaemia. At present there is no direct evidence linking the phosphorylation of eIF2alpha to the anaemia observed in *rps19* morphants. Clarifying this key point will be a priority in future studies.

To date all my studies have necessarily been carried out in zebrafish embryos. It would be desirable to have adult (or at least older) zebrafish carrying RP gene mutations to facilitate further studies. This will require generation of a stable line using either TILLING or zinc finger nuclease technology (see 1.2.2). Optimally the study of an allelic series of zebrafish carrying mutations corresponding to those seen in human DBA would be most informative. This would allow the assessment of the phenotypes of zebrafish with "true" haploinsufficiency and potential for in vivo genetic modifier and chemical screens. In addition, it is critical that findings from the zebrafish are validated with studies in humans. This goal could be achieved using cells from DBA patients (who are not transfusion dependent or on therapy). However, such patients are rare and their samples are in great demand. Several groups have successfully grown haematopoietic cells (of all lineages) from the rare CD34$^+$ blood progenitor cells found in peripheral blood, (D Higgs personal communication) but it is not known if such cells are present at normal frequency or proliferative capacity in DBA patients. An alternate strategy for using primary cells is to use cord blood or mobilised CD34$^+$ cells, knockdown

RPS19 using lentiviral vectors and differentiate the cells down the erythroid lineage as described by Ebert et al (2008).

In conclusion, a morpholino knockdown model of DBA and MDS 5q-syndrome has been developed. It is demonstrated that p53-mediated mechanisms can ameliorate, but, not completely correct the anaemia observed in RP-morphants. It is shown that the anaemia does not result from effects mediated by p63 or p73, both members of the p53 family. Finally, it is clear that the integrated stress response is activated in *rps19* morphants, independent of p53 status, but this is not associated with significant Chop-induced cell death in erythroid cells since loss of Chop cannot rescue the anaemia.

8. Final discussion, conclusions and future work

This final discussion chapter will focus on three major areas related to the work described in this thesis. Firstly, I will discuss the limitations of current zebrafish screening approaches, and new strategies of zebrafish screening in development to identify novel genes and pathways relevant to human disease. Secondly, I will discuss the work described in Chapter 7 and suggest hypotheses for the role of the integrated stress response in the pathogenesis of anaemia in patients with both DBA and MDS. Finally, potential future studies using zebrafish to model ribosomal gene mutations will be considered.

8.1   The use of zebrafish to identify novel genes and pathways relevant to human disease

Like all animal models used to shed light on human diseases, the use of zebrafish to study human diseases has its fair share of sceptics. The evidence presented in this thesis argues that the zebrafish is an excellent model system for the study of embryonic haematopoiesis. In particular, genes involved in ribosome biogenesis are highly conserved between the zebrafish and humans, facilitating the development of cross-reactive reagents and implying the likely conservation of pathways in fish and in mammals. The zebrafish affords several specific advantages over other systems. In comparison to more simple organisms such as yeast, worms and flies, zebrafish are small vertebrates with the capacity for forward genetic studies. In common with mammals, they have a closed vascular system and beating heart and are genetically diploid. Long-term cryopreservation of zebrafish sperm and in vitro fertilisation techniques are also established enabling the storage of zebrafish lines for future use. The cost and space required to maintain a zebrafish facility is modest when compared to maintaining mouse facilities, a particularly important consideration in view of the current economic climate. Zebrafish progeny can also be generated in extremely large numbers and can reach sexual maturity within 8 weeks. This makes the generation of adult zebrafish with complex genotypes a feasible prospect. The zebrafish haematopoietic system develops extremely rapidly with definitive haematopoiesis predominating as early as by 5 dpf. Progress of blood development can be studied in vivo over time with the assistance of a wide array of transgenic lines since the embryos develop outside the mother. The recent power of this approach has been demonstrated by several landmark papers

defining the emergence of HSCs from vascular precursors in zebrafish (Bertrand et al, 2010; Kissa & Herbomel, 2010).

8.1.1 Screening for novel haematopoietic genes using the zebrafish

The zebrafish is first and foremost a developmental model and as such my future studies using the zebrafish will capitalise on this strength, while aiming to generate novel reagents that will aid rapid and effective screens. Although current methods are effective, there is clear scope for improvement in the efficiency of zebrafish screening methods. The genetic screen described in Chapter 3 that identified the role of Ddx18 in myeloid development has some specific drawbacks. WISH as the primary screening method is not optimal. 4–5 day old embryos are extremely sensitive to varying amounts of proteinase K digestion and the repeated washes requires over the course of the 3 day protocol (often resulting in poor staining or dismembered embryos). Since this screen was performed, considerable progress has been made in the study of fate mapping of blood development in the zebrafish embryo (Bertrand et al, 2008; Bertrand et al, 2007). In light of these findings, it would be essential for future screens to focus on time points when primitive and definitive haematopoiesis could be reliably distinguished. Based on current knowledge, such time points would be 16–18 hpf for primitive myelopoiesis and 5 dpf for definitive haematopoiesis. Studies of intermediate time points will be confounded by a mixture of both primitive and definitive myelopoiesis, whereas studies at later time points will be technically restricted as RNA rescue or morpholino experiments may not be feasible given the expected half-lives of these reagents. Rapid histochemical assays for myelopoiesis (such as Sudan Black and myeloperoxidase) have now been optimised and provide an excellent alternative to ISH for primary screens. The availability of antibodies for use in zebrafish research is also rapidly expanding with several companies now either specifically generating zebrafish antibodies or testing antibodies with specificity for other species for cross-reactivity with zebrafish. Antibodies which work in whole mount immunofluorescence (or immunohistochemistry) also provide an excellent alternative or adjuvant for secondary screening, allowing assessment of levels of protein expression rather than transcript. Several key haematopoietic transcription factors have now been targeted for the generation of commercially available antibodies and will be useful tools for future study (Anaspec, CA, USA). While the screen in Chapter 3 was

specifically designed to identify genes involved in myelopoiesis, particularly granulopoiesis, with the view to identifying novel genes associated with AML or MDS, a more rational approach might be to screen for defects in HSC production using Runx1 or Cmyb. Both of these transcription factors have transgenic lines available as well as zebrafish-specific antibodies (although they remain to be validated in immunohistochemical assays). The utility of using these genes for chemical genetic screening has already been demonstrated by North and colleagues (North et al, 2007). Thus a primary screen could be performed in vivo using double or single transgenic lines, with a secondary screen using whole mount immunohistochemistry for Runx1 and or Cmyb.

Using the viral insertional library developed by Nancy Hopkins laboratory (Amsterdam et al, 2004a) for the screen also introduces bias in the genes identified in the screen. The primary screen that generated the library was based on genes essential for development and thus these genes are almost all embryonic lethal mutations. Many of the alleles also result from intronic insertions and thus are more likely to be hypomorphic alleles. Therefore haploinsufficient phenotypes may have been missed (since heterozygosity will more likely result in greater than 50% gene expression) and genes with specific haematopoietic defects may also have been missed since they will not necessarily result in lethality. An example such a gene that would likely have been missed in this screen is the recently described Runx1 mutant which has 20% viability to adulthood in contrast to mammalian Runx1 knockouts which are homozygous lethal (Sood et al, 2010). Viral insertional mutagenesis as a screening strategy is also biased for other reasons. Viral insertion sites are not randomly distributed throughout the genome, but, the virus has preferential sites of insertion as evidenced by the generation of two or more either identical or closely related alleles in some loci (Amsterdam et al, 2004a). Thus the coverage of the genome from this type of screen is relatively small and there are likely to be more novel genes affecting myeloid development yet to be identified.

8.1.2 Screening for novel cancer genes in the zebrafish

The ultimate hypothesis-driven goal of screens for genes resulting in abnormal myelopoiesis was to identify mutations or viral insertions in genes that were also involved in human myeloid malignancies. To date the Look laboratory has sequenced the coding regions of three of the genes associated with reduced

213

myeloid cell numbers in zebrafish mutants in patients with AML and /or MDS patients at a total cost of over $30,000. While my data and that of others suggests that all three of the genes may have a role in human AML/MDS (previously unreported SNPs were identified for two of three genes, and the third has been reported as one of the most markedly down-regulated genes in MDS (Sridhar et al, 2009)), abnormalities in these genes were observed in a small proportion of AML/MDS patients and validation of their roles and driver rather than passenger mutations is lacking. In addition the time- and cost-effectiveness of this as a strategy for identification of novel cancer associated genes is questionable. This is particularly true as the next generation of high throughput genome-wide re-sequencing technology is becomes available at an increasingly affordable time and cost. Already the entire genomes of 2 patients with normal karyotype AML have been sequenced identifying several novel mutated genes potentially involved in the pathogenesis of MDS and AML (Ley et al, 2008; Mardis et al, 2009). Notably, while several candidate genes were identified in the whole-genome sequencing studies, none of the likely candidates were mutated in subsequent sequencing of an additional 100 patients (Mardis et al, 2009), with only one coding variant (IDH1-R132C) identified in more than one sample in the other study (Mardis et al, 2009). This brings into question whether discovery of bonefide disease-associated mutations may be reaching saturation. Have all the common genetic mutations in AML/MDS now been identified? Within the coming years it seems likely that re-sequencing of cohorts of patients with AML and MDS of all subtypes will provide complete and comprehensive coverage of the human "AML-ome" and "MDS-ome" to determine the majority of disease-causing mutations as yet unidentified. Therefore, while I strongly believe that the zebrafish is an excellent model for identification of novel genes involved in haematopoiesis and the hypothesis that some such genes might be involved in the development of cancers is true, I believe the most valuable role for the future of zebrafish screens pertaining to human disease lies in the generation of knockout and transgenic models in which to perform modifier or chemical screens.

8.1.3 Generation of new models for modifier screens

The studies described in Chapter 6 confirmed that the zebrafish is a viable model system in which to study NPM1-mediated diseases. In addition, collaborative

studies with Niccolo Bolli have identified that NPMc+ expression in zebrafish embryos results in the relocation of zebrafish *npm1* genes to the cell cytoplasm. This parallels the abnormal sub-cellular localisation of NPMc seen in human AML patients with NPM mutations. In zebrafish, NPMc+ expression also resulted in an increase in definitive HSCs, providing insight into possible mechanisms for clonal dominance in NPMc+-expressing HSCs (Bolli and Payne et al, 2010). In order to capitalise on these findings and generate a model amenable to future screens, the Look laboratory has generated transgenic zebrafish lines expressing the mutated human NPMc+ allele under the control of the ubiquitous beta-actin promoter. One potential confounding issue when using such transgenic zebrafish models is the presence of four wild-type *npm1* alleles. Based on work in cell culture it is likely that the balance between WT and mutated alleles is required to retain a significant proportion of WT NPM1 in the cytoplasm, thereby disrupting tumour-suppressor ARF and p53 pathways (Cheng et al, 2007). In the zebrafish, with its four WT *npm1* alleles, this balance may be more of a challenge to achieve. Since loss of *npm1* genes *per se* also resulted in haematological abnormalities and may mirror aspects of 5q MDS, 2 different strategies to develop stable knockout models of *npm1a* and *npm1b* are being used. Both strategies use zinc-finger technology. In the first, in-silico-designed zinc fingers to each *npm1* gene have been injected into zebrafish embryos and these are now mating adults. The second strategy also uses zinc fingers but in this case the fingers are generated to specifically bind their target in vitro using a bacterial-2-hybrid system prior to injection into the one-cell stage zebrafish embryo. If a stable mutant for Npm1a and Npm1b can be generated these will be bred to the *Tg(beta actin:NPMc+;cmlc2:EGFP)*. This will aim to modify the balance of NPMc+ to WT *npm1*. Future studies on these lines will focus on chemical screens to identify compounds which can normalize the number of HSCs *(Tg(beta actin:NPMc+;cmlc2:EGFP)*. Such screens in WT embryos have already resulted in the generation of novel therapeutics for haematopoietic stem cell transplantation demonstrating the potential power of this approach (Lord et al, 2007; North et al, 2007).

While a major utility of the zebrafish is the ability to perform embryonic screens, some groups (including the Look laboratory) have tackled the challenge of modifier screens in transgenic tumour-prone adult zebrafish. The capacity to identify tumour-modifying genes (either enhancers or suppressors) could both

enhance knowledge of disease biology and reveal alternative pathways for therapeutic intervention. There are considerable technical challenges to unbiased screens in adults. One primary issue is that tumour-prone animals must have a predictable, reproducible and preferably narrow time window during which they develop tumours. For this to be a process amenable to screening, animals also need to be relatively young when they develop tumours (while still being of breeding age in order to ensure the line can be propagated). Even if these parameters can be met then screening for disease-modifying mutations still poses major space and mapping issues. Screening for haploinsufficient disease-modifying genes is the most straight-forward approach. However, unless there is also a homozygous embryonic phenotype also evident from the same mutation, then mapping the disease-modifying allele is virtually impossible by current positional cloning methods. A further potential drawback of this screening strategy is that novel methods for identifying disease-modifiers using xenogeneic transplantation of human leukaemias with pooled RNAi gene knockdown are now available. Such strategies may be more attractive to researchers since not only does this system utilise primary human cells in a mammalian model, it knocks down several genes in tandem, each of which is barcoded for rapid identification of the RNAi (or shRNA) causing the effect. An alternative approach in zebrafish that might circumvent the technical challenges associated with the development of adult zebrafish screens is to identify embryonic phenotypes that are indicative of later development of cancer. Although this may sound implausible, several recent zebrafish mutants or transgenics have been assessed as both embryos and adults and there is growing evidence that defective embryonic haematopoiesis in these models may directly reflect the development of adult leukaemia or bone marrow failure. In particular the recently described $runx1^{w84x}$ mutations are homozygous-viable to adulthood in 20% of cases. All embryos display absence of $Tg(cd41:GFP)$, expressing HSCs between 36 hpf and 5 dpf, as well as absence of definitive lineage-specific cells. Twenty percent of embryos recover and survive to adulthood, although they continue to show a "bone marrow" failure phenotype with thrombocytopenia, and leukopenia, suggesting that the embryonic deficiency of HSCs exerts an influence on adult haematopoiesis (Sood et al, 2010). Although it is well established that humans with loss of runx1 are predisposed to developing AML and/or MDS (familial thrombocytopenia with predisposition to AML (FTP-AML)) it is not yet known

whether zebrafish with *runx1^{w84x}* mutations go on to develop AML/MDS. The development of overt leukaemia in this model could result from a "second hit" mutation as is likely to be the case in the pathogenesis of AML in FTP-AML. Another study showing embryonic disturbances of haematopoiesis and adult leukaemia in zebrafish was recently presented in abstract form at the American Society of Haematology, where knockdown of the zinc finger protein programmed cell death domain 2 (PDCD2) resulted in a marked reduction in *runx1*-expressing HSC while transgenic expression of aberrant splice variants of PDCD2 isolated from AML patients resulted in the development of AML in adult zebrafish (Kramer et al, 2009). If such correlative phenotypes could be definitively validated the utility of zebrafish to screen for modifiers would be greatly enhanced.

8.1.4   Chemical and automated screens in zebrafish

Several pioneering groups have demonstrated the considerable potential for using zebrafish to identify novel compounds that can modulate many aspects of vertebrate biology. One recent example of this is the study by North et al. identifying prostaglandins as mediators of HSC production (North et al, 2007). Not only has the relevance of this pathway been validated in murine studies but similar compounds were also identified in the studies from Randall Peterson's laboratory to identify modifiers of the differentiation block induced by AML1:ETO in a heat shock-inducible transgenic zebrafish model (Yeh et al, 2009). Further studies from these and other groups have been focusing on novel rapid throughput automated screening techniques, ranging from the robotisation of the injection process to high-throughput whole embryo screening for fluorescence (Vogt et al, 2009; C Grabher personal communication and H Spaink personal communication).   More   information   is   available   from **http:/zfpharma.com/products_disease_screening-sequencing.html.**

8.2   Determining the role of the integrated stress response on anaemia in DBA and MDS

While it seems likely that p53 stabilisation and apoptosis or cell cycle arrest are major contributors in the anaemia observed in RP-deficient diseases such as DBA and MDS, the experiments performed in Chapter 7 of this thesis demonstrated that a p53-independent mechanism contributes anaemia in RP-deficient zebrafish. This may have be the result of activation of the integrated stress response (ISR), resulting in phosphorylation of eIF2alpha on serine 51. It is

possible that components of this pathway contribute to the development of anaemia in RP-deficiency in a p53-independent manner and may serve as a pathway in which to explore novel therapeutics for these diseases. Several key questions remain to be addressed regarding the role of the ISR in RP deficiency which will form the scientific basis of my future studies. An overview of the ISR is shown in Figure 8-3 where genes highlighted in green reflect those genes which result in anaemia when knocked out in murine models.

8.2.1 Does phosphorylation of EIF-2alpha contribute to the anaemia in RP deficiency?

Determining a direct link between phosphorylation of eIF-2alpha and the anaemia observed in RP morphants is critical to definitively show a causal link between anaemia and the ISR. The simplest genetic means to do this would be to knockdown *eif-2alpha* using morpholinos. However this strategy would be likely to result in lethality given the essential role of eIF-2alpha in translation initiation. A possible strategy to avoid this issue would be to titrate the level of eIF-2alpha to try and rescue with anaemia. This strategy is feasible since there is an excellent cross-reactive antibody to detect the level of eIF-2alpha protein but may be technically challenging since the effects of a given dose of morpholino can be variable due to a degree of mosaic expression. A third possibility is to knockdown eIF-2alpha in the zebrafish while simultaneously over-expressing a kinase-dead variant of human EIF-2alpha, where S51 is mutated to S51A (Vattem & Wek, 2004). The desired effect would be to maintain sufficient eIF-2alpha for translation initiation while removing its capacity to be phosphorylated at the critical serine residue. This strategy might also result in some developmental abnormalities since it is likely that phosphorylation of eIF-2alpha is required physiologically during development; however it may still be possible to observe improvements in blood production. The uses of human EIF-2alpha contructs are preferable over zebrafish constructs since *eif-2alpha* is duplicated in the zebrafish genome. Both zebrafish and human have extremely high homology (Figure 8-1) suggesting probable conservation of function. It is possible however that even if the phosphorylation of eIF-2alpha does not correlate with anaemia in *rps19* morphants, another arm of the ISR may mediate the anaemia. This is most likely to depend on the specific kinase responsible for phosphorylation of eIF-2alpha and the triggers for kinase activation.

```
zfish eif2alpha        mpglscrfyqhrfpevedvvmvnvrsiaemgayvsllleynniegmilllselsrrrirsin
zfish eif2alpha-like   mpalssrfyqhrfpevedvvmvnvrsiaemgayvsllleynniegmilllselsrrrirsin
human EIF2ALPHA        MPGLSCRFYQHKFPEVEDVVMVNVRSIAEMGAYVSLLEYNNIEGMILLSELSRRRIRSIN
                       **.**.*****:*******************************************

klirigrnecvvvirvdkekgyidlskrrvspeeaikcedkftksktvysilrhvaevleytkdeqleslfqrtawvfdekykkpg
klirigrnecvvvirvdkekgyidlskrrvspeeaikcedkftksktvysilrhvaevleytkdeqleslyqrtawvfdekykrpg
KLIRIGRNECVVVIRVDKEKGYIDLSKRRVSPEEAIKCEDKFTKSKTVYSILRHVAEVLEYTKDEQLESLFQRTAWVFDDKYKRPG
*****************************************************************:********:***:**

ygaydvfkqavsdpaildgldlteeernvlidninrrltpqavkiradievacygyegidavkealraglncsteampikinliap
ygaydvfkqavsdpaildclelteeeravlidninrrltpqavkiradievacygyegidavkealragltcstecmpikinliap
YGAYDAFKHAVSDPSILDSLDLNEDEREVLINNINRRLTPQAVKIRADIEVACYGYEGIDAVKEALRAGLNCSTENMPIKINLIAP
*****.**:*****:*** *:*.*:** ***:***********************************.**** *********

pryvmttttlerteglsvlnqamaaikerieekrgvfnvqmepkvvtdtdetelqrqlerlerenaevdgdddaeemeakted
pryvmttttlerteglsvlnqamavikekieekrgvfniqmepkvvtdtdetelarqlerlerenaevdgdddaeemeakted
PRYVMTTTTLERTEGLSVLSQAMAVIKEKIEEKRGVFNVQMEPKVVTDTDETELARQMERLERENAEVDGDDDAEEMEAKAED
*******************.****.***:*********:**************** **:********************:**
```

hs EIF2ALPHA:zfish Eif2alpha = 94.3% identical;   hs EIF2ALPHA:zfish Eif2alpha-like = 93.7% identical;

Figure 8-1 : Clustal W alignment of zebrafish and human EIF-2alpha

Legend Figure 8-1: Clustal W alignment of zebrafish eIF-2alpha and eIF2alpha-like amino acid sequences with human EIF-2ALPHA amino acid sequence. * mark identical amino acids, : are similar and . less similar. Yellow boxed region shows conserved serine residue required for GDP:GTP recycling and translation shutdown in response to stress.

8.2.2 Which kinase phosphorylates eIF2alpha in response to RP deficiency?

Four different kinases are known to phosphorylate EIF-2alpha in mammals; PKR-like ER-localised eIF2α kinase *(*PERK), protein kinase regulated by RNA (PKR), general control non-derepressible 2 (GCN2) kinase and haem regulated inhibitory (HRI) kinase (Figure 8-2). Each kinase is stimulated by unique environmental cues within the cell which are also likely to be tissue-specific. Three of the four kinases, PKR, GCN2 and HRI, are expressed in erythroid cells and thus are candidates as kinases that could contribute to the anaemia resulting from stress pathway induction.

8.2.2.1 PERK

PERK is not expressed in erythroid cells. While it is possible that non-cell autonomous factors could contribute to anaemia via activation of PERK (and cell automony was not demonstrated in the experiments shown in Chapter 7), this kinase is the least likely to contribute significantly to the anaemia in Rps19 deficiency. Supporting this are preliminary studies I have performed showing that loss of Rps19 did not show any increase in the expression of ER chaperone BiP, which is associated with the PERK-dependent ER stress pathway.

8.2.2.2 PKR

PKR functions as part of the innate immune system and is classically activated by binding of double stranded RNA (dsRNA) to two RNA binding motifs. This results in a shift from inactive PKR monomers to active PKR dimeric forms, as a consequence of trans-autophosphorylation (Dar et al, 2005; Dey et al, 2005a, 2005b) This mechanism provides defence against viral RNA while the majority of endogenous small RNAs are masked from PKR activation by nucleoside modifications and the absence of 5' triphosphate (Karikó et al, 2005; Nallagatla et al, 2007; Nallagatla et al, 2008). A plausible mechanism by which PKR could be activated by RP deficiencies is suggested by the observation that PKR binds the 40S ribosomal subunit. Evidence from one study identified that dsRNA and ribosomes compete for binding at the RBM. Ribosome bound PKR is unable to activate the trans-autophosphorylation required for activation of PKR, but instead acts as an inhibitor of PKR activation (Raine et al, 1998). Moreover, there are

some endogenous RNA species capable of activating PKR including interferon mRNA and tumor necrosis factor-α mRNA. In addition a role in viral immunity, PKR is also thought to have tumour suppressive function since it is a p53-response gene (Yoon et al, 2009). Transcriptional activation of PKR by p53 is unlikely to be the mechanism of eIF-2alpha phosphorylation in the context of RP loss since eIF2alpha is also phosphorylated in p53 mutant embryos. Thus on balance, the likelihood that PKR is the primary kinase responsible for eIF2alpha phosphorylation in my model is relatively low.

8.2.2.3 GCN2 kinase

GCN2 is the most highly conserved kinase among those capable of phosphorylating eIF-2alpha, with homologues identified in all eukaryotes. The main identified stress factors which activate GCN2 are nutrient deficiency, UV irradiation and proteasome inhibition. GCN2-deficient mice are relatively normal under basal conditions but develop rapid muscle wasting within days of deprivation of the amino acid leucine (Anthony et al, 2004). Activation of GCN2 by UV irradiation may be an indirect result of nutritional deficiency since it has been shown that UVB irradiation generates nitric oxide free radicals (NO*) which deplete L-arginine and cause a relative nutritional deficiency. GCN2 is also activated by proteasome inhibition using the proteasome inhibitor MG132 (Jiang & Wek, 2005); however, this may be cell-type specific as some studies suggest that it is primarily HRI kinase that is responsible for this effect (Yerlikaya et al, 2008).

Recent evidence has identified that translation is impaired in DBA patients and that this impairment can respond to the administration of L-Leucine in vitro (Cmejlova et al, 2006). Further studies have also suggested that some DBA patients may have a clinical response to the administration of L-leucine supplements (Pospisilova et al, 2007). The rationale behind L-leucine administration in these studies stems from its role as a stimulator of translation via the EIF4F binding complex (Anthony et al, 2000). This complex is required along with EIF2 for translation initiation although the pathways are thought to be independent of one another. Leucine therefore may act solely as a translational stimulator in DBA patients, but it is also possible that there is a relative deficiency of leucine in RP-deficient cells which results in activation of GCN2 and phosphorylation of eIF-2alpha. This not only makes GCN2 an attractive candidate

kinase for phosphorylation of eIF-2alpha in my model but also suggests that translation inhibition mediated by the eIF4F complex may also occur in RP-deficient states.

8.2.2.4 HRI kinase

By far the most attractive candidate kinase to phosphorylate eIF-2alpha in RP-deficient erythroid cells is the HRI kinase. In erythroid cells, the balance between haem and globin synthesis is finely tuned as the correct stoichiometry of the three components of haemoglobin (haem, α-globin and β-globin) is essential to prevent the deleterious effects of excess globins as seen in thalassaemias or haemolytic anaemias. HRI kinase functions primarily to maintain the balance between haem and globin synthesis in erythroid cells. HRI kinase contains two haem-binding sites. When haem levels are sufficient, any excess haem not required for incorporation into haemoglobin binds the haem-binding sites within HRI. One of these haem binding sites is reversible, and in relative haem-deficient states will be free of bound haem. The absence of bound haem at this site leads to autophosphorylation of HRI, dimerisation and activation of the kinase activity to phosphorylate eIF-2alpha (Bauer et al, 2001). The result is shut down of globin synthesis to preserve the balance of haem and globin, and prevent damage to the cell associated with excess globin chains. The protective effect of HRI kinase has been demonstrated in HRI kinase knockout mice. Under basal conditions HRI$^{-/-}$ mice have normal embryonic erythropoiesis and as adults show macrocytosis and mild hyperchromia. When fed an iron deficient diet the mice became markedly anaemic with splenomegaly and normochromic anaemia and increased apoptosis of erythroid precursors compared to iron-deficient HRI$^{+/+}$ controls, and Heinz body preparations demonstrate large globular precipitates of free globin chains in HRI$^{-/-}$ mice (Han et al, 2001). The role of HRI kinase in two inherited forms of anaemia has also been studied (Han et al, 2005). HRI knockout mice were bred to ferrochelatase$^{-/-}$ mice. Ferrochelatase mutations are found in cases of human erythropoietic porphyria and result in failure to incorporate iron into protoporphyrin IX, the final step in haem biosynthesis (Tutois et al, 1991). Ferrochelatase$^{-/-}$ mice are therefore haem deficient and provide an in vivo model to test of the effects of HRI loss in haem deficiency. Ferrochelatase$^{-/-}$;HRI$^{-/-}$ mice have more severe anaemia, liver and skin effects than their ferrochelatase$^{-/-}$ siblings, and also develop red cell globin inclusions confirming

222

that HRI kinase exerts a protective effect in this condition not only in erythroid cells but also in other tissues utilising haem containing enzymes. HRI$^{-/-}$ mice were also bred to β-thalasemia mice which resulted in embryonic lethality from profound anaemia. β-thalasemia is not thought to be a haem-deficient state, however; HRI is known to be activated in haem-replete reticulocytes in response to denatured proteins. Activation of HRI by a change in its migration was confirmed in β-thalasemia mice, although phosphorylation of EIF-2alpha in response to this was not addressed. This study showed that HRI kinase is essential not only for the maintenance of the balance between haem and globin in haem deficiency but also in other anaemic states (Han et al, 2005).

Legend Figure 8-2 : Scheme of key components of the Eif-2alpha pathway of translational regulation in erythroid cells. All proteins highlighted in green give rise to anaemia during development or adult life in mouse knockout models (Lu et al, 2004). The major kinase regulating eIF-2alpha phosphorylation in erythroid cells is HRI kinase allowing balance of haem and globin synthesis.
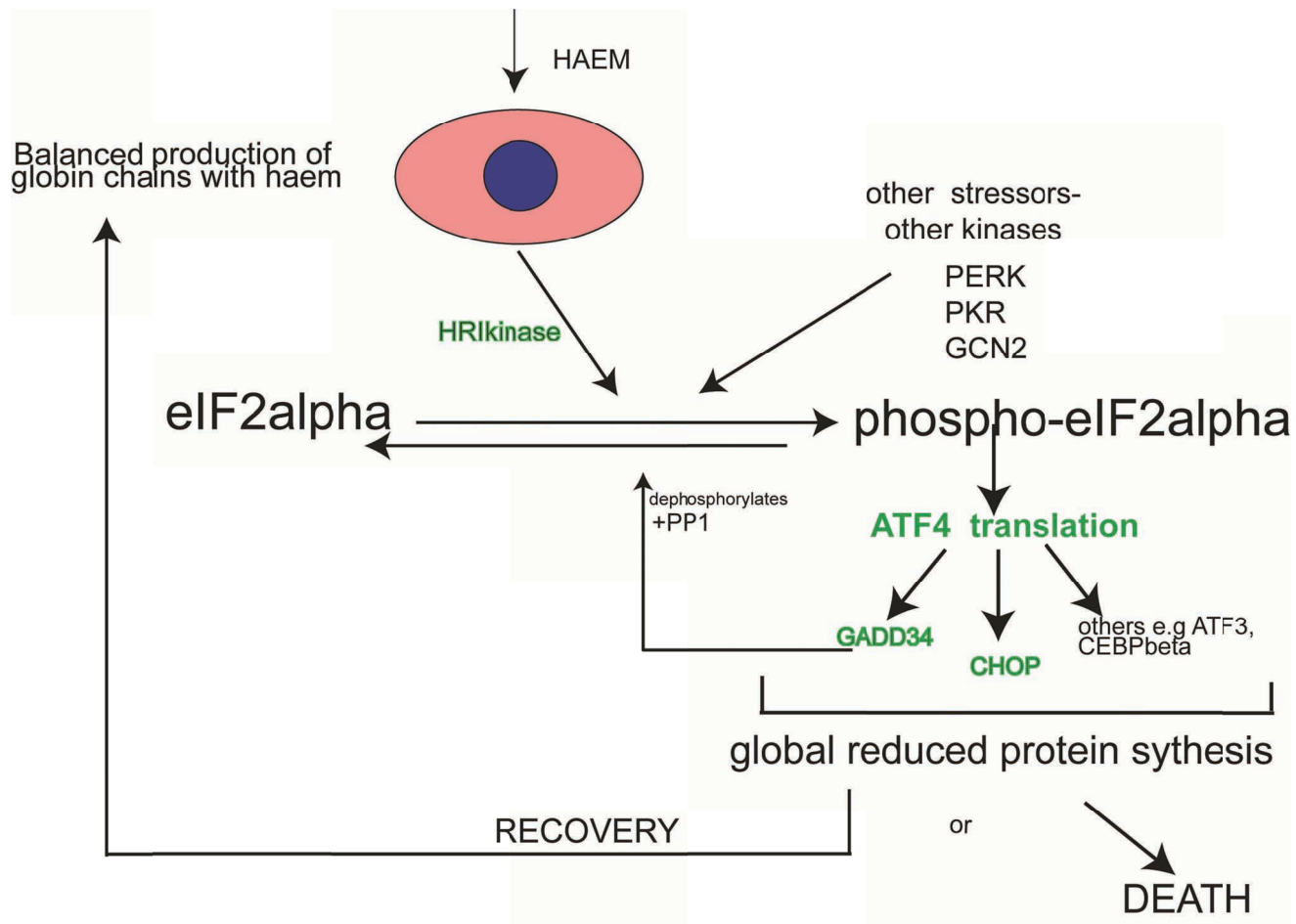
Figure 8-2 : Cartoon of stress response pathways

Haem levels in DBA have not been assessed, but, indirect evidence suggests that there is likely to be haem excess rather than deficiency. This comes from mainly anecdotal evidence that there is a relative increase in the levels of iron overload observed in transfused DBA patients compared to non-DBA patients receiving the same transfusion volume. Translation efficiency is reduced RP-deficient cells from DBA patients indicating that denatured proteins are unlikely to provide the stimulus for HRI kinase activation. Therefore, while HRI kinase, given its relative tissue specificity for erythroid cells and maintenance of equilibrium in inherited and acquired anaemias is the clear forerunner as candidate kinase to phosphorylate eIF-2alpha in our RP-deficient model, the mechanism whereby RP-deficient states might lead to this activation remains unclear.

8.2.3   Balance between haem and globin – is FLVCR1 the key?

Haem, a structure manufactured within all cells by enzymes located within the cytosol and mitochondria, consists of a porphyrin ring with central iron core. All cells have a need for haem since it is a constituent of some of several essential haemoproteins and enzymes; however, 80% of the body's haem is incorporated in haemoglobin within red blood cells. Production of haemoglobin is regulated during erythroid differentiation such that increasing amounts of haemoglobin are produced as the cells differentiate. Furthermore the presence of haem is able to regulate the differentiation of erythroid cells. In mammalian erythrocytes all the haemoglobin required for the lifespan of the cell is generated by the time the cell is terminally differentiated and has extruded its nucleus and organelles, since no further protein production can occur after this point.

Feline leukaemia virus subgroup C receptor 1 (FLVCR1) was identified as the cell surface receptor for the feline leukaemia virus subgroup C (FeLV-C) in cats. Cats infected with FeLV-C develop profound anaemia with reduced capacity to form CFU-Erythroid colonies. Infection with the virus resulted in reduced expression of FLVCR1 on the cell surface of erythroid cells. It was shown that intracellular haem content was inversely proportional to the expression of FLVCR1 on the cell surface, suggesting that FLVCR1 may function as a haem exporter (Quigley et al, 2004). Mice deficient in *Flvcr1* develop a macrocytic anaemia and constitutional features resembling DBA (Keel et al, 2008). A search for mutations in *FLCVR1* in DBA patients did not identify any abnormalities; however, DBA patient erythroid cells exhibit a number of splice variants of FLVCR1 not found in normal erythroid

cells prematurely truncating the protein and results in reduced expression of FLVCR1 on the cell surface (Rey et al, 2008). In addition, knockdown of RPS19 in K562 cells reduces FLVCR1 protein levels and increases the amount of alternately spliced FLVCR1. Thus there appears to be a link between expression level of FLVCR1 and the anaemia observed with loss of RPS19.

It has been hypothesised that loss of cell surface FLVCR1 results in increased intracellular haem, increased oxidative damage and death by apoptosis. An alternate, complementary hypothesis is that aberrant FLVCR1 cell surface expression is able to mediate EIF-2alpha phosphorylation. This may occur as a result of relative L-arginine deficiency that may occur as a result of excess haem leading to activation of GCN2 (Omodeo-Sale et al, 2010).

8.2.4   Are the effectors of the ISR translated in response to EIF2alpha phosphorylation in RP-deficient states?

One possible explanation for the anaemia observed in *rps19* morphants is that phosphorylation of Eif-2alpha is an appropriate physiological response to ribosomal stress that should allow activation of pathways required for repair of the cell, and that it is a component of the repair pathway that is aberrant in *rps19* morphants. This hypothesis is supported by the observation that the majority of mRNAs capable of bypassing the translation block imposed by phospho-EIF-2alpha and mediating the "recovery or death" decisions made by cells are regulated at the translational level by the presence of short, non-coding upstream open reading frames (uORF). The primary regulator of this process is the transcription factor ATF4. ATF4 carries two uORFs which are highly conserved between zebrafish and humans (Figure 8-3A). In mammalian cell culture systems it appears that the all three ORFS (two upstream ORFs and the coding ORF) are recognised by the ribosome which attempts to translate the proceeding nucleotide sequence. Under basal conditions, in the presence of only the first uORF with the ATG of the second mutated, the main coding reading frame is constitutively "ON" and ATF4 is translated. Conversely in the presence of only the second uORF (with the first ATG mutated) the coding reading frame is "OFF". Phosphorylation of EIF-2alpha has no effect on translation levels in the presence of only one uORF. In the presence of both uORFs under basal conditions ATF4 is only translated at very low levels, but, when the cell becomes stressed and EIF-

2alpha is phosphorylated, there is a marked increase in the level of ATF4 translation (Vattem & Wek 2004). This is depicted in the cartoon in Figure 8-3B. The proposed mechanism for this is that phosphorylated-EIF-2alpha results in impaired production of EIF2-GTP-tRNAi^{met} ternary complex formation and inefficient ribosomal scanning. Thus the second "inhibitory" reading frame is skipped and the ATF4 coding region is translated. It is therefore conceivable that in the presence of RP-deficiency this "skipping" mechanism is aberrant and ATF4 is not translated. This in turn could lead to a failure to activate repair pathways normally implemented to allow the cell to recover.

Legend Figure 8-3: (A) Conservation of the uORFs of ATF4 in human, mouse and zebrafish species. Atf4 is duplicated in zebrafish. uORF1 is shown in red, uORF2 is shown in blue and Atf4 coding region is denoted by lower case lettering. The uORF structural organisation is highly conserved indicating that the distances between them may play a critical role in ATF4 translation. (B) Schematic cartoon of ATF4 reading frame function. X marks mutated ATG of uORF. Green shows the ATF4 coding region. Intensity of green denotes the level of protein expression of ATF4 under the specified conditions. Thus uORF1 is required for activating, uORF2 is inhibitory and both uORFs are required for optimal response to stress when EIF-2alpha is phosphorylated (Figure adapted from Lu et al, 2004 and Vattem & Wek, 2004).

Figure 8-3 : Atf4 uORFs are conserved from mammals to zebrafish and required for stress induced translation responses

8.3 Future studies using zebrafish to model diseases of ribosomal protein gene mutations

Using zebrafish to study aspects of human ribosomal protein gene mutations (or deletions) is very appealing for several reasons. First, the majority of RP genes and associated proteins involved in ribosome biogenesis are highly conserved between mammals and zebrafish, not only attesting the importance of such genes through evolution but implying conserved function. Given the high levels of conservation, validation of findings at the protein level can be facilitated with an array of cross-reacting antibodies, a limitation of studies in zebrafish when less-conserved proteins are under investigation. Second the zebrafish is an ideal genetic model in which to study the development of the haematopoietic system since it is diploid and transparent until 5 dpf (or later if pigment mutant strains are utilised). The major factor limiting future studies of disease-associated RPs is the lack of stable lines to assess the effects on adult haematopoiesis. In the case of DBA there are to date 9 genes with described mutations in RPs and all other RPs have been sequenced with no mutations validated in the registry of patients at the Children's Hospital Boston (Doherty et al, 2010). There are several zebrafish viral insertional mutant lines that carry insertions in ribosomal protein genes. These lines originated from the viral insertional screen performed in Nancy Hopkins laboratory (the same library used for the myeloid screen in Chapter 3 of this thesis). The majority of these lines (17 of 28) are tumour-prone in heterozygous adults, giving rise to a spectrum of tumours that are commonly associated with p53 mutations in both zebrafish and humans (Amsterdam et al, 2004b; Berghmans et al, 2005; Lai et al, 2009; MacInnes et al, 2008). Of the genes known to be mutated in DBA (*RPS7 RPS19*, *RPS24*, *RPS17*, *RPL35A, RPL5, RPS10, RPS26,* and *RPL11)* only *rps7* and *rpl11* are found in this cohort of zebrafish insertional mutants. Rps7 mutant zebrafish are tumour-prone with around 50% of adults dying as a result of tumour development. In contrast Rpl11 mutants do not show any increase in tumour formation (Lai et al, 2009). It is notable that both *rps7* and *rpl11* mutants contain insertions within the first intron, suggesting they may be hypomorphic alleles. Regardless of this, the study of these mutants by Lai et al. did not identify any correlation between mRNA levels of the mutant RP genes; however protein levels were not assessed, limiting the conclusions which can be drawn about the relative contribution of Rps7 or Rpl11

levels to tumorigenesis in these fish. Studies of the haematopoietic system in these zebrafish have not been performed, which is most likely because *RPS7* and *RPL11* mutations are relatively recent observations in DBA. My future studies in this field would begin with investigation of the two available DBA alleles with the primary goal of determining whether heterozygous mutants have normal blood development.

For my future studies I would aim to generate stable lines carrying *rps14* and *rps19* mutant alleles. TILLING is in progress for both of these genes at the Sanger Centre in Cambridge (UK) and I have assessed the ZIFIT databases for the presence of putative zinc finger sites for zinc finger nuclease mediated mutagenesis. Zinc finger target sites are present for both genes using either in silico based zinc finger construction and OPEN based bacterial-2-hybrid strategies (Maeder et al, 2009; Meng et al, 2008).

In RP-deficient patients' ribosome biogenesis is impaired. A recent landmark paper from Ingolia et al (2009) has capitalised on the knowledge that ribosomes bind mRNA at the site of translation initiation and leave a "footprint" there, approximately 30 nucleotides long (Ingolia et al, 2009). Ribosome foot printing of budding yeast under normal and starved conditions was achieved using simple RNAse digestion of total RNA extract. A parallel sample of randomly fragmented mRNAs was used as controls. Deep whole genome sequencing was then performed followed by a comparative analysis between the ribosome footprint sequence and the mRNA random fragmented RNA. Such ribosome profiling and sequencing represents an extremely powerful tool for examining the effects of impaired ribosome biogenesis has on translation of haematopoietic and other mRNAs. Since the sequencing primers used in such whole genome methods are universal this method has no species specificity. The zebrafish model is ideal for application of this new technology, as large numbers of fish can be generated, erythroid cells can be sorted using transgenic animals, and mature erythroid cells are nucleated (thus containing RNA). Although mature human erythroid cells do not contain RNA it has been shown that the target cell where ribosomal haploinsufficiency has its effect is in the nucleated erythroid progenitor stage. I would aim in future studies to utilise ribosomal footprint sequencing to determine the specific effects of translated RNAs on erythroid cells by ribosomal foot printing carried out using RP-heterozygous animals and controls. Erythroid

specificity would be attained using *Tg(gata1:dsRED2)* lines to allow identification of live anaemic heterozygotes as it is likely that homozygotes are embryonic lethal. It is probable that there are common genes and pathways affected by RP loss, however, there may also be differences between RP-proteins particularly RPS14 and those that result in DBA. Thus, I would aim to use zebrafish that carry mutations in *rps19* and *rps14* that most closely represent the most common genetic lesions in DBA and MDS5q respectively. Since it is unlikely that sufficient RNA from DBA patients will be available from peripheral blood samples validation would be carried out in primary human CD34+ cells with siRNA/shRNA knockdown of RPS19 and RPS14 (Ebert et al, 2008). For validation and further study of the effects specific to RPS14 loss, primary MDS patient samples with loss of 5q would add critical clinical relevance to the findings and are more likely to be available given such patients routinely undergo bone marrow examination.

8.4 Concluding remarks

The data presented in this thesis demonstrates the power of the zebrafish model in the study of haematopoiesis with relevance to human disease. It is serendipitous that I embarked on a project to address the function of Ddx18 in haematopoiesis. For many months I did not consider the relevance of the literature on Has1p in ribosome biogenesis in yeasts to human haematopoiesis. It was only during my subsequent studies of NPM1 and particularly RPS19 and RPS14 that a common thread of ribosome biogenesis began to emerge.

I believe that using the zebrafish to study the highly conserved process of ribosome biogenesis will provide relevant and translatable information about human diseases associated with ribosomal protein deficiencies. Marriage of detailed genetic analysis in this simple model organism can now be complemented by the analysis of the translated proteome using cutting edge whole genome sequencing of ribosomal foot printing. Coupled with in vitro studies in primary human cells I believe we can begin to unravel and clarify novel pathways that will facilitate our understanding of disease biology, and lead to the generation of novel therapeutics.

References cited

Abdelhaleem M (2002) The novel helicase homologue DDX32 is down-regulated in acute lymphoblastic leukemia. *Leukemia Research* **26:** 945-954

Adams SP, Sahota SS, Mijovic A, Czepulkowski B, Padua RA, Mufti GJ, Guinn BA (2002) Frequent expression of HAGE in presentation chronic myeloid leukaemias. *Leukemia* **16:** 2238-2242

Adzhubei IA, Schmidt S, Peshkin L, Ramensky VE, Gerasimova A, Bork P, Kondrashov AS, Sunyaev SR (2010) A method and server for predicting damaging missense mutations. *Nat Meth* **7:** 248-249

Alberts B, Johnson A, Lewis J, Raff M, Roberts K, Walter P (2008) *Molecular Biology of the Cell*, fifth - reference edition edn.: Garland Science.

Albiero E, Madeo D, Bolli N, Giaretta I, Bona ED, Martelli MF, Nicoletti I, Rodeghiero F, Falini B (2007) Identification and functional characterization of a cytoplasmic nucleophosmin leukaemic mutant generated by a novel exon-11 NPM1 mutation. *Leukemia*

Alcalay M, Tiacci E, Bergomas R, Bigerna B, Venturini E, Minardi SP, Meani N, Diverio D, Bernard L, Tizzoni L, Volorio S, Luzi L, Colombo E, Lo Coco F, Mecucci C, Falini B, Pelicci PG, for the Gruppo Italiano Malattie Ematologiche Maligne dell'Adulto Acute Leukemia Working P (2005) Acute myeloid leukemia bearing cytoplasmic nucleophosmin (NPMc+ AML) shows a distinct gene expression profile characterized by up-regulation of genes involved in stem-cell maintenance. *Blood* **106:** 899-902

Amigo JD, Ackermann GE, Cope JJ, Yu M, Cooney JD, Ma D, Langer NB, Shafizadeh E, Shaw GC, Horsely W, Trede NS, Davidson AJ, Barut BA, Zhou Y, Wojiski SA, Traver D, Moran TB, Kourkoulis G, Hsu K, Kanki JP, Shah DI, Lin HF, Handin RI, Cantor AB, Paw BH (2009) The role and regulation of friend of GATA-1 (FOG-1) during blood development in the zebrafish. *Blood* **114:** 4654-4663

Amsterdam A, Burgess S, Golling G, Chen W, Sun Z, Townsend K, Farrington S, Haldi M, Hopkins N (1999) A large-scale insertional mutagenesis screen in zebrafish. *Genes and Development* **13:** 2713-2724

Amsterdam A, Nissen RM, Sun Z, Swindell EC, Farrington S, Hopkins N (2004a) Identification of 315 genes essential for early zebrafish development. *Proceeding of the National Academy of Sciences U S A* **101:** 12792-12797

Amsterdam A, Sadler K, Lai K, Farrington S, Bronson R, Lees J, Hopkins N (2004b) Many ribosomal protein genes are cancer genes in zebrafish. *PLoS Biology* **2:** E139

Anderson KL, Smith KA, Conners K, McKercher SR, Maki RA, Torbett BE (1998) Myeloid development is selectively disrupted in PU.1 null mice. *Blood* **91:** 3702-3710

Anthony J, Yoshizawa F, Anthony T, Vary T, Jefferson L, Kimball S (2000) Leucine stimulates translation initiation in skeletal muscle of postabsorptive rats via a rapamycin-sensitive pathway. *Journal of Nutrition* **130:** 2413-2419

Anthony T, McDaniel B, Byerley R, McGrath B, Cavener D, McNurlan M, Wek R (2004) Preservation of liver protein synthesis during dietary leucine deprivation occurs at the expense of skeletal muscle mass in mice deleted for eIF2 kinase GCN2. *The Journal of Biological Chemistry* **279:** 36553-36561

Anur P, Nemecek ER, Kurre P (2009) The evolving spectrum of 'non-classical' Diamond-Blackfan anaemia – a case of eADA positive pancytopenia in a young adult. *British Journal of Haematology* **145:** 428-430

Badhai J, Fröjmark A-S, Razzaghian HR, Davey E, Schuster J, Dahl N (2009a) Posttranscriptional down-regulation of small ribosomal subunit proteins correlates with reduction of 18S rRNA in RPS19 deficiency. *FEBS Letters* **583:** 2049-2053

Badhai J, Fröjmark A, J Davey E, Schuster J, Dahl N (2009b) Ribosomal protein S19 and S24 insufficiency cause distinct cell cycle defects in Diamond-Blackfan anemia. *Biochimica et Biophysica Acta* **1792:** 1036-1042

Ball SE, McGuckin CP, Jenkins G, Gordon-Smith EC (1996) Diamond-Blackfan anaemia in the U.K.: analysis of 80 cases from a 20-year birth cohort. *British Journal of Haematology* **94:** 645-653

Barbazuk WB, Korf I, Kadavi C, Heyen J, Tate S, Wun E, Bedell JA, McPherson JD, Johnson SL (2000) The syntenic relationship of the zebrafish and human genomes. *Genome Research* **10:** 1351-1358

Barlow JL, Drynan LF, Hewett DR, Holmes LR, Lorenzo-Abalde S, Lane AL, Jolin HE, Pannell R, Middleton AJ, Wong SH, Warren AJ, Wainscoat JS, Boultwood J, McKenzie AN (2010) A p53-dependent mechanism underlies macrocytic anemia in a mouse model of human 5q- syndrome. *Nature Medicine* **16:** 59-66

Bauer B, Rafie-Kolpin M, Lu L, Han A, Chen J (2001) Multiple autophosphorylation is essential for the formation of the active and stable homodimer of heme-regulated eIF2alpha kinase. *Biochemistry* **40:** 11543-11551

Bennett CM, Kanki JP, Rhodes J, Liu TX, Paw BH, Kieran MW, Langenau DM, Delahaye-Brown A, Zon LI, Fleming MD, Look AT (2001) Myelopoiesis in the zebrafish, Danio rerio. *Blood* **98:** 643-651

Berghmans S, Murphey RD, Wienholds E, Neuberg D, Kutok JL, Fletcher CD, Morris JP, Liu TX, Schulte-Merker S, Kanki JP, Plasterk R, Zon LI, Look AT (2005) tp53 mutant zebrafish develop malignant peripheral nerve sheath tumors. *Proceedings of National Academy of Sciences U S A* **102:** 407-412

Bernstein KA, Granneman S, Lee AV, Manickam S, Baserga SJ (2006) Comprehensive mutational analysis of Yeast DEXD/H Box RNA helicases involved in large ribosomal subunit biogenesis. *Molecular and Cellular Biology* **26:** 1195-1208

Bertrand JY, Chi NC, Santoso B, Teng S, Stainier DY, Traver D (2010) Haematopoietic stem cells derive directly from aortic endothelium during development. *Nature* **464**:108-111

Bertrand JY, Kim AD, Teng S, Traver D (2008) CD41+ cmyb+ precursors colonize the zebrafish pronephros by a novel migration route to initiate adult hematopoiesis. *Development* **135:** 1853-1862

Bertrand JY, Kim AD, Violette EP, Stachura DL, Cisson JL, Traver D (2007) Definitive hematopoiesis initiates through a committed erythromyeloid progenitor in the zebrafish embryo. *Development* **134:** 4147-4156

Bertwistle D, Sugimoto M, Sherr CJ (2004) Physical and functional interactions of the Arf tumor suppressor protein with nucleophosmin/B23. *Molecular and Cellular Biology* **24:** 985-996

Boisset JC, van Cappellen W, Andrieu-Soler C, Galjart N, Dzierzak E, Robin C (2010) In vivo imaging of haematopoietic cells emerging from the mouse aortic endothelium. *Nature* **464**:116-120

Bolli N, De Marco MF, Martelli MP, Bigerna B, Pucciarini A, Rossi R, Mannucci R, Manes N, Pettirossi V, Pileri SA, Nicoletti I, Falini B (2009) A dose-dependent tug of war involving the NPM1 leukaemic mutant, nucleophosmin, and ARF. *Leukemia* **23:** 501-509

Bolli N, Nicoletti I, De Marco MF, Bigerna B, Pucciarini A, Mannucci R, Martelli MP, Liso A, Mecucci C, Fabbiano F, Martelli MF, Henderson BR, Falini B. (2007) Born to be exported: COOH-terminal nuclear export signals of different strength ensure cytoplasmic accumulation of nucleophosmin leukemic mutants. *Cancer Research* **67:** 6230-6237.

Bolli N, Payne EM, Grabher C, Lee JS, Johnston AB, Falini B, Kanki JP, Look AT (2010) Expression of the cytoplasmic NPM1 mutant (NPMc+) causes the expansion of hematopoietic cells in zebrafish. *Blood* **115:** 3329-3340

Boocock GR, Morrison JA, Popovic M, Richards N, Ellis L, Durie PR, Rommens JM (2003) Mutations in SBDS are associated with Shwachman-Diamond syndrome. *Nature Genetics* **33:** 97-101

Borze I, Juvonen E, Ninomiya S, Jee KJ, Elonen E, Knuutila S (2010) High-resolution oligonucleotide array comparative genomic hybridization study and methylation status of the RPS14 gene in de novo myelodysplastic syndromes. *Cancer Genetics and Cytogenetics* **197:** 166-173

Botlagunta M, Vesuna F, Mironchik Y, Raman A, Lisok A, Winnard P, Jr., Mukadam S, Van Diest P, Chen JH, Farabaugh P, Patel AH, Raman V (2008) Oncogenic role of DDX3 in breast cancer biogenesis. *Oncogene* **27:** 3912-3922

Boultwood J, Fidler C, Lewis S, Kelly S, Sheridan H, Littlewood TJ, Buckle VJ, Wainscoat JS (1994) Molecular mapping of uncharacteristically small 5q deletions in two patients with the 5q- syndrome: delineation of the critical region on 5q and identification of a 5q- breakpoint. *Genomics* **19:** 425-432

Boultwood J, Fidler C, Soularue P, Strickson AJ, Kostrzewa M, Jaju RJ, Cotter FE, Fairweather N, Monaco AP, Muller U, Lovett M, Jabs EW, Auffray C, Wainscoat JS (1997) Novel genes mapping to the critical region of the 5q- syndrome. *Genomics* **45:** 88-96

Brownlie A, Donovan A, Pratt SJ, Paw BH, Oates AC, Brugnara C, Witkowska HE, Sassa S, Zon LI (1998) Positional cloning of the zebrafish sauternes gene: a model for congenital sideroblastic anaemia. *Nature Genetics* **20:** 244-250

Brownlie A, Hersey C, Oates AC, Paw BH, Falick AM, Witkowska HE, Flint J, Higgs D, Jessen J, Bahary N, Zhu H, Lin S, Zon L (2003) Characterization of embryonic globin genes of the zebrafish. *Developmental Biology* **255:** 48-61

Brunham LR, Singaraja RR, Pape TD, Kejariwal A, Thomas PD, Hayden MR (2005) Accurate prediction of the functional significance of single nucleotide polymorphisms and mutations in the *ABCA1* gene. *PLoS Genetics* **1:** e83

Burns CE, DeBlasio T, Zhou Y, Zhang J, Zon L, Nimer SD (2002) Isolation and characterization of runxa and runxb, zebrafish members of the runt family of transcriptional regulators. *Experimental Hematology* **30:** 1381-1389

Burns CE, Galloway JL, Smith AC, Keefe MD, Cashman TJ, Paik EJ, Mayhall EA, Amsterdam AH, Zon LI (2009) A genetic screen in zebrafish defines a hierarchical network of pathways required for hematopoietic stem cell emergence. *Blood* **113:** 5776-5782

Chakraborty A, Uechi T, Higa S, Torihara H, Kenmochi N (2009) Loss of ribosomal protein L11 affects zebrafish embryonic development through a p53-dependent apoptotic response. *PLoS One* **4:** e4152

Chan FY, Robinson J, Brownlie A, Shivdasani RA, Donovan A, Brugnara C, Kim J, Lau BC, Witkowska HE, Zon LI (1997) Characterization of adult alpha- and beta-globin genes in the zebrafish. *Blood* **89:** 688-700

Chen J, Jette C, Kanki JP, Aster JC, Look AT, Griffin JD (2007) NOTCH1-induced T-cell leukemia in transgenic zebrafish. *Leukemia* **21:** 462-471

Cheng K, Grisendi S, Clohessy JG, Majid S, Bernardi R, Sportoletti P, Pandolfi PP (2007) The leukemia-associated cytoplasmic nucleophosmin mutant is an oncogene with paradoxical functions: Arf inactivation and induction of cellular senescence. *Oncogene* **26:** 7391-7400

Cheng R, Ford BL, O'Neal PE, Mathews CZ, Bradford CS, Thongtan T, Barnes DW, Hendricks JD, Bailey GS (1997) Zebrafish (*Danio rerio*) p53 tumor suppressor gene: cDNA sequence and expression during embryogenesis. *Molecular Marine Biology and Biotechnology* **6:** 88-97

Childs S, Weinstein BM, Mohideen MA, Donohue S, Bonkovsky H, Fishman MC (2000) Zebrafish dracula encodes ferrochelatase and its mutation provides a model for erythropoietic protoporphyria. *Current Biology* **10:** 1001-1004

Chiocchetti A, Gibello L, Carando A, Aspesi A, Secco P, Garelli E, Loreni F, Angelini M, Biava A, Dahl N, Dianzani U, Ramenghi U, Santoro C, Dianzani I (2005) Interactions between RPS19, mutated in Diamond-Blackfan anemia, and the PIM-1 oncoprotein. *Haematologica* **90:** 1453-1462

Cmejlova J, Dolezalova L, Pospisilova D, Petrtylova K, Petrak J, Cmejla R (2006) Translational efficiency in patients with Diamond-Blackfan anemia. *Haematologica* **91:** 1456-1464

Colombo E, Marine JC, Danovi D, Falini B, Pelicci PG (2002) Nucleophosmin regulates the stability and transcriptional activity of p53. *Nature Cell Biology* **4:** 529-533

Craven SE, French D, Ye W, de Sauvage F, Rosenthal A (2005) Loss of Hspa9b in zebrafish recapitulates the ineffective hematopoiesis of the myelodysplastic syndrome. *Blood* **105:** 3528-3534.

Crowhurst MO, Layton JE, Lieschke GJ (2002) Developmental biology of zebrafish myeloid cells. *International Journal of Developmental Biology* **46:** 483-492

Cuomo ME, Knebel A, Morrice N, Paterson H, Cohen P, Mittnacht S (2008) p53-Driven apoptosis limits centrosome amplification and genomic instability downstream of NPM1 phosphorylation. *Nature Cell Biology* **10:** 723-730

Danilova N, Sakamoto KM, Lin S (2008) Ribosomal protein S19 deficiency in zebrafish leads to developmental abnormalities and defective erythropoiesis through activation of p53 protein family. *Blood* **112:** 5228-5237

Dar A, Dever T, Sicheri F (2005) Higher-order substrate recognition of eIF2alpha by the RNA-dependent protein kinase PKR. *Cell* **122:** 887-900

Dayyani F, Wang J, Yeh J-RJ, Ahn E-Y, Tobey E, Zhang D-E, Bernstein ID, Peterson RT, Sweetser DA. (2008) Loss of TLE1 and TLE4 from the del(9q) commonly deleted region in AML cooperates with AML1-ETO to affect myeloid cell proliferation and survival. *Blood* **111:** 4338-4347.

de Oliveira JF, Sforca ML, Blumenschein TM, Goldfeder MB, Guimaraes BG, Oliveira CC, Zanchin NI, Zeri AC (2010) Structure, dynamics, and RNA interaction analysis of the human SBDS protein. *Journal of Molecular Biology* **396:** 1053-1069

Deisenroth C, Zhang Y (2010) Ribosome biogenesis surveillance: probing the ribosomal protein-Mdm2-p53 pathway. *Oncogene* **29:** 4253-4260

Detrich HW, 3rd, Kieran MW, Chan FY, Barone LM, Yee K, Rundstadler JA, Pratt S, Ransom D, Zon LI (1995) Intraembryonic hematopoietic cell migration during vertebrate development. *Proceedings of the National Academy of Sciences U S A* **92:** 10713-10717

Dey M, Cao C, Dar A, Tamura T, Ozato K, Sicheri F, Dever T (2005a) Mechanistic link between PKR dimerization, autophosphorylation, and eIF2alpha substrate recognition. *Cell* **122:** 901-913

Dey M, Trieselmann B, Locke E, Lu J, Cao C, Dar A, Krishnamoorthy T, Dong J, Sicheri F, Dever T (2005b) PKR and GCN2 kinases and guanine nucleotide exchange factor eukaryotic translation initiation factor 2B (eIF2B) recognize overlapping surfaces on eIF2alpha. *Molecular and Cellular Biology* **25:** 3063-3075

Dixon J, Hovanes K, Shiang R, Dixon M (1997) Sequence analysis, identification of evolutionary conserved motifs and expression analysis of murine tcof1 provide further evidence for a potential function for the gene and its human homologue, TCOF1. *Hum Molecular Genetics* **6:** 727-737

Dixon J, Jones N, Sandell L, Jayasinghe S, Crane J, Rey J, Dixon M, Trainor P (2006) Tcof1/Treacle is required for neural crest cell formation and proliferation deficiencies that cause craniofacial abnormalities. *Proceedings of the National Academy of Sciences U S A* **103:** 13403-13408

Dodd ME, Hatzold J, Mathias JR, Walters KB, Bennin DA, Rhodes J, Kanki JP, Look AT, Hammerschmidt M, Huttenlocher A (2009) The ENTH domain protein Clint1 is required for epidermal homeostasis in zebrafish. *Development* **136:** 2591-2600

Doherty L, Sheen M, Vlachos A, Choesmel V, O'Donohue M, Clinton C, Schneider H, Sieff C, Newburger P, Ball S, Niewiadomska E, Matysiak M, Glader B, Arceci R, Farrar J, Atsidaftos E, Lipton J, Gleizes P, Gazda H (2010) Ribosomal protein genes RPS10 and RPS26 are commonly mutated in Diamond-Blackfan anemia. *American Journal of Human Genetics* **86:** 222-228

Donovan A, Brownlie A, Dorschner MO, Zhou Y, Pratt SJ, Paw BH, Phillips RB, Thisse C, Thisse B, Zon LI (2002) The zebrafish mutant gene chardonnay (cdy) encodes divalent metal transporter 1 (DMT1). *Blood* **100:** 4655-4659

Donovan A, Brownlie A, Zhou Y, Shepard J, Pratt SJ, Moynihan J, Paw BH, Drejer A, Barut B, Zapata A, Law TC, Brugnara C, Lux SE, Pinkus GS, Pinkus JL, Kingsley PD, Palis J, Fleming MD, Andrews NC, Zon LI (2000) Positional cloning of zebrafish ferroportin1 identifies a conserved vertebrate iron exporter. *Nature* **403:** 776-781

Dougan S, Warga R, Kane D, Schier A, Talbot W (2003) The role of the zebrafish nodal-related genes squint and cyclops in patterning of mesendoderm. *Development* **130:** 1837-1851

Downs JA, Lowndes NF, Jackson SP (2000) A role for Saccharomyces cerevisiae histone H2A in DNA repair. *Nature* **408:** 1001-1004

Doyon Y, McCammon JM, Miller JC, Faraji F, Ngo C, Katibah GE, Amora R, Hocking TD, Zhang L, Rebar EJ, Gregory PD, Urnov FD, Amacher SL (2008) Heritable targeted gene disruption in zebrafish using designed zinc-finger nucleases. *Nature Biotechnology* **26:** 702-708

Draptchinskaia N, Gustavsson P, Andersson B, Pettersson M, Willig TN, Dianzani I, Ball S, Tchernia G, Klar J, Matsson H, Tentler D, Mohandas N, Carlsson B, Dahl N (1999) The gene encoding ribosomal protein S19 is mutated in Diamond-Blackfan anaemia. *Nature Genetics* **21:** 169-175

Driever W, Solnica-Krezel L, Schier AF, Neuhauss SC, Malicki J, Stemple DL, Stainier DY, Zwartkruis F, Abdelilah S, Rangini Z, Belak J, Boggs C (1996) A genetic screen for mutations affecting embryogenesis in zebrafish. *Development* **123:** 37-46

Dubaele S, Chène P (2007) Cellular studies of MrDb (DDX18). *Oncology Research* **16:** 549-556

Ebert BL, Galili N, Tamayo P, Bosco J, Mak R, Pretz J, Tanguturi S, Ladd-Acosta C, Stone R, Golub TR, Raza A (2008) An erythroid differentiation signature predicts response to lenalidomide in myelodysplastic syndrome. *PLoS Medicine* **5:** e35

Eisen JS, Smith JC (2008) Controlling morpholino experiments: don't stop making antisense. *Development* **135:** 1735-1743

Emery B, de la Cruz J, Rocak S, Deloche O, Linder P (2004) Has1p, a member of the DEAD-box family, is required for 40S ribosomal subunit biogenesis in Saccharomyces cerevisiae. *Molecular Microbiology* **52:** 141-158

Enomoto T, Lindstrom MS, Jin A, Ke H, Zhang Y. (2006) Essential role of the B23/NPM core domain in regulating ARF binding and B23 stability. J*ournal of Biological Chemistry* **281**: 18463-18472.

Falini B, Bigerna B, Pucciarini A, Tiacci E, Mecucci C, Morris SW, Bolli N, Rosati R, Hanissian S, Ma Z, Sun Y, Colombo E, Arber DA, Pacini R, La Starza R, Verducci Galletti B, Liso A, Martelli MP, Diverio D, Pelicci PG, Lo Coco F, Martelli MF (2006a) Aberrant subcellular expression of nucleophosmin and NPM-MLF1 fusion protein in acute myeloid leukaemia carrying t(3;5): a comparison with NPMc+ AML. *Leukemia* **20:** 368-371

Falini B, Bolli N, Liso A, Martelli MP, Mannucci R, Pileri S, Nicoletti I (2009) Altered nucleophosmin transport in acute myeloid leukaemia with mutated NPM1: molecular basis and clinical implications. *Leukemia* **23:** 1731-1743

Falini B, Bolli N, Shan J, Martelli MP, Liso A, Pucciarini A, Bigerna B, Pasqualucci L, Mannucci R, Rosati R, Gorello P, Diverio D, Roti G, Tiacci E, Cazzaniga G, Biondi A, Schnittger S, Haferlach T, Hiddemann W, Martelli MF, Gu W, Mecucci C, Nicoletti I.

(2006b) Both carboxy-terminus NES motif and mutated tryptophan(s) are crucial for aberrant nuclear export of nucleophosmin leukemic mutants in NPMc+ AML. *Blood* **107:** 4514-4523.

Falini B, Martelli MP, Bolli N, Bonasso R, Ghia E, Pallotta MT, Diverio D, Nicoletti I, Pacini R, Tabarrini A, Verducci Galletti B, Mannucci R, Roti G, Rosati R, Specchia G, Liso A, Tiacci E, Alcalay M, Luzi L, Volorio S, Bernard L, Guarini A, Amadori S, Mandelli F, Pane F, Lo Coco F, Saglio G, Pelicci PG, Martelli MF, Mecucci C (2006c) Immunohistochemistry predicts nucleophosmin (NPM) mutations in acute myeloid leukemia. *Blood* **108:** 1999-2005

Falini B, Mecucci C, Tiacci E, Alcalay M, Rosati R, Pasqualucci L, La Starza R, Diverio D, Colombo E, Santucci A, Bigerna B, Pacini R, Pucciarini A, Liso A, Vignetti M, Fazi P, Meani N, Pettirossi V, Saglio G, Mandelli F, Lo-Coco F, Pelicci PG, Martelli MF (2005b) Cytoplasmic nucleophosmin in acute myelogenous leukemia with a normal karyotype. *The New England journal of medicine* **352:** 254-266

Foley JE, Yeh JR, Maeder ML, Reyon D, Sander JD, Peterson RT, Joung JK (2009) Rapid mutation of endogenous zebrafish genes using zinc finger nucleases made by Oligomerized Pool ENgineering (OPEN). *PLoS ONE* **4:** e4348

Fukuda T, Yamagata K, Fujiyama S, Matsumoto T, Koshida I, Yoshimura K, Mihara M, Naitou M, Endoh H, Nakamura T, Akimoto C, Yamamoto Y, Katagiri T, Foulds C, Takezawa S, Kitagawa H, Takeyama K, O'Malley BW, Kato S (2007) DEAD-box RNA helicase subunits of the Drosha complex are required for processing of rRNA and a subset of microRNAs. *Nature Cell Biology* **9:** 604-611

Fuller-Pace FV (2006) DExD/H box RNA helicases: multifunctional proteins with important roles in transcriptional regulation. *Nucleic Acids Research* **34:** 4206-4215

Fumagalli S, Di Cara A, Neb-Gulati A, Natt F, Schwemberger S, Hall J, Babcock GF, Bernardi R, Pandolfi PP, Thomas G (2009) Absence of nucleolar disruption after impairment of 40S ribosome biogenesis reveals an rpL11-translation-dependent mechanism of p53 induction. *Nature Cell Biology* **11:** 501-508

Gaiano N, Allende M, Amsterdam A, Kawakami K, Hopkins N (1996) Highly efficient germ-line transmission of proviral insertions in zebrafish. *Proceedings of the National Academy of Sciences U S A* **93:** 7777-7782

Galloway JL, Wingert RA, Thisse C, Thisse B, Zon LI (2005) Loss of gata1 but not gata2 converts erythropoiesis to myelopoiesis in zebrafish embryos. *Developmental Cell* **8:** 109-116

Ganapathi KA, Austin KM, Lee CS, Dias A, Malsch MM, Reed R, Shimamura A (2007) The human Shwachman-Diamond syndrome protein, SBDS, associates with ribosomal RNA. *Blood* **110:** 1458-1465

Gates MA, Kim L, Egan ES, Cardozo T, Sirotkin HI, Dougan ST, Lashkari D, Abagyan R, Schier AF, Talbot WS (1999) A genetic linkage map for zebrafish: comparative analysis and localization of genes and expressed sequences. *Genome Research* **9:** 334-347

Gering M, Patient R (2005) Hedgehog signaling is required for adult blood stem cell formation in zebrafish embryos. *Developmental Cell* **8:** 389-400

Gering M, Rodaway AR, Gottgens B, Patient RK, Green AR (1998) The SCL gene specifies haemangioblast development from early mesoderm. *EMBO Journal* **17:** 4029-4045

Gering M, Yamada Y, Rabbitts TH, Patient RK (2003) Lmo2 and Scl/Tal1 convert non-axial mesoderm into haemangioblasts which differentiate into endothelial cells in the absence of Gata1. *Development* **130:** 6187-6199

Ghioni P, Bolognese F, Duijf PHG, van Bokhoven H, Mantovani R, Guerrini L (2002) Complex transcriptional effects of p63 Isoforms: Identification of novel activation and repression domains. *Molecular and Cellular Biology* **22:** 8659-8668

Golling G, Amsterdam A, Sun Z, Antonelli M, Maldonado E, Chen W, Burgess S, Haldi M, Artzt K, Farrington S, Lin SY, Nissen RM, Hopkins N (2002) Insertional mutagenesis in zebrafish rapidly identifies genes essential for early vertebrate development. *Nature Genetics* **31:** 135-140

Grandori C, Mac J, Siëbelt F, Ayer D, Eisenman R (1996) Myc-Max heterodimers activate a DEAD box gene and interact with multiple E box-related sites in vivo. *EMBO Journal* **15:** 4344-4357

Grisendi S, Bernardi R, Rossi M, Cheng K, Khandker L, Manova K, Pandolfi PP (2005) Role of nucleophosmin in embryonic development and tumorigenesis. *Nature* **437:** 147-153

Grisendi S, Mecucci C, Falini B, Pandolfi PP (2006) Nucleophosmin and cancer. *Nature Reviews Cancer* **6:** 493-505

Haffter P, Granato M, Brand M, Mullins MC, Hammerschmidt M, Kane DA, Odenthal J, van Eeden FJ, Jiang YJ, Heisenberg CP, Kelsh RN, Furutani-Seiki M, Vogelsang E, Beuchle D, Schach U, Fabian C, Nusslein-Volhard C (1996) The identification of genes with unique and essential functions in the development of the zebrafish, *Danio rerio*. *Development* **123:** 1-36

Hall C, Flores MV, Storm T, Crosier K, Crosier P (2007) The zebrafish lysozyme C promoter drives myeloid-specific expression in transgenic fish. *BMC Developmental Biology* **7:** 42

Han A, Fleming M, Chen J (2005) Heme-regulated eIF2alpha kinase modifies the phenotypic severity of murine models of erythropoietic protoporphyria and beta-thalassemia. *Journal of Clinical Investigation* **115:** 1562-1570

Han A, Yu C, Lu L, Fujiwara Y, Browne C, Chin G, Fleming M, Leboulch P, Orkin S, Chen J (2001) Heme-regulated eIF2alpha kinase (HRI) is required for translational regulation and survival of erythroid precursors in iron deficiency. *EMBO Journal* **20:** 6909-6918

Hegedus Z, Zakrzewska A, Agoston VC, Ordas A, Racz P, Mink M, Spaink HP, Meijer AH (2009) Deep sequencing of the zebrafish transcriptome response to mycobacterium infection. *Molecular Immunology* **46:** 2918-2930

Heinrichs S, Kulkarni R, Bueso-Ramos C, Levine R, Loh M, Li C, Neuberg D, Kornblau S, Issa J, Gilliland D, Garcia-Manero G, Kantarjian H, Estey E, Look A (2009) Accurate detection of uniparental disomy and microdeletions by SNP array analysis in myelodysplastic syndromes with normal cytogenetics. *Leukemia* **23:** 1605-1613

Henn A, Cao W, Licciardello N, Heitkamp SE, Hackney DD, De La Cruz EM (2010) Pathway of ATP utilization and duplex rRNA unwinding by the DEAD-box helicase, DbpA. *Proceedings of the National Academy of Sciences* **107:** 4046-4050

Herbomel P, Thisse B, Thisse C (1999) Ontogeny and behaviour of early macrophages in the zebrafish embryo. *Development* **126:** 3735-3745

Herrera J, Savkur R, Olson M (1995) The ribonuclease activity of nucleolar protein B23. *Nucleic Acids Research* **23:** 3974-3979

Hilbert M, Karow A, Klostermeier D (2009) The mechanism of ATP-dependent RNA unwinding by DEAD box proteins. *Biological Chemistry* **390:** 1237-1250

Hogan B, Layton J, Pyati U, Nutt S, Hayman J, Varma S, Heath J, Kimelman D, Lieschke G (2006) Specification of the primitive myeloid precursor pool requires signaling through Alk8 in zebrafish. *Current Biology* **16:** 506-511

Hölzel M, Orban M, Hochstatter J, Rohrmoser M, Harasim T, Malamoussi A, Kremmer E, Längst G, Eick D (2010) Defects in 18 S or 28 S rRNA processing activate the p53 pathway. *Journal of Biological Chemistry* **285:** 6364-6370

Horsfield JA, Anagnostou SH, Hu JK, Cho KH, Geisler R, Lieschke G, Crosier KE, Crosier PS (2007) Cohesin-dependent regulation of Runx genes. *Development* **134:** 2639-2649

Hsu K, Traver D, Kutok JL, Hagen A, Liu TX, Paw BH, Rhodes J, Berman JN, Zon LI, Kanki JP, Look AT (2004) The pu.1 promoter drives myeloid gene expression in zebrafish. *Blood* **104:** 1291-1297

Ingolia NT, Ghaemmaghami S, Newman JRS, Weissman JS (2009) Genome-Wide analysis in vivo of translation with nucleotide resolution using ribosome profiling. *Science* **324:** 218-223

Jaju RJ, Boultwood J, Oliver FJ, Kostrzewa M, Fidler C, Parker N, McPherson JD, Morris SW, Muller U, Wainscoat JS, Kearney L (1998) Molecular cytogenetic delineation of the critical deleted region in the 5q- syndrome. *Genes Chromosomes and Cancer* **22:** 251-256

Janov AJ, Leong T, Nathan DG, Guinan EC (1996) Diamond-Blackfan anemia. Natural history and sequelae of treatment. *Medicine (Baltimore)* **75:** 77-78

Jiang H, Jiang L, Wek R (2007) The eukaryotic initiation factor-2 kinase pathway facilitates differential GADD45a expression in response to environmental stress. *Journal of Biological Chemistry* **282:** 3755-3765

Jiang H, Wek R (2005) Phosphorylation of the alpha-subunit of the eukaryotic initiation factor-2 (eIF2alpha) reduces protein synthesis and enhances apoptosis in response to proteasome inhibition. *Journal of Biological Chemistry* **280:** 14189-14202

Jin H, Xu J, Wen Z (2007) Migratory path of definitive hematopoietic stem/progenitor cells during zebrafish development. *Blood* **109:** 5208-5214

Jones N, Lynn M, Gaudenz K, Sakai D, Aoto K, Rey J, Glynn E, Ellington L, Du C, Dixon J, Dixon M, Trainor P (2008) Prevention of the neurocristopathy Treacher Collins syndrome through inhibition of p53 function. *Nature Medicine* **14:** 125-133

Jorgensen P, Nishikawa JL, Breitkreutz B-J, Tyers M (2002) Systematic identification of pathways that couple cell growth and division in yeast. *Science* **297:** 395-400

Jorgensen P, Tyers M (2004) How cells coordinate growth and division. *Current Biology* **14:** R1014-1027

Jost JP, Schwarz S, Hess D, Angliker H, Fuller-Pace FV, Stahl H, Thiry S, Siegmann M (1999) A chicken embryo protein related to the mammalian DEAD box protein p68 is tightly associated with the highly purified protein-RNA complex of 5- MeC-DNA glycosylase. *Nucleic Acids Research* **27:** 3245-3252

Kalev-Zylinska ML, Horsfield JA, Flores MV, Postlethwait JH, Vitas MR, Baas AM, Crosier PS, Crosier KE (2002) Runx1 is required for zebrafish blood and vessel development and expression of a human RUNX1-CBF2T1 transgene advances a model for studies of leukemogenesis. *Development* **129:** 2015-2030

Karikó K, Buckstein M, Ni H, Weissman D (2005) Suppression of RNA recognition by Toll-like receptors: the impact of nucleoside modification and the evolutionary origin of RNA. *Immunity* **23:** 165-175

Karow A, Klostermeier D (2009) A conformational change in the helicase core is necessary but not sufficient for RNA unwinding by the DEAD box helicase YxiN. *Nucleic Acids Research* **37:** 4464-4471

Keel S, Doty R, Yang Z, Quigley J, Chen J, Knoblaugh S, Kingsley P, De Domenico I, Vaughn M, Kaplan J, Palis J, Abkowitz J (2008) A heme export protein is required for red blood cell differentiation and iron homeostasis. *Science* **319:** 825-828

Kim R, Emi M, Tanabe K, Murakami S (2006) Role of the unfolded protein response in cell death. *Apoptosis* **11:** 5-13

Kishi S, Bayliss PE, Uchiyama J, Koshimizu E, Qi J, Nanjappa P, Imamura S, Islam A, Neuberg D, Amsterdam A, Roberts TM (2008) The identification of zebrafish mutants showing alterations in senescence-associated biomarkers. *PLoS Genetics* **4:** e1000152

Kissa K, Herbomel P (2010) Blood stem cells emerge from aortic endothelium by a novel type of cell transition. *Nature* **646:** 112-115

Kissa K, Murayama E, Zapata A, Cortes A, Perret E, Machu C, Herbomel P (2008) Live imaging of emerging hematopoietic stem cells and early thymus colonization. *Blood* **111:** 1147-1156

Korgaonkar C, Hagen J, Tompkins V, Frazier AA, Allamargot C, Quelle FW, Quelle DE (2005) Nucleophosmin (B23) targets ARF to nucleoli and inhibits its function. *Molecular and Cellular Biology* **25:** 1258-1271

Kosmider O, Gelsi-Boyer V, Slama L, Dreyfus F, Beyne-Rauzy O, Quesnel B, Hunault-Berger M, Slama B, Vey N, Lacombe C, Solary E, Birnbaum D, Bernard OA, Fontenay M (2010) Mutations of IDH1 and IDH2 genes in early and accelerated phases of myelodysplastic syndromes and MDS/myeloproliferative neoplasms. *Leukemia* **24:** 1094-1096

Kramer JJ, Minakhina S, Campbell N, Marshall S, Piso K, Rabson AB, Steward R, Schaar D, Sabaawy H (2009) Alternative Splicing of PDCD2 Regulates Hematopoietic Stem Cell Specification, and Drives Multilineage Leukemia Development. *ASH Annual Meeting Abstracts* **114:** 258

Kurki S, Peltonen K, Latonen L, Kiviharju TM, Ojala PM, Meek D, Laiho M (2004) Nucleolar protein NPM interacts with HDM2 and protects tumor suppressor protein p53 from HDM2-mediated degradation. *Cancer Cell* **5:** 465-475

Lai K, Amsterdam A, Farrington S, Bronson R, Hopkins N, Lees J (2009) Many ribosomal protein mutations are associated with growth impairment and tumor predisposition in zebrafish. *Developmental Dynamics* **238:** 76-85

Lambert B, Buckle M (2006) Characterisation of the interface between nucleophosmin (NPM) and p53: Potential role in p53 stabilisation. *FEBS Letters* **580:** 345-350

Lambertsson A (1998) The minute genes in *drosophila* and their molecular functions. *Advances in Genetics* **38:** 69-134

Langenau DM, Keefe MD, Storer NY, Guyon JR, Kutok JL, Le X, Goessling W, Neuberg DS, Kunkel LM, Zon LI (2007) Effects of RAS on the genesis of embryonal rhabdomyosarcoma. *Genes and Development* **21:** 1382-1395

Langenau DM, Traver D, Ferrando AA, Kutok JL, Aster JC, Kanki JP, Lin S, Prochownik E, Trede NS, Zon LI, Look AT (2003) Myc-induced T cell leukemia in transgenic zebrafish. *Science* **299:** 887-890

Langheinrich U, Hennen E, Stott G, Vacun G (2002) Zebrafish as a model organism for the identification and characterization of drugs and genes affecting p53 signaling. *Current Biology* **12:** 2023-2028

Le Beau MM, Espinosa R, 3rd, Neuman WL, Stock W, Roulston D, Larson RA, Keinanen M, Westbrook CA (1993) Cytogenetic and molecular delineation of the smallest commonly deleted region of chromosome 5 in malignant myeloid diseases. *Proceedings of the National Academy of Sciences U S A* **90:** 5484-5488

Le Guyader D, Redd M, Colucci-Guyon E, Murayama E, Kissa K, Briolat V, Mordelet E, Zapata A, Shinomiya H, Herbomel P (2008) Origins and unconventional behavior of neutrophils in developing zebrafish. *Blood* **111:** 132-141

Le HY, Zhang Y, Liu H, Ma LH, Jin Y, Huang QH, Chen Y, Deng M, Chen Z, Chen SJ, Liu TX (2008) eena Promotes myeloid proliferation through stimulating ERK1/2 phosphorylation in zebrafish. *J Biol Chem* **283:** 17652-17661

Le X, Langenau DM, Keefe MD, Kutok JL, Neuberg DS, Zon LI (2007) Heat shock-inducible Cre/Lox approaches to induce diverse types of tumors and hyperplasia in transgenic zebrafish. *Proc Natl Acad Sci U S A* **104:** 9410-9415

Lee RK, Stainier DY, Weinstein BM, Fishman MC (1994) Cardiovascular development in the zebrafish. II. Endocardial progenitors are sequestered within the heart field. *Development* **120:** 3361-3366

Lee S, Chen J, Zhou G, Shi RZ, Bouffard GG, Kocherginsky M, Ge X, Sun M, Jayathilaka N, Kim YC, Emmanuel N, Bohlander SK, Minden M, Kline J, Ozer O, Larson RA, LeBeau MM, Green ED, Trent J, Karrison T, Liu PP, Wang SM, Rowley JD (2006) Gene expression profiles in acute myeloid leukemia with common translocations using SAGE. *Proceedings of the National Academy of Sciences U S A* **103:** 1030-1035

Ley TJ, Mardis ER, Ding L, Fulton B, McLellan MD, Chen K, Dooling D, Dunford-Shore BH, McGrath S, Hickenbotham M, Cook L, Abbott R, Larson DE, Koboldt DC, Pohl C, Smith S, Hawkins A, Abbott S, Locke D, Hillier LW, Miner T, Fulton L, Magrini V, Wylie T, Glasscock J, Conyers J, Sander N, Shi X, Osborne JR, Minx P, Gordon D, Chinwalla A, Zhao Y, Ries RE, Payton JE, Westervelt P, Tomasson MH, Watson M, Baty J, Ivanovich J, Heath S, Shannon WD, Nagarajan R, Walter MJ, Link DC, Graubert TA, DiPersio JF, Wilson RK (2008) DNA sequencing of a cytogenetically normal acute myeloid leukaemia genome. *Nature* **456:** 66-72

Li J, Sejas DP, Burma S, Chen DJ, Pang Q. (2007) Nucleophosmin suppresses oncogene-induced apoptosis and senescence and enhances oncogenic cooperation in cells with genomic instability. *Carcinogenesis* **6:** 1163-1170

Li J, Sejas DP, Rani R, Koretsky T, Bagby GC, Pang Q (2006) Nucleophosmin regulates cell cycle progression and stress response in hematopoietic stem/progenitor cells. *Journal of Biological Chemistry* **281:** 16536-16545

Li L, Monckton EA, Godbout R (2008) A role for DEAD box 1 at DNA double-strand breaks. *Molecular and Cellular Biology* **28:** 6413-6425

Liang XH, Fournier MJ (2006) The helicase Has1p is required for snoRNA release from pre-rRNA. *Molecular and Cellular Biology* **26:** 7437-7450

Liao EC, Paw BH, Peters LL, Zapata A, Pratt SJ, Do CP, Lieschke G, Zon LI (2000) Hereditary spherocytosis in zebrafish riesling illustrates evolution of erythroid beta-spectrin structure, and function in red cell morphogenesis and membrane stability. *Development* **127:** 5123-5132

Lieschke GJ, Oates AC, Paw BH, Thompson MA, Hall NE, Ward AC, Ho RK, Zon LI, Layton JE (2002) Zebrafish SPI-1 (PU.1) marks a site of myeloid development independent of primitive erythropoiesis: implications for axial patterning. *Developmental Biology* **246:** 274-295

Lin HF, Traver D, Zhu H, Dooley K, Paw BH, Zon LI, Handin RI (2005) Analysis of thrombocyte development in CD41-GFP transgenic zebrafish. *Blood* **106:** 3803-3810

Lin S, Gaiano N, Culp P, Burns JC, Friedmann T, Yee JK, Hopkins N (1994) Integration and germ-line transmission of a pseudotyped retroviral vector in zebrafish. *Science* **265:** 666-669

Lindqvist L, Oberer M, Reibarkh M, Cencic R, Bordeleau M-E, Vogt E, Marintchev A, Tanaka J, Fagotto F, Altmann M, Wagner G, Pelletier J (2008) Selective pharmacological targeting of a DEAD box RNA helicase. *PLoS ONE* **3:** e1583

Lipton JM, Atsidaftos E, Zyskind I, Vlachos A (2006) Improving clinical care and elucidating the pathophysiology of Diamond Blackfan anemia: an update from the Diamond Blackfan Anemia Registry. *Pediatric Blood Cancer* **46:** 558-564

Liu JM, Ellis SR (2006) Ribosomes and marrow failure: coincidental association or molecular paradigm? *Blood* **107:** 4583-4588

Lohrum M, Ludwig R, Kubbutat M, Hanlon M, Vousden K (2003) Regulation of HDM2 activity by the ribosomal protein L11. *Cancer cell* **3:** 577-587

Lord A, North T, Zon L (2007) Prostaglandin E2: making more of your marrow. *Cell Cycle* **6:** 3054-3057

Lu J, Guo S, Ebert BL, Zhang H, Peng X, Bosco J, Pretz J, Schlanger R, Wang JY, Mak RH, Dombkowski DM, Preffer FI, Scadden DT, Golub TR (2008) MicroRNA-mediated control of cell fate in megakaryocyte-erythrocyte progenitors. *Developmental Cell* **14:** 843-853

Lu PD, Harding HP, Ron D (2004) Translation reinitiation at alternative open reading frames regulates gene expression in an integrated stress response. *The Journal of Cell Biology* **167:** 27-33

Lyons SE, Lawson ND, Lei L, Bennett PE, Weinstein BM, Liu PP (2002) A nonsense mutation in zebrafish gata1 causes the bloodless phenotype in vlad tepes. *Proceedings of the National Academy of Science U S A* **99:** 5454-5459

Lyons SE, Shue BC, Lei L, Oates AC, Zon LI, Liu PP (2001) Molecular cloning, genetic mapping, and expression analysis of four zebrafish c/ebp genes. *Gene* **281:** 43-51

MacInnes A, Amsterdam A, Whittaker C, Hopkins N, Lees J (2008) Loss of p53 synthesis in zebrafish tumors with ribosomal protein gene mutations. *Proceedings of the National Academy of Science U S A* **105:** 10408-10413

Maeder M, Thibodeau-Beganny S, Sander J, Voytas D, Joung J (2009) Oligomerized pool engineering (OPEN): an 'open-source' protocol for making customized zinc-finger arrays. *Nature Protocols* **4:** 1471-1501

Mardis ER, Ding L, Dooling DJ, Larson DE, McLellan MD, Chen K, Koboldt DC, Fulton RS, Delehaunty KD, McGrath SD, Fulton LA, Locke DP, Magrini VJ, Abbott RM, Vickery TL, Reed JS, Robinson JS, Wylie T, Smith SM, Carmichael L, Eldred JM, Harris CC, Walker J, Peck JB, Du F, Dukes AF, Sanderson GE, Brummett AM, Clark E, McMichael JF, Meyer RJ, Schindler JK, Pohl CS, Wallis JW, Shi X, Lin L, Schmidt H, Tang Y, Haipek C, Wiechert ME, Ivy JV, Kalicki J, Elliott G, Ries RE, Payton JE, Westervelt P, Tomasson MH, Watson MA, Baty J, Heath S, Shannon WD, Nagarajan R, Link DC, Walter MJ, Graubert TA, DiPersio JF, Wilson RK, Ley TJ (2009) Recurring mutations found by sequencing an acute myeloid leukemia genome. *The New England Journal of Medicine* **361:** 1058-1066

Mathias JR, Dodd ME, Walters KB, Rhodes J, Kanki JP, Look AT, Huttenlocher A (2007) Live imaging of chronic inflammation caused by mutation of zebrafish Hai1. *Journal of Cell Science* **120:** 3372-3383

Mathias JR, Perrin BJ, Liu TX, Kanki J, Look AT, Huttenlocher A (2006) Resolution of inflammation by retrograde chemotaxis of neutrophils in transgenic zebrafish. *Journal of Leukocyte Biology* **80:** 1281-1288

McGowan K, Li J, Park C, Beaudry V, Tabor H, Sabnis A, Zhang W, Fuchs H, de Angelis M, Myers R, Attardi L, Barsh G (2008) Ribosomal mutations cause p53-mediated dark skin and pleiotropic effects. *Nature Genetics* **40:** 963-970

McKercher S, Torbett B, Anderson K, Henkel G, Vestal D, Baribault H, Klemsz M, Feeney A, Wu G, Paige C, Maki R (1996) Targeted disruption of the PU.1 gene results in multiple hematopoietic abnormalities. *EMBO Journal* **15:** 5647-5658

Meng X, Noyes MB, Zhu LJ, Lawson ND, Wolfe SA (2008) Targeted gene inactivation in zebrafish using engineered zinc-finger nucleases. *Nature Biotechnology* **26:** 695-701

Menne TF, Goyenechea B, Sanchez-Puig N, Wong CC, Tonkin LM, Ancliff PJ, Brost RL, Costanzo M, Boone C, Warren AJ (2007) The Shwachman-Bodian-Diamond syndrome protein mediates translational activation of ribosomes in yeast. *Nature Genetics* **39:** 486-495

Merlat A, Lai J, Sterkers Y, Demory J, Bauters F, Preudhomme C, Fenaux P (1999) Therapy-related myelodysplastic syndrome and acute myeloid leukemia with 17p deletion. A report on 25 cases. *Leukemia* **13:** 250-257

Moore P, Steitz T (2002) The involvement of RNA in ribosome function. *Nature* **418:** 229-235

Morris S, Kirstein M, Valentine M, Dittmer K, Shapiro D, Look A, Saltman D (1995) Fusion of a kinase gene, ALK, to a nucleolar protein gene, NPM, in non-Hodgkin's lymphoma. *Science* **267:** 316-317

Morris S, Kirstein M, Valentine M, Dittmer K, Shapiro D, Saltman D, Look A (1994) Fusion of a kinase gene, ALK, to a nucleolar protein gene, NPM, in non-Hodgkin's lymphoma. *Science* **263:** 1281-1284

Murayama E, Kissa K, Zapata A, Mordelet E, Briolat V, Lin HF, Handin RI, Herbomel P (2006) Tracing hematopoietic precursor migration to successive hematopoietic organs during zebrafish development. *Immunity* **25:** 963-975

Nallagatla S, Hwang J, Toroney R, Zheng X, Cameron C, Bevilacqua P (2007) 5'-triphosphate-dependent activation of PKR by RNAs with short stem-loops. *Science* **318:** 1455-1458

Nallagatla S, Toroney R, Bevilacqua P (2008) A brilliant disguise for self RNA: 5'-end and internal modifications of primary transcripts suppress elements of innate immunity. *RNA Biology* **5:** 140-144

Narla A, Ebert BL (2010) Ribosomopathies: human disorders of ribosome dysfunction. *Blood* **115:** 3196-3205

Neveling K, Bechtold A, Hoehn H (2007) Genetic instability syndromes with progeroid features. *Zeitschrift für Gerontologie und Geriatrie* **40:** 339-348

Niethammer P, Grabher C, Look AT, Mitchison TJ (2009) A tissue-scale gradient of hydrogen peroxide mediates rapid wound detection in zebrafish. *Nature* **459:** 996-999

Nissen P, Hansen J, Ban N, Moore P, Steitz T (2000) The structural basis of ribosome activity in peptide bond synthesis. *Science* **289:** 920-930

North TE, Goessling W, Walkley CR, Lengerke C, Kopani KR, Lord AM, Weber GJ, Bowman TV, Jang I-H, Grosser T, FitzGerald GA, Daley GQ, Orkin SH, Zon LI (2007) Prostaglandin E2 regulates vertebrate haematopoietic stem cell homeostasis. *Nature* **447:** 1007-1011

Nurse P, Masui Y, Hartwell L (1998) Understanding the cell cycle. *Nature Medicine* **4:** 1103-1106

Ofir-Rosenfeld Y, Boggs K, Michael D, Kastan M, Oren M (2008) Mdm2 regulates p53 mRNA translation through inhibitory interactions with ribosomal protein L26. *Molecular Cell* **32:** 180-189

Okuda M (2002) The role of nucleophosmin in centrosome duplication. *Oncogene* **21:** 6170-6174

Okuda M, Horn HF, Tarapore P, Tokuyama Y, Smulian AG, Chan PK, Knudsen ES, Hofmann IA, Snyder JD, Bove KE, Fukasawa K (2000) Nucleophosmin/B23 is a target of CDK2/cyclin E in centrosome duplication. *Cell* **103:** 127-140

Omodeo-Sale F, Cortelezzi L, Vommaro Z, Scaccabarozzi D, Dondorp A (2010) Dysregulation of L-arginine metabolism and bioavailability associated to free plasma heme. *American Journal of Physiology - Cell Physiology* **299:** c148-154

Orrù S, Aspesi A, Armiraglio M, Caterino M, Loreni F, Ruoppolo M, Santoro C, Dianzani I (2007) Analysis of the ribosomal protein S19 interactome. *Molecular and Cellular Proteomics* **6:** 382-393

Oyadomari S, Mori M (2003) Roles of CHOP//GADD153 in endoplasmic reticulum stress. *Cell Death and Differentiation* **11:** 381-389

Palade GE (1955) A small particulate component of the cytoplasm. *Journal of Biophysical and Biochemical Cytology* **1:** 59-68

Patton EE, Widlund HR, Kutok JL, Kopani KR, Amatruda JF, Murphey RD, Berghmans S, Mayhall EA, Traver D, Fletcher CD, Aster JC, Granter SR, Look AT, Lee C, Fisher DE, Zon LI (2005) BRAF mutations are sufficient to promote nevi formation and cooperate with p53 in the genesis of melanoma. *Current Biology* **15:** 249-254

Paw BH (2001) Cloning of the zebrafish retsina blood mutation: a genetic model for dyserythropoiesis and erythroid cytokinesis. *Blood Cells, Molecules and Diseases* **27:** 62-64

Paw BH, Davidson AJ, Zhou Y, Li R, Pratt SJ, Lee C, Trede NS, Brownlie A, Donovan A, Liao EC, Ziai JM, Drejer AH, Guo W, Kim CH, Gwynn B, Peters LL, Chernova MN, Alper

SL, Zapata A, Wickramasinghe SN, Lee MJ, Lux SE, Fritz A, Postlethwait JH, Zon LI (2003) Cell-specific mitotic defect and dyserythropoiesis associated with erythroid band 3 deficiency. *Nature Genetics* **34:** 59-64

Pellagatti A, Cazzola M, Giagounidis A, Perry J, Malcovati L, Della Porta MG, Jadersten M, Killick S, Verma A, Norbury CJ, Hellstrom-Lindberg E, Wainscoat JS, Boultwood J (2010a) Deregulated gene expression pathways in myelodysplastic syndrome hematopoietic stem cells. *Leukemia* **24:** 756-764

Pellagatti A, Hellstrom-Lindberg E, Giagounidis A, Perry J, Malcovati L, Della Porta MG, Jadersten M, Killick S, Fidler C, Cazzola M, Wainscoat JS, Boultwood J (2008) Haploinsufficiency of RPS14 in 5q- syndrome is associated with deregulation of ribosomal- and translation-related genes. *British Journal of Haematology* **142:** 57-64

Pellagatti A, Marafioti T, Paterson JC, Barlow JL, Drynan LF, Giagounidis A, Pileri SA, Cazzola M, McKenzie ANJ, Wainscoat JS, Boultwood J (2010b) Induction of p53 and up-regulation of the p53 pathway in the human 5q- syndrome. *Blood* **115:** 2721-2723

Perdahl E, Naprstek B, Wallace W, Lipton J (1994) Erythroid failure in Diamond-Blackfan anemia is characterized by apoptosis. *Blood* **83:** 645-650

Poppe B, Vandesompele J, Schoch C, Lindvall C, Mrozek K, Bloomfield CD, Beverloo HB, Michaux L, Dastugue N, Herens C, Yigit N, De Paepe A, Hagemeijer A, Speleman F (2004) Expression analyses identify MLL as a prominent target of 11q23 amplification and support an etiologic role for MLL gain of function in myeloid malignancies. *Blood* **103:** 229-235

Pospisilova D, Cmejlova J, Hak J, Adam T, Cmejla R (2007) Successful treatment of a Diamond-Blackfan anemia patient with amino acid leucine. *Haematologica* **92:** e66-67

Prakash K, Tuteja R (2010) A novel DEAD box helicase Has1p from Plasmodium falciparum: N-terminal is essential for activity. *Parasitology International* **59:** 271-277

Quigley JG, Yang Z, Worthington MT, Phillips JD, Sabo KM, Sabath DE, Berg CL, Sassa S, Wood BL, Abkowitz JL (2004) Identification of a human Heme exporter that Is essential for erythropoiesis. *Cell* **118:** 757-766

Raaijmakers MHGP, Mukherjee S, Guo S, Zhang S, Kobayashi T, Schoonmaker JA, Ebert BL, Al-Shahrour F, Hasserjian RP, Scadden EO, Aung Z, Matza M, Merkenschlager M, Lin C, Rommens JM, Scadden DT (2010) Bone progenitor dysfunction induces myelodysplasia and secondary leukaemia. *Nature* **464:** 852-857

Raine DA, Jeffrey IW, Clemens MJ (1998) Inhibition of the double-stranded RNA-dependent protein kinase PKR by mammalian ribosomes. *FEBS Letters* **436:** 343-348

Ramenghi U, Garelli E, Valtolina S, Campagnoli MF, Timeus F, Crescenzio N, Mair M, Varotto S, D'Avanzo M, Nobili B, Massolo F, Mori PG, Locatelli F, Gustavsson P, Dahl N, Dianzani I (1999) Diamond-Blackfan anaemia in the Italian population. *British Journal of Haematology* **104:** 841-848

Ramensky V, Bork P, Sunyaev S (2002) Human non-synonymous SNPs: server and survey. *Nucleic Acids Research* **30:** 3894-3900

Ransom DG, Haffter P, Odenthal J, Brownlie A, Vogelsang E, Kelsh RN, Brand M, van Eeden FJ, Furutani-Seiki M, Granato M, Hammerschmidt M, Heisenberg CP, Jiang YJ, Kane DA, Mullins MC, Nusslein-Volhard C (1996) Characterization of zebrafish mutants with defects in embryonic hematopoiesis. *Development* **123:** 311-319

Redner RL, Rush EA, Faas S, Rudert WA, Corey SJ (1996) The t(5;17) variant of acute promyelocytic leukemia expresses a nucleophosmin-retinoic acid receptor fusion. *Blood* **87:** 882-886

Renshaw SA, Loynes CA, Trushell DM, Elworthy S, Ingham PW, Whyte MK (2006) A transgenic zebrafish model of neutrophilic inflammation. *Blood* **108:** 3976-3978

Rentzsch F, Bakkers J, Kramer C, Hammerschmidt M (2004) Fgf signaling induces posterior neuroectoderm independently of Bmp signaling inhibition. *Developmental Dynamics* **231:** 750-757

Rentzsch F, Kramer C, Hammerschmidt M (2003) Specific and conserved roles of TAp73 during zebrafish development. *Gene* **323:** 19-30

Rey MA, Duffy SP, Brown JK, Kennedy JA, Dick JE, Dror Y, Tailor CS (2008) Enhanced alternative splicing of the FLVCR1 gene in Diamond Blackfan anemia disrupts FLVCR1 expression and function that are critical for erythropoiesis. *Haematologica* **93:** 1617-1626

Rhodes J, Amsterdam A, Sanda T, Moreau L, McKenna K, Heinrichs S, Ganem N, Ho K, Neuberg D, Johnston A, Ahn Y, Kutok J, Hromas R, Wray J, Lee C, Murphy C, Radtke I, Downing J, Fleming M, MacConaill L, Amatruda J, Gutierrez A, Galinsky I, Stone R, Ross E, Pellman D, Kanki J, Look A (2009) Emi1 maintains genomic integrity during zebrafish embryogenesis and cooperates with p53 in tumor suppression. *Molecular and Cellular Biology* **29:** 5911-5922

Rhodes J, Hagen A, Hsu K, Deng M, Liu TX, Look AT, Kanki JP (2005) Interplay of pu.1 and gata1 determines myelo-erythroid progenitor cell fate in zebrafish. *Developmental Cell* **8:** 97-108

Ribeil JA, Zermati Y, Vandekerckhove J, Cathelin S, Kersual J, Dussiot M, Coulon S, Moura IC, Zeuner A, Kirkegaard-Sorensen T, Varet B, Solary E, Garrido C, Hermine O (2007) Hsp70 regulates erythropoiesis by preventing caspase-3-mediated cleavage of GATA-1. *Nature* **445:** 102-105

Ridanpaa M, van Eenennaam H, Pelin K, Chadwick R, Johnson C, Yuan B, vanVenrooij W, Pruijn G, Salmela R, Rockas S, Makitie O, Kaitila I, de la Chapelle A (2001) Mutations in the RNA component of RNase MRP cause a pleiotropic human disease, cartilage-hair hypoplasia. *Cell* **104:** 195-203

Robb L, Lyons I, Li R, Hartley L, Köntgen F, Harvey R, Metcalf D, Begley C (1995) Absence of yolk sac hematopoiesis from mice with a targeted disruption of the scl gene. *Proceedings of the National Academy of Science U S A* **92:** 7075-7079

Robu ME, Larson JD, Nasevicius A, Beiraghi S, Brenner C, Farber SA, Ekker SC (2007) p53 Activation by knockdown technologies. *PLoS Genetics* **3:** e78

Rocak S, Emery B, Tanner NK, Linder P (2005) Characterization of the ATPase and unwinding activities of the yeast DEAD-box protein Has1p and the analysis of the roles of the conserved motifs. *Nucleic Acids Research* **33:** 999-1009

Rubbi CP, Milner J (2003) Disruption of the nucleolus mediates stabilization of p53 in response to DNA damage and other stresses. *EMBO Journal* **22:** 6068-6077

Ruggero D, Grisendi S, Piazza F, Rego E, Mari F, Rao PH, Cordon-Cardo C, Pandolfi PP (2003) Dyskeratosis congenita and cancer in mice deficient in ribosomal RNA modification. *Science* **299:** 259-262

Samuels BL, Larson RA, Le Beau MM, Daly KM, Bitter MA, Vardiman JW, Barker CM, Rowley JD, Golomb HM (1988) Specific chromosomal abnormalities in acute nonlymphocytic leukemia correlate with drug susceptibility in vivo. *Leukemia* **2:** 79-83

Savkur R, Olson M (1998) Preferential cleavage in pre-ribosomal RNA byprotein B23 endoribonuclease. *Nucleic Acids Research* **26:** 4508-4515

Scott E, Simon M, Anastasi J, Singh H (1994) Requirement of transcription factor PU.1 in the development of multiple hematopoietic lineages. *Science* **265:** 1573-1577

Sekiguchi T, Hayano T, Yanagida M, Takahashi N, Nishimoto T (2006) NOP132 is required for proper nucleolus localization of DEAD-box RNA helicase DDX47. *Nucleic Acids Research* **34:** 4593-4608

Sengoku T, Nureki O, Nakamura A, Kobayashi S, Yokoyama S (2006) Structural basis for RNA unwinding by the DEAD-box protein Drosophila Vasa. *Cell* **125:** 287-300

Shafizadeh E, Paw BH, Foott H, Liao EC, Barut BA, Cope JJ, Zon LI, Lin S (2002) Characterization of zebrafish merlot/chablis as non-mammalian vertebrate models for severe congenital anemia due to protein 4.1 deficiency. *Development* **129:** 4359-4370

Shaw GC, Cope JJ, Li L, Corson K, Hersey C, Ackermann GE, Gwynn B, Lambert AJ, Wingert RA, Traver D, Trede NS, Barut BA, Zhou Y, Minet E, Donovan A, Brownlie A, Balzan R, Weiss MJ, Peters LL, Kaplan J, Zon LI, Paw BH (2006) Mitoferrin is essential for erythroid iron assimilation. *Nature* **440:** 96-100

Sidi S, Sanda T, Kennedy RD, Hagen AT, Jette CA, Hoffmans R, Pascual J, Imamura S, Kishi S, Amatruda JF, Kanki JP, Green DR, D'Andrea AA, Look AT (2008) Chk1 suppresses a caspase-2 apoptotic response to DNA damage that bypasses p53, Bcl-2, and caspase-3. *Cell* **133:** 864-877

Singleton MR, Dillingham MS, Wigley DB (2007) Structure and mechanism of helicases and nucleic acid translocases. *Annual Reviews Biochemistry* **76:** 23-50

Sobeck A, Stone S, Landais I, de Graaf B, Hoatlin ME (2009) The Fanconi anemia protein FANCM is controlled by FANCD2 and the ATR/ATM pathways. *Journal of Biological Chemistry* **284:** 25560-25568

Sood R, English MA, Belele CL, Jin H, Bishop K, Haskins R, McKinney MC, Chahal J, Weinstein BM, Wen Z, Liu PP (2010) Development of multi-lineage adult hematopoiesis in the zebrafish with a runx1 truncation mutation. *Blood* **115:** 2806-2809

Sportoletti P, Grisendi S, Majid SM, Cheng K, Clohessy JG, Viale A, Teruya-Feldstein J, Pandolfi PP (2008) Npm1 is a haploinsufficient suppressor of myeloid and lymphoid malignancies in the mouse. *Blood* **111:** 3859-3862

Sridhar K, Ross D, Tibshirani R, Butte A, Greenberg P (2009) Relationship of differential gene expression profiles in CD34+ myelodysplastic syndrome marrow cells to disease subtype and progression. *Blood* **114:** 4847-4858

Stachura DL, Reyes JR, Bartunek P, Paw BH, Zon LI, Traver D (2009) Zebrafish kidney stromal cell lines support multilineage hematopoiesis. *Blood* **114:** 279-289

Stainier DY, Fouquet B, Chen JN, Warren KS, Weinstein BM, Meiler SE, Mohideen MA, Neuhauss SC, Solnica-Krezel L, Schier AF, Zwartkruis F, Stemple DL, Malicki J, Driever W, Fishman MC (1996) Mutations affecting the formation and function of the cardiovascular system in the zebrafish embryo. *Development* **123:** 285-292

Stainier DY, Lee RK, Fishman MC (1993) Cardiovascular development in the zebrafish. I. Myocardial fate map and heart tube formation. *Development* **119:** 31-40

Stainier DY, Weinstein BM, Detrich HW, 3rd, Zon LI, Fishman MC (1995) Cloche, an early acting zebrafish gene, is required by both the endothelial and hematopoietic lineages. *Development* **121:** 3141-3150

Stockhammer OW, Zakrzewska A, Hegedus Z, Spaink HP, Meijer AH (2009) Transcriptome profiling and functional analyses of the zebrafish embryonic innate immune response to Salmonella infection. *Journal of Immunology* **182:** 5641-5653

Streisinger G (1984) Attainment of minimal biological variability and measurements of genotoxicity: production of homozygous diploid zebra fish. *National Cancer Institute Monographs* **65:** 53-58

Sunyaev S, Kuznetsov E, Rodchenkov I, Tumanyan V (1997) Protein sequence-structure compatibility criteria in terms of statistical hypothesis testing. *Protein Engineering* **10:** 635-646

Sznajer Y, Baumann C, David A, Journel H, Lacombe D, Perel Y, Blouin P, Segura JF, Cezard JP, Peuchmaur M, Vulliamy T, Dokal I, Verloes A (2003) Further delineation of the congenital form of X-linked dyskeratosis congenita (Hoyeraal-Hreidarsson syndrome). *European Journal of Pediatrics* **162:** 863-867

Theissen B, Karow A, Köhler J, Gubaev A, Klostermeier D (2008) Cooperative binding of ATP and RNA induces a closed conformation in a DEAD box RNA helicase. *Proceedings of the National Academy of Sciences U S A* **105:** 548-553

Thompson MA, Ransom DG, Pratt SJ, MacLennan H, Kieran MW, Detrich HW, 3rd, Vail B, Huber TL, Paw B, Brownlie AJ, Oates AC, Fritz A, Gates MA, Amores A, Bahary N, Talbot WS, Her H, Beier DR, Postlethwait JH, Zon LI (1998) The cloche and spadetail genes differentially affect hematopoiesis and vasculogenesis. *Developmental Biology* **197:** 248-269

Traver D, Paw BH, Poss KD, Penberthy WT, Lin S, Zon LI (2003) Transplantation and in vivo imaging of multilineage engraftment in zebrafish bloodless mutants. *Nature Immunology* **4:** 1238-1246

Tutois S, Montagutelli X, Da Silva V, Jouault H, Rouyer-Fessard P, Leroy-Viard K, Guénet JL, Nordmann Y, Beuzard Y, Deybach JC (1991) Erythropoietic protoporphyria in the house mouse. A recessive inherited ferrochelatase deficiency with anemia, photosensitivity, and liver disease. *The Journal of Clinical Investigation* **88:** 1730-1736

Uechi T, Nakajima Y, Chakraborty A, Torihara H, Higa S, Kenmochi N (2008) Deficiency of ribosomal protein S19 during early embryogenesis leads to reduction of erythrocytes in a zebrafish model of Diamond-Blackfan anemia. *Human Molecular Genetics* **17:** 3204-3211

Uhlmann-Schiffler H, Kiermayer S, Stahl H (2009) The DEAD box protein Ddx42p modulates the function of ASPP2, a stimulator of apoptosis. *Oncogene* **28:** 2065-2073

Valencia A, Cervera J, Such E, Sanz MA, Sanz GF (2008) Lack of RPS14 promoter aberrant methylation supports the haploinsufficiency model for the 5q- syndrome. *Blood* **112:** 918

Van den Berghe H, Michaux L (1997) 5q-, twenty-five years later: a synopsis. *Cancer Genetics and Cytogenetics* **94:** 1-7

van der Sar AM, Spaink HP, Zakrzewska A, Bitter W, Meijer AH (2009) Specificity of the zebrafish host transcriptome response to acute and chronic mycobacterial infection and the role of innate and adaptive immune components. *Molecular Immunology* **46:** 2317-2332

van Riggelen J, Yetil A, Felsher DW (2010) MYC as a regulator of ribosome biogenesis and protein synthesis. *Nature Reviews Cancer* **10:** 301-309

van Rooijen E, Voest EE, Logister I, Korving J, Schwerte T, Schulte-Merker S, Giles RH, van Eeden FJ (2009) Zebrafish mutants in the von Hippel-Lindau tumor suppressor

display a hypoxic response and recapitulate key aspects of Chuvash polycythemia. *Blood* **113:** 6449-6460

Vardiman JW (2010) The World Health Organization (WHO) classification of tumors of the hematopoietic and lymphoid tissues: An overview with emphasis on the myeloid neoplasms. *Chemico-Biological Interactions* **184:** 16-20

Vattem K, Wek R (2004) Reinitiation involving upstream ORFs regulates ATF4 mRNA translation in mammalian cells. *Proceedings of the National Academy of Science U S A* **101:** 11269-11274

Vlachos A, Ball S, Dahl N, Alter BP, Sheth S, Ramenghi U, Meerpohl J, Karlsson S, Liu JM, Leblanc T, Paley C, Kang EM, Leder EJ, Atsidaftos E, Shimamura A, Bessler M, Glader B, Lipton JM, on behalf of the participants of the Sixth Annual Daniella Maria Arturi International Consensus C (2008) Diagnosing and treating Diamond Blackfan anaemia: results of an international clinical consensus conference. *British Journal of Haematology* **142:** 859-876

Vogt A, Cholewinski A, Shen X, Nelson S, Lazo J, Tsang M, Hukriede N (2009) Automated image-based phenotypic analysis in zebrafish embryos. *Developmental Dynamics* **238:** 656-663

Walne AJ, Dokal I (2009) Advances in the understanding of dyskeratosis congenita. *British Journal of Haematology* **145:** 164-172

Wang W, Budhu A, Forgues M, Wang XW (2005) Temporal and spatial control of nucleophosmin by the Ran-Crm1 complex in centrosome duplication. *Nature Cell Biology* **7:** 823-830

Warga R, Kane D, Ho R (2009a) Fate mapping embryonic blood in zebrafish: multi- and unipotential lineages are segregated at gastrulation. *Developmental Cell* **16:** 744-755

Warga RM, Kane DA, Ho RK (2009b) Fate mapping embryonic blood in zebrafish: multi- and unipotential lineages are segregated at gastrulation. *Developmental Cell* **16:** 744-755

Weinstein BM, Schier AF, Abdelilah S, Malicki J, Solnica-Krezel L, Stemple DL, Stainier DY, Zwartkruis F, Driever W, Fishman MC (1996) Hematopoietic mutations in the zebrafish. *Development* **123:** 303-309

Westerfield M (2000) *The zebrafish book. A guide for the laboratory use of zebrafish (Danio rerio)*, 4th edition. The University of Oregon Press.

Willett CE, Cortes A, Zuasti A, Zapata AG (1999) Early hematopoiesis and developing lymphoid organs in the zebrafish. *Developmental Dynamics* **214:** 323-336

Willig TN, Niemeyer CM, Leblanc T, Tiemann C, Robert A, Budde J, Lambiliotte A, Kohne E, Souillet G, Eber S, Stephan JL, Girot R, Bordigoni P, Cornu G, Blanche S,

Guillard JM, Mohandas N, Tchernia G (1999) Identification of new prognosis factors from the clinical and epidemiologic analysis of a registry of 229 Diamond-Blackfan anemia patients. DBA group of Societe d'Hematologie et d'Immunologie Pediatrique (SHIP), Gesellshaft fur Padiatrische Onkologie und Hamatologie (GPOH), and the European Society for Pediatric Hematology and Immunology (ESPHI). *Pediatr Res* **46:** 553-561

Willman CL, Sever CE, Pallavicini MG, Harada H, Tanaka N, Slovak ML, Yamamoto H, Harada K, Meeker TC, List AF and Tadatsugu Taniguchi. (1993) Deletion of IRF-1, mapping to chromosome 5q31.1, in human leukemia and preleukemic myelodysplasia. *Science* **259:** 968-971

Wise C, Chiang L, Paznekas W, Sharma M, Musy M, Ashley J, Lovett M, Jabs E (1997) TCOF1 gene encodes a putative nucleolar phosphoprotein that exhibits mutations in Treacher Collins Syndrome throughout its coding region. *Proceedings of the National Academy of Science U S A* **94:** 3110-3115

Wong JM, Collins K (2006) Telomerase RNA level limits telomere maintenance in X-linked dyskeratosis congenita. *Genes and Development* **20:** 2848-2858

Wu MH, Yung BY (2002) UV stimulation of nucleophosmin/B23 expression is an immediate-early gene response induced by damaged DNA. *Journal of Biological Chemistry* **277:** 48234-48240

Xie D, Hofmann WK, Mori N, Miller CW, Hoelzer D, Koeffler HP (2000) Allelotype analysis of the myelodysplastic syndrome. *Leukemia* **14:** 805-810

Yeh JR, Munson KM, Elagib KE, Goldfarb AN, Sweetser DA, Peterson RT (2009) Discovering chemical modifiers of oncogene-regulated hematopoietic differentiation. *Nature Chemical Biology* **5:** 236-243

Yerlikaya A, Kimball S, Stanley B (2008) Phosphorylation of eIF2alpha in response to 26S proteasome inhibition is mediated by the haem-regulated inhibitor (HRI) kinase. *Biochemistry Journal* **412:** 579-588

Yi CH, Yuan J (2009) The Jekyll and Hyde functions of caspases. *Developmental Cell* **16:** 21-34

Yoneda-Kato N, Look AT, Kirstein MN, Valentine MB, Raimondi SC, Cohen KJ, Carroll AJ, Morris SW (1996) The t(3;5)(q25.1;q34) of myelodysplastic syndrome and acute myeloid leukemia produces a novel fusion gene, NPM-MLF1. *Oncogene* **12:** 265-275

Yoon A, Peng G, Brandenburger Y, Zollo O, Xu W, Rego E, Ruggero D (2006) Impaired control of IRES-mediated translation in X-linked dyskeratosis congenita. *Science* **312:** 902-906

Yoon C-H, Lee E-S, Lim D-S, Bae Y-S (2009) PKR, a p53 target gene, plays a crucial role in the tumor-suppressor function of p53. *Proceedings of the National Academy of Sciences U S A* **106:** 7852-7857

Yung B, Chan P (1987) Identification and characterization of a hexameric form of nucleolar phosphoprotein B23. *Biochimistre Biophysica Acta* **925:** 74-82

Zaffran S, Chartier A, Gallant P, Astier M, Arquier N, Doherty D, Gratecos D, Sémériva M (1998) A Drosophila RNA helicase gene, pitchoune, is required for cell growth and proliferation and is a potential target of d-Myc. *Development* **125:** 3571-3584

Zhang DE, Zhang P, Wang ND, Hetherington CJ, Darlington GJ, Tenen DG (1997) Absence of granulocyte colony-stimulating factor signaling and neutrophil development in CCAAT enhancer binding protein alpha-deficient mice. *Proceedings of the National Academy of Sciences U S A* **94:** 569-574

Zhao N, Stoffel A, Wang PW, Eisenbart JD, Espinosa R, 3rd, Larson RA, Le Beau MM (1997) Molecular delineation of the smallest commonly deleted region of chromosome 5 in malignant myeloid diseases to 1-1.5 Mb and preparation of a PAC-based physical map. *Proceedings of the National Academy of Sciences U S A* **94:** 6948-6953

Zhu Y, Poyurovsky MV, Li Y, Biderman L, Stahl J, Jacq X, Prives C (2009) Ribosomal protein S7 Is both a regulator and a substrate of MDM2. *Molecular Cell* **35:** 316-326

Appendix 1 – Morpholinos sequences

npm1a ATG/5'UTR   TAATGTTATCCTC**CAT**TTTTGCGCG

npm1a ATG/5'UTR   TAATcTTATCgTC**gAT**TTTaGCcCG (5bp mm)

npm1a E2-I2   AAGAAACATCACATACCATTCTAAC

npm1a E3-I3   TTATGACCAAGTCTACTTACACTTG

npm1b ATG/5'UTR   GACCCATCTGTTCGAGATC**CAT**GTC

npm1b ATG/5'UTR   GAgCCATgTGTTCGAcATC**gAT**cTC (5bp mm)

npm1b E2-I2   TCAAATATTCATCTTCCTCACCGAC

p53 ATG/5'UTR   GCGC**CAT**TGCTTTGCAAGAATTG

std control   CCTCTTACCTCAGTTACAATTTATA <small>(targets human beta globin intronic mutation)</small>

ddx18 E1-I1   CAACGTAAATACATTACCTTCGCTG

ddx18 E2-I2   AGCATCATTAAACACTCACTGGATG

ddx18 ATG/5'UTR   GAATCTT**CAT**CTGCATGTCCGCCAT

ddx18 5bp mismatch   GAATgTT**gAT**CTcCATcTCCGGCAT

rps19 splice   AAACATGAAAAACTCACCAGCTCTG

rps19 atg   CACTGTTACACCACCTGG**CAT**CTTG

rps14 E2-I2   CAGGTTTTCAGGATACATACTTGCC

chop Splice MO   CGATTCCAGACGCTACTGACCTCTG

p63 Splice MO   AAAGAGTGGCATACCGTCATTGAAC

p73 5'UTR MO   GGATGTTGGACAATCCACCGCAGGG

Appendix 2 – Oligonucleotide sequences

zebrafish beta actin

forward: 5'-CTGGTCGTTGACAACGGCT-3'

reverse: 5'-TCCATCACAATACCAGTAGT-3'

ddx18^{*hi1727*} genotyping

ddx18 forward: 5'-GCGGACATGCAGATGAAGAT-3'

reverse viral (nltr3):   5'- CTGTTCCATCTGTTCCTGAC-3'

reverse WT allele: 5'-CATTAAATCACACATAGCCACGA-3'

zebrafish *ddx18* cloning

forward: 5'-CGC**GGATCC**CATGGCGGACATGCAGAT-3'

reverse: 5'-CCG**CTCGAG**CGGACTGATCAGAGCTCCTC

sequencing primers: 5'-CGTGCTGAAGGAGTTGATGA-3'

                    5'-GTTCCCCTGAGTGAGTGAGTTTGAATTCTCC-3'

human *DDX18* cloning

forward: 5'-CG**GGATCC**TGTTGGGCAGAATGTCACAC-3'

reverse: 5'-A**CTCGAG**AAGGAAGGCATGTGTTCAGTG-3'

sequencing primer: 5'-TCCTCTTCAAACCCCACATC-3'

                 5'-GCTTGATAATGGGTGGCAGT-3'

Human *DDX18* PCR cloning from pCMVSport-6 (open biosystems)

Forward: 5'-GGCACTTGTTGGGCAG**GAATTC**ACACCTGCCG-3'

Reverse: 5'-GCAGGCAGTTCTCTCACTGAACACATG**GGATCC**TTTC-3'

human site directed mutagenesis

hsDDX18_g548a: 5'-GGATACTTCGTTTGCTTCTCTATATAATCTTGTCAATGA AAACACTC-3'

hsDDX18_g548a-r: 5'-AGTGTTTTCATTGACAAGATTATATAGAGAAGCAAAC GAAGTATCC-3'

hsDDX18_g1111a: 5'–GCCACCCAAACTCGAAAAATTGAAGACCTGGCAA-3'

hsDDX18_g1111a-r: 5'-TTGCCAGGTCTTCAATTTTTCGAGTTTGGGTGGC-3'

hsDDX18_g1861a: 5'-TCAAGGTGCCTCCCTTCATTGATCTGAACGTCAAC-3'

hsDDX18_g1861a-r:5'–GTTGACGTTCAGATCAATGAAGGGAGGCACCTTGA-3'

zebrafish *ddx18* short probe

forward: 5'-GGCTATTCATGGGAAGCAGA-3'
reverse: 5'-TGTAGGCCTCCTGAGCTGAT-3'

zebrafish *npm1a* cloning and morphotyping

forward: 5'-G**GGATCC**CGCTTCCTGCACTCGTGTTCGCTGAC-3'
reverse: 5'-GC**TCTAGA**GCGGCCATTCTGAAACCCACTATTC-3'

zebrafish *npm1b* cloning (and morphotyping)

forward: 5'-CG**GGATCC**GCGCAAAATGGAGGATAAC-3'
reverse: 5'-A**CTCGAG**CGCAGACTTCTGCTGCACT-3'

zebrafish *rps14* cloning (and morphotyping)

forward: 5'-G**GAATTC**CCACACATAGCAATGGCTCCT-3'
reverse: 5'-GC**TCTAGA**GCGACACTTTATTCTGAAAAATATCCAA-3'

zebrafish *rps19* cloning

forward: 5'- CG**GGATCC**CAAGATGCCAGGTGGTGTAA-3'

reverse: 5'-A**CTCGAG**CTGGTTTCCAACAAAAGTTTATTTTAC-3'

zebrafish *p63* morphotyping

forward: 5'-CTACAACAACGATCATGCTCAAAAC-3'

reverse: 5-AGTAATGGAATCCTCCACGTATT-3'

zebrafish *xbp1* alternate splicing
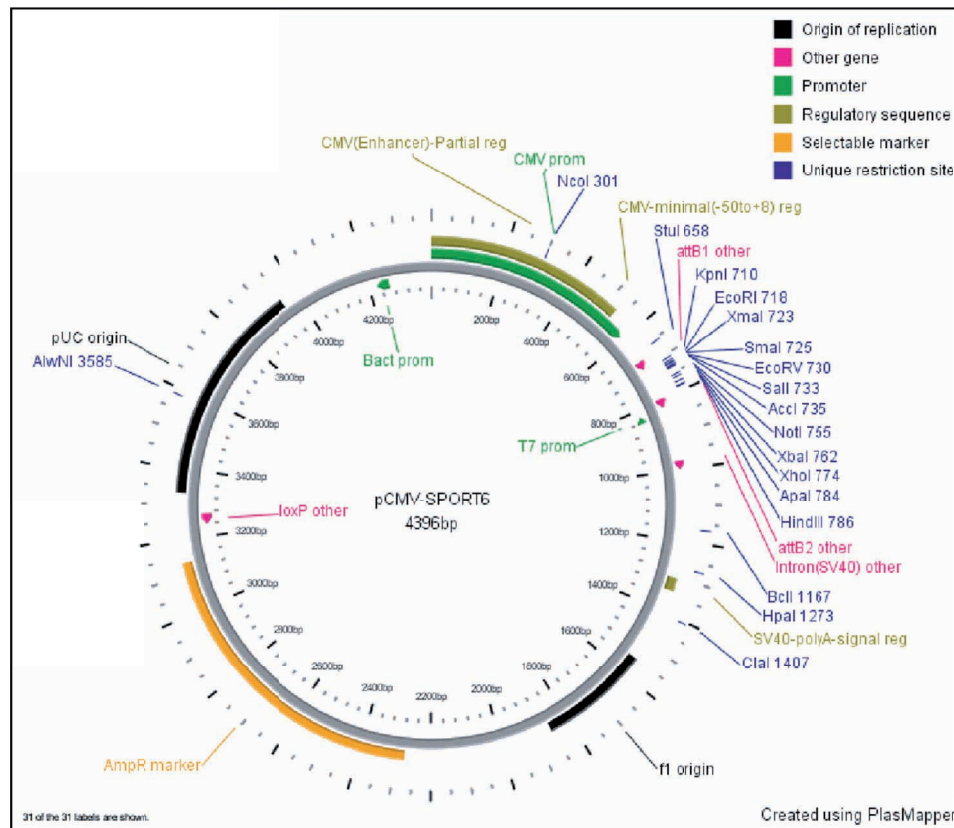
forward: 5'-CCTTGGAAACAAAGGAGCAG-3'

reverse: 5'- CCAGGGCTGTGAGTATCCAT-3

** bold underlined text denotes restriction enzyme linkers added to the sequence.

Appendix 3 – Plasmid maps and sequences

Clone: pCMV-SPORT6 Human *DDX18*

Source: Open Biosystems

Product Page(click to open)
Catalog Number   MHS1010-57628
Clone Id   3452935
Cluster   Hs.363492
Description   Human MGC Verified FL cDNA (IRAT)
Detailed Description   NIH_MGC_10
Accessions   BC001238,BC001238.1,BE541297,BE541297.1
Host Strain   DH10B
Tissuechoriocarcinoma
Species   Homo sapiens
Location   3-b-2
3' Restriction Site   NotI
5' Restriction Site   SalI
Vector NamepCMV-SPORT6
Vector Type   Mammalian Expression
Antibiotic Information   Ampicillin (Concentration: 100 µg/ml, Resistant Range: 50-200 µg/ml)
Sequencing Primerssp6, T7, -21M13, M13 reverse
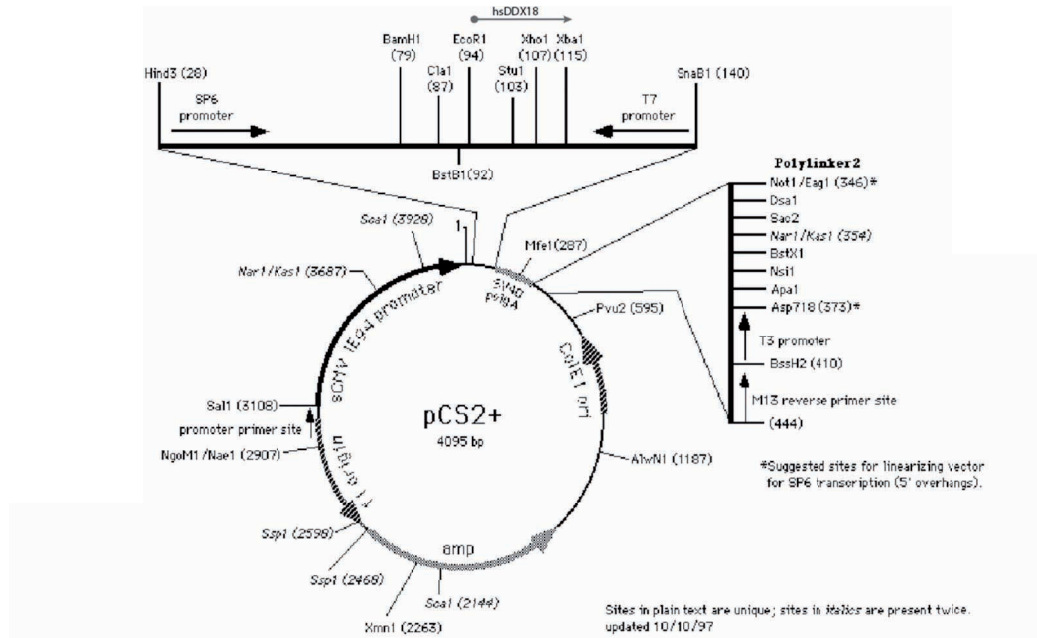Vector Name   pCMV-SPORT6
Vector Type Mammalian Expression
Antibiotic Information   Ampicillin (Concentration: 100 µg/ml, Resistant Range: 50-200 µg/ml)
Sequencing Primers   sp6, T7, -21M13, M13 reverse

Clone: pCS2-Human *DDX18*

Source: Open Biosystems subcloned by Elspeth Payne

Subcloned from pCMVSport-6 using restriction digest with EcoR1 and Xba1

Verified by sequencing :

```
atgtcacacctgccgatgaaactcctgcgtaagaagatcgagaagcggaacctcaaattgcggcagcggaacctaaagtt
tcaggggggcctcaaatctgaccctatcggaaactcaaaatggagatgtatctgaagaaacaatgggaagtagaaaggtta
aaaaatcaaaacaaaagcccatgaatgtgggcttatcagaaactcaaaatggaggcatgtctcaagaagcagtgggaaat
ataaaagttacaaagtctccccagaaatccactgtattaagcaatggagaagcagcaatgcagtcttccaattcagaatc
aaaaaagaaaaagaagaaaaagagaaaaatggtgaatgatgctgagcctgatacgaaaaaagcaaaaactgaaaacaaag
ggaaatctgaagaagaaagtgccgagactactaaagaaacagaaataatgtggagaagccagataatgatgaagatgag
agtgaggtgcccagtctgcccctgggactgacaggagcttttgaggatacttcgtttgcttctctatgtaatcttgtcaa
tgaaaacactctgaaggcaataaaagaaatgggttttacaaacatgactgaaattcagcataaaagtatcagaccacttc
tggaaggcagggatcttctagcagctgcaaaaacaggcagtggtaaaaccctggcttttctcatccctgcagttgaactc
attgttaagttaaggttcatgcccaggaatggaacaggagtccttattctctcacctactagagaactagccatgcaaac
ctttggtgttcttaaggagctgatgactcaccacgtgcatacctatggcttgataatgggtggcagtaacagatctgctg
aagcacagaaacttggtaatgggatcaacatcattgtggccacaccaggccgtctgctggaccatatgcagaataccca
ggatttatgtataaaaacctgcagtgtctggttattgatgaagctgatcgtatcttggatgtggggtttgaagaggaatt
aaagcaaattattaaacttttgccaacacgtagacagactatgctctttctgccacccaaactcgaaaagttgaagacc
tggcaaggatttctctgaaaaaggagccattgtatgttggcgttgatgatgataaagcgaatgcaacagtggatggtctt
gaacagggatatgttgtttgtccttctgaaaagagattccttctgctctttacattccttaagaagaaccgaaagaagaa
gcttatggtcttcttttcatcttgtatgtctgtgaaataccactatgagttgctgaactacattgatttgcccgtcttgg
ccattcatggaaagcaaaagcaaaataagcgtacaaccacattcttccagttctgcaatgcagattcgggaacactattg
tgtacggatgtggcagcgagaggactagacattcctgaagtcgactggattgttcagtatgaccctccggatgaccctaa
ggaatatattcatcgtgtgggtagaacagccagaggcctaaatgggagagggcatgccttgctcattttgcgcccagaag
aattgggttttcttcgctacttgaaacaatccaaggttccattaagtgaatttgacttttcctggtctaaaatttctgac
attcagtctcagcttgagaaattgattgaaaagaattactttcttcataagtcagcccaggaagcatataagtcatacat
acgagcctatgattcccattctctgaaacagatctttaatgttaataacctaaatttgcctcaggttgctctgtcatttg
gtttcaaggtgcctcccttcgttgatctgaacgtcaacagtaatgaaggcaagcagaaaaagcgaggaggtggtggtgga
tttggctaccagaaaaccaagaaagttgagaaatccaaaatctttaaacacattagcaagaaatcatctgacagcaggca
gttctctcactgaacacatgccttcctttcatcttgaataactttgtcctaa
```

Adds 5' Xma1, Sma1, EcoRV into pCS2;

3' Not1 (retained from original cloning); Linearise with ApaI /Transcribe with Sp6

Clone: pCRII zebrafish ddx18 short probe

Source:TA cloned from PCR product derived from 30hpf cDNA
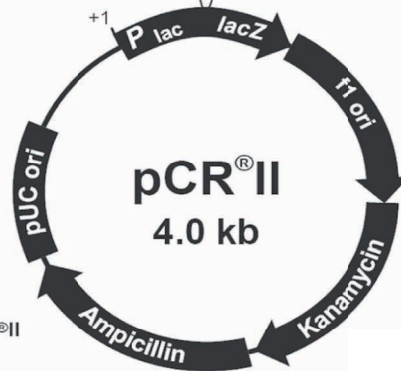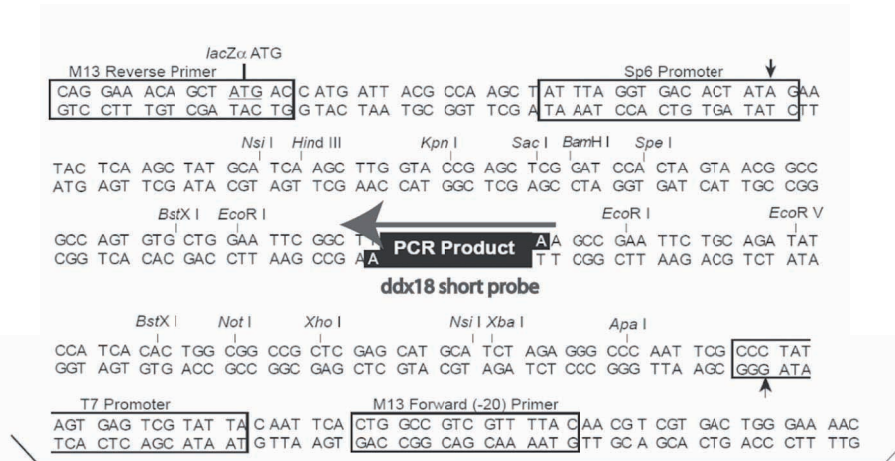
Comments for pCR®II
3971 nucleotides

LacZα gene: bases 1-587
M13 Reverse priming site: bases 205-221
Sp6 promoter: bases 239-256
T7 promoter: bases 404-423
M13 (-20) Forward priming site: bases 431-446
f1 origin: bases 588-1025
Kanamycin resistance ORF: bases 1359-2153
Ampicillin resistance ORF: bases 2171-3031
pUC origin: bases 3176-3849

size - 404bp
sequence

gggaagcagaaacagacaaagagaaccacaacgtttttccagttctgtaatgcagattctggcattctcctctgtacgga
tgtggctgccagaggtttggatatccccgaagtagactggattgttcagtttgacccacctgatgatcctaaggagtaca
tccatcgtgttggacgaacagctcgtggtattaatggaagaggacatgcactgctgatcctgaggccagaggagcttggc
tttttacgattcctcaagcaggccaaagttcccctgagtgagtttgaattctcctggacaaaaatctcagatattcaatc
tcagttggataaactgatcgagaaaaactactaccttcacaaatcagctcaggaggcctacaaatcctatgtcagagctt
atga

Clone: pCS2+ npm1a full length cDNA

Source: PCR cloned with restriction enzyme linkers from 30hpf cDNA (Elspeth Payne)
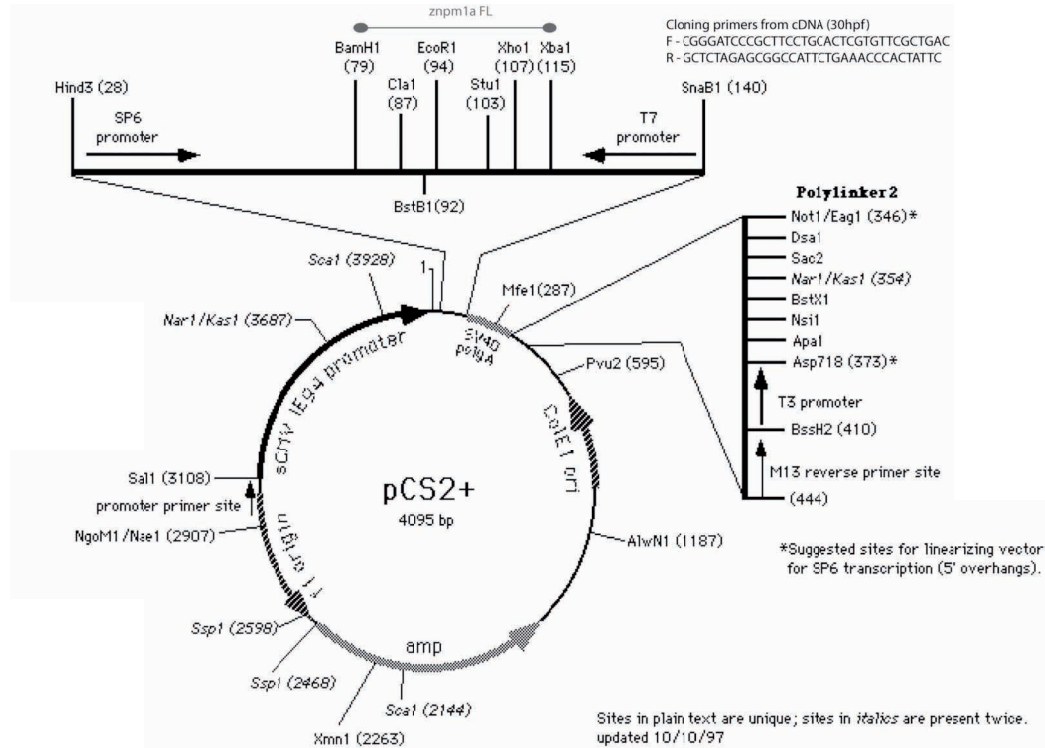
Clone: pCS2+ npm1b full length cDNA

Source: PCR cloned with restriction enzyme linkers from 30hpf cDNA (Elspeth Payne)
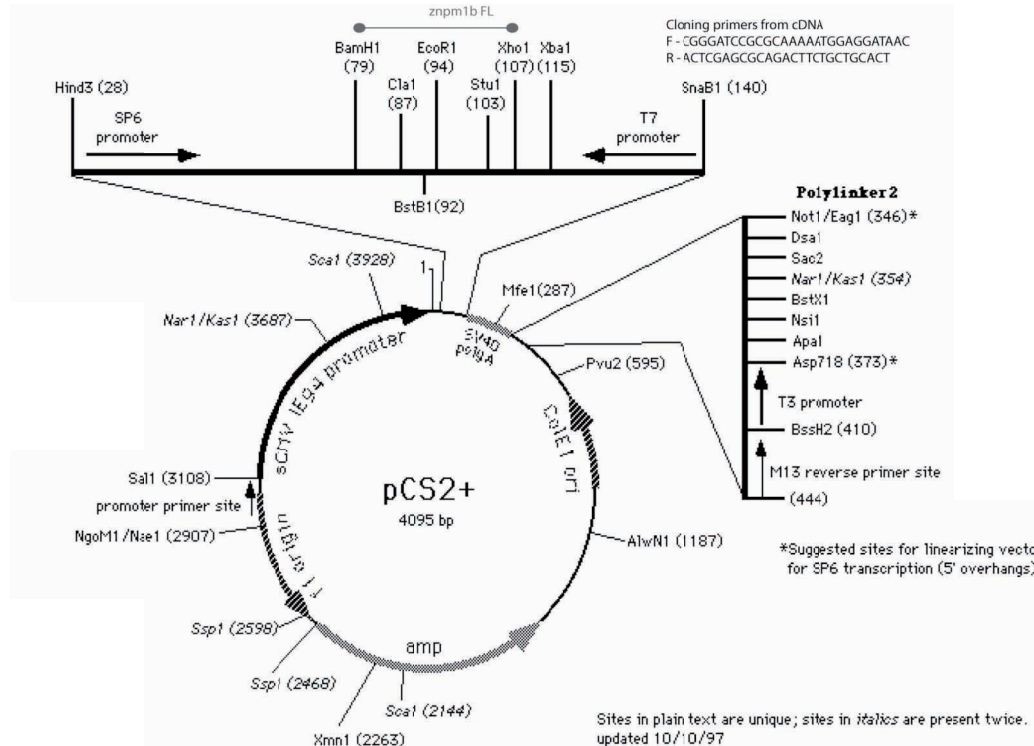

```
atggaggataacattaaagacctcagccgaccccagatgtatttgtttggttgttcgttgaaggctgacaag
aaagagcacaaagttgacctggatgatgatgaggctgaacatcagctgtcacttaagtcggtgtgtttgggt
gccgaggcggaggataaaattccacaccgtggagatggagggattgacttacgatggcaaaaccaccaaaatc
acacttgctgtattgaaaccatccgttctgccttctttaagtctgggcggttttgaggtcactcctcctgtg
tcctttcgtctgcagtccggaggggggccggtctacatcagcggtcaacattttgtcagtgtcaaagagtca
gatgatgaggatgaggaggaagaggagaacaacacttcaccggtgaagagaccgtccaacatgaccctcgcc
aaagtgcctcagaaaaagctgaaaatggatgaggatgaagacagcgatgatgatgatgacgacgacgacgat
gatgatgatgatgaagaggatgatgacaaacaagaaaagcctgctgtaaagagccctgtcaaatccact
caaaaaactccagagaagaagaaaagtgcagataagcagaatggctctccagacaagaaagcagggacatca
gggaagcccccaaactcagacaccgcagaaagtaaaagacaagtctgctgcagggccttctgggaagactccc

agcattcccagcctgagtgaagtcaaaagcaaacttacatcagcagctaaagaggggaagccatttccaaag
acggaacagaagttcgagaacttcgctagaagctctttcaagatctctgataagcaagtgatcaaagacctt
tggaactttgtacaatcactaaaaaagtaa
```
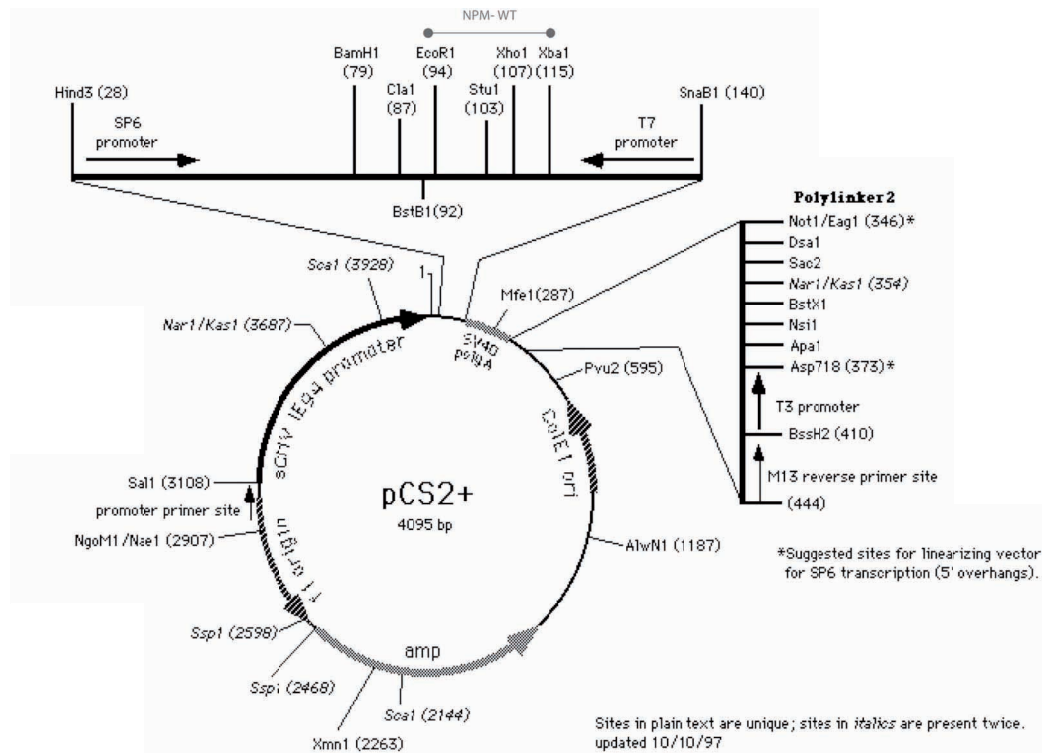
Clone: pCS2+ human *NPM1* full length cDNA

Source: subcloned as described in Chapter 6 (Original Clone Niccolo Bolli)

Clone: pCS2+ zebrafish rps14 full length cDNA

Source: PCR cloned with restriction enzyme linkers from 30hpf cDNA (Elspeth Payne)
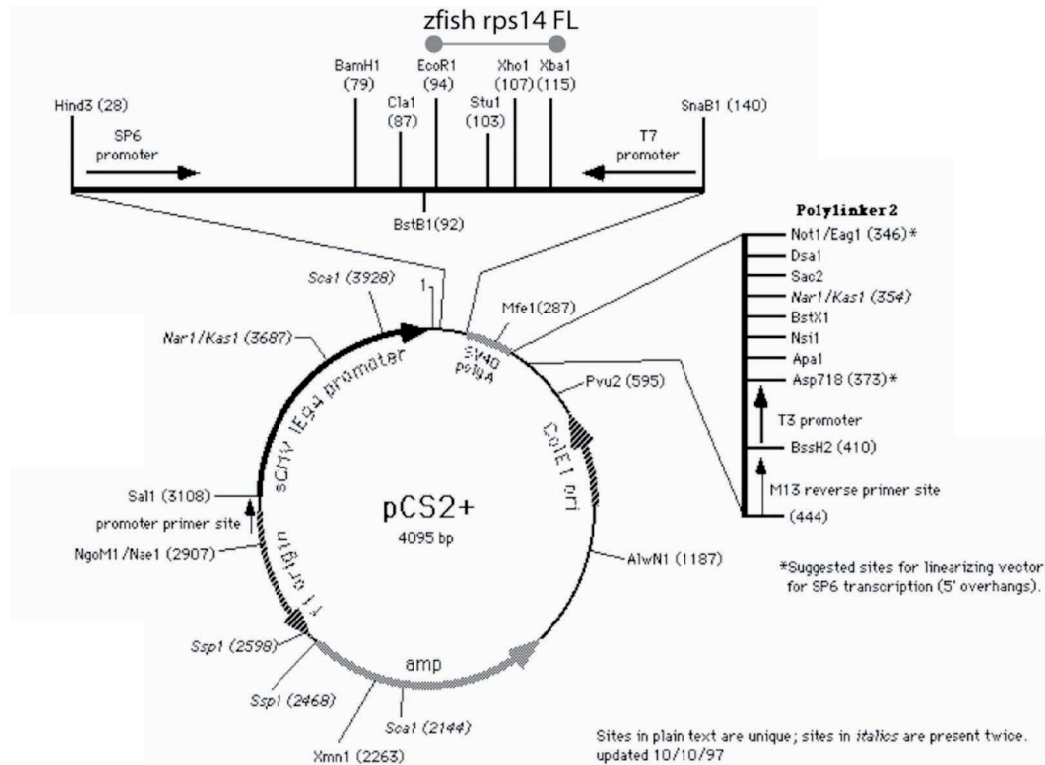
cloning primers
Forward (EcoR1 linker) GGAATTCCCACACATAGCAATGGCTCCT
Reverse (Xba1 linker) GCTCTAGAGCGACACTTTATTCTGAAAAATATCCAA
SEQUENCE :

CACACATAGCAATGGCTCCTCGCAAGGGTAAGGAAAAGAAGGAAGAGCAGGTCATCAGCCTAGGAC
CTCAGGTAGCTGAGGGGGAGAATGTGTTTGGAGTTTGTCACATCTTCGCATCCTTCAACGACACCT
TTGTGCACGTCACTGATCTGTCTGGCAAAGAAACAATTTGCCGTGTGACTGGTGGGATGAAGGTGA
AGGCCGACAGAGATGAGTCTTCTCCTTATGCTGCTATGTTGGCAGCTCAGGATGTGGCTCAAAAGT
GCAAAGAGCTGGGCATCACTGCTCTGCACATCAAGCTGAGGGCCACTGGTGGAAACAGAACCAAGA
CTCCTGGACCAGGGGCACAGTCTGCCCTCAGGGCTCTAGCTCGTTCCGGCATGAAGATTGGTCGTA
TCGAGGACGTCACCCCCATTCCATCAGACAGCACCCGCAGAAAGGGAGGTCGTCGTGGACGTCGTC
TGTAATCTATTGGATATTTTTCAGAATAAAGTGTC

267

Appendix 4 – Supplier information

Supplier	Address	URL
Abcam	1 Kendall Square, Ste 341 Cambridge, MA 02139-1517 USA **Phone:** 617 225 2272 **Fax:** 866 739 9884	**www.abcam.com**
Agencourt (Now Beckman-Coulter Genomics)	Danvers, MA, United States **Phone:** 1 800 361 7780	**www.beckmangenomics.com/genomic_services.html**
Ambion	2130 Woodward St. Austin, TX 78744-1832 USA **Phone:** 512 651-0200 **Fax:** +1 512 651-0201	**www.ambion.com**
Ana Spec	AnaSpec 34801 Campus Drive Fremont, CA 94555 Phone: 510-791-9560 Fax: 510-791-9572	**www.anaspec.com/**
Applied Biosystems	Division Headquarters 850 Lincoln Centre Drive Foster City, CA 94404 U.S.A. **Phone:** 650-638-5800 **Fax:** 650-638-5884	**www.appliedbiosystems.com**
Bethyl Labs	P.O. Box 850 Montgomery, Texas 77356 U.S. **Phone:** 936-597-6111 **Fax:** 936-597-6105	**www.bethyl.com**
Corning	One Riverfront Plaza NY 14831 USA **Phone:** 607-974-9000	**www.corning.com**
DNASTAR, Inc.	3801 Regent Street Madison, WI 53705 USA **Phone:** 608-258-7420 **Fax :** 608-258-7439	**www.dnastar.com**

Gene Tools, LLC	Gene Tools, LLC One Summerton Way Philomath, OR 97370 **Phone:** 541-929-7840 **Fax:** 541-929-7841	**www.gene-tools.com**
Genewiz, Inc	GENEWIZ, Inc. 115 Corporate Blvd. South Plainfield, NJ 07080 USA **Phone:** 1-908-222-0711 **Fax:** 1-908-333-4511	**www.genewiz.com/**
GraphPad Software	2236 Avenida de la Playa La Jolla, CA 92037 USA support@graphpad.com	**www.graphpad.com**
Invitrogen	1600 Faraday Ave Carlsbad California 92008 USA **Phone:** 800-955-6288	**www.invitrogen.com**
New England Biolabs	240 County Road Ipswich, MA 01938-2723 **Phone:** 978-927-5054	**www. neb.com**
Open Biosystems	601 Genome Way Ste. 2100 Huntsville, AL 35806 USA **Phone:** 888-412-2225	**www.thermo.com/openbiosystems**
Operon Biotechnologies, Inc	2211 Seminole Drive Huntsville, Alabama 35805, USA **Phone:** 800-688-2248 **Fax:** 251-252-7794	**https://operon.com**
Qiagen Inc	27220 Turnberry Lane Valencia CA 91355 **Phone:** 800-426-8157 **Fax:** 800-718-2056	**www.qiagen.com**
Roche	Roche Applied Science 9115 Hague Road P.O. Box 50414 Indianapolis, IN 46250-0414 USA	**www.roche-applied-science.com**
Sigma-Aldrich	PO Box 14508	**www.sigmaaldrich.com**

	St. Louis, MO 63178 USA **Phone:** 800-325-5832 **Fax:** 800-240-4668	
SoftGenetics, LLC.	100 Oakwood Ave, Suite 350 State College, PA 16803, USA **Phone:** 814-237-9340 **Fax:** 814-237-9343	**www.softgenetics.com**
Stratagene (now Agilent Technologies, Inc.)	5301 Stevens Creek Boulevard Santa Clara, CA 95051-7201, USA **Phone:** 1-800-227-9770	**www.genomics.agilent.com**
Vector Labs	30 Ingold Road Burlingame, CA 94010, USA **Phone:** 650-697-3600 **Fax:** 650-697-0339	**www.vectorlabs.com/**
Znomics Inc	Znomics, Inc. 2611 SW 3rd Ave, Suite 200 Portland, OR 97201, USA **Phone:** 503-827-5271 **Fax:** 503-228-3290	**www.znomics.com**

Appendix 5 - **Published manuscripts arising from this work**

Expression of the cytoplasmic NPM1 mutant (NPMc+) causes the expansion of hematopoietic cells in zebrafish

*Niccolò Bolli,[1,2] *Elspeth M. Payne,[1,3] Clemens Grabher,[1,4] Jeong-Soo Lee,[1] Adam B. Johnston,[1] Brunangelo Falini,[2] John P. Kanki,[1] and A. Thomas Look[1,5]

[1]Department of Pediatric Oncology, Dana-Farber Cancer Institute, Harvard Medical School, Boston, MA; [2]Institute of Hematology, University of Perugia, Perugia, Italy; [3]Institute of Cancer, Barts and the London School of Medicine, London, United Kingdom; [4]Karlsruhe Institute of Technology, Forschungszentrum Karlsruhe, Karlsruhe, Germany; and [5]Division of Hematology/Oncology, Department of Pediatrics, Children's Hospital, Harvard Medical School, Boston, MA

Mutations in the human nucleophosmin (*NPM1*) gene are the most frequent genetic alteration in adult acute myeloid leukemias (AMLs) and result in aberrant cytoplasmic translocation of this nucleolar phosphoprotein (NPMc+). However, underlying mechanisms leading to leukemogenesis remain unknown. To address this issue, we took advantage of the zebrafish model organism, which expresses 2 genes orthologous to human *NPM1*, referred to as *npm1a* and *npm1b.* Both genes are ubiquitously expressed, and their knockdown produces a reduction in myeloid cell numbers that is specifically rescued by *NPM1* expression. In zebrafish, wild-type human NPM1 is nucleolar while NPMc+ is cytoplasmic, as in human AML, and both interact with endogenous zebrafish Npm1a and Npm1b. Forced NPMc+ expression in zebrafish causes an increase in *pu.1*+ primitive early myeloid cells. A more marked perturbation of myelopoiesis occurs in p53^{m/m} embryos expressing NPMc+, where *mpx*+ and *csf1r*+ cell numbers are also expanded. Importantly, NPMc+ expression results in increased numbers of definitive hematopoietic cells, including erythromyeloid progenitors in the posterior blood island and *c-myb/cd41*+ cells in the ventral wall of the aorta. These results are likely to be relevant to human NPMc+ AML, where the observed NPMc+ multilineage expression pattern implies transformation of a multipotent stem or progenitor cell. (*Blood*. 2010;115(16):3329-3340)

Introduction

Nucleophosmin (NPM1) is a ubiquitous multifunctional phosphoprotein, which is normally located in the nucleolus but has nucleocytoplasmic shuttling activity. Known functions of NPM1 include roles in ribosome biogenesis and control of centrosome duplication.[1] NPM1 also regulates the tumor suppressors p14^{ARF2,3} and p53,[4] and is up-regulated by cellular stresses such as DNA damage.[5] *Npm1*^{+/−} heterozygous mice are viable, and show a hematologic syndrome similar to human myelodysplastic syndrome (MDS), suggesting a role of Npm1 in hematopoiesis.[6] Moreover, *Npm1*^{+/−} mice show genomic instability and a greater propensity to develop hematologic malignancies, defining *Npm1* as a haploinsufficient tumor suppressor.[7] Heterozygous gain of function mutations in *NPM1* are the most frequent genetic abnormalities found in human acute myeloid leukemia (AML), occurring in 30% of all adult cases.[8] Such mutations of *NPM1* appear to be specific to AML, as they do not occur in other human cancers.[8,9] In the absence of FLT3-ITDs, mutated *NPM1* in adult AML has been associated with a better prognosis.[10] Because of its distinctive biologic and clinical features,[11] *NPM1*-mutated AML has been included as a new provisional entity in the 2008 World Health Organization (WHO) classification of human myeloid neoplasms.[12] Consequently, *NPM1* mutational analysis is now performed routinely on adults diagnosed with AML.[10,11]

NPM1 expression is normally detected primarily in the nucleolus, but when mutated it aberrantly relocates to the cytoplasm.[13]

More than 50 mutations have been described that lead to this aberrant localization, and thus the term NPM1 cytoplasmic–positive (NPMc+) has been used to define cytoplasmic mutants that are found in AML.[8] Mechanisms underlying the aberrant localization of NPMc+ have been identified,[14,15] and studies have shown that NPMc+ can function as an oncogene in vitro[16] and disrupt murine hematopoiesis;[17] however, the critical steps leading to leukemic transformation of NPMc+-expressing cells remain unknown.

The zebrafish is a powerful vertebrate disease model system. Several human and murine oncogenes involved in leukemogenesis cause leukemia and disrupt normal hematopoiesis in the zebrafish, providing strong support of the zebrafish as a relevant model system to study mechanisms underlying human leukemia.[18-20] Two distinct waves of zebrafish hematopoiesis have been described. Primitive hematopoiesis is characterized by the generation of embryonic erythrocytes in the intermediate cell mass (ICM)[21] and a distinct population of primitive macrophages that arise from the anterior lateral plate mesoderm (ALPM).[22] Definitive hematopoiesis consists of 2 phases: at first, transient erythromyeloid progenitors (EMPs) form in the posterior blood island (PBI) starting around 24 hours postfertilization (hpf),[23] followed by the appearance of hematopoietic stem cells (HSCs) in the ventral wall of the dorsal aorta by 30 hpf, in a region that is thought to be equivalent to the mammalian aorta-gonad-mesonephros (AGM).[24] These HSCs

---

then colonize the thymus and the kidney, the hematopoietic organ in adult zebrafish.[24]

We have used the zebrafish model to study the physiologic role of Npm1 and the perturbation in hematopoiesis induced by NPMc+ expression. We identified 2 zebrafish orthologs of the human *NPM1* gene, *npm1a* and *npm1b*, and determined that these genes are required for normal hematopoiesis. Furthermore, we have shown for the first time that *NPMc+* expression causes expansion of primitive and definitive hematopoietic cells in vivo, establishing a platform to further investigate the mechanisms through which NPMc+ contributes to leukemic transformation.

Methods

Zebrafish, microinjections, and WISH

Wild-type AB stocks of *Danio rerio*, the transgenic lines Tg(*pu.1*:EGFP),[25] Tg(*c-myb*:EGFP),[26] Tg(*cd41*:EGFP),[27] Tg(*gata1*:DsRED),[28] Tg(*lmo2*:DsRed),[29] and Tg(*gata1*:EGFP),[30] and the mutant line *tp53*$^{zdf1/zdf1}$ (*tp53*$^{M214K/M214K}$, referred to in the text as p53$^{m/m}$)[31] were maintained as described.[32] mRNAs were injected into 1-cell–stage embryos at the indicated amounts. Morpholinos (MOs) targeting the 5′UTR/ATG codon or splice donor sites of *npm1a*, *npm1b*, and control morpholinos, were designed by Gene-Tools LLC. Sequences are given in Table 1. MO concentrations were titrated to the lowest dose resulting in phenotypes: 1.6 ng each for *npm1a* and *npm1b* ATG MOs, 8 ng and 4 ng for *npm1a* splice donor MOs (exon2-intron2(2) and exon3-intron3, respectively), and 4 ng for *npm1b* splice donor MO (exon2-intron2). For experiments in p53-deficient backgrounds, NPM1- or NPMc+–encoding mRNAs were injected into the p53$^{m/m}$ line or with the p53 MO (1.6 ng)[33] in the Tg(*pu.1*:EGFP) line. Observed increases in enhanced green fluorescent protein–positive (EGFP$^+$) cells in the Tg(*pu.1*:EGFP) line expressing NPMc+ served as an indicator for NPMc+ function.

Developmental staging of injected zebrafish embryos and uninjected controls was determined by somite number. Embryos were fixed in 4% paraformaldehyde (PFA), and assays for mRNA expression using whole-mount in situ hybridization (WISH) were performed as described.[34] Embryos were visualized and imaged with a Nikon SMZ1500 zoom stereomicroscope (Nikon Instruments Inc) using the NIS-Elements software (Nikon Instruments Inc). Some WISH embryos were postfixed in 4% PFA and embedded in 1.5% agar/5% sucrose, equilibrated in 30% sucrose, and cryosectioned (20 μm). All animal protocols were approved by the Dana-Farber Animal Care and Use Committee.

Cloning of human and zebrafish NPM1 cDNAs and RNA production

Full-length NPM1 cDNA (wild-type and mutated) were subcloned in the pCS2$^+$ or p3X-FLAG vector (Sigma) from pGEM-T-easy-NPM1 and

Table 1. MO sequences

Gene	Target	MO sequence
npm1a	ATG/5′UTR	TAATGTTATCCTC**CAT**TTTTGCGCG
npm1a	ATG/5′UTR 5-bp mismatch	TAATcTTATCgTC**gAT**TTTaGCcCG
npm1a	Exon2-intron2 splice donor (2)*	AAGAAACATCACATACCATTCTAAC
npm1a	Exon3-intron3 splice donor	TTATGACCAAGTCTACTTACACTTG
npm1b	ATG/5′UTR	GACCCATCTGTTCGAGATC**CAT**GTC
npm1b	ATG/5′UTR 5-bp mismatch	GAgCCATgTGTTCGAcATC**gAT**cTC
npm1b	Exon2-intron2 splice donor	TCAAATATTCATCTTCCTCACCGAC
p53	ATG/5′UTR	GCGC**CAT**TGCTTTGCAAGAATTC
Std cont	Human β-globin intron mutation	CCTCTTACCTCAGTTACAATTTATA

Bold letters indicate the ATG codon; lowercase letters, mismatched residues; and Std cont, standard control.

*(2) is the 1 working morpholino of 2 tested (supplemental Figure 1F, available on the *Blood* Web site; see the Supplemental Materials link at the top of the online article).

Table 2. Oligonucleotide sequences

Primer	Sequence
Npm1a forward *Bam*H1	5′-CG**GGATCC**CGCTTCCTGCACTCGTGTTCGCTGAC-3′
Npm1a reverse *Xba*I	5′-GC**TCTAGA**GCGGCCATTCTGAAACCCACTATTC-3′
Npm1b forward *Bam*HI	5′-CG**GGATCC**GCGCAAAATGGAGGATAAC-3′
Npm1b reverse *Xho*I	5′-A**CTCGAG**CGCAGACTTCTGCTGCACT-3′
β-actin forward	5′-CTGGTCGTTGACAACGGCT-3′
β-actin reverse	5′-TCCATCACAATACCAGTAGT-3′

Bold letters indicate restriction enzyme sites.

pGEM-T-easy-NPMmutA.[8] Full-length cDNA encoding EGFP-NPM1 (wild-type and mutated) were subcloned in pCS2$^+$ from pEGFP-C1-NPM1 and pEGFP-C1-NPMmutA.[8] Full-length cDNA of the 2 zebrafish *NPM1* orthologs *npm1a* and *npm1b* were reverse transcription–polymerase chain reaction (RT-PCR)–amplified from 24 hpf AB embryos. Primers for full-length *npm1a* coding region amplification were designed based on the published NCBI sequence (NM_199428), while those for *npm1b* were based on overlapping expressed sequence tag (EST) sequences and the recently annotated Zv8 sequence BC093285 (Table 2). Full-length *npm1a* and *npm1b* amplicons were cloned into pCRII-Topo Dual Promoter vector (Invitrogen), from which WISH probes were made, and then into pCS2$^+$, pEGFP-C1, and pDsRed-Monomer-C1 expression vectors (Clontech). All constructs were verified by sequencing. All mRNAs were transcribed from pCS2$^+$ using the mMessage mMachine kit (Ambion).

Comparative analysis and identification of synteny to human 5q35.1-5q35.2

Genes located in 5q35.1-5q35.2 were identified using the National Center for Biotechnology Information (NCBI) Mapviewer.[35] Zebrafish orthologs for genes in this region were identified using a "reciprocal best-hit" analysis as described.[36] TBLASTN searches were applied for human protein sequences and BLASTX or TBLASTN searches for zebrafish cDNA sequences or proteins, respectively (Ensembl Zv7). Comparative analysis between the human and the 2 zebrafish protein sequences used the Clustal W algorithm.[37]

RT-PCR, protein extraction, WB, and coimmunoprecipitation studies

Total RNA from zebrafish embryos at various stages of development was extracted using Trizol (Invitrogen) following the manufacturer's instructions. RT-PCR was performed on RNA using the Qiagen One-Step RT-PCR Kit using gene-specific primers. Primers used for npm1a and npm1b amplification spanned the full-length coding sequence. Primers used for β-actin amplification spanned 2 introns. Primer sequences are provided in Table 2. Protein lysates were obtained from single-cell suspensions of approximately 20 zebrafish embryos per condition. Embryos were dissociated with 0.5% trypsin (GIBCO), and protein extraction, Western blot (WB), and coimmunoprecipitation studies were carried out as described.[14] Antibodies used were anti-NPM1, clone 376;[8] anti–β-tubulin (Abcam); anti-GFP (Roche); and anti-FLAG (Sigma).

Fluorescence analysis in zebrafish embryos and 293T cells

For cytospins (Figure 3A-F), 24-hpf embryos injected with EGFP-NPM1 or EGFP-NPMc+ at the indicated doses were dissociated with 0.5% trypsin (GIBCO). The cell suspension was fixed in 4% PFA. A total of 10^5 cells were spun onto glass slides and mounted with ProLong Gold Antifade reagent with DAPI (Molecular Probes). For confocal analysis of EGFP$^+$ cells from whole embryos (Figure 3H-I), 24-hpf embryos injected with EGFP-NPM1 (50 ng) or EGFP-NPMc+ (10 ng) were fixed in 4% PFA, deyolked, and flat-mounted on glass slides with ProLong Gold Antifade reagent with DAPI (Molecular Probes). 293T cells (Figure 4) were seeded on glass coverslips and transfected 24 hours later using Fugene 6 (Roche).

In cotransfection experiments, plasmids were used at equimolar ratios. At 24 hours after transfection, cells were rinsed in phosphate-buffered saline (PBS), fixed in PFA (10 minutes), and mounted on glass slides with ProLong Gold Antifade reagent with DAPI (Molecular Probes). Whole-mount anti–activated caspase-3 and anti-GFP immunostaining (Figure 6) were performed as follows: embryos fixed in 4% PFA were rinsed in PDT (PBST, 0.3% Triton-X, and 1% DMSO), blocked in CAB (10% HI-FBS, 2% BSA in PBST), and incubated with primary antibodies (rabbit anti–activated caspase-3 [BD Biosciences] and mouse anti-GFP [Molecular Probes]) in CAB (1:500). Embryos were then washed in PDT, blocked in CAB, and incubated with secondary antibodies (anti–mouse AlexaFluor-488–conjugated and anti–rabbit AlexaFluor-568–conjugated; Molecular Probes) in CAB (1:200). Acridine orange stains were performed as previously described.[38] Confocal images of 32-hpf Tg(cd41:EGFP), Tg(gata1:dsRed);(c-myb:EGFP), and Tg(lmo2:dsRed);(gata1:EGFP) transgenic embryos injected with NPM1 (50 ng) or NPMc+ (10 ng; Figure 7) were taken from live embryos mounted in 1% low-melting point agarose.

Analysis of zebrafish by flow cytometry

Specific hematopoietic subpopulations from adult dissected kidney marrows were obtained as described.[28] Transgenic embryos were dissociated in liberase blendzyme 3 (Roche) for 30 to 60 minutes at 32°C. Embryos were gently dissociated using a pipette tip, passed through a 40-μM filter, and washed 3 times in cold PBS. Tg(pu.1:EGFP) were labeled with annexin V–phycoerythrin (PE) to assess apoptosis.[38]

DNA content of pu.1:EGFP+ cells was determined by hypotonic propidium iodide (PI) staining of EGFP+ cells sorted on a MoFlo cell sorter (DAKO Cytomation). Fluorescence-activated cell sorter (FACS) analysis of c-myb:EGFP+ cells was conducted in dissected trunks of embryos, gating on the FSC^HIGH population as described in Bertrand et al.[24] Data from Tg(c-myb:EGFP), Tg(pu.1:EGFP), and double Tg(gata1:EGFP);Tg(lmo2:dsRed) cell suspensions were acquired on a FACS-Canto II (BD Biosciences). Dead c-myb:EGFP and pu.1:EGFP cells were excluded by PI staining. Data were analyzed using FlowJo (TreeStar) or Modfit LT (Verity Software).

Results

Identification of 2 zebrafish NPM1 genes

Zebrafish often have 2 copies of genes orthologous to a single mammalian gene as a result of genomic duplication during teleost evolution.[39] To identify the zebrafish npm1 gene(s), the human NPM1 amino acid sequence was used in a TBLASTN search using the Ensembl, University of California Santa Cruz (UCSC), and NCBI platforms. A total of 2 loci were identified, including an annotated zebrafish npm1 gene on chromosome 10 whose protein product exhibits 51% identity to NPM1, and multiple overlapping ESTs encoded by a novel locus on
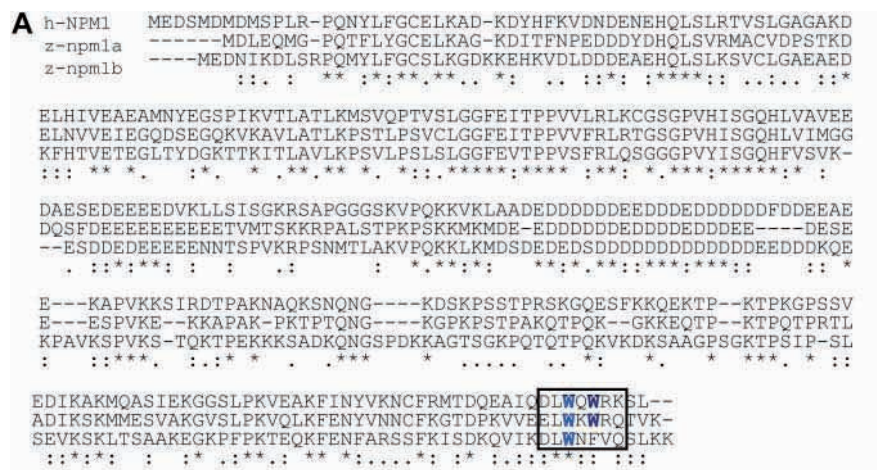
Figure 1. Identification of 2 putative zebrafish npm1 genes. (A) Clustal W alignment of human NPM1 (top row), zebrafish Npm1a (middle row), and Npm1b (bottom row) proteins. * indicates identical residues; colon (:), highly similar residues; and period (.), similar residues. Critical tryptophan residues necessary for nucleolar localization are highlighted in blue in the boxed area. (B) The genomic loci surrounding human NPM1 on chromosome 5q35.1 (top row) are syntenic with the regions where npm1a (on chromosome 10) and npm1b (on chromosome 14) are located in the zebrafish genome (bottom row left and right, respectively). (C) RT-PCRs showing npm1a (top row) and npm1b (middle row) expression levels. β-actin expression levels are used as a loading control (bottom row). Left: npm1a and npm1b embryonic expression was assessed from whole embryos at the indicated time points. Right: RT-PCRs from precursor, lymphoid, myeloid, and erythroid cells sorted from adult kidney marrow (gating strategy based on forward- and side-scatter plots[28]). (D,F,G,I) npm1a or npm1b WISH assays in 24-hpf or 48-hpf embryos, lateral view, anterior to the left, dorsal upwards. (E,H) Close-up dorsal view (anterior to the left) of the brain and anterior trunk in flat-mounted, deyolked 24-hpf embryos stained with npm1a or npm1b probes. Digoxigenin-labeled RNA probes encoding the full-length npm1a and npm1b sequences were transcribed from linearized cDNA constructs using the DIG RNA labeling kit (Roche) following manufacturer instructions.
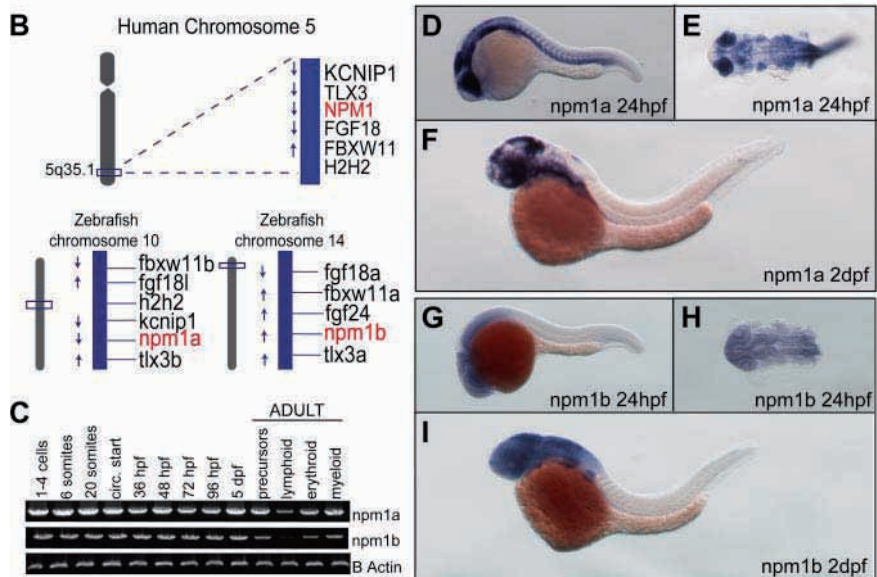
chromosome 14, corresponding to a gene with 48% identity to NPM1 (Figure 1A). In silico analysis of the putative proteins encoded by the 2 genes shows that critical NPM1 functional domains are conserved in both Npm1 zebrafish proteins, including the C-terminal tryptophan residues implicated in nucleolar localization[14] (Figure 1A boxed area; supplemental Figure 1A-B). Furthermore, the genomic regions surrounding both zebrafish npm1 genes showed high degrees of synteny with human 5q35.1, the locus of human NPM1 (Figure 1B). Thus, each of these genes is orthologous to NPM1; we refer to these genes as npm1a (chromosome 10) and npm1b (chromosome 14). Both zebrafish npm1 genes are expressed maternally and throughout the first 5 days of development (Figure 1C). They are also both expressed in all hematopoietic compartments of the adult kidney marrow (Figure 1C). To investigate the spatial expression pattern of npm1a and npm1b, we performed WISH and found that both npm1a and npm1b are ubiquitously expressed at 24 hpf, with highest levels in the developing brain, eye, and somites (Figure 1D-E and 1G-H, respectively). By 2 days after fertilization (dpf), expression was most prominent in the brain and fin-buds (Figure 1F,I).

Knockdown of npm1a and npm1b leads to myeloid cell loss

To determine whether the zebrafish npm1 genes had a role in hematopoiesis, each gene was knocked down using antisense MOs. Initial studies were carried out using 5′UTR/ATG MOs. Embryos were analyzed for myeloid peroxidase (mpx) expression by WISH at 2 dpf. Knockdown of each gene individually lead to a significant reduction in the number of mpx-expressing cells (Figure 2A,D,G,M). When npm1a and npm1b were knocked-down simultaneously, the effect on mpx-expressing cell numbers was markedly increased (Figure 2J,M). Embryos injected with both MOs together showed developmental abnormalities, with a smaller head and eyes and a shortened yolk extension (Figure 2J; arrow and arrowhead). We further validated the specificity of this phenotype by testing several MOs directed at splice donor sites of npm1a and npm1b. Combined knockdown of npm1a and npm1b using the splice donor site MOs
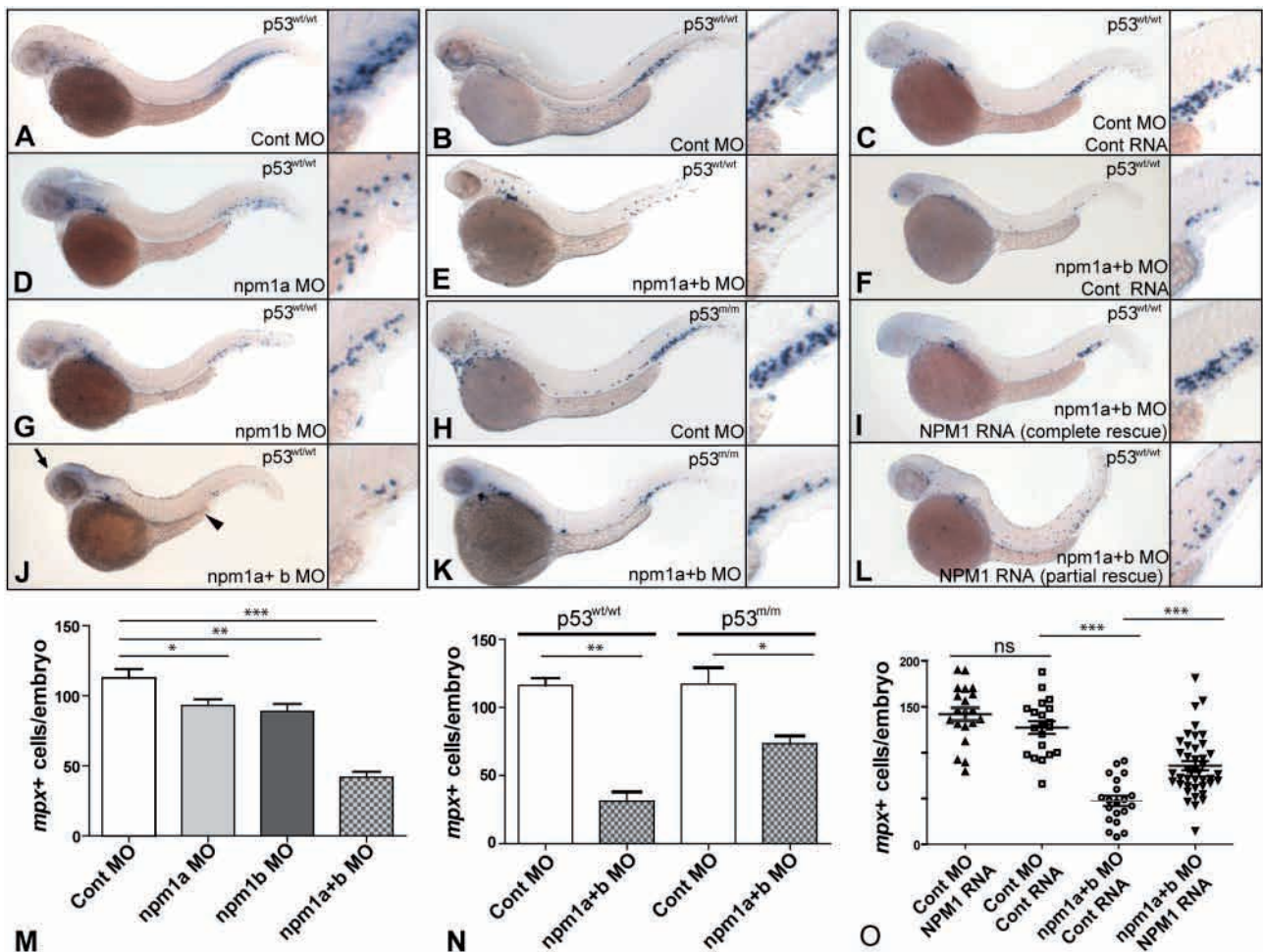
Figure 2. Knockdown of npm1a and npm1b leads to loss of myeloid cells. (A-L) WISH for mpx in 48-hpf embryos, lateral view, anterior to the left, dorsal upwards. (A,D,G,J,M) Knockdown of npm1 genes results in loss of mpx-expressing myeloid cells. A significant difference is seen in myeloid cell numbers when each gene is knocked-down individually (npm1a in panel D and npm1b in panel G, quantified in panel M); this effect is at least additive in the double knockdown (npm1a + npm1b in panel J, quantified in panel M). (B,E,H,K,N) mpx expression is reduced upon npm1 knockdown compared with controls in both the p53$^{wt/wt}$ (B,E) and p53$^{m/m}$ (H,K) backgrounds (quantified in panel N). (C,F,I,L,O) Loss of mpx expression by knockdown of npm1 (F) can be rescued completely (I) or partially (L) by NPM1 RNA injection (10 pg). No differential expression of mpx is observed when 10 pg NPM1 or 10 pg control RNA (C) are injected with a control MO (quantified in panel O). npm1a MO indicates 5′UTR MO (1.4 ng); npm1b MO, 5′UTR MO (1.4 ng); npm1(a+b), npm1a MO + npm1b MO (1.4 ng each); control MO, npm1a 5-bp mismatch + npm1b 5-bp mismatch at 1.4 ng each. Error bars represent SEM. ns indicates not significant; *$P < .02$; **$P < .01$; ***$P < .001$ (Student t test). Complete rescue in panel I is defined as mpx$^+$ cell numbers per embryo greater than the lower limit of the 95% confidence interval of the control RNA/control MO-injected embryos. Partial rescue in panel L is defined as mpx$^+$ cells/embryos greater than the upper limit of the 95% confidence interval of the npm1(a+b) MO but below the lower limit of the 95% confidence interval of the control RNA/control MO-injected embryos.

Figure 3. Mutated human NPM1 is aberrantly expressed in the cytoplasm of zebrafish cells. (A-F) Epifluorescence analysis of EGFP-NPM1 (A-C) and EGFP-NPMc+ (D-F) subcellular localization in cytospins of zebrafish cells after mRNA injection at the indicated amounts. NPM1 or NPMc+ proteins are shown in green, and nuclei are counterstained in blue with DAPI. Cells were visualized with a Zeiss Axio imager Z1 microscope using a Zeiss 63×/1.4 numeric aperture (NA) Apochromat oil lens (Carl Zeiss). Images were acquired with Openlab software (Perkin Elmer). (G) WB analysis of protein extracts from NPM1 (top left 3 lanes) and NPMc+ (top right 3 lanes) mRNA-injected embryos. NPM1 expression levels at each mRNA dose are shown along with β-tubulin expression as a loading control (bottom row). The arrows indicate the doses used for subsequent experiments. (H-I) Confocal microscopy of EGFP-NPM1 subcellular localization in zebrafish embryos at 24 hpf injected with 10 pg of EGFP-NPM1 mRNA (H) and 50 pg EGFP-NPMc+ mRNA (I). NPM1 protein is shown in green, while nuclei are counterstained in blue with DAPI. Images of cells were taken in the dorsal trunk region, shown in the insert (H), with a Zeiss LSM 510 META 2-Photon confocal microscope (Carl Zeiss), using a Zeiss 63×/1.4 NA Apochromat oil lens (Carl Zeiss). Images were acquired with the Zeiss LSM 510 software (Carl Zeiss). The EGFP expression patterns shown were representative of cells throughout the embryo.
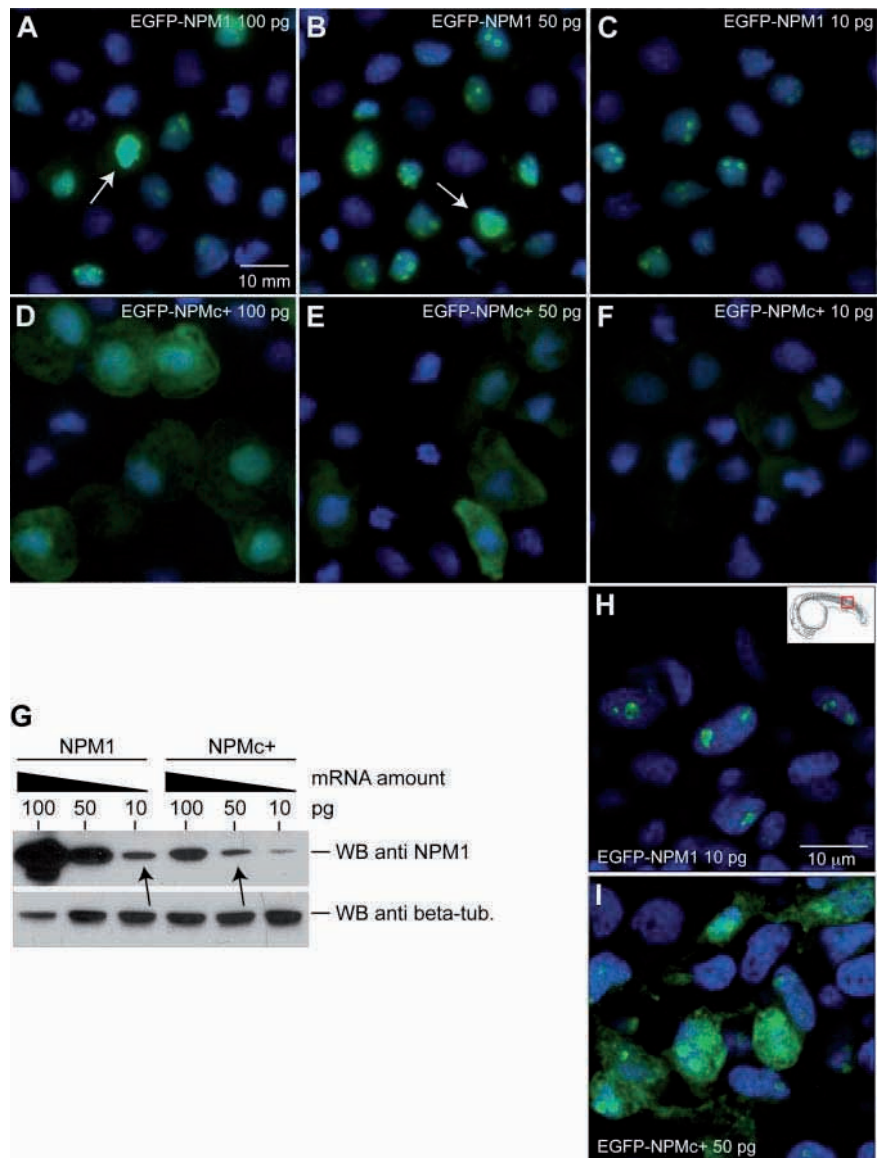

led to the same myeloid phenotype in these morphants as that induced by the 5′UTR/ATG-targeted double morphants (supplemental Figure 1C-D; quantified in supplemental Figure 1E). Knockdown of each gene was confirmed by RT-PCR and sequencing of the products to demonstrate the introduction of a premature stop codon in aberrantly spliced products (supplemental Figure 1F). Because it is known that some MOs can induce p53-dependent cell death as an off-target effect,[40] we knocked-down npm1a and npm1b in the p53[m/m] line and analyzed mpx expression by WISH at 2 dpf. Compared with control MO-injected p53[wt/wt] (Figure 2B) and p53[m/m] (Figure 2H) embryos, injection of npm1(a+b) MO in p53[m/m] embryos led to a significant reduction of mpx expression (Figure 2K), similar to that observed in p53[wt/wt] (Figure 2E; quantifications in Figure 2N). These findings show that the loss of myeloid cells seen after knockdown of npm1a and npm1b is not a result of p53-dependent MO-induced toxicity.

To functionally validate npm1a and npm1b as true orthologs of human NPM1, we tested whether NPM1 expression could rescue the npm1 knockdown phenotype. We injected 1-cell–stage embryos with NPM1 RNA or control (mCherry-encoding) RNA along with npm1(a+b) MOs or mismatch controls. Although control RNA injection had no effect in the context of control MO or npm1(a+b)

double morphants (Figure 2C,F; quantified in Figure 2O), injection of NPM1 mRNA (10 pg) rescued both the myeloid and developmental defects when injected into npm1(a+b) double morphants. Complete rescue was observed in 15% of embryos (Figure 2I), and a partial rescue was seen in 75% of embryos (Figure 2L). Importantly, NPM1 mRNA injection along with the control MO had no effect on the number of mpx cells (quantified in Figure 2O). These results demonstrate that npm1a and npm1b are true orthologs of NPM1.

Mutated human NPM1 is aberrantly expressed in the cytoplasm of zebrafish cells

To test whether NPMc+ was aberrantly localized to the cytoplasm in the zebrafish, as in humans, we injected mRNAs encoding NPMc+ or NPM1 fused to EGFP. The mRNAs were injected into 1-cell–stage embryos at doses up to 100 pg. At the highest dose, embryos appeared normal, and injected and uninjected embryos were morphologically indistinguishable by brightfield microscopic examination at 20 somites. NPM1 protein subcellular localization was assessed using cytospins of cell suspensions obtained from EGFP-NPM1– and EGFP-NPMc+–injected embryos at 24 hpf
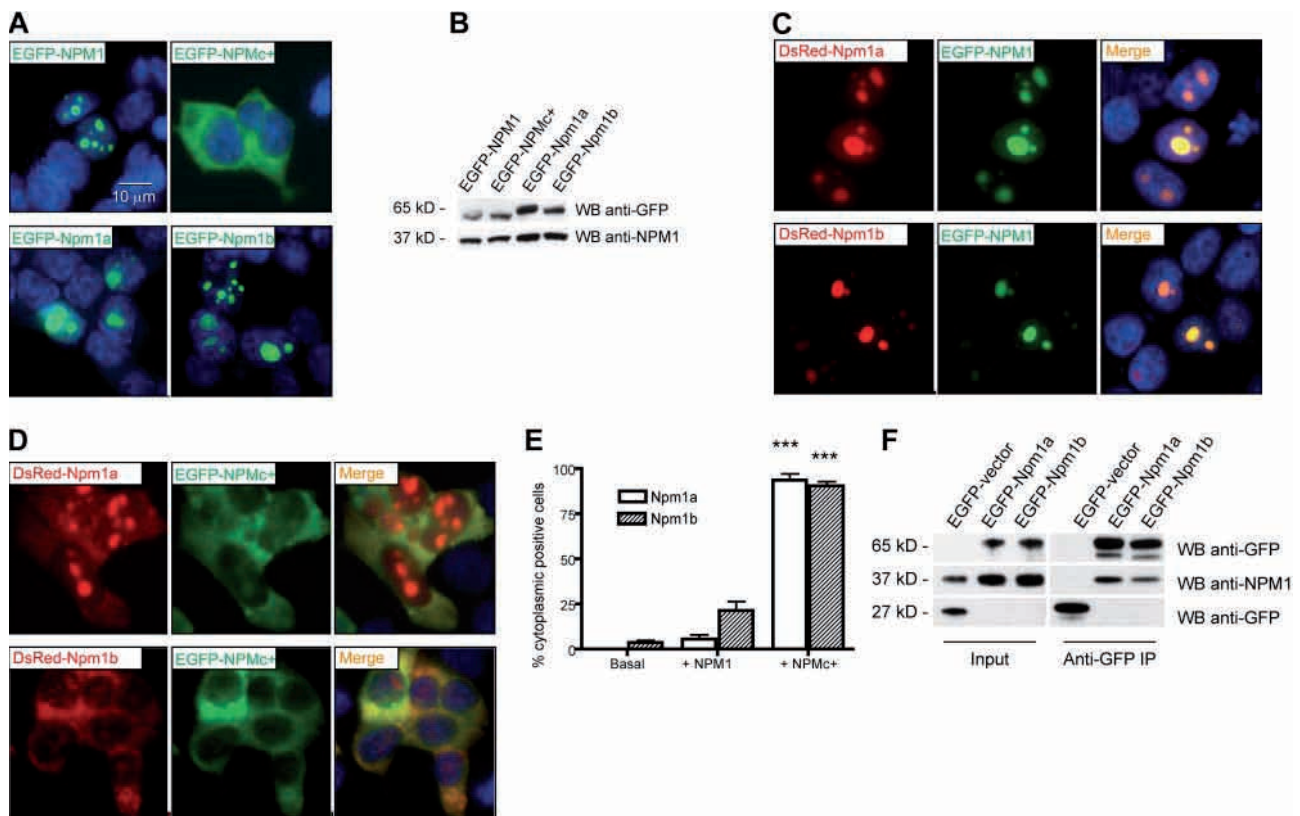
Figure 4. Zebrafish npm1 orthologs interact with human NPM1 protein. (A) Epifluorescent images of 293T cells transfected with pEGFP-C1 expression vector encoding NPM1 (top left), NPMc+ (top right), Npm1a (bottom left), or Npm1b (bottom right). Expressed proteins are shown in green; nuclei are counterstained in blue with DAPI. (B) Anti-GFP WB analysis of protein lysates from transfected cells shown in Figure 2A. Levels of transfected proteins (top row) are shown along with levels of endogenous NPM1 (bottom row). (C) Epifluorescent images of 293T cells cotransfected with pEGFP-C1-NPM1 and pDsRed-monomer-C1 encoding zebrafish Npm1a (top row) or Npm1b (bottom row). Colocalization areas between Npm1a or Npm1b (in red, left column) and NPM1 (in green, middle column) are shown in yellow in the merged images (right column). Nuclei are counterstained in blue with DAPI. (D) Epifluorescent images of 293T cells cotransfected with pEGFP-C1-NPM1c+ and pDsRed-monomer-C1 encoding Npm1a (top row) or Npm1b (bottom row). Colocalization areas between Npm1a or Npm1b (in red, left column) and NPMc+ (in green, middle column) are shown in yellow in the merged images (right column). Nuclei are counterstained in blue with DAPI. All fluorescent images were acquired with a Zeiss Axio imager Z1 microscope using a Zeiss 63×/1.4 NA Apochromat oil lens (Carl Zeiss) and Openlab software (Perkin Elmer). (E) Quantification of the Npm1a and Npm1b delocalization by NPMc+. Bars indicate the percentage of cells with aberrant Npm1a (□) or Npm1b (▨) cytoplasmic expression (with or without residual nucleolar positivity). Error bars indicate SD. *Statistically significant differences between the NPMc+-injected and both NPM1-injected and uninjected embryos (***$P < .001$; Student t test). More than 200 cells were counted in 3 different microscopic fields for this analysis. (F) Anti-GFP coimmunoprecipitation assays of 293T cells transfected with the empty pEGFP-C1 vector, pEGFP-C1-Npm1a, or pEGFP-C1-Npm1b. Left panels, input; right panels, anti-GFP coimmunoprecipitation lanes. Top row: anti-GFP WB, detecting EGFP-Npm1a and EGFP-Npm1b fusion proteins. Middle row: anti-NPM1 WB, detecting endogenous NPM1. Bottom row: anti-GFP WB, detecting EGFP expressed by the empty vector. In the anti-GFP immunoprecipitation lanes, a dimmer band under the EGFP-Npm1a and EGFP-Npm1b bands probably represents a degradation product of the fusion protein, as it is also visible in the input lanes at longer exposures.

(Figure 3A-F). At low mRNA concentrations (10 pg), EGFP-NPM1 expression was restricted to nucleoli (Figure 3C), while at higher doses (50 and 100 pg), the protein was found to leak into the nucleoplasm and sometimes the cytoplasm of cells (arrows in Figure 3A-B), possibly because of overexpression artifacts. By contrast, NPMc+ was expressed in the cell cytoplasm at all mRNA concentrations (Figure 3D-F), consistent with observations in human NPMc+ AML cases.[8,13] In mammalian cells, NPMc+ cytoplasmic localization is dependent on the presence of a novel nuclear export signal (NES) created by the mutation,[14] and thus this function appears conserved in zebrafish.

We performed WB analysis to determine protein expression levels in lysates from NPM1 or NPMc+ mRNA–injected embryos, and found that wild-type protein levels were much higher than those of NPMc+ at each mRNA dose (Figure 3G). Thus, we selected mRNA doses that yielded comparable protein levels, injecting 10 pg for NPM1 and 50 pg for NPMc+ (2 black arrows in Figure 3G) in all subsequent assays. We validated these selected doses in vivo by analyzing the EGFP-NPM1 and EGFP-NPMc+ protein subcellular localization in embryos by confocal microscopy (Figure 3H-I), confirming the nucleolar restriction of NPM1 and the cytoplasmic distribution of NPMc+ in the vast majority of cells.

Zebrafish NPM1 orthologs interact with human NPM1 proteins

Current evidence supports the hypothesis that the NPMc+ mutant protein heterodimerizes with NPM1 (encoded by the residual normal allele) and may function by shuttling this and other partners out of the nucleus.[13,41] To test whether we could study this mechanism in the zebrafish model, we examined the ability of NPMc+ to interact with zebrafish Npm1 proteins. EGFP- or DsRed-tagged Npm1a and Npm1b were expressed with fluorophore-tagged NPM1 or NPMc+ proteins in human 293T cells to assay for colocalization. First, we confirmed that both EGFP-Npm1a and EGFP-Npm1b were expressed in the nucleoli of cells (Figure 4A bottom left and right, respectively), as was NPM1 (compare with EGFP-NPM1 in Figure 4A top left; and to the cytoplasmic localization of EGFP-NPMc+, top right). WB analysis of transfected cells confirmed that all the proteins were expressed at comparable levels (Figure 4B). When coexpressed with EGFP-NPM1, both DsRed-Npm1a and DsRed-Npm1b colocalized with it in the nucleoli of cells (Figure 4C top and bottom rows, respectively). However, when either Npm1a or Npm1b were coexpressed with EGFP-NPMc+, they became aberrantly expressed in the cytoplasm, with or without residual nucleolar expression, in more than 90% of cells (Figure 4D top and bottom rows, respectively; quantification in Figure 4E). These observations
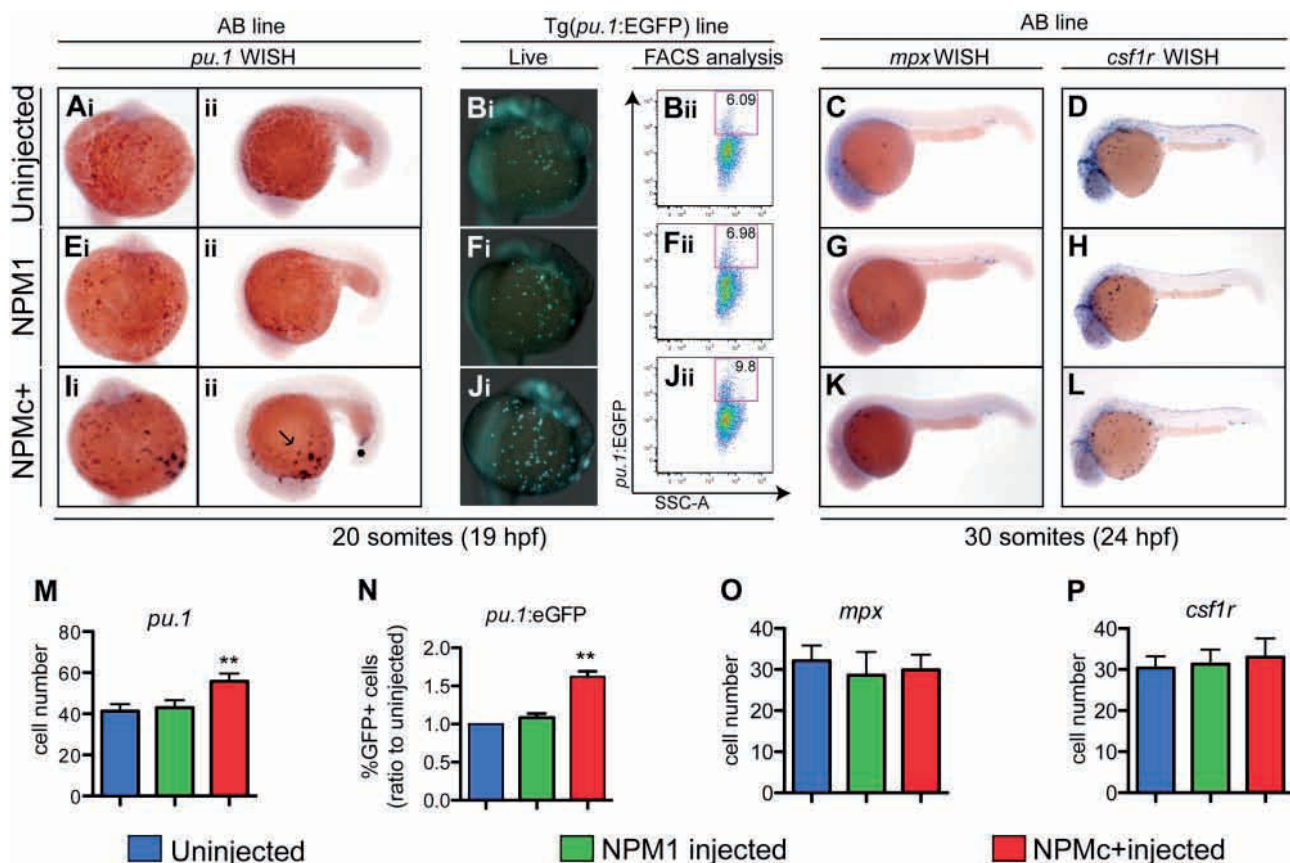
Figure 5. NPMc+ increases the number of primitive myeloid cells in zebrafish embryos. (Ai-Aii,Ei-Eii,Ii-Iii,M) WISH assays of AB embryos showing *pu.1* expression at 20 somites (19 hpf) in ventral views, anterior to the top (A,E,Ii), and lateral views anterior to the left, dorsal upwards (Aii,Eii,Iii). *pu.1*-expressing cells are shown as dark purple dots that increase in number with NPMc+ expression (Ii-Iii). (M) *pu.1*[+] cell number quantification shows a statistically significant increase upon NPMc+ expression (20 embryos counted per condition). (B,F,J) *pu.1* expression analysis in the Tg(*pu.1*:EGFP) line at 20 somites (19 hpf). Ventral views, anterior to the top, of the ALPM and yolk of live Tg(*pu.1*:EGFP) transgenic zebrafish embryos, uninjected (Bi), or injected with NPM1 10 pg (Fi) or NPMc+ 50 pg (Ji) mRNA. Green cells indicate cells expressing EGFP under the control of the *pu.1* promoter. NPMc+ expression causes a marked increase in EGFP[+] cell numbers that disperse widely across the embryo's yolk (Ji). FACS analysis of Tg(*pu.1*:EGFP) embryos, uninjected (Bii), or injected with NPM1 10 pg (Fii) or NPMc+ 50 pg (Jii) mRNA. *EGFP* expression is shown in the y-axis and is increased upon NPMc+ expression (Jii). (N) Quantification of the percentage of EGFP^{+} cells in 3 independent FACS experiments, each including 50 heterozygous Tg(*pu.1*:EGFP) embryos per condition, normalized to the percentage of EGFP^{+} cells of uninjected embryos. (C-D, G-H, K-L, O-P) WISH assays showing lateral views (anterior to the left, dorsal upwards) of 30 somites (24 hpf) embryos stained for *mpx* (C,G,K) or *csf1r* expression (D,H,L). No significant change in expression of any of these markers is observed. The number of *mpx* and *csf1r* cells is quantified in panels O and P, respectively (20 embryos counted per condition). Note that the *csf1r* probe also stains xanthophores in the dorsal trunk of the embryo. In all graphs, error bars represent SEM. *Statistically significant differences between the NPMc+-injected and both NPM1-injected and uninjected embryos (**P < .005; Student *t* test). In histograms, blue indicates uninjected control embryos; green, NPM1-injected embryos; and red, NPMc+-injected embryos.

indicate that NPMc+ can act in a dominant fashion to redistribute the 2 zebrafish Npm1 proteins to the cytoplasm, similar to human NPM1 (supplemental Figure 2A).[14,41]

To show that human and zebrafish NPM1 proteins can directly bind to each other, we carried out coimmunoprecipitation experiments. Figure 4F shows that an anti-GFP antibody can pull down both EGFP-Npm1a and EGFP-Npm1b along with endogenous NPM1 from transfected 293T cell lysates. In the reciprocal experiment, FLAG-tagged NPM1 and NPMc+ were able to pull down EGFP-tagged Npm1a and Npm1b (supplemental Figure 2B-C). These data demonstrate that NPMc+ can directly interact with zebrafish Npm1 proteins to affect subcellular localization processes, and validates our rationale for testing the consequences of NPMc+ expression in the developing hematopoietic system of zebrafish embryos.

NPMc+ increases the number of primitive myeloid cells in zebrafish embryos

To determine the effects of NPMc+ expression on primitive hematopoiesis, we injected in vitro–transcribed mRNAs encoding NPMc+ (and NPM1 as control) into 1-cell–stage zebrafish embryos, and assayed markers of hematopoietic cell subpopulations

by WISH. We found that expression of NPMc+, but not of NPM1, caused an increase in the number of *pu.1*^{+} cells at 20 somites compared with controls (Figure 5A,E,I; quantified in Figure 5M). These findings were also confirmed by counting *EGFP*^{+} cells in the Tg(*pu.1*:EGFP) transgenic line[25] that expresses EGFP under the control of the *pu.1* promoter (Figures 5Bi,Fi,Ji) and by flow cytometric analysis in the same line (Figures 5Bii,Fii,Jii; quantified in Figure 5N). To determine whether other markers of differentiating early myeloid cells were also expanded, we used probes to detect *mpx* and *csf1r* expression at 30 somites. Surprisingly, we found that neither of these markers was significantly affected by NPMc+ expression compared with NPM1-injected or uninjected embryos (Figure 5C-D,G-H,K-L; quantified in Figure 5O-P).

NPMc+ expression causes an increase in the number of primitive mpx[+] and csf1r^{+} cells in the absence of functional p53

We then asked whether we could see a more marked perturbation of primitive myeloid cell development in the absence of p53. Upon NPMc+ expression *pu.1* cells were increased in the p53[m/m] line at the 20-somite stage to a similar extent as observed in the wild-type background, while NPM1 expression had no effect compared with

uninjected embryos (Figure 6A,E,I; quantified in Figure 6M). Interestingly, we also observed increased numbers of *mpx*- and *csf1r*-expressing cells at the 30-somite stage, providing evidence that a p53-dependent process is required to prevent the increase in mpx^+ and $csf1r^+$ early myeloid cells induced by NPMc+ (Figure 6C,G,K and Figure 6D,H,L; quantified in Figure 5N-O, respectively). Furthermore, abnormally located *pu.1*- and *mpx*-expressing

cells were also observed in the dorsal trunk and head regions in these fish (Figure 6Iii,K arrows). Additional evidence that NPMc+ perturbs the differentiation of myeloid precursors comes from $EGFP^+$ sorted cells from 30-somite Tg(*pu.1*:EGFP) embryos injected with p53 MO and either NPM1 or NPMc+. Giemsa-stained cytospin slides showed a significant difference in morphology. NPMc+-expressing cells were larger and exhibited more open

Figure 6.

chromatin, consistent with a more immature phenotype than control and NPM1-expressing cells (Figure 6B,F,J).

### NPMc+ expression causes apoptotic cell death in zebrafish embryos

To determine the mechanism whereby NPMc+ expression resulted in an increase in *pu.1*-expressing early myeloid cells and, later, in *mpx*+ and *csf1r*+ cells only when p53 was not functional, we used the supravital dye acridine orange to assess cell death due to NPMc+ at 30 somites. NPM1 expression has no effect in hematopoiesis, and therefore served as a control. NPMc+ caused a dramatic increase in cell death detected throughout the embryo, particularly in the eye and brain (Figure 6Ri). In contrast, NPM1-injected embryos (Figure 6Qi) only showed a slight increase in the number of dead cells compared with control uninjected embryos (Figure 6Pi). To further dissect the mechanism of cell death, we also assayed injected embryos for activated caspase-3, which is expressed in apoptotic cells. NPMc+-injected embryos (Figure 6Rii), but not NPM1-injected or uninjected embryos (Figure 6Qii and 6Pii, respectively) showed increased activated caspase-3 staining in the brain and eye, and in cells in the ALPM region (Figure 6Rii arrow). This region corresponds to the location of developing myeloid precursors and suggests that *pu.1*+ cells could be undergoing apoptosis. To test this hypothesis, we injected NPM1 or NPMc+ in the Tg(*pu.1:EGFP*) transgenic line, and analyzed embryos for the coexpression of activated caspase-3 (in red) and EGFP (in green). NPMc+-injected embryos showed an increase in both signals compared with uninjected and NPM1-injected embryos (Figure 6Piii,Qiii,Riii); however, colocalization of red and green in the same cell was not detected. These findings were confirmed by FACS annexin-V analysis in Tg(*pu.1*:EGFP) transgenic embryos: NPMc+-injected embryos showed an increase in apoptosis as a whole (supplemental Figure 3A-C) that was not markedly evident in *pu.1:EGFP*+ cells (supplemental Figure 3D-F). Furthermore, the cell-cycle profile in sorted EGFP+ cells from Tg(*pu.1*:EGFP) animals showed no difference between control and NPMc+-injected embryos (supplemental Figure 3G-I). Given the marked increase in apoptotic cells evident in NPMc+-injected embryos, we examined the role of p53 in NPMc+-induced cell death. Both wild-type and mutated NPM1 proteins were expressed in the p53$^{m/m}$ line, and acridine orange and anti–activated

caspase-3 assays were performed. These assays showed a marked reduction in cell death and apoptosis in p53$^{m/m}$ (Figure 6Riv-v, respectively) compared with p53$^{wt/wt}$ NPMc+-injected embryos (Figure 6Ri-ii), suggesting that the apoptotic phenotype elicited by NPMc+ is p53-dependent.

NPMc+ increases the number of definitive hematopoietic cells in zebrafish embryos

To investigate whether NPMc+ expression affects definitive hematopoietic cell numbers, we examined the expression of the integrin *cd41* and the transcription factors *c-myb* and *runx1*, which label definitive HSCs starting between 30 and 36 hpf.[24] First, we used Tg(*cd41*:EGFP) transgenic fish to analyze expression of GFP^{Low} cells in the AGM region (Figure 7A black box).[24,42] Confocal microscopy showed that NPMc+ expression caused an increase in numbers of *cd41*-EGFP^{Low}–expressing cells between the dorsal aorta and the cardinal vein (brackets in Figure 7C,F,I; quantified in Figure 7L), the expected region for developing HSCs, and an increase in EGFP+ cells in the pronephric ducts, ventral to the AGM[24] (arrows in Figure 7C,F,I). Next, we analyzed *c-myb* expression by WISH, and found that NPMc+, but not NPM1, expression causes an increase in the numbers of *c-myb*–expressing cells at 32 hpf (supplemental Figure 4Ai,Ei,Ii; quantified in supplemental Figure 4M). Histologic cross-sections of these embryos confirmed *c-myb*–expressing cells were correctly localized between the ventral wall of the dorsal aorta and the cardinal vein (ie, the AGM region), and NPMc+-injected embryos showed ventral and lateral expansion of these cells within this domain (supplemental Figure 4Aii-iii,Eii-iii,Iii-iii). Importantly, NPMc+ expression caused the same increase in the number of *c-myb*–expressing cells in the AGM of p53$^{m/m}$ embryos (supplemental Figure 4D,H,L; quantified in supplemental Figure 4P). Next, we injected NPM constructs into double-transgenic embryos Tg(*c-myb*:EGFP);(*gata1*:DsRED). Z-stack images obtained by confocal microscopy in the AGM region (Figure 7A black box) confirmed that NPMc+ expression increased the number of EGFP+ cells expressed from the *c-myb* promoter relative to controls at 32 hpf (Figure 7Di,Gi,Ji). This observed increase in *c-myb*+ cells was confirmed by FACS analysis (supplemental Figure 4B,F,J; quantified in supplemental Figure 4N). As *c-myb* is also expressed in the ICM at this stage,[43] it was important to exclude the possibility that the observed increase

Figure 6. NPMc+ expression causes an increase in the number of primitive *mpx*+ and *csf1r*+ cells in the absence of functional p53 and causes p53-dependent apoptotic cell death. (Ai-Aii, Ei-Eii, Ii-Iii, M) *pu.1* WISH assays in homozygous p53 mutant embryos at 20 somites (19 hpf), uninjected (Ai-Aii), or injected with NPM1 10 pg (Ei-Eii) or NPMc+ 50 pg (Ii-Iii). Embryos are shown in ventral (Ai,Ei,Ii; anterior to the top) and lateral (Aii,Eii,Iii; anterior to the left, dorsal upwards) views. *pu.1*-expressing cells are indicated by dark purple spots and are increased in embryos injected with NPMc+, 50 pg (Ii-Iii). (M) *pu.1*+ cell number quantification shows a statistically significant increase upon NPMc+ expression (20 embryos counted per condition). (B,F,J) Giemsa stain of cystospins of *EGFP*+ cells sorted from Tg(*pu.1:EGFP*) embryos at 30 somites (24 hpf), injected with p53 MO 1.6 ng alone (B) or in combination with either NPM1 10 pg (F) or NPMc+ 50 pg (J). NPMc+ expression results in larger cells with more immature morphology (J). Images were acquired with a Zeiss Axio imager Z1 microscope using a Zeiss 63×/1.4 NA Apochromat Oil lens (Carl Zeiss) and Openlab software (Perkin Elmer). (C-D, G-H, K-L, N-O) *mpx* (C,G,K) and *csf1r* (D,H,L) WISH are shown in lateral views (anterior to the left, dorsal upwards) of homozygous p53 mutant embryos at 30 somites (24 hpf) uninjected (C-D) or injected with NPM1 10 pg (G-H) or NPMc+ 50 pg (K-L). Note that *mpx* and *csf1r* expression is markedly expanded upon NPMc+ expression and p53 loss (K-L). The number of *mpx* and *csf1r* cells is quantified in panels N and O, respectively (20 embryos counted per condition). Note that the *csf1r* probe also stains xanthophores in the dorsal trunk of the embryo. Error bars represent SEM. *Statistically significant differences between the NPMc+-injected and both NPM1-injected and uninjected embryos (**P < .005; ***P < .001; Student *t* test). In histograms, blue indicates uninjected control embryos; green, NPM1-injected embryos; and red, NPMc+-injected embryos. (P-R) Wild-type p53 embryos are shown either uninjected (Pi-Piii), or expressing NPM1 (Qi-Qiii) or NPMc+ (Ri-Riii). All embryos are at 30 somites (24 hpf) and shown in lateral views of the head and anterior trunk, anterior to the left and dorsal upwards. Acridine orange staining (green indicate dead or dying cells) of embryos uninjected (Pi), or injected with NPM1 10 pg (Qi) or NPMc+ 50 pg (Ri) mRNA. An increase in dying cells is observed upon NPMc+ expression (Ri). Activated caspase-3 immunostaining (green indicates cells in apoptosis) of embryos uninjected (Pii), or injected with NPM1 10 pg (Qii) or NPMc+ 50 pg (Rii) mRNA. Increased numbers of apoptotic cells are observed in NPMc+-injected embryos (Rii), forming aggregates on the yolk (arrow). Anti–activated caspase-3 and anti-GFP immunostaining in Tg(*pu.1:EGFP*) transgenic embryos (red spots indicate cells that express the cleaved form of caspase-3, and green spots indicate cells expressing EGFP under the control of the *pu.1* promoter), uninjected (Piii), or injected with NPM1 10 pg (Qiii) or NPMc+ 50 pg (Riii) mRNA. Note in panel Riii the increase in activated caspase-3–expressing cells that surround and lie adjacent to EGFP+ cells, but do not colocalize with them. Homozygous mutant p53 embryos are shown uninjected (Piv-Pv), or expressing either NPM1 (Qiv-Qv) or NPMc+ (Riv-Rv). All embryos are at 30 somites (24 hpf) shown in lateral views of the head and anterior trunk, anterior to the left and dorsal upwards. Acridine orange staining of embryos uninjected (Piv) or injected with NPM1 10 pg (Qiv) or NPMc+ 50 pg mRNA (Riv) show no difference in the number of dead or dying cells. Anti–activated caspase-3 staining of embryos uninjected (Pv) or injected with either NPM1 10 pg (Qv) or NPMc+ 50 pg (Rv) mRNA show no difference in the number of apoptotic cells. Embryos were equilibrated in glycerol and visualized with a Nikon SMZ1500 zoom stereomicroscope (Nikon) using a 488 nm filter for the EGFP signal and 568 nm filter for the red signal. Images were acquired with NIS-Elements software (Nikon).
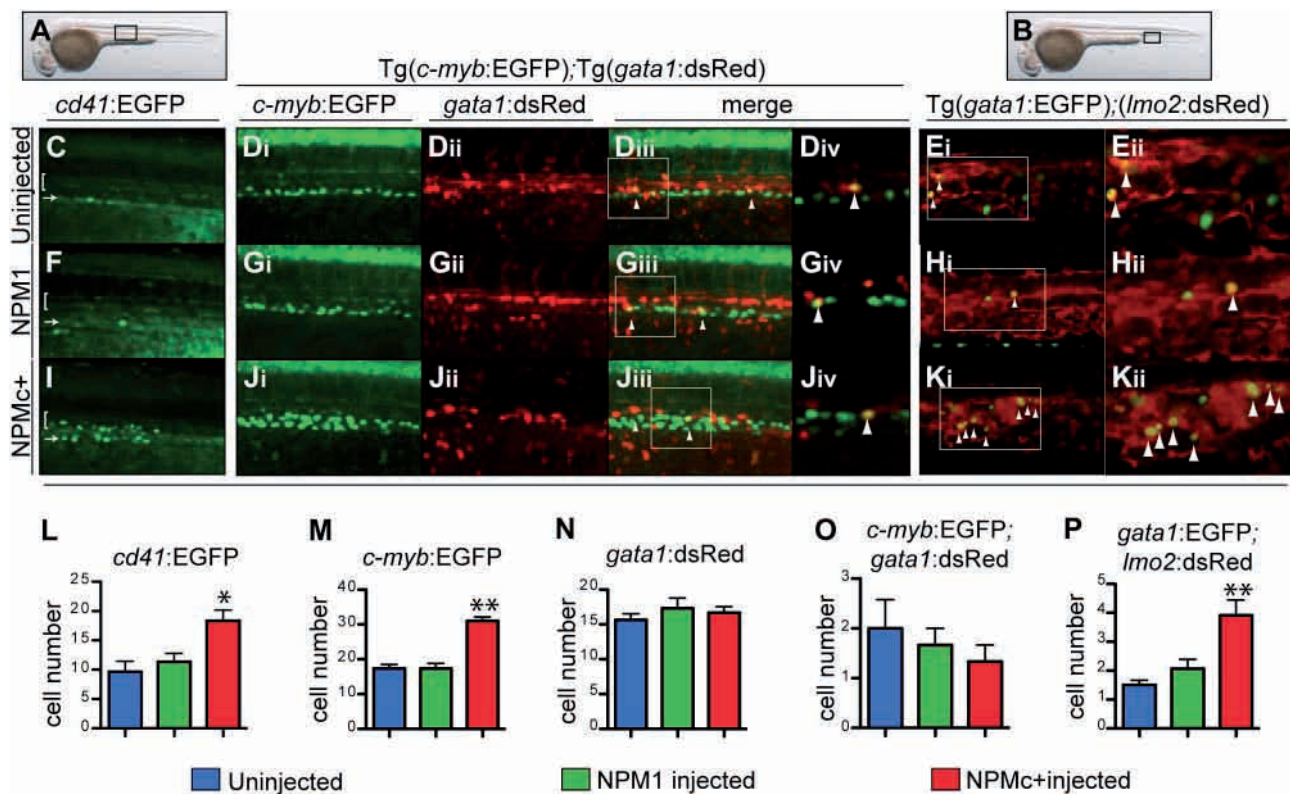
Figure 7. NPMc+ increases the number of definitive hematopoietic cells in zebrafish embryos. (A-B) Brightfield images of a 32-hpf embryo (lateral view, anterior to the left, dorsal upwards) where a black box shows the region of the AGM (A) or of the PBI (B), where subsequent images were taken. (C,F,I,L) Confocal images taken from the AGM region of live 32-hpf Tg(*cd41*:EGFP) transgenic zebrafish embryos (black box in panel A), uninjected (C), or injected with NPM1 10 pg (F) or NPMc+ 50 pg (I) mRNA. Green cells indicate expression of EGFP under the control of the *cd41* promoter. The bracket highlights *cd41*low EGFP+ cells in the AGM region, while the arrow points at the renal EGFP+ population located in the region of the pronephric ducts. EGFP+ cells in the AGM field were counted and showed increased numbers upon NPMc+ expression (L). Images were captured on a Yokogawa spinning disk confocal microscope using a 10×/0.3 NA Plan-fluor phase objective. (Di-iv, Gi-iv, Ji-iv, M-O) Confocal images taken from the AGM region of live 32-hpf Tg(*c-myb*:EGFP);(*gata1*:DsRed) transgenic zebrafish embryos (black box in panel A), uninjected (Di-Div), or injected with NPM1 10 pg (Gi-Giv) or NPMc+ 50 pg (Ji-Jiv) mRNA. Green indicates cells expressing EGFP under the control of the *c-myb* promoter; red indicates cells expressing DsRed under the control of the *gata1* promoter; yellow indicates cells coexpressing both genes (highlighted by arrowheads). The white boxes in panels Diii, Giii, and Jiii indicate an area, magnified in a single Z-stack slice (Div,Giv,Jiv), showing how single slices were used to quantify the number of yellow cells. NPMc+ expression causes an increase in EGFP+ cell numbers in the field of analysis (quantified in panel M) without affecting numbers of cells expressing DsRed under the control of the *gata1* promoter (quantified in panel N) or double-positive cells (quantified in panel O by counting yellow cells in 3 different Z-stack slices in each of 4 embryos). Images were taken as for Tg(*cd41*:EGFP) embryos. (E,H,K,P) Confocal images taken from the PBI region of live 32-hpf Tg(*gata1*:EGFP);(*lmo2*:DsRed) transgenic zebrafish embryos (black box in panel B), uninjected (E), or injected with NPM1 10 pg (H) or NPMc+ 50 pg (K) mRNA. Green indicates cells expressing EGFP under the control of the *gata1* promoter; red indicates cells expressing DsRed under the control of the *lmo2* promoter; yellow indicates cells coexpressing both genes (highlighted by arrowheads). NPMc+ expression causes an increase in cells expressing both genes (K), quantified in panel P by counting yellow cells in 3 different Z-stack slices in each of 4 embryos. Images are single Z-stack slices, and the white boxes in panels Ei, Hi, and Ki indicates an area magnified in panels Eii, Hii, and Kii. Images were acquired on a Yokogawa spinning disk confocal microscope using a 20×/0.75 NA Plan-Apo DIC objective. All confocal images were acquired using the Andor IQ software. Analysis of images was performed using ImageJ software. Error bars represent SEM. *Statistically significant differences between the NPMc+-injected and both NPM1-injected and uninjected embryos (*$P < .05$, **$P < .005$; Student t test). In histograms blue indicates uninjected control embryos; green, NPM1-injected embryos; and red, NPMc+-injected embryos.

in *c-myb*–expressing cells did not result from developmentally delayed erythrocytes that can also express *c-myb*. We found that the number of *gata1*:DsRed+ cells was not increased in NPMc+-injected embryos (Figure 7Dii,Gii,Jii; quantified in Figure 7N; also shown by *gata1* WISH; supplemental Figure 5C,F,I). Importantly, we demonstrated that the number of cells coexpressing *c-myb* and *gata1* (yellow cells) was not increased in embryos expressing NPMc+ (arrowheads in Figure 7Diii,Giii,Jiii; magnified single Z-sections showing boxed yellow cells in Figure 7Div,Giv,Jiv; quantified in Figure 7O). Therefore, the increase in *c-myb* was not due to increased numbers of erythroid precursors. To confirm that NPMc+ causes an increase in HSCs in the AGM, we also analyzed *runx1* expression, but surprisingly found that the numbers of *runx1*+ cells were unchanged in NPMc+-injected embryos relative to controls at both the 28- and 32-hpf time points (supplemental Figure 5A-B,D-E,G-H).

We then addressed whether expression of NPMc+ affected the EMP population, which can be identified by gata1/lmo2BRIGHT

coexpressing cells in the PBI.[23] Confocal microscopic analysis of the PBI region (Figure 7B black box) in double-transgenic Tg(*gata1*:EGFP);(*lmo2*:DsRed) embryos injected with NPMc+ showed a marked increase in numbers of gata1-lmo2 double-positive cells relative to controls (Figure 7E,H,K; quantified in Figure 7P). We confirmed these findings by FACS analysis and found similar increases in the numbers of EMPs upon expression of NPMc+ (supplemental Figure 4C,G,K; quantified in supplemental Figure 4O), again underscoring the finding that NPMc+ perturbs definitive hematopoiesis in the zebrafish embryo.

Discussion

In this report, we have used the zebrafish embryo as a model to examine the role of NPMc+ in hematopoiesis. We identified 2 *npm1* genes orthologous to human *NPM1* and have shown that

loss of both zebrafish *npm1* genes results in a defect in myelopoiesis, which was partially redundant between the 2 genes. This myeloid phenotype is consistent with findings reported in an *Npm1* mouse knockout model,[6] and could be rescued by forced NPM1 expression, indicating functional conservation between human and zebrafish NPM1. Zebrafish embryos injected with human NPMc+-encoding mRNA demonstrated abnormal cellular localization of the mutated protein in the cell cytoplasm, similar to human NPMc+ AML cells, while normal human NPM1 was localized exclusively in the nucleolus. We also demonstrated that both NPM1 and NPMc+ could bind to the zebrafish Npm1 orthologs and regulate their subcellular localization.

We demonstrated that NPMc+ expression perturbs primitive myelopoiesis by examining cells expressing the myeloid markers *pu.1*, *mpx*, and *csf1r*. While *pu.1* is mostly expressed in myeloid precursors at the 20-somite stage,[25] *mpx* is a marker of primitive and definitive granulocytes, and at 30 somites is also expressed in differentiating macrophages.[22] *csf1r* is the zebrafish ortholog of the human macrophage colony-stimulating factor receptor. It is expressed in precursor and mature macrophages on the yolk sac, and in xanthophores of the skin.[44] Interestingly, NPMc+ expression resulted in a striking increase in the number of early *pu.1*-expressing myeloid cells, but only caused a corresponding increase in the numbers of *mpx*- or *csf1r*-expressing myeloid cells later in development in the absence of functional p53. Although our data also showed that NPMc+ expression elicited a generalized p53-dependent apoptotic response, we were unable to demonstrate that the p53-dependent apoptotic cell death was occurring specifically in *pu.1*-expressing myeloid cells upon NPMc+ expression. Technical limitations using reporter zebrafish lines expressing EGFP under the control of the *pu.1* promoter may preclude this analysis, because the EGFP signal is known to be degraded early in the course of apoptosis, and therefore a myeloid apoptotic cell might not simultaneously express both EGFP and cleaved caspase-3 or annexin V. Alternatively, apoptosis could occur within a *pu.1*⁻, *mpx*⁺, and *csf1r*⁺ myeloid cell population at a later stage or a p53-dependent, nonapoptotic cell death process such as senescence could explain these observations. Taken together, these data suggest that NPMc+ expression perturbs primitive hematopoiesis by promoting the early expansion of *pu.1*⁺ myeloid cells, and this phenotype is even more pronounced in a p53-deficient background where *mpx*⁺ and *csf1r*⁺ cells are also expanded. The correlation between p53 mutational status and the extent of the phenotype elicited by NPMc+ is intriguing, because p53 mutations rarely occur in NPMc+ AMLs.[11] However, it has been shown that NPMc+ binds to and inactivates the tumor suppressor p14^ARF in mammalian cells, thus inhibiting the p53 response to oncogene activation.[13] Zebrafish and other teleosts lack a homolog of mammalian p14^ARF,[45] and thus our finding that a p53-dependent apoptotic response is activated by NPMc+ expression may reflect an oncogene-associated cell stress response, which is not evident in human NPMc+ AML cells due to inhibition of p14^ARF by NPMc+. These data are also consistent with the myeloproliferative phenotype elicited by NPMc+ expression in a transgenic mouse model,[17] and may be relevant to human AML. Other oncogenes involved in human AML have been shown to disrupt primitive hematopoiesis in zebrafish.[46,47] Moreover, the phenotype induced by the RUNX1:ETO oncoprotein in zebrafish primitive hematopoiesis has been successfully used in a large-scale screen for chemical modifiers,[48] again underscoring the relevance and strengths of the zebrafish system.

Although the transient nature of NPMc+ protein expression after mRNA injection prevents the study of zebrafish hematopoiesis beyond 32 hpf, our data show that definitive hematopoiesis is perturbed by NPMc+, which has important implications for the role of this protein in leukemogenesis. We found that *c-myb*– and *cd41*:EGFP-expressing cells were increased in the ventral wall of the aorta of NPMc+-injected embryos, suggesting that presumptive HSC numbers are increased due to its expression. However, the number of cells expressing *runx1* remains normal at this time. *Runx1* acts upstream of *c-myb* in the development of normal HSCs,[49] suggesting that NPMc+ may expand a *c-myb*⁺/*cd41*⁺ subpopulation of HSCs in which *runx1* expression has already been down-regulated. Alternatively, NPMc+ may specifically down-regulate the expression of *runx1* in these cells. We also showed that NPMc+ expression increases the numbers of *gata1*⁺/*lmo2^BRIGHT* double-positive cells in the PBI, indicating expansion of EMPs, the first multipotent, definitive hematopoietic progenitors to develop in both mice and zebrafish. Unlike normal HSCs, EMPs express both *c-myb* and *cd41* but only very low levels of *runx1*, suggesting these could be the main cells targeted by NPMc+ at this time point. However, given the correct anatomical location of *c-myb*-EGFP– and *cd41*-EGFP–expressing cells, we favor the hypothesis that both EMPs and HSCs are expanded by NPMc+. Importantly, it has been recently reported that NPMc+ is expressed in the leukemia-initiating cell fraction of human NPMc+ AMLs.[50,51] In addition, mutated NPMc+ can be found in granulocytic, monocytic, erythroid, and megakaryocytic cells in the bone marrow of patients with NPMc+ AML.[52] These data suggest that a multipotent stem or progenitor cell is the cell of origin for NPMc+ leukemias. Thus, the increase in definitive EMPs and HSCs promoted by NPMc+ expression in zebrafish is likely related to the role of NPMc+ in myeloid leukemogenesis, and provides a tractable in vivo system for study of the mechanisms through which hematopoietic development is perturbed in the presence of NPMc+.

Authorship

Contribution: N.B. and E.M.P. designed and performed research and wrote the manuscript; C.G. contributed important new reagents and analyzed and interpreted data; A.B.J. and J.-S.L. performed research; B.F. designed research and provided important reagents; and J.P.K. and A.T.L. designed research, analyzed data, and wrote the manuscript.

Conflict-of-interest disclosure: B.F. has applied for a patent on the clinical use of NPM1 mutants. The remaining authors declare no competing financial interests.

Correspondence: Niccolò Bolli and A. Thomas Look, Dana-Farber Cancer Institute, Mayer Bldg, Rm M630, 44 Binney St, Boston, MA 02115; e-mail: niccolo_bolli@dfci.harvard.edu, thomas_look@dfci.harvard.edu.

References

1. Grisendi S, Mecucci C, Falini B, Pandolfi PP. Nucleophosmin and cancer. *Nat Rev Cancer.* 2006; 6(7):493-505.

2. Bertwistle D, Sugimoto M, Sherr CJ. Physical and functional interactions of the Arf tumor suppressor protein with nucleophosmin/B23. *Mol Cell Biol.* 2004;24(3):985-996.

3. Korgaonkar C, Hagen J, Tompkins V, et al. Nucleophosmin (B23) targets ARF to nucleoli and inhibits its function. *Mol Cell Biol.* 2005;25(4): 1258-1271.

4. Colombo E, Marine JC, Danovi D, Falini B, Pelicci PG. Nucleophosmin regulates the stability and transcriptional activity of p53. *Nat Cell Biol.* 2002; 4(7):529-533.

5. Wu MH, Yung BY. UV stimulation of nucleophosmin/B23 expression is an immediate-early gene response induced by damaged DNA. *J Biol Chem.* 2002;277(50):48234-48240.

6. Grisendi S, Bernardi R, Rossi M, et al. Role of nucleophosmin in embryonic development and tumorigenesis. *Nature.* 2005;437(7055):147-153.

7. Sportoletti P, Grisendi S, Majid SM, et al. Npm1 is a haploinsufficient suppressor of myeloid and lymphoid malignancies in the mouse. *Blood.* 2008;111(7):3859-3862.

8. Falini B, Mecucci C, Tiacci E, et al. Cytoplasmic nucleophosmin in acute myelogenous leukemia with a normal karyotype. *N Engl J Med.* 2005; 352(3):254-266.

9. Liso A, Bogliolo A, Freschi V, et al. In human genome, generation of a nuclear export signal through duplication appears unique to nucleophosmin (NPM1) mutations and is restricted to AML. *Leukemia.* 2008;22(6):1285-1289.

10. Schlenk RF, Dohner K, Krauter J, et al. Mutations and treatment outcome in cytogenetically normal acute myeloid leukemia. *N Engl J Med.* 2008; 358(18):1909-1918.

11. Falini B, Nicoletti I, Martelli MF, Mecucci C. Acute myeloid leukemia carrying cytoplasmic/mutated nucleophosmin (NPMc+ AML): biologic and clinical features. *Blood.* 2007;109(3):874-885.

12. Arber D, Brunning RD, Le Beau MM, et al. Acute myeloid leukaemia with recurrent genetic abnormalities. In: Swerdlow SH et al, eds. *WHO Classification of Tumours of Haematopoietic and Lymphoid Tissues.* Lyon, France: International Agency for Research on Cancer (IARC). 2008; 110-123.

13. Falini B, Bolli N, Liso A, et al. Altered nucleophosmin transport in acute myeloid leukaemia with mutated NPM1: molecular basis and clinical implications. *Leukemia.* 2009;23:1731-1743.

14. Falini B, Bolli N, Shan J, et al. Both carboxy-terminus NES motif and mutated tryptophan(s) are crucial for aberrant nuclear export of nucleophosmin leukemic mutants in NPMc+ AML. *Blood.* 2006;107(11):4514-4523.

15. Bolli N, Nicoletti I, De Marco MF, et al. Born to be exported: COOH-terminal nuclear export signals of different strength ensure cytoplasmic accumulation of nucleophosmin leukemic mutants. *Cancer Res.* 2007;67(13):6230-6237.

16. Cheng K, Grisendi S, Clohessy JG, et al. The leukemia-associated cytoplasmic nucleophosmin mutant is an oncogene with paradoxical functions: Arf inactivation and induction of cellular senescence. *Oncogene.* 2007;26(53):7391-7400.

17. Cheng K, Sportoletti P, Ito K, et al. The cytoplasmic NPM mutant induces myeloproliferation in a transgenic mouse model. *Blood.* 2010;115(16): 3341-3345.

18. Langenau DM, Traver D, Ferrando AA, et al. Myc-induced T cell leukemia in transgenic zebrafish. *Science.* 2003;299(5608):887-890.

19. Bertrand JY, Traver D. Hematopoietic cell development in the zebrafish embryo. *Curr Opin Hematol.* 2009;16(4):243-248.

20. Payne E, Look T. Zebrafish modelling of leukaemias. *Br J Haematol.* 2009;146(3):247-256.

21. Detrich HW 3rd, Kieran MW, Chan FY, et al. Intraembryonic hematopoietic cell migration during vertebrate development. *Proc Natl Acad Sci U S A.* 1995;92(23):10713-10717.

22. Le Guyader D, Redd MJ, Colucci-Guyon E, et al. Origins and unconventional behavior of neutrophils in developing zebrafish. *Blood.* 2008;111(1): 132-141.

23. Bertrand JY, Kim AD, Violette EP, Stachura DL, Cisson JL, Traver D. Definitive hematopoiesis initiates through a committed erythromyeloid progenitor in the zebrafish embryo. *Development.* 2007;134(23):4147-4156.

24. Bertrand JY, Kim AD, Teng S, Traver D. CD41+ cmyb+ precursors colonize the zebrafish pronephros by a novel migration route to initiate adult hematopoiesis. *Development.* 2008;135(10): 1853-1862.

25. Hsu K, Traver D, Kutok JL, et al. The pu.1 promoter drives myeloid gene expression in zebrafish. *Blood.* 2004;104(5):1291-1297.

26. North TE, Goessling W, Walkley CR, et al. Prostaglandin E2 regulates vertebrate haematopoietic stem cell homeostasis. *Nature.* 2007;447(7147): 1007-1011.

27. Lin HF, Traver D, Zhu H, et al. Analysis of thrombocyte development in CD41-GFP transgenic zebrafish. *Blood.* 2005;106(12):3803-3810.

28. Traver D, Paw BH, Poss KD, Penberthy WT, Lin S, Zon LI. Transplantation and in vivo imaging of multilineage engraftment in zebrafish bloodless mutants. *Nat Immunol.* 2003;4(12):1238-1246.

29. Zhu H, Traver D, Davidson AJ, et al. Regulation of the lmo2 promoter during hematopoietic and vascular development in zebrafish. *Dev Biol.* 2005;281(2):256-269.

30. Long Q, Meng A, Wang H, Jessen JR, Farrell MJ, Lin S. GATA-1 expression pattern can be recapitulated in living transgenic zebrafish using GFP reporter gene. *Development.* 1997;124(20):4105-4111.

31. Berghmans S, Murphey RD, Wienholds E, et al. tp53 mutant zebrafish develop malignant peripheral nerve sheath tumors. *Proc Natl Acad Sci U S A.* 2005;102(2):407-412.

32. Westerfield M. The zebrafish book: a guide for the laboratory use of zebrafish (*Danio rerio*). 4th edition. Eugene, OR: University of Oregon Press, 2000.

33. Langheinrich U, Hennen E, Stott G, Vacun G. Zebrafish as a model organism for the identification and characterization of drugs and genes affecting p53 signaling. *Curr Biol.* 2002;12(23):2023-2028.

34. Bennett CM, Kanki JP, Rhodes J, et al. Myelopoiesis in the zebrafish, *Danio rerio. Blood.* 2001; 98(3):643-651.

35. National Center for Biotechnology Information (NCBI). Mapviewer. Available at: http://www.ncbi.nlm.nih.gov.ezp-prod1.hul.harvard.edu/mapview/. Accessed August 2006.

36. Barbazuk WB, Korf I, Kadavi C, et al. The syntenic relationship of the zebrafish and human genomes. *Genome Res.* 2000;10(9):1351-1358.

37. European Informatics Institute. Clustal W algorithm. Available at: http://www.ebi.ac.uk/Tools/clustalw2/index.html. Accessed January 2009.

38. Sidi S, Sanda T, Kennedy RD, et al. Chk1 suppresses a caspase-2 apoptotic response to DNA damage that bypasses p53, Bcl-2, and caspase-3. *Cell.* 2008;133(5):864-877.

39. Gates MA, Kim L, Egan ES, et al. A genetic linkage map for zebrafish: comparative analysis and localization of genes and expressed sequences. *Genome Res.* 1999;9(4):334-347.

40. Robu ME, Larson JD, Nasevicius A, et al. p53 activation by knockdown technologies. *PLoS Genet.* 2007;3(5):e78.

41. Bolli N, De Marco MF, Martelli MP, et al. A dose-dependent tug of war involving the NPM1 leukaemic mutant, nucleophosmin, and ARF. *Leukemia.* 2009;23(3):501-509.

42. Kissa K, Murayama E, Zapata A, et al. Live imaging of emerging hematopoietic stem cells and early thymus colonization. *Blood.* 2008;111(3): 1147-1156.

43. Thompson MA, Ransom DG, Pratt SJ, et al. The cloche and spadetail genes differentially affect hematopoiesis and vasculogenesis. *Dev Biol.* 1998;197(2):248-269.

44. Hall C, Flores MV, Storm T, Crosier K, Crosier P. The zebrafish lysozyme C promoter drives myeloid-specific expression in transgenic fish. *BMC Dev Biol.* 2007;7:42.

45. Gilley J, Fried M. One INK4 gene and no ARF at the Fugu equivalent of the human INK4A/ARF/INK4B tumour suppressor locus. *Oncogene.* 2001;20(50):7447-7452.

46. Kalev-Zylinska ML, Horsfield JA, Flores MV, et al. Runx1 is required for zebrafish blood and vessel development and expression of a human RUNX1-CBF2T1 transgene advances a model for studies of leukemogenesis. *Development.* 2002;129(8):2015-2030.

47. Liu TX, Rhodes J, Deng M, et al. Dominant-interfering C/EBPalpha stimulates primitive erythropoiesis in zebrafish. *Exp Hematol.* 2007;35(2): 230-239.

48. Yeh JR, Munson KM, Elagib KE, Goldfarb AN, Sweetser DA, Peterson RT. Discovering chemical modifiers of oncogene-regulated hematopoietic differentiation. *Nat Chem Biol.* 2009;5(4):236-243.

49. Burns CE, Galloway JL, Smith AC, et al. A genetic screen in zebrafish defines a hierarchical network of pathways required for hematopoietic stem cell emergence. *Blood.* 2009;113(23):5776-5782.

50. Martelli MP, Pettirossi V, Bonifacio E, et al. Evidence for CD34+ hematopoietic progenitor cell involvement in acute myeloid leukemia with NPM1 gene mutation: implications for the cell of origin [abstract]. *Blood.* 2008;112(11):Abstract 307.

51. Taussig DC, Vargaftig J, Miraki-Moud F, et al. Leukemia initiating cells from some acute myeloid leukemia patients with mutated nucleophosmin reside in the CD34- fraction. *Blood.* 2010;115(10): 1976-1984.

52. Pasqualucci L, Liso A, Martelli MP, et al. Mutated nucleophosmin detects clonal multilineage involvement in acute myeloid leukemia: Impact on WHO classification. *Blood.* 2006;108(13):4146-4155.